A Mathematical Model of the Potassium Homeostasis in Saccharomyces cerevisiae

vorgelegt von

Matthias Kahm

am

15.12.2011

aus Diez

Angefertigt mit der Genehmigung der Mathematisch-Naturwissenschaftlichen Fakultät der Rheinischen Friedrich-Wilhelms-Universität Bonn.

Erstgutachter: Prof. Dr. Maik Kschischo
Zweitgutachter: Prof. Dr. Wolfgang Alt

Tag der mündlichen Prüfung: 21.06.2012
Erscheinungsjahr   2012

Diese Dissertation ist auf dem Hochschulserver der ULB Bonn

`http://hss.ulb.uni-bonn.de/diss_online`

elektronisch publiziert.

Zusammenfassung

Die Aufrechterhaltung eines inneren Gleichgewichts ist Kennzeichen allen Lebens. Jeder Organismus benötigt Mechanismen welche bestimmte Parameter in vorgegebene Grenzen einregeln. Die Hefe *Saccharomyces cerevisiae* ist der Lage ihre zytosolische Kalium Konzentration zwischen 200 und 300 mM zu halten; bei begrenztem ebenso wie übermäßigem externen Kaliumangebot. Zur Klärung der dazu notwendigen Mechanismen wurde ein mathematisches Modell der Kaliumhomöostase entwickelt.

Aufgrund einer engen Kopplung schließt die Betrachtung der Kaliumflüsse mindestens die Aktivität der Protonentransporter mit ein. Dies betrifft inbesondere die Plasmamembran ATPase Pma1. Das aktive Auswärtspumpen von H^+ erhält das Membranpotential und liefert die notwendige Energie für alle zellulären Transportvorgänge.

Eine Beschreibung der einzelnen Transporter konnte oftmals aus elektrophysiologischen Messungen abgeleitet werden. Als zentraler Bestandteil wird das Membranpotential mittels einer Kondensatorgleichung modelliert. Das Membranpotential dient der Energetisierung und Kopplung des Ionentransports.

Modellerweiterungen wurden für das Volumen, den Ammoniumtransport und Metabolismus, sowie für den Puffereffekt der CO_2 assoziierten Reaktionen entwickelt. Die Kalibrierung der Modellparameter erfolgt über ein Experiment, bei dem der zeitliche Verlauf der internen Kaliumkonzentration unter externem Kaliummangel bestimmt wurde.

Als zentrale Fragestellung wurde untersucht welcher Prozess die Dynamik der internen Kaliumkonzentration bestimmt. Nach systematischen Tests geeigneter Regulationsmechanismen, konnten die Aktuatoren der Kaliumhomöostase durch die Methode des *Reverse Tracking* ermittelt werden. Diese neue Methode dient der Schätzung des zeitlichen Verlaufes eines Modellparamters welcher notwendig ist um ein dynamisches Modell gegebenen Daten anzupassen.

Als testbare Modellhypothese wird vorgeschlagen, dass die Hefezelle auf plötzlichen externen Kaliumabfall mit einem rasch erhöhten H^+-Ausfluss reagiert. Der Effekt liegt dabei in der Energetisierung der Kaliumaufnahme. Dies kann zum Einen über eine verstärkte Produktion von CO_2 und zum Anderen über die Aktivierung der Protonenpumpe Pma1 geschehen. Experimente können schließlich die Beteilung beider Prozesse bei der Regulation der Kaliumkonzentration belegen.

Contents

Symbols

Physical units:

- V: Volt

- A: Ampere

- C: Coulomb (A · s)

- S: Siemens (A/V)

- J: Joule (C · V)

- F: Farad (C/V)

- K: Kelvin

- L: Liter

- Pa: Pascal

Variables:

- [.] square brackets indicate concentrations

- $[.]_i$ the subscript i denotes internal (cytosolic) concentrations

- $[.]_o$ the subscript o denotes outer (surrounding) concentrations

- $[.]^0$ the subscript *zero* indicates initial values

- J mass fluxes

- I electric current densities

- I_K the subscript denotes the ion related to the current (or flux)

- $I^{Trk1,2}$ the superscript denotes the transport system related to the current (or flux)

- $E = \frac{RT}{zF} \frac{[.]_o}{[.]_i}$ equilibrium potential of a transporter (Nernst potential in case of a uniport)

- E_K the subscript indicate the respecting ion for the equilibrium potential

Constants:

- $F = 96\,485\,000\,\mu C/mmol$ Faraday's constant

- $R = 8314.5\,\mu J/mmol/K$ ideal gas constant

- $T = 293\,K$ temperature

- $R \cdot T = 2.4361\,10^6\,\frac{\mu J}{mmol}$

- z valence of a respecting ion, unless otherwise stated $z = 1$

- $e = 1.6 \cdot 10^{-13}\mu C$ elementary charge

- $F/(R \cdot T) = 39.6 \, \frac{1}{\text{V}}$

- $(R \cdot T)/F = 0.025 \, \text{V}$

- $\mathcal{R} = \frac{volume}{surface} = \frac{\frac{4}{3}\pi \, r^3}{4\pi \, r^2} = \frac{r}{3} \approx 7.5 \cdot 10^{-5} \, \text{cm}$, for a spherical cell with $r = 2.28 \cdot 10^{-4} \text{cm}$ and a volume of 50 fL

- $1/\mathcal{R} = \frac{surface}{volume} = \frac{3}{r} \approx 13\,000 \, \frac{1}{\text{cm}}$

Conversions:

- $\text{mg}_{\text{dryweight}} = 0.3 \cdot \text{mg}_{\text{wetweight}}$

- $1 \frac{\text{nmol}}{\text{mg}} \rightarrow 0.5 \, \text{mM}$

- $\frac{\text{pA}}{cell} \rightarrow \frac{1}{3} \cdot \frac{\mu\text{A}}{\text{cm}^2}$

- $\frac{\text{pA}}{cell} \rightarrow 6.22 \cdot 10^{-5} \frac{\text{mmol}}{\text{cm}^3 \, \text{s}}$

- $\frac{\text{nmol}}{\text{mg min}} \rightarrow 5 \cdot 10^{-4} \frac{\text{mmol}}{\text{cm}^3 \, \text{min}} = \frac{5}{60} \cdot 10^{-4} \frac{\text{mmol}}{\text{cm}^3 \, \text{s}}$

- $\frac{\text{nmol}}{\text{mg min}} \rightarrow 8.33 \cdot 10^{-6} \frac{\text{mmol}}{\text{cm}^3 \, \text{s}}$

- $\frac{\text{mmol}}{\text{s g}_{\text{protein}}} \rightarrow 30.87 \frac{\mu\text{A}}{\text{cm}^2}$

Special symbol:

↻ Indicates data sets and experiments which were performed as a consequence of the modeling process

Preamble

This work was integrated in the SysMo ERA-NET project TRANSLUCENT. As a transnational funding initiative SysMO (*S*ystems *B*iology of *M*icro*O*rganisms) supports consortia of modelers and wet lab scientist to investigate a certain topic. The aim of TRANSLUCENT was a systems level understanding of yeast cation homeostasis.

The generated data consists of expression profiles, protein interaction networks, growth and transport characterization, flux measurements, time courses for various intracellular species, the cell volume, the construction of knock-out mutants and many more.

For the modeling process such a collaboration offers the opportunity to request necessary data directly from the experimenters. It allows the design of experiments to test and verify certain model hypothesis. Under such fruitful conditions a mathematical model is understood as a tool to enhance the knowledge about the underlying model organism.

Consequently, the underlying idea is a data driven modeling approach, where the modelers request experiments which presumably support the model building process. Many of those experiments, which were designed by the author in close collaboration with the project partners were used in the present work. The comprehensive list of experiments can be found in the Appendix 4.5. However, the data is owed by the researches and still not published in most cases. This explains, why the reader is often referred to unpublished material. Nevertheless, the most relevant findings will be presented and the model predictions will be supported by experimental data.

1 Introduction

Life is a most complex phenomenon. Since the existence of cells was known, biologists investigate the function and interaction of the different cell parts. Systems biology has developed theoretical concepts about a systematic approach to cellular processes, metabolic fluxes (Sanders et al. 1983), cell communication, excitability (Bezanilla 2002) and adaption to environment. In recent times the development of experimental techniques and methodology (high-throughput measurements, microscope, fluorescence) as well as the development of powerful computers have contributed to a revolution in biology. A process that is fruitful for both disciplines.

The amount of data and the wide field of biology requires more and more interdisciplinary efforts. Biologists need to understand mathematical terms and expressions; mathematicians have to learn that under the same conditions, the same protocol and a precise prearrangement the biological organism might behave different in each experiment.

Systems biology is not only driven by curiosity but by hard economic interest. The prospect of design or modeling a microorganism to produce substances is often cheaper (to use the cell factory) than developing an industrial process. However, biotechnological applications need a reliable fundamental knowledge about an organism to use it efficiently in engineering. In fact, the reason why microorganism are extensively studied is the aim to recruit them for special purposes, e.g. production of pharmacological relevant proteins, production of ethanol, cleaning of wastewater etc. (Klemme 2004).

A model is an abstract representation of a process. The development of a model can clarify fundamental concepts and points out gaps in current knowledge. Modeling assists experimentations by fast and cheap simulations. The most powerful aspect of modeling is to make testable predictions.

The modeling process starts with the acquisition of the present knowledge about the process of interest. In close collaboration with experimental scientists, this knowledge serves to develop a first model concept. At this stage it may already turn out, that additional aspects require investigations before the concept can be translated into a mathematical description. Once the first model version is achieved, a dynamic cycle is entered. The model simulation lead to predictions, which requires experimental validation. The acceptance or falsification of model hypothesis generates new biological knowledge, which can be used to further improve the model. The repeated cycle of prediction, validation and model adaptation drives the biological knowledge, see Figure 1.1.

Each organism faces a changing environment. This brings the need of capable control mechanisms to keep the inner state of the organism in a viable range. The auto-regulation of a homeostatic state is a characteristic of life.

Yeast is widely used by humans since ancient times. The utilization ranges from classic brewery and bakery applications to the production of biofuel. Furthermore yeast serves as a model organism to clarify diseases. An example is studies about early apoptose triggers in cancer therapy (Gourlay et al. 2006). A basic property of yeast is its salt stress resistance. Yeast cells can survive micromolar
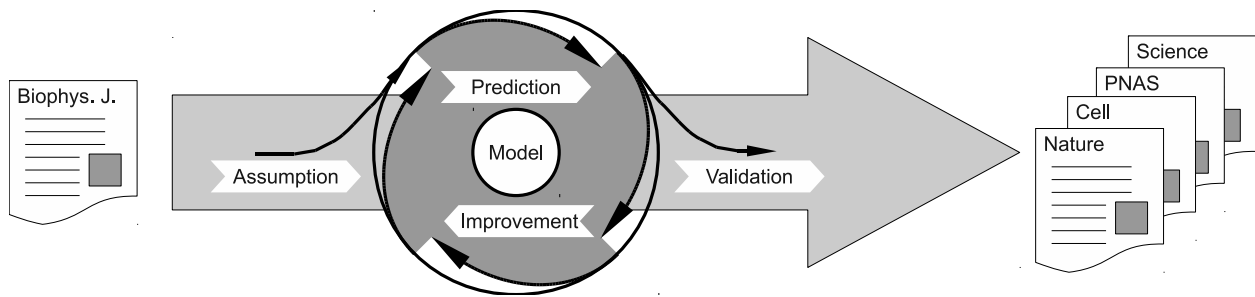
Figure 1.1: *Modeling process. A continuous sequence of model predictions, experimental validation and model adaptations*

to molar concentrations of potassium and sodium. This appears as a worthwhile topic to study, since salt stress resistance is also a desired property of crops in salinization soils. To put in a nutshell, Rodriguez-Navarro (2000) states, since fungi live closely to humans, animals and plants, everything that affects fungi, affects economy, ecology and health. The variety of applications rise many interesting biological questions. This work is mainly focused on the maintenance of the intracellular potassium under a reduced external potassium supply. Fundamental to this investigation is the development of a predictive model. This thesis provides a first attempt to model the response of *Saccharomyces cerevisae* to a shortage of potassium. Therefore, the modeling process itself is important in this work.

Structure of the thesis

The following Section 1.1 gives an introduction in the biological background of this work.

Chapter 2 is composed of two parts. The first one introduces all relevant experiments and data sets and the second one reveals the model building process. It will be shown how the presented data is used to derive mathematical descriptions for e.g. the membrane transporters and it also explains the different stages of the model.

The main results are presented in Chapter 3. The model simulations are used to better understand the potassium starvation experiments of Navarrete et al. (2010) (see Section 2.1.3) and to reveal the basic biophysical processes which can not directly be observed in the wet lab experiments. The most regulatory processes necessary for the maintenance of potassium homeostasis are predicted by the model. These predictions are then compared to validation experiments.

1.1 Yeast as a model organism

The cell-walled, budding yeast *Saccharomyces cerevisae* is a well studied organism, which combines an easy handling and experimental tractability. As an unicellular, eukaryotic fungus it has similarities to higher cells. Thus, the knowledge about principal physiological processes in yeast can often be transferred to other organisms. For example, many methods in molecular genetics were developed using yeast cells. Research on yeast significantly contributed to the understanding of the cell cycle, signaling pathways, the properties of the cytoskeleton proteins like actin and tubulin and transport mechanisms (Botstein and Fink 1988). In addition, *Saccharomyces cerevisiae* is an organism which can be used for stable heterologous expression and analysis of their properties of

many plant and animal genes; see Bertl and Slayman (1990) and references therein.

With a fully characterized genome (Goffeau et al. 1996) and an exhaustive computerized search for possible transport proteins (Nelissen et al. 1997) yeast appears as a suitable organism to study the transport of alkali-metal ions, such as potassium or sodium. In natural environments yeast usually faces low external concentrations of the required potassium and plenty of the toxic sodium (Rodriguez-Navarro 2000). To keep an optimum intracellular potassium concentration of 200-300 mM and a high potassium/sodium ratio yeast cells uses three different strategies (Sychrova 2004): (1) discrimination of potassium and sodium at the level of influx, ensured by a low affinity of the transporters to sodium, (2) extrusion of toxic ions and (3) sequestration into organelles. Based on measurements on potassium and sodium content, Kolacna et al. (2005) suggests a constant sum of intracellular potassium and sodium, which means, that the increase of one species leads to a decrease of the other one. This result matches the observation of Rodriguez-Navarro (2000), that sodium seems to be less toxic to the cell in potassium limiting conditions, helping to maintain the cell volume and pH.

1.1.1 Potassium

Potassium is required for many physiological functions such as protein synthesis, enzyme activation and regulation of the cell cycle. Potassium is also involved in the cell volume regulation and the maintenance of the intracellular pH and the membrane potential (Ariño et al. (2010); Rodriguez-Navarro (2000); Sychrova (2004) and references therein). These effects will also be visible in the later model simulations. The connections between potassium and other cellular parameters are described below.

As the most abundant cation in yeast the intracellular[1] potassium concentration is maintained around 200-300 mM. However, this value can differ between strains and according to the composition of the external medium (Haro and Rodriguez-Navarro 2002; Kuroda et al. 2004; Ramos and Rodriguez-Navarro 1986; Rivetta et al. 2005; Sychrova 2004). The related ascomycete *Neurospora crassa* has similar potassium requirements (Rodriguez-Navarro and Ramos 1984).

In many environments potassium concentration is in the micromolar range (Rodriguez-Navarro 2000). Therefore the cells have to keep potassium inside against a very steep concentration gradient. Yeast cells are able to grow under 10 μM-2.5 M K^+ and <1.5 M Na^+ (Ariño et al. 2010), with 0.5 mM K^+ to 1 mM K^+ (Bañuelos et al. 2002; Rodriguez-Navarro and Ramos 1984) being enough to support the maximum growth rate. Experiments where the cells were kept in very low potassium concentrations for a long time revealed intracellular K^+ concentrations around 220 nmol/mg dryweight (Bertl et al. 2003), 100 mM/kg cellwater (Kuroda et al. 2004) and 60 nmol/mg dryweight (Navarrete et al. 2010). Ramos and Rodriguez-Navarro (1986) reported that potassium starvation could not decrease the K^+ content much below 230 nmol/mgdryweight. This led to the conviction of many biologists, that yeast cells can keep a residual potassium concentration of around 100 mM[2] even under very low potassium conditions.

---

[1]Note: the compartmentalization of species in organelles or the vacuole is currently not fully characterized and hardly accessible by experimental procedures. In this work the whole cell is treated as *one* compartment and the terms *intracellular*, *lumenal* and *cytosolic* are used as synonyms for the whole cell interior.

[2]According to the calculations in Section 2.1.3, 1 nmol/mg$_{dry}$ corresponds roughly to 0.5 mM.

1.1.2 Membrane potential

The membrane potential is generated by an excess of negative charges at the cytosolic side of the plasma membrane. Although containing a bulk of negative charges such as inorganic and organic anions like carboxylic acids, mono and diester phosphates, the cell interior maintains an electroneutral state at any time (Rodriguez-Navarro 2000); see Section 2.2.3 and Appendix 4.9

The constraint of macroscopic electroneutrality requires compensatory fluxes for each charge that is moved over the membrane. For example, Rodriguez-Navarro (2000) reports that a potassium loss, is partly balanced by the uptake of H^+. Nevertheless, a loss of potassium goes in parallel with a hyperpolarization of the membrane (Navarrete et al. 2010), since only 6000 charges per μm^2 are sufficient to shift the membrane potential by 100 mV; see Section 2.2.3 and Appendix 4.9. For a diameter of 5-10 μm the cell surface is 80-300 μm^2.

The value of the membrane potential is still under discussion. Rodriguez-Navarro (2000) reported a membrane potential of -300 mV in fungi and -230 mV in plants and suggested the membrane potential of *S. cerevisiae* could be close to that of *N. crassa*, which is below -300 mV (Gradmann et al. 1978). Rodriguez-Navarro (2000) states, that values in older publications, suggesting values around -100 mV are probably underestimated especially in small fungi cells due to leakage effects between the recording electrode and the membrane. However, a recent publication of Jennings and Cui (2008) suggests a membrane potential in the range of -50 to -120 mV. On the contrary, Sanders et al. (1983) assumes a membrane potential of -300 to -200 mV. A definite answer can not be given until a technique for a direct membrane potential measurement in *S. cerevisiae* is available. This work assumes a membrane potential around -300 mV since such a value is favored by the authors of a recent review (Ariño et al. 2010).

1.1.3 pH

S. cerevisiae requires a low external pH for optimal growth. For an external pH around 5, the intracellular pH was reported to be around 7 pH in the exponential growth phase (Navarrete et al. 2010). Potassium starved cells are known to have a more acidic intracellular pH of 6-6.5 pH; (Navarrete et al. 2010; Rodriguez-Navarro 2000) and references therein. The vacuole has a more acidic pH than the cytosol with a pH below 4.8 pH (Brett et al. 2005). Finding striking similarities between the computed isoelectric points of the yeast proteome, Brett et al. (2006) raises the hypothesis that the proteome itself could encode the pH of the different cellular compartments.

The intracellular pH is influenced by potassium via the tight coupling of potassium and proton fluxes. As mentioned above, the uptake and efflux of potassium is partly balanced by respective proton fluxes to ensure electroneutrality. Actually, the uptake of potassium is driven by the active proton extrusion via the ATPase Pma1, see Section 1.2. This implies, although proton buffer mechanisms might quickly restore the pH, that the uptake of potassium goes in parallel with an increase of the pH (and *vice versa*).

The cells interior has a certain protein buffer capacity which is caused by effects of amino acids, negative macromolecules or a metabolic CO_2 production. This means means that not every proton entering or leaving the cell contributes to the pH. An appropriate value for the buffer capacitance was not found in publications, but using measurements from various sources, a buffer capacity around 200 mmol/pH was be inferred; see Section 2.2.11.

1.1.4 Cell volume

The diameter of a typical yeast cell is 5-10 μm, whereas haploid strains are usually smaller than diploids ones and the shape depicts a flatted sphere. The influence on the cell volume arises from potassium's contribution to the internal osmotic pressure. Since the total concentration of osmotic active substances in the cell is estimated as 600-700 mM by Gennemark et al. (2006), potassium could be responsible for almost fifty percent of the internal pressure. In most environments the internal osmotic pressure is higher than the external one (Rodriguez-Navarro 2000). Without the inward directed turgor pressure created by the rigid cell wall, an influx of water would occur, leading to a swelling and possible rupture of the cell membrane.

Since yeast can survive a vast range of external salt concentrations, it needs efficient volume regulation capabilities to prevent swelling and extensive shrinkage. A system which is used by the cell especially in hyper-osmotic conditions is the HOG-pathway (*H*igh *O*smolarity *G*lycerol) controlled glycerol production (Gennemark et al. 2006; Reed et al. 1987). Glycerol is accumulated inside the cell to increase the internal osmotic pressure in order to prevent an excessive loss of water. The contrary effect is achieved by the opening the Fps1 channels, which allow the efflux of glycerol (Gennemark et al. 2006).

1.1.5 Other ionic species

Sodium and lithium are toxic to cells. Sodium enters the cell presumably via the potassium uptake systems (Haro and Rodriguez-Navarro 2002; Sychrova 2004). Another uptake route is via the inorganic phosphate-sodium symport Pho89 (Martinez and Persson 1998). The accumulation of sodium is prevented by a limited uptake, sequestration in the vacuole and an efficient efflux, where the extrusion is mainly via Ena1-5 ATPases (Platara et al. 2006) and the antiporter Nha1 (Prior et al. 1996). For cells growing in standard medium, Kolacna et al. (2005) found a sodium level around 13 mM (original unit 25.5 mmol/g dry weight, unit conversion see Section 2.1.3).

Ammonium is a preferred nitrogen source for *S. cerevisiae*. The uptake of ammonium is performed by the MEP system, which is composed of a whole family of transporters (Marini et al. 1997, 1994). Inside the cell, ammonium is quickly integrated into amino acids. The amino acids, that were not used by the cell can be released by the SPS system, a system consisting of different amino acid transporters. Especially in the absence of potassium, ammonium is known to have toxic effects on the cell (reduced cell growth). In a fed-batch experiment Hess et al. (2006) observed, that under potassium limiting conditions the amino acid extrusion is enlarged in the presence of high external NH_4^+. Since ammonium is similar in size and charge to potassium, these authors hypothesize, that ammonium could enter the cell under potassium starvation via potassium transporters, especially Trk1,2. However, unpublished material by Joaquin Ariño indicates a rather low cytosolic concentration of around 4 mM in a rich medium and 10 mM under potassium starvation; for experimental conditions according to Navarrete et al. (2010).

S. cerevisiae requires only traces of chloride for normal growth Rodriguez-Navarro (2000). Since the cytosolic concentration of chloride is higher than expected, if Cl^- uptake would only occur by passive processes. Some authors suggest a proton-chloride symport mechanism (Jennings and Cui 2008; Roberts et al. 2001). According to Kuroda et al. (2004) a cytosolic chloride concentration far above 1 mM hinders the potassium uptake via Trk1,2. Similarly, Rivetta et al. (2005) reports
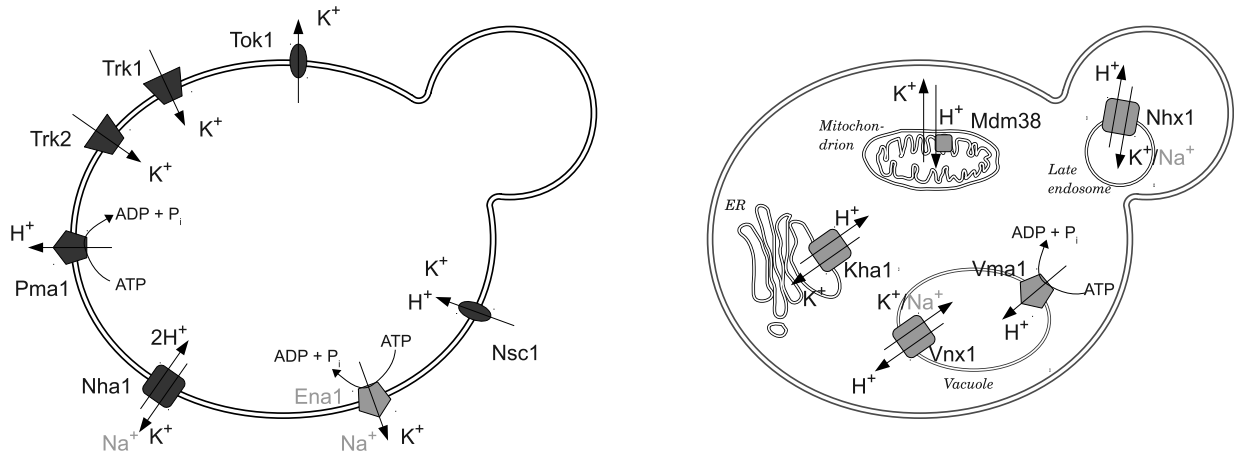
Figure 1.2: *Schema of the main plasma membrane (left) and organelle (right) transport proteins. Light gray colored species and transporters are not considered in the biophysical model. For a detailed description of transporters see Section 1.3.*

high cytosolic chloride (>30 mM) to short circuit the proton pump and to hinder the proton-driven nutrient transporters. Thus, typical cytosolic chloride concentrations are given to be 50-150 μM (Coury and Brodsky 1999; Jennings and Cui 2008), whereas the vacuolar concentration can be higher around 1 mM (Jennings and Cui 2008).

Calcium serves as an intracellular signaling molecule and is kept in a 50-200 nM for a vast range of external Ca^{2+} (Cui and Kaandorp 2006).

1.2 Potassium homeostasis in S. cerevisiae

The cell membrane separates the living cell from the environment, which allows the cell to establish specific intracellular conditions. Sophisticated plasma membrane transport mechanisms are required to supply nutrients and ions requested for cellular functions.

The two main classes of cellular transporters are the carriers and the channels (Alberts et al. 2002). The channels are aqueous pores, which allow the movement of ions of a certain size or charge. The simplest model of a channel is a system consisting of a selectivity filter, the pore region and a gate. After passing the filter, the substance is transported by a sequential binding to several domains in the pore region. However, the interaction between the ions and the protein is rather low. This allows a very fast transport. The state of a channel can be controlled by ligands, the membrane potential or mechanic forces. Electrophysiological measurements revealed a stochastic switch between open and closed states. This means, that a single channel opens and closes randomly, whereas the probability for a certain state depends on the variable which mediates the gating (Weiss 1996a). The transport direction of a channel protein is determined passively by the electrochemical gradient of the transported substance.

The carriers[3] depict a more complex class of cellular transporters. A specific substance can bind to the protein and is transported through the membrane by several, reversible conformation changes. The close interaction between the substrate and the carrier leads to a lower transport rate compared to channels. Carriers can exist in various forms. The simplest is the uniport, which

---

[3]also denoted as transporters or carrier proteins

Name	Number	Type	Substrates	Main function	Reference
Pma1	1 260 000	ATPase	H^+	H^+ efflux	Buch-Pedersen et al. (2006); Serrano (1983)
Trk1	unknown	uniporter	K^+ (Rb^+)	K^+ uptake	Gaber et al. (1988); Ko et al. (1990)
Trk2	unknown	uniporter	K^+ (Rb^+)	K^+ uptake	Ko et al. (1990); Petrezsélyová et al. (2011)
Tok1	unknown	channel	K^+	K^+ efflux	Bertl et al. (1993); Ketchum et al. (1995)
Nha1	1480	antiporter	H^+, K^+, Na^+	K^+/Na^+ efflux	Bañuelos et al. (2002); Prior et al. (1996)
Nsc1	unknown	channel	K^+, H^+	unknown	Bihler et al. (1998, 2002)
Ena1	600	ATPase	$Na^+, K^+,$	K^+/Na^+ efflux	Platara et al. (2006); Ruiz and Arino (2007)

Table 1.1: *Overview of the main plasma membrane transporters. The number of molecules per cell is taken from www.yeastgenome.org.*

allows the transport of *one* species per turn-over cycle. Contrary, a symport is able to transport two identical or different substances in the same direction, whereas the antiport mediates the transport of substances in both directions.

The movement of an ion along an electrochemical gradient is called passive transport or facilitated diffusion. To allow a transport against an electrochemical gradient, the transport process must be coupled to a source of energy. In case of the symport and antiport, the electrochemical gradient of one substance can be used to drive the transport of the other species. This kind of transport is called secondary active transport.

The primary active transport is generally mediated by the ATPases, is a special type of carrier. The chemical energy stored in the ATP molecule is used to energize the necessary conformational change to pump a substrate against its electrochemical gradient. More general: the chemical energy of ATP is converted into electrochemical energy. As a source for ATP synthesis yeast prefers glucose, whereas fructose and mannose can be metabolized in the same glycolytic pathway as glucose (Serrano 1983).

In the following the mechanism of potassium and proton fluxes in *S. cerevisiae* is described. The focus is on the main function of the relevant transport systems; see Figure 1.2 and Table 1.1. For more detailed description of the respective transporters see Section 1.3.

The core players in potassium homeostasis are: Pma1 (H^+ extrusion), Trk1,2 (K^+ uptake) and the counteracting Nha1 (K^+ release, H^+ uptake); see Figure 1.2. In the budding yeast *S. cerevisiae* the plasma membrane ATPase Pma1 is the primary source of energy for all secondary active membrane transport systems. As a vital transport system, Pma1 extrudes one H^+ per ATP and generates an inward directed chemical proton gradient, which energizes the transport of ions as well as the uptake of nutrients such as sugars and amino acids (Serrano 1988). The steady extrusion of positive charges generates a negative membrane potential, which attracts positively charged species like potassium.

The Trk1 and Trk2 systems (denoted as Trk1,2) use the energy stored in the membrane potential to accumulate the intracellular potassium against a steep concentration gradient (Bertl et al. 2003). Since the membrane potential is generated by the activity of the proton pump Pma1, there is a tight coupling between the outward directed proton flux and the uptake of potassium. The characterization of potassium uptake driven by proton extrusion was already investigated in the 1940s (Rothstein and Bruce 1958) and is generally accepted[4]. Sychrova (2004) describes Pma1 as

[4]See section 2.2 in Rodriguez-Navarro (2000) to find numerous references for related experiments and detailed information

the provider and Trk1,2 as the main consumer of the electrochemical proton gradient.

The uptake of potassium does not stop at a certain maximum potassium concentration, but is controlled by a steady influx and efflux (Bañuelos et al. 2002; Sychrova 2004). An answer, why evolution has developed such a mechanism can be hardly given. A possible explanation may be found in the metabolism. For many decades it is known, that metabolic active yeast cells tend to acidify their environment (Lopéz et al. (1999) and references therein). Since the outward directed proton flux energizes the potassium uptake, a metabolic active cell permanently creates the condition for potassium uptake. This gives the need to limit the internal K^+ concentration by capable efflux systems. However, the question what comes first, the proton releasing metabolism or the usage of the proton extrusion for potassium supply is a classical *chicken or the egg* problem.

The proton and potassium fluxes are coupled by the antiporter Nha1. It is active at low external pH and uses the electrochemical proton gradient to remove potassium (and sodium) from the cytosol (Prior et al. 1996). The mechanism of energization provides a functional connection between potassium uptake and release: An increase in the Pma1 activity leads to an increase of the cytosolic K^+ (mainly via Trk1,2) and also pH. Assuming a constant external pH, the activity of Pma1 enlarges the inward directed proton gradient, which drives Nha1. Thus, the resulting increase in the activity of Nha1 counterbalances (1) the potassium uptake and (2) restores the intracellular pH. A similar effect is caused at the level of the organelles, where the proton/potassium antiporters use the proton gradient to drive the potassium sequestration. It is hypothesized, that this tight coupling of proton and potassium fluxes contributes to a very stable system, where disturbances are quickly counteracted; see also Section 3.2.5.

Besides Nha1 the outward rectifying potassium channel Tok1 could also mediate potassium extrusion. However, Tok1 is known to have a low open probability for negative membrane voltages (Bertl et al. 2003; Johansson and Blatt 2006).

A large proton influx arises from the activity of various nutrient (e.g. amino acid) transporters, which utilize the inward directed proton gradient. An additional proton and also potassium uptake may occur via the calcium-blocked putative channel Nsc1p. Furthermore, the transport (uptake and efflux) of H^+ and K^+ can happen by weakly expressed transport systems (e.g. Qdr2p, Pmp3p) and unspecific processes.

1.3 Main transport systems in S. cerevisiae

This section provides some details for the relevant transport systems about their function, effects of mutations and their regulation mechanism. It is not claimed of being complete, but gives the references to relevant publications. For an overview how the knowledge of potassium homeostasis evolved over the decades see Ariño et al. (2010); Borst-Pauwels (1981); Rodriguez-Navarro (2000).

1.3.1 Pma1

The electrochemical force generated by the P-type plasma membrane ATPase Pma1 energizes all cellular transport processes. A knockout of the related gene or a longer inhibition (e.g. by vanadate Bowman and Slayman (1979)) of the pump finally leads to cell death. Corresponding to its central role, Pma1 is the major plasma membrane protein with more than 10^6 molecules per cell, which represents 15% of all plasma membrane proteins (Ghaemmaghani 2003; Serrano 1988). Per one

molecule of ATP, one proton is extruded from the cell. However, it was reported for the related ascomycete *N. crassa*, that the stoichiometry can change to $2\,H^+$ per 1 ATP under energy restricting conditions, e.g. lack of glucose (Warncke and Slayman 1980).

The turnover rate of one Pma1 molecule was estimated as 20-100 H^+ per second (Serrano 1988). This corresponds to a mass flux of $8 \cdot 10^{-4}$ to $4 \cdot 10^{-3} \frac{mmol}{cm^3\,s}$ and current density of 6-30 $\frac{\mu A}{cm^2}$; see Section 2.2.9 for detailed calculation. Pma1 utilizes most of the cell's ATP (Serrano 1980), whereas the estimated fraction of ATP consumption ranges from 20% to 60% (Martinez-Muñoz and Peña 2005; Morsomme et al. 2000).

As the central transport system, Pma1 is tightly regulated. For example, glucose serves as a signal for transcriptional and post-transcriptional modifications of the Pma1 activity. Serrano (1983) reported a rapid activation by presumably a direct ATPase activation since the proton efflux occurs without a raise in the ATP level and the phenomenon occurs too rapid to be explained by the activation of ATP synthesis. However, the author states that glucose metabolism seems to be required for ATPase activation. An additional effect of glucose is the enhancement of the *PMA1* transcription by the TUF, RAP1 and GRF1 transcription factors (Rao et al. 1993).

Further post-transcriptional regulation of Pma1 may occur via phosphorylation by the Ptk2 kinase, which increases the transport capacity of Pma1 (Eraso et al. 2006). Estrada et al. (1996) found the kinases Yck1,2 to decrease Pma1's activity. Buch-Pedersen et al. (2006) reported, that intracellular potassium could bind to Pma1 and uncouples the ATP hydrolytic activity from H^+ transport. This mechanism might act as a safety valve, hindering H^+ extrusion, when enough potassium is inside the cell. However, a detailed control mechanism for Pma1 is still not characterized (Ariño et al. 2010).

1.3.2 Trk1 and Trk2

The notation Trk1,2, which can often be found in the literature, is used as an abbreviation for the Trk1 and Trk2 system. This does not tend to imply that there is a kind of complex or physical interaction between both proteins. Such properties are not supported by any results so far (Ariño et al. 2010).

The TRK1 and TRK2 genes encode the most prominent potassium uptake transporters (Bihler et al. 2002; Ko et al. 1990; Madrid et al. 1998). Although the relevance of both systems may vary from strain to strain, it is accepted that Trk1 is a fast, high affinity system mediating the majority of the inward potassium flux and ensuring the growth in surroundings containing potassium below $1\,mM$. On the contrary, Trk2 is reported to be a low affinity system of minor relevance under normal conditions (Kuroda et al. 2004; Ramos et al. 1994). Recent studies revealed, that the overexpression of Trk2 can substitute a missing Trk1 system (Michel et al. 2006; Petrezsélyová et al. 2011). This implies, that the role of the Trk1 and Trk2 systems rather depends on their expression level than on a functional difference.

Although the role of Trk1,2 as the main potassium uptake system is out of question, the detailed function and protein structure of the Trk1,2 system is still under scientific discussion. According to Haro and Rodriguez-Navarro (2002) both systems appear to have two ion binding sites with one site highly specific to potassium. For the other site various ions (K^+, H^+ and Na^+) have been proposed (Kuroda et al. 2004), but Haro and Rodriguez-Navarro (2002) state, that Trk1 normally

transports two identical ions, namely potassium.

Inspired by studies of a proton-potassium symport in the related ascomycete *Neurospora crassa* (Rodriguez-Navarro et al. 1986) and theoretical thoughts about the necessary energy for K^+ uptake, Rodriguez-Navarro (2000) propose that Trk1,2 might be a $K^+ - H^+$ symporter. This hypothesis is also raised by (Bihler et al. 1998; Borst-Pauwels 1993). In contrast, Haro and Rodriguez-Navarro (2002) report no changes of the Trk1,2 activity in the range of 4-8 pH, which is unlikely, if Trk1,2 is driven by an inward directed proton gradient. The same authors pose the question whether both binding sites contribute to the transport or one site serves only for activation. Based on Rubio et al. (1995) Joaquin Ariño and colleagues (Ariño et al. 2010) state, that a potassium-sodium symport mechanism can not be ruled out. Calero et al. (2000) also report, that Trk1,2 allows a Na^+ uptake and the transporter increases its ability to discriminate between K^+ and Na^+ in the presence of sodium.

There is also a chloride channel like behavior known for Trk1,2 proteins. According to Rivetta et al. (2005), this is rather a secondary than an evolved function, since it is only observable in cells with an artificially raised cytosolic chloride concentrations ($\gg 1$ mM).

It was also hypothesized, that ammonium could leak via Trk1,2 under potassium limiting conditions (Hess et al. 2006). It is also known, that Trk1,2 can rapidly change its transport kinetics under K^+ shortage, changing from a low/medium to a high affinity mode to ensure the potassium supply (Navarrete et al. 2010; Ramos et al. 1994; Ramos and Rodriguez-Navarro 1986).

trk1Δ mutants need potassium in the millimolar range to grow and *trk1,2Δ* double mutants are not able to grow in potassium concentrations below 10 mM, but their growth rate similar to wildtype cells for external K^+ above 50 mM. At external potassium concentrations above 1 mM, the missing of either Trk1 or Trk2 has no effect on growth (Bertl et al. 2003).

trk1Δ mutants are not only defective in potassium uptake but are also hyperpolarized (Haro and Rodriguez-Navarro 2002; Madrid et al. 1998; Ramos et al. 1994). The idea is, that Trk1,2 is the consumer of the energy provided by the Pma1 ATPase (Petrezsélyová et al. 2011) and if no energy is consumed by Trk1,2, a higher level of energy is stored in the more negative membrane potential. In addition, experimental findings shown in Section 2.1.6 indicate a higher level of Pma1 activity in *trk1Δ* mutants. The known hyperpolarization helps unspecific or low expressed potassium transporters to ensure potassium uptake, as it was proposed by Madrid et al. (1998); Ramos et al. (1994); see also potassium uptake experiments in Appendix 4.4.

Contrary to *TRK2*, which's expression undergoes a complex regulation (Vidal et al. 1995), no evidence was found for the transcriptional regulation of Trk1 (Ariño et al. 2010). On the post-transcriptional level several proteins have been identified to regulate Trk1,2. Positive regulators are the kinases Hal4, Hal5 (Goosens et al. 2000; Mulet et al. 1999) and Snf1 (Ariño et al. 2010) and the dephosphorylating calcineurin pathway (Mendoza et al. 1994). The protein phosphatases Ppz1, Ppz2 (Merchan et al. 2004) and the SR-protein kinase Sky1 (Forment et al. 2002) are negative regulators for Trk1,2. Ppz1 itself is negatively regulated by Hal3 (Yenush et al. 2002). The pH dependent interaction of Ppz1 and Hal3 was proposed to act as a pH sensor in order to control the potassium concentration and pH (Yenush et al. 2005).

However, the proof of direct phosphorylation of Trk1,2 by Hal4,5p or its dephosphorylation by Ppz1,2p is still missing.

1.3.3 Nha1

The antiporter Nha1 is necessary for high salt stress resistance, by preventing toxic cytosolic concentrations Brett et al. (2005). It consumes the proton gradient to lift sodium (analogue lithium) or potassium (analogue rubidium) out of the cell Prior et al. (1996); Sychrova (2004). Contrary to the sodium ATPase Ena1 it is active at low external pH (Ruiz and Arino 2007). As an additional function, Bañuelos et al. (2002) suggested, that in case of a sudden alkalinization of the cytosol Nha1 might act as a safety valve by using the outward directed potassium gradient to drive in some protons.

According to Ohgaki et al. (2005) two protons are exchanged for one sodium or potassium, whereas the affinity of both species is very similar. Thus, contrary to the organelle proton/potassium antiporters, Nha1 is an electrogenic system with a net uptake of one positive charge per turn. However, this finding of Ohgaki et al. (2005) is subject of current scientific discussion.

The transcription is very low and the expression can not induced by salt stress, osmotic effects or pH changes Banuelos et al. (1998). However, the deletion or overexpression of *NHA1* has significant influence on the potassium content; see Bañuelos et al. (2002) and Table 2.6. Furthermore, several studies revealed a contribution of Nha1 to the cell cycle, maintenance of the membrane potential, regulation of the pH and response to osmotic or saline shocks (Kinclova-Zimmermannova and Sychrova 2004; Kinclova-Zimmermannova et al. 2006; Maresova et al. 2006).

The deletion of *NHA1* results in a more alkaline cytosolic pH (Brett et al. 2005; Sychrova 2004) and the overexpression of *NHA1* results in a hyperpolarization of the membrane (Kinclova-Zimmermannova et al. 2006); for a possible explanation see Section 3.1 and Figure 3.3.

Since Nha1 is a very stable protein with a halftime around six hours (Ariño et al. 2010), the regulation of Nha1 rather happens on the post-transcriptional level. The C-terminus has been identified as a potential target of regulation mechanisms, e.g. phosphorylation by the Hog1 kinase under osmotic stress (Kinclova-Zimmermannova and Sychrova 2004).

The Sit4 phosphatase was found to increase the potassium efflux via Nha1, whereas a direct interaction between Sit4 and Nha1 was not shown so far Ariño et al. (2010). Sit4 itself is modulated by Sap155 (negative modulator) and Sap185 (positive modulator) (Manlandro et al. 2005).

Based on growth characteristics and the potassium content, Bañuelos et al. (2002) suggested a potassium or pH dependent cross-talk between Nha1 and Trk1,2.

1.3.4 Tok1

Tok1 is an outward rectifying potassium channel, which is active at positive and low negative membrane voltages (Ketchum et al. 1995; Loukin and Saimi 1999). It was also reported by Vergani et al. (1998), that the activity of Tok1 is modulated by external potassium, which might close the channel above $3\,\mathrm{mM}$. Although the biophysical properties of the system has been studied extensively by electrophysiological measurements (Bertl et al. 2003; Johansson and Blatt 2006), its physiological role is still unclear since *tok1*Δ mutants do not show growth defects (Ariño et al. 2010). However, recent potassium content measurements by José Ramos confirmed a higher potassium concentration in *tok1*Δ mutants (personal communication).

Bertl et al. (1998) suggest, that Tok1 releases K^+ to restore the membrane potential, when potassium is accumulated inside the cell. A relationship between Tok1 and the membrane potential

was also shown by Maresova et al. (2006), who report a depolarization in $tok1\Delta$ mutants and a hyperpolarization in a strain overexpressing *TOK1*. On the contrary, there is also evidence of a Tok1 mediated potassium uptake (Fairman et al. 1999). Thus, Tok1 deserves further investigations.

1.3.5 Nsc1

Nsc1 represents a very-low-affinity uptake route for potassium and protons (Sychrova 2004). The name Nsc1 refers to *non-selective channel* and indicates the putative transporters ability to mediate fluxes of various monovalent (NH_4^+, Li^+) and divalent cations (Ariño et al. 2010; Bertl et al. 2003). Although a respective gene could not be identified, Trk1,2 and Tok1 independent potassium currents were revealed by electrophysiological measurements (Bertl et al. 2003; Bihler et al. 2002). Bertl et al. (2003) found that under conditions where Nsc1 is reduced in its activity cells are more dependent on the presence of Trk1,2. This indicates that the unspecific potassium current relevantly contributes to potassium uptake.

Nsc1 is blocked by external pH <4 (Bihler et al. 2002) and also by divalent cations and especially Ca^{2+} (Bertl et al. 2003). Bihler et al. (2002) observed a decrease in the Nsc1 mediated current with elevated levels of external calcium in the range of 10 μM to 10 mM, whereas 1 to 10 mM are enough to inhibit the Nsc1 activity. In personal communication Prof. Clifford Slayman[5] states 1 mM of external calcium as a critical concentration. Below that value he assumes the Nsc1 mediated proton influx would be principally large enough to short circuit the proton pump. Therefore he suggested, that Pma1 must be regulated in dependence of the Nsc1 activity. However, the role of Nsc1 requires further research.

1.3.6 Further systems

The systems described below, will not be explicitly implemented in the model since they are not active under the considered conditions or their function is not extensively characterized yet. Nevertheless, they may be relevant in future considerations and can contribute to a mechanistic understanding of potassium homeostasis- in particular the coupling of proton and potassium fluxes.

Ena1   *ENA1* is one of four (some strains five) genes expressing a P-type ATPase. It mainly serves to detoxify sodium and lithium, but also extrudes potassium (Platara et al. 2006). *ENA1* is not expressed under standard conditions and activated by sodium, osmotic stress and especially by alkaline pH (Ruiz and Arino 2007), where no inward directed proton gradient exists. Since Nha1 is deactivated under such a condition the function of detoxification is performed by Ena1 (Sychrova 2004). *ENA1-4* are expressed usually at very low level resulting in a constitutive activity. The *ENA1* gene is highly regulated and can be induced by salt, pH, and osmotic stress. Complementary to Nha1, Ena1 is active at rather alkaline pH (Sychrova 2004). *ENA1* is controlled mainly by gene regulation and has been extensively studied (Platara et al. 2006). This involves regulation pathways such as the HOG osmoresponsive pathway and the calcineurin pathway (Ariño et al. (2010) and references therein).

---

[5]Yale University, New Haven, USA; co-author of Bertl et al. (2003); Bihler et al. (2002)

Qdr2 and Pmp3   The Pmp3 (Navarre and Goffeau 2000) and Qdr2 (Vargas et al. 2007) systems depict weakly expressed potassium/sodium transporters with a marginal contribution to potassium supply (Ariño et al. 2010). These systems might be relevant for potassium uptake in *trk1,2Δ* mutants.

Vma1 and Vnx1   The interplay of Vma1 and Vnx1 serves to sequestrate potassium in the vacuole. Vma1 is a V-type ATPase localized in the vacuolar membrane and responsible to acidify the vacuole (around 5 pH). This maintains a proton gradient -directed from the vacuole to the cytosol- which drives the potassium-proton antiporter Vnx1p (Brett et al. 2005).

Further antiporters   Nhx1p is localized in late endosomes and is responsible for potassium and sodium sequestration in pre-vacuolar vesicles Brett et al. (2005). It contributes to the maintenance of the pH, potassium homeostasis and osmotic regulation. Based on studies using *nha1Δ-nhx1Δ*, Brett et al. (2005) suggested a more dominant role of Nhx1p in regulating pH and K^+.

The potassium-proton antiporter Kha1p localized in the membrane of Golgi apparatus serves for the similar purpose as Nhx1p (potassium and sodium sequestration, pH regulation). However, Maresova and Sychrova (2005) reported that growth defects in *nhx1Δ* mutants can not be recovered by an overexpression of Kha1p. This implies a less relevant role of Kha1p compared to Nhx1p.

Although the respecting transporter is left to be identified, a potassium/proton antiporter has been shown in the inner mitochondrial membrane and the gene product of *MDM38* was identified to be indispensable for its function (Nowikovsky et al. 2004). Due to a very negative inner mitochondrial membrane potential around -150 mV, potassium is attracted and taken up via specific cation channels (Nowikovsky et al. 2004). To prevent an excessive accumulation of potassium, the antiporter uses the inward directed proton gradient to remove potassium from the mitochondrial matrix (Zotova et al. 2010).

2 Materials and Methods

This chapter consists of two parts. The first one describes the data and methods used for the modeling process and the *in silico* simulations. This part will mainly focus on the potassium starvation experiment of Navarrete et al. (2010), which will serve for model calibration in later stages of this work.

The second part provides the details of the model building process. It introduces the basic model approach, which deals with the description of the fluxes mediated by each of the transport systems. This approach allows to simulate even the knock-out of certain transporters. In addition, further model extensions will be developed to overcome limitations of the basic approach.

Terms and definitions

For a clear reference, the following definitions are introduced.

Membrane potential

In the literature the term *increase of the membrane potential* is often used to describe the hyperpolarization. The idea behind such a term is the increase of stored energy or the increase in the absolute value of the membrane potential. Since the membrane potential is defined as negative, a hyperpolarization means, strictly mathematically spoken, a decrease of the membrane potential. To avoid confusions, the following convention is used in the present work.

- The hyperpolarization, will be termed as a *decrease of the membrane potential*. Equivalently the term *a more negative membrane potential* is used.

- The depolarization, will be termed as an *increase of the membrane potential*. Equivalently the term *a more positive membrane potential* is used.

Unit convention

In this work the units follow a standard convention, which is unless otherwise stated:

- concentrations are expressed in $\frac{\mathrm{mmol}}{\mathrm{cm}^3}$

- mass fluxes in $\frac{\mathrm{mmol}}{\mathrm{cm}^3\,\mathrm{s}}$

- electric current densities in $\frac{\mu\mathrm{A}}{\mathrm{cm}^2}$

Physical units

- V: Volt

- A: Ampere

- C: Coulomb (A · s)

- S: Siemens (A/V)

- J: Joule (C · V)

- F: Farad (C/V)

- K: Kelvin

- L: Liter

Definition of variables

- [.] square brackets indicate concentrations

- $[.]_i$ the subscript i denotes internal (cytosolic) concentrations

- $[.]_o$ the subscript o denotes outer (surrounding) concentrations

- $[.]^0$ the superscript *zero* indicates initial values

- $[.]^*$ the superscript * indicates stationary values

- J mass fluxes

- I electric current densities

- I_K the subscript denotes the ion related to the current (or flux)

- $I^{Trk1,2}$ the superscript denotes the transport system related to the current (or flux)

- $E = \frac{RT}{zF} \frac{[.]_o}{[.]_i}$ equilibrium potential of a transporter (Nernst potential in case of a uniport)

- E_X the subscript indicates the respecting ion X for the equilibrium potential

Definition of constants

- $F = 96\,485\,000\,\mu C/mmol$ Faraday's constant

- $R = 8314.5\,\mu J/mmol/K$ ideal gas constant

- $T = 293\,K$ temperature

- $R \cdot T = 2.4361\,10^6\,\frac{\mu J}{mmol}$

- z valence of a respecting ion, unless otherwise stated $z = 1$

- $e = 1.6 \cdot 10^{-13} \mu C$ elementary charge

- $F/(R \cdot T) = 39.6 \, \frac{1}{\mathsf{V}}$

- $(R \cdot T)/F = 0.025 \, \mathsf{V}$

- $\mathcal{R} = \frac{volume}{surface} = \frac{\frac{4}{3}\pi \, r^3}{4\pi \, r^2} = \frac{r}{3} \approx 7.5 \cdot 10^{-5} \, \mathsf{cm}$, for a spherical cell with $r = 2.28 \cdot 10^{-4}\mathsf{cm}$ and a volume of 50 fL

- $1/\mathcal{R} = \frac{surface}{volume} = \frac{3}{r} \approx 13\,000 \, \frac{1}{\mathsf{cm}}$

Sign convention

The sign convention for mass fluxes is *influx negative.* Thus $J < 0$ indicates the uptake of species (anions and cations). Since the relation between mass flux and current density reads

$$I = z \cdot F \cdot J \cdot \frac{volume}{surface}, \tag{2.1}$$

the current induced by anions with valence $z < 0$ has an opposite sign than the respective mass flux. Table 2.1 gives the overview of currents, fluxes and their sign.

	Current I	Flux J
Cations	< 0, influx	< 0, influx
Cations	> 0, efflux	> 0, efflux
Anions	< 0, efflux	< 0, influx
Anions	> 0, influx	> 0, efflux

Table 2.1: *The table gives an overview of the sign convention for the movement of anions and cations.*

Software

Data from literature figures was collected by the free software tool `g3data`[1]. It allows to define the location and scaling of the axes in an image by mouse clicks and keyboard input. The data points can than be interactively selected and the respective coordinates are exported to a text file for further processing.

All necessary calculations were performed on a Dell workstation, 2.8 GH, Duo Core, 4 GB, SUSE Linux 10.2, with Matlab, version 7.4.336 (R2007a). Related toolboxes were the Optimization Toolbox (V3.1.1) for data fits, the Symbolic Math Toolbox (V3.2) as well as the `ode15s` solver from the base package .

Standard deviations

In all figures, error bars indicate 95% confidence intervals.

Experiments initiated by the modeling process

This thesis contains several data sets which were initiated by the author during the modeling process. These experiments which were only performed to support the dynamic cycle of prediction, evaluation and improvement are marked with the symbol $\boxed{\circlearrowright}$. A comprehensive list of all experiments that were requested by the author is given in the Appendix 4.5.

---

[1]Jonas Frantz, `http://www.frantz.fi/software/g3data.php`

2.1 Data

Below, the data used to derive or calibrate the model is given. A fundamental problem underlying biological data from various sources, is the limited comparability. This is not only due to different experimental setups and various yeast strains, but also because of different technical devices. In order to compare data from different sources, a suitable unit conversion is required. Thus, for each of the following data sets, the units were converted to the standard. Since a unit conversion in a biological background is always dependent on simplifying assumptions, the presented conversions have to be considered only as an estimation. The reader will note, that although the different unit conversions were derived independently, the results are in good agreement.

2.1.1 Current-voltage relationships

The paper from Kuroda et al. (2004), gives the current-voltage relationship for the main potassium uptake system Trk1,2. The measurements are performed for both Trk proteins together and do not allow for a distinction between Trk1 and Trk2; raw data see Figure 2.1. The data points are the mean of 3-5 independent readings. Standard deviations were not presented in the publication.

To perform the experiment with yeast, the authors used *pmr1Δ* mutants. Pmr1 is a golgi apparatus calcium pump and the lack of this pump results in larger yeast cells, which are easier to handle in a patch-clamp experiment. The diameter of the cells is stated to be 10 μm^2. Due to Bihler et al. (1998), who found no apparent deviations from wild type plasma membrane currents in *pmr1Δ* mutants, the authors of Kuroda et al. (2004) refer the *pmr1Δ* as wildtype.

The electro-physiological measurements were obtained under four different conditions. The external KCl concentration was either 150 mM, 10 mM, 1 mM or 50 μM and the internal potassium concentrations was 30 mM in all four cases. Since the work of Kuroda et al. (2004) revealed that unphysiologically chloride concentrations lead to a chloride efflux via Trk1,2 and a concomitant potassium insensitivity of Trk1,2, the pipette solution contained only 1.2 mM of chloride. The pH in the recording buffer was 5.5 pH and in the pipette solution 7 pH.

To detect the currents, which are mediated by Trk1,2 only, the experiment was performed two times. First, the current-voltage relationships for the wildtype were generated. The experiment was repeated for the *trk1,2Δ* mutant under the same conditions. The currents visible in this second experiment could not be mediated by Trk1,2 but may cover all other potassium transport currents and electrode leakage. The authors explicitly state that the origins of these currents are not yet known. Subtracting the currents obtained from the *trk1,2Δ* mutant from those of the wildtype gives the leak corrected Trk1,2 current-voltage relationship. It is worth to note, that the observed potassium leak did not agree with a pure cellular potassium leak. In this case, it is to be expected, that the zero crossing of the data corresponds to the Nernst potential for potassium, what was not the case here. This discrepancy might be explained by other leakage currents arising from the experimental set up (e.g. electrode leak) or by the involvement of other particles, or random stoichiometric changes in the unspecific potassium transport.

Figure 2.1 visualizes the raw data of the wildtype and the *trk1,2Δ* mutant. The sign convention of the presented currents is *uptake: negative*. For negative membrane voltages, the Trk1,2 currents show a clear uptake. The efflux visible for positive membrane potentials is stated to be mediated by Tok1, which is known to open for positive voltages.
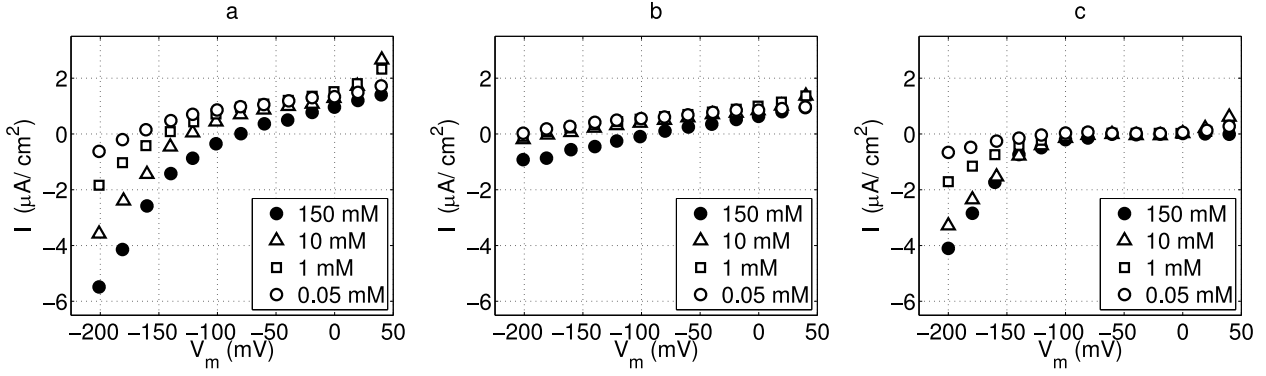
Figure 2.1: *The figure presents the data of Kuroda et al. (2004) (a) gives the current voltage relationship for the wildtype (pmr1Δ mutant), panel (b) shows linear potassium currents for trk1,2Δ and panel (c) gives the difference between (a) and (b).*

Unit conversion

In Kuroda et al. (2004) the current was originally expressed in $\frac{\text{pA}}{\text{cell}}$, and the diameter of a typical cell used in this experiments was stated to be $10\,\mu\text{m}^2$. Assuming a sphere shape, the cell has a volume of $2.66 \cdot 10^{-10}\,\text{cm}^3 = 266\,\text{fL}$ and a surface of $314\,\mu\text{m}^2$. Thus, the conversion of the current can be achieved by changing the reference to surface of a single cell:

$$\frac{\text{pA}}{cell} = \frac{\text{pA}}{314\,\mu\text{m}^2} \tag{2.2}$$

$$= \frac{10^{-6}\,\mu\text{A}}{314 \cdot 10^{-8}\,\text{cm}^2} \tag{2.3}$$

$$\approx \frac{1}{3} \cdot \frac{\mu\text{A}}{\text{cm}^2}\,. \tag{2.4}$$

The particle flux can be modeled by using the equation $I = zF \cdot J \cdot \frac{vol}{surf}$:

$$\frac{\mu\text{A}}{\text{cm}^2}/\left(zF\,\frac{vol}{surf}\right) = \frac{\mu\text{A}}{\text{cm}^2}/\left(96\,485\,000\,\frac{\mu\text{C}}{\text{mmol}}\,\frac{5.24 \cdot 10^{-10}\,\text{cm}^3}{314 \cdot 10^{-8}\,\text{cm}^2}\right) \tag{2.5}$$

$$= \frac{\mu\text{A}}{\text{cm}^2}/\left(96\,485\,000\,\frac{\mu\text{C}}{\text{mmol}} \cdot 1.67 \cdot 10^{-4}\,\text{cm}\right) \tag{2.6}$$

$$= \frac{\mu\text{A}}{\text{cm}^2}/\left(96\,485\,000\,\frac{\mu\text{C}}{\text{mmol}} \cdot 1.67 \cdot 10^{-4}\,\text{cm}\right) \tag{2.7}$$

$$= \frac{\mu\text{A}}{\text{cm}^2}/\left(1.61 \cdot 10^4\,\frac{\mu\text{C} \cdot \text{cm}}{\text{mmol}}\right)\,. \tag{2.8}$$

Thus the following relationships are suggested as an appropriate unit conversion:

$$\frac{\text{pA}}{cell} \,\widehat{=}\, \frac{1}{3} \cdot \frac{\mu\text{A}}{\text{cm}^2} \tag{2.9}$$

$$\frac{\text{pA}}{cell} \,\widehat{=}\, 6.22 \cdot 10^{-5}\,\frac{\text{mmol}}{\text{cm}^3\,\text{s}}\,. \tag{2.10}$$

For the raw data this yields fluxes of approximately $10^{-4}\,\frac{\text{mmol}}{\text{cm}^2\,\text{s}}$. For the current density one finds values around $3\,\frac{\mu\text{A}}{\text{cm}^2}$ (see Figure 2.1 c). The proposed unit conversion was solely based on the known cell size and uses no further assumptions.

2.1.2 Rubidium fluxes

To study the molecular mechanism of potassium transport via Trk1 Haro and Rodriguez-Navarro (2002) measured the uptake of Rb^+ as a K^+ analogue in potassium starved and azide treated cells (strain $W\Delta 3$).

Both measurements (starved and azide treated cells) tend to support a kinetic model, which suggests, that Trk1 co-transports two identical ions. To reveal the influx kinetics of Rb^+, the authors reduced the potassium content inside the cells. For this purpose two strategies were followed. One was a simple potassium starvation procedure. In potassium starved cells Trk1 develops a high affinity mode, allowing the uptake of K^+ even in the micromolar range. Because the micromolar traces of potassium in the recording buffer are assumed to interfere with the Rb^+ the authors used azide-treated cells in their first approach. Azide reduces the potassium content in *S. cerevisiae* (Ramos and Rodriguez-Navarro 1986; Rothstein and Bruce 1958) and also sets Trk1 to a medium affinity state in which micromolar concentrations of potassium are not taken up by the transporter.

Figure 2.2 gives the raw data as well as the proposed data fit according to the multi state model developed by the authors. The figure shows the current density (representing influx) of Rb^+ in response to different external concentrations of Rb^+. The influx is measured as the initial uptake rate after the addition of the respective Rb^+ concentration. Each of the given data points is the mean of four independent readings. Standard deviations are not reported.

The influx is modeled by the authors as

$$J = \frac{V_{max} \cdot [Rb^+]_o}{[Rb^+]_o^2 + K_1 \cdot [Rb^+]_o + K_2} \,. \tag{2.11}$$

The solid line in Figure 2.2 gives the data fit according to the above equation. For the starved cells, the data fit deviates from the data points. This may have been caused by the following problem: The authors state, that in this case K_2 could not be estimated due to the contaminant potassium in the medium. Nevertheless, they present a data fit in their publication, without mentioning, which value was used for K_2. Therefore, K_2 is set to zero in Figure 2.2. It may be, that the deviation between the model and the data does also exist in the paper, but is not clearly visible, due to the representation of the data as a kind of Eadie-Hofstee plot. In addition, the Figure 2.2 shows a linear regression line corresponding to a logarithmic dependence from the external Rb^+ concentration. Apparently, the regression line depicts an acceptable approximation of the given data.

A huge caveat concerning the data is the missing control of the membrane potential and possible concentration dependencies of the kinetic parameters. This will be overcome by the simple model in Section 2.2.4.

Unit conversion

The original unit in Haro and Rodriguez-Navarro (2002) is given as $\frac{nmol}{mg\,min}$, where mg refers to the dry weight. Here the relationship

$$\frac{nmol}{mg} \,\hat{=}\, \frac{1}{2}\, mM = 5 \cdot 10^{-4} \frac{mmol}{cm^3} \,, \tag{2.12}$$
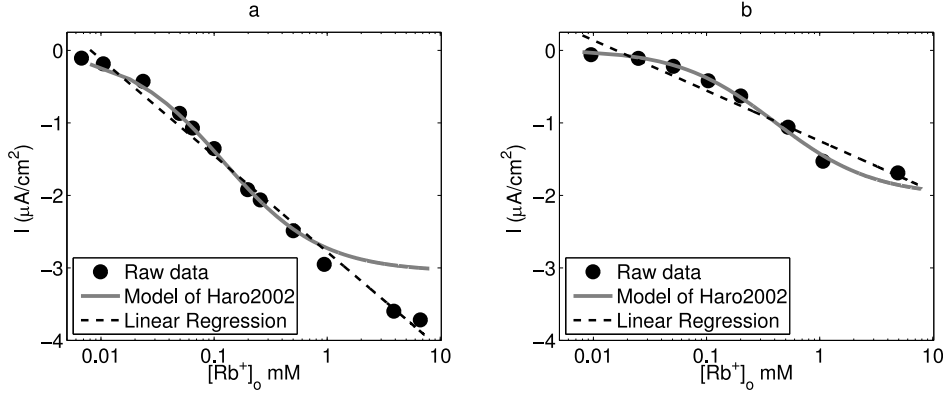
Figure 2.2: *The data points give the raw data of Haro and Rodriguez-Navarro (2002), (left, starved cells: right, azide treated cells). The units were converted from flux $\frac{nmol}{mg_{dry}}$ to current density $\frac{\mu A}{cm^2}$ (see Section 2.1.2 for details on data conversion). The gray line represents the mathematical description given in the article.*

derived in Section 2.1.3 is used

$$\frac{\text{nmol}}{\text{mg min}} \quad \hat{=} \quad 5 \cdot 10^{-4} \frac{\text{mmol}}{\text{cm}^3 \text{min}} = \frac{5}{60} \cdot 10^{-4} \frac{\text{mmol}}{\text{cm}^3 \text{s}} \tag{2.13}$$

$$\frac{\text{nmol}}{\text{mg min}} \quad \hat{=} \quad 8.33 \cdot 10^{-6} \frac{\text{mmol}}{\text{cm}^3 \text{s}} . \tag{2.14}$$

Thus a flux of $20 \frac{\text{nmol}}{\text{mg min}}$ in the raw data is converted to $1.67 \frac{\text{mmol}}{\text{cm}^3 \text{s}}$. The conversion to electric current density suffers from an unknown cell size; here a diameter of $6\,\mu\text{m}$ (sphere shape) is assumed

$$8.33 \cdot 10^{-6} \frac{\text{mmol}}{\text{cm}^3 \text{s}} \cdot F \frac{vol}{surf} = 0.08 \frac{\mu A}{\text{cm}^2} . \tag{2.15}$$

Therefore the following relationship is suggested

$$\frac{\text{nmol}}{\text{mg min}} \quad \hat{=} \quad 0.08 \frac{\mu A}{cm^2} . \tag{2.16}$$

2.1.3 Potassium starvation measurements

Navarrete et al. (2010) investigated the effects of potassium starvation on the potassium content, cell volume, pH and membrane potential in wild type (strain BY4741) and Trk1,2 double mutants; see Figure 2.3 and Figure 2.4. These experiments will be used for the model calibration in Chapter 3. Cells were grown in high potassium (50 mM KCL), washed with K^+ free YNB medium and transferred to YNB medium without potassium (traces of KCL left: 15 μM). Apart from the washing procedure the medium contains 2% glucose during the whole experiment.

	wildtype		trk1,2Δ	
	0 h	5 h	0 h	5 h
volume (fL)	48.2	37.3	48.2	42.7
concentration (mM)	196	31	212	125
amount of substance (fmol)	9.4	1.2	10.3	5.2

Table 2.2: *Cell volume, potassium concentration and the amount of potassium before and after five hours of starvation for the wildtype and trk1,2Δ mutant. In the wildtype, not only the concentration, but also the amount of potassium tremendously has decreased after five hours.*
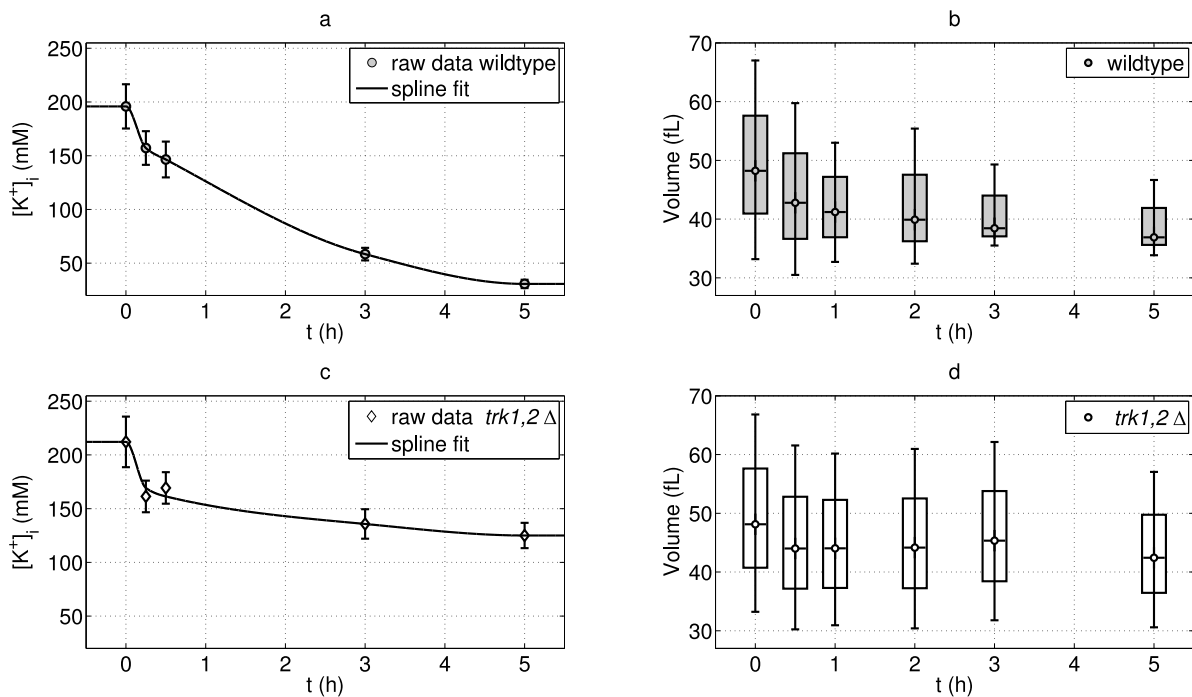
Figure 2.3: *Effects of potassium starvation on potassium content (a,c) and cell volume (b,d). The data is taken from Fig. 4 and Fig. 6 in Navarrete et al. (2010). The first time point refers to a measurement performed right after the washing and before transfer to potassium free medium. The other time points indicate samples drawn after a certain period of starvation in potassium free medium. The lines represent spline fits and depict an estimation of the potassium concentration time courses. This course will serve as a time dependent reference value in the reverse tracking approach in Section 3.2.*

Potassium As can be seen in Figure 2.3 (b) the loss of potassium coincides with a reduction of the cell volume. The volume reduces from 48 fL at time point zero to 37 fL after five hours of starvation; see Table 2.2 for a comparison of concentration, volume and amount of substance. Similar to the changes in potassium concentration, the shrinking of the cell is faster in the first hour and slows down later on. Since it is known that potassium is a relevant osmolyte in yeast, the reduction of volume as a direct effect of potassium loss seems logical. Navarrete et al. (2010) mention that about 50% of the cells are able to complete the cell cycle at time point zero.

At the beginning of the experiment in Figure 2.3 (b) the cell size distribution is broad and rather symmetric. This distribution becomes more asymmetric for later time points with a large tail on the left side. This means that there are very small cells, what indicates a relevant number of cells has completed the cell cycle. The lack of potassium could then prevent the cells from growing and from producing biomass (role of K^+ in metabolic processes) or even swelling (role of K^+ as an osmolyte). Altogether, it appears certain, that the observed volume reduction is not only due to the loss of potassium, but also supported by cell division processes.

The *trk1,2Δ* mutants in Figure 2.3 c behave differently compared to the wildtype. The intracellular potassium concentration changes from around 200 mM to 130 mM after five hours of starvation. At the first sight it appears not plausible, why cells lacking the main potassium uptake system should keep a higher level of potassium. The authors of Navarrete et al. (2010) hypothesized, that the known hyperpolarization of *trk1,2Δ* mutants supports the maintenance of potassium. The volume decreases in parallel with the potassium from 48 fL to 42.7 fL. In contrast to the wildtype, the distribution of the cell size stays symmetric at any time point.
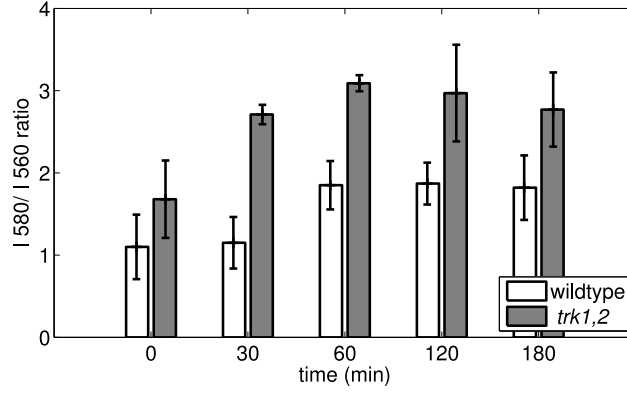
Figure 2.4: *Relative membrane voltage for the experiment of Navarrete et al. (2010). Time point zero represents the measurement before the transfer to the potassium free medium. The other time points refer to the period of starvation. The increase in the I 560/ I 580 ratio indicates a hyperpolarization of the membrane. The drop of external potassium causes a hyperpolarization in the wildtype and in the trk1,2Δ mutant, whereas the hyperpolarization is more pronounced in trk1,2Δ. After 60 minutes a constant membrane potential is maintained.*

pH ⟳ The original pH measurements of Navarrete et al. (2010) show a rather constant pH, both for *trk1,2Δ* (around 6.5 pH) and wildtype (around 7 pH). Several repetitions performed by Silvia Petrezsélyová and Daniel Ganser revealed a slow pH decrease in of 0.3-0.5 units during five hours of starvation.

Membrane potential The measurement of the relative membrane potential in Figure 2.4 b shows the hyperpolarization of the membrane under potassium starvation. This finding highlights the role of potassium in the maintenance of the membrane potential. The data also shows the known hyperpolarization of the *trk1,2Δ* mutant. In both cases the hyperpolarization reaches a stable level after 30-60 minutes of starvation. In later sections of this work, the reader will note, that the simulated membrane potential shows a more rapid dynamics.

Volume In the measurements, the volume decreases from 48 fL to 37 fL in the wildtype, and from 48 fL to 42.7 fL in the *trk1,2Δ* mutant. As it was stated earlier, the measurements might not only reflect osmotic effects. Thus, it is tried to quantify the effect of cell division. The authors of Navarrete et al. (2010) state, that at the beginning of the experiment 50% of the wildtype and 17% of the double mutant are able to fulfill the cell cycle. Assuming, that the cells being able to divide *will* divide once during the five hours of starvation allows an estimate of the cell volume at the end of the experiment

$$\hat{V}_{wt} = \frac{50 \cdot 48\,\text{fL} + 100 \cdot 24\,\text{fL}}{150} = 32\,\text{fL} \tag{2.17}$$

$$\hat{V}_{trk1,2} = \frac{83 \cdot 48\,\text{fL} + 34 \cdot 24\,\text{fL}}{117} = 42\,\text{fL}\,, \tag{2.18}$$

where the estimated value for the *trk1,2Δ* is close to the data point at 5h; see Table 2.2. In personal communication the authors reported, that the biomass is only slightly increased in the experiments, but the optical density increases by 20% after five hours of starvation, both in wildtype and *trk1,2Δ*. For the *trk1,2Δ* mutant the authors did not expect a production of biomass under these conditions, whereas the wildtype is assumed to be capable in growing.

K_m (mM)

Strain	0 min.	15 min.	30 min.	60 min.	120 min.	180 min.	300 min.
BY4717	6.21	0.31	0.14	0.13	0.13	0.14	0.16
trk1,trk2	20.1	-	20.1	-	-	20.4	-

Capacity V_{max} (mM/min)

Strain	0 min.	15 min.	30 min.	60 min.	120 min.	180 min.	300 min.
BY4717	2.56	4.455	4.82	7.7	13.4	12.45	13.6
trk1,trk2	2.62	-	3.15	-	-	2.64	-

Table 2.3: *Affinity and capacity derived from Rb^+ uptake measurements (Navarrete et al. 2010). After a certain time of starvation in potassium free medium the Rb^+ uptake kinetics were monitored. While the Trk1,2 transporter obviously changes to a high affinity mode after 15 minutes, the capacity increase more slowly over several hours. The conversion from the original unit* nmol/mg/min *was achieved by the factor 0.5 (see Section 2.1.3). According to personal informations from the authors, the affinity for potassium is five times higher than for rubidium.*

If (as a very rough estimation) the increase in the optical density is assumed to be proportional to the increase in the cell volume an improved estimate for the wildtype can be given by

$$\hat{V}_{wt} \quad = \quad 32\,\text{fL} \cdot (1 + 20/100) = 38.4\,\text{fL}\,, \tag{2.19}$$

which is close to the value measured after five hours of starvation (37 fL). It can be concluded, that the cell division and cell growth processes balance each other, and that the changes in the volume observed in the data can be mainly explained by osmotic effects. However, a more direct distinction between osmotic effects, cell growth and cell division is currently not possible[2].

Kinetic properties Table 2.3 reflects the change of the rubidium (a potassium analogue) uptake kinetics after a certain time of potassium starvation in the wildtype and Trk1,2 mutant. The authors assume a Michaelis-Menten-kinetics like behavior for the uptake and give a respective K_m (affinity: $1/K_m$) and V_{max} (capacity). According to personal communication with the authors the capacity for potassium and rubidium is similar, whereas the affinity is five times higher for potassium. At the beginning of the starvation experiment one can find a rapid decrease (within 15 min) of K_m from 6.21 mM to 0.31 mM. This indicates the ability of the the transport systems to rapidly cope with potassium limiting conditions by becoming sensitive for concentrations in the micromolar range. After 30 minutes the K_m is rather stable at 140 μM (standard deviations are not available).

The different time scales of K_m and V_{max} might indicate different levels of regulation. The affinity could change due to biophysical properties of the transport systems or quick regulation processes such as phosphorylations, while the capacity might depend on gene regulation processes, providing more transport systems in the cell membrane. It is remarkable, that in the double mutant, both kinetic parameters do not vary over time. This shows that Trk1,2 is responsible for the observed changes.

---

[2] ↻ The presumption, that cell growth effects are visible in the data is also supported by unpublished repetitions of the experiment, where the cell volume (wildtype) even increases after one hour of starvation.
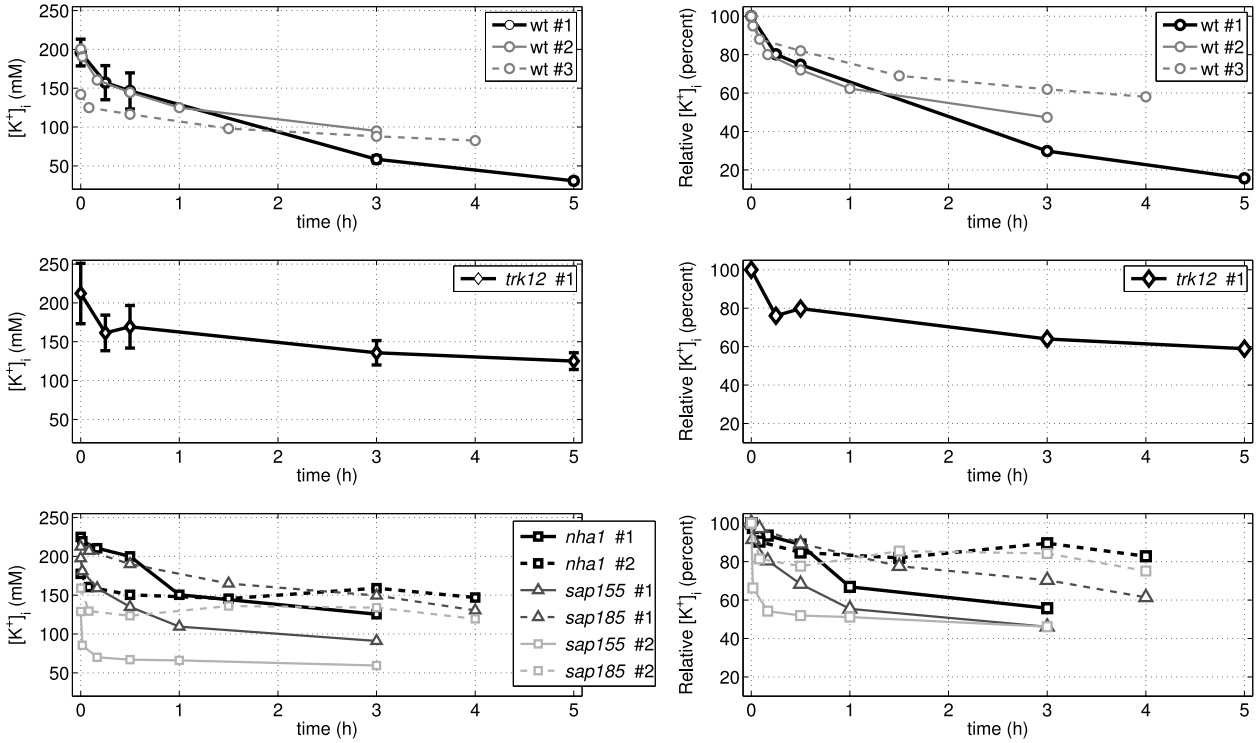
Figure 2.5: *All available measurements for the protocol of Navarrete et al. (2010). The left panels give the potassium concentration for the wildtype, trk1,2Δ and nha1Δ mutant. The sap155Δ mutant is defective in the Nha1 repressor, leading to a lower potassium concentration at the end of the recording. The deletion of the activator SAP185 has the opposite effect. For each of the nha1Δ, sap155Δ and sap185Δ mutants only two replicates were available. The right panels show the potassium data relative to the first data point. All cases show the same dynamic behavior. The potassium drop is fast in the first 30-60 minutes followed by a slower reduction. It can be hypothesized, that in each case there is a similar mechanism governing this behavior.*

Additional starvation experiments ⟲ To complete the starvation data of Navarrete et al. (2010) additional measurements on the wild type, *trk1,2*Δ and *nha1*Δ mutants were made; see Figure 2.5. Despite the large natural variability, the cells exhibit a similar potassium dynamics: a rapid loss in the first hour is followed by a smoother potassium reduction later on.

Composition of medium

According to Gennemark et al. (2006) the extracellular osmotic pressure Π_o generated by the medium can be calculated from the concentrations $[X]_o$, respective moieties m and osmotic coefficient ϕ.

$$\Pi_o = RT \sum_{j=1}^{n} [X]_o \cdot m_j \cdot \phi_j \,, \tag{2.20}$$

where R and T refers to the ideal gas constant and the temperature. Table 2.4 gives the composition[3] of YNB ForMedium^{TM} supplemented with 2% glucose (micro nutrients neglected). In the given

---

[3]As provided by personal with communication Guido Hasenbrink and also available from the manufacturers website www.formedium.com

Specie	value $\frac{g}{L}$	molec. weight $\frac{g}{mol}$	conc. mM	moieties	osm. coeff. ϕ
$(NH_4)_2\ SO_4$	4	113	35.4	3	0.77
$(NH_4)_3\ PO_4$	0.92	149.1	6.2	4	0.77
$MgSO_4$	0.5	120.4	4.2	2	0.61
NaCl	0.1	58.4	1.7	2	0.93
$CaCl_2$	0.1	112	0.9	2	0.85
Amino acid mix	1.285	138	9.3	1	1
Glucose	20	180.2	111	1	1.01

Table 2.4: *Osmotic coefficients were taken from Robinson and Stokes (1959) 476ff. The average molecular weight of amino acids is given by Follmann (2001), p. 88. The respective osmotic coefficient is assumed to be 1, which is sufficiently close to the values for arginine and lysine given in Bonner (1982) ($\phi_{Arg} = 0.981$, $\phi_{Lys} = 0.940$ at a concentration of 100 mM and a temperature of 298.15 K).*

case one find the extracellular osmotic pressure

$$\Pi_o = 230.47 \, \text{mM} \, RT \, . \tag{2.21}$$

The osmotic coefficients in Robinson and Stokes (1959) are determined for a single substance solved in pure water at a concentration of 100 mM. For technical reasons it is difficult to determine the coefficients for lower concentrations. However, the interaction between solvent and solute becomes less relevant for decreasing concentrations and the osmotic coefficient draws near one. The interaction of a colloquial of substances with the solvent and each other can be complex. Thus the calculated external osmotic pressure is only an estimation of the magnitude of that effect.

Unit conversion

The unit of $\frac{\text{nmol}}{\text{mg}_{dry}}$ is often used to give the cellular content of a certain molecular species. Since the mathematical model deals with concentrations, a respective conversion is needed. A conversion could be achieved by multiplying the original unit with the ratio of dry weight (w_{dry}) to volume (vol). To estimate the dry weight it is assumed that the density (ρ) of a typical yeast cell is ten percent higher than that of water: $\rho_{cell} = 1100 \frac{\text{mg}}{\text{cm}^3}$. Using a ratio of dry weight to wet weight of $r_{d/w} = 0.3$, allows to give an estimate for the dry weight of a typical yeast cell by $w_{dry} = vol \cdot \rho_{cell} \cdot r_{d/w}$, yielding the desired conversion[4].

$$\frac{\text{nmol}}{\text{mg}} \cdot \frac{w_{dry}}{vol} \ = \ 10-6\frac{\text{mmol}}{\text{mg}} \cdot \frac{vol \cdot \rho_{cell} \cdot r_{d/w}}{vol} \tag{2.22}$$

$$= \ 10-6\frac{\text{mmol}}{\text{mg}} \cdot \rho_{cell} \cdot r_{d/w} \tag{2.23}$$

$$= \ 10-6\frac{\text{mmol}}{\text{mg}} \cdot 1100\frac{\text{mg}}{\text{cm}^3} \cdot 0.3 \tag{2.24}$$

$$= \ 3.3 \cdot 10^{-4}\frac{\text{mmol}}{\text{cm}^3} = 0.33 \, \text{mM} \tag{2.25}$$

Thus $1\frac{\text{nmol}}{\text{mg}} \widehat{=} 0.33$ mM. However, this relationship is not satisfactory. The raw data of Navarrete et al. (2010) presents a potassium content of $390\frac{\text{nmol}}{\text{mg}}$ for unstarved cells. This would lead to a cytosolic potassium concentration of 130 mM, which is far below commonly accepted values ($200 - 300$ mM).

---

[4]For comments on the cell weight, the reader is referred to Appendix 4.6

Besides uncertainties in $r_{d/w} = 0.3$ and ρ_{cell}, the conversion suffers from treating the whole cell volume as a space for potassium dilution. The fraction of the non osmotic volume of a cell is estimated by Gennemark et al. (2006) as $k_1 = 0.37$. This leads to the conclusion, that the overall potassium amount is concentrated only in about two thirds of the cell volume, which results in the relationship

$$1\frac{\text{nmol}}{\text{mg}} \mathrel{\widehat{=}} \frac{3}{2} \cdot 0.33\,\text{mM} \approx 0.5\,\text{mM}\,. \tag{2.26}$$

Using that relationship, the potassium concentration at the beginning of the mentioned experiment is around 200mM. Measurements of the intracellular potassium content, performed in the same laboratory, with the same strain and the same growth medium, indicate that the maximum potassium content kept by BY4741 is around $600\,\frac{\text{nmol}}{\text{mg}}$ for potassium concentrations above $1\,\text{mM}$ in the medium (see Section 2.1.4). According to the suggested conversion factor of 0.5 the observed content corresponds to $300\,\text{mM}$. Leading to plausible results in both cases, the suggested conversion appears reasonable. In addition it should be mentioned that, Cerbon and Calderon (1994) use a conversion factor of 0.435 for *Saccharomyces carlsbergensis* and Rosas et al. (1994) use a factor of 0.5 in *S. cerevisiae*.

Depending on various and sometimes unknown aspects like the cell volume, it is not possible to give an accurate conversion in every case. A unit conversion on a biological background has to be considered as an estimation and not as an exact calculation, but the requirement of comparability justifies to assume a reasonable and suitable conversion method. Whether the suggested values can hold in a context apart from this work needs to be clarified in each individual case.

Another problem lies in the very likely change of the cell composition during starvation by means of cell division processes, osmotic effects or the known strengthening of the cell wall under starvation. This might be the reason, why the conversion leads to a very low potassium concentration of around $30\,\text{mM}$ after five hours of starvation. This is contradictory to the conviction of many biologists, that yeast cells keep a residual potassium concentration of around $100\,\text{mM}$ even under long term starvation. Therefore it is likely that the real potassium concentration is higher at the end of the observed time interval.

2.1.4 Stable potassium experiments

⟳ The intracellular K^+ is known to be rather stable at 200-300 mM under normal conditions. However, a dynamic system can show even more than one steady state. For a better understanding of the system it is relevant to determine whether the K^+ content can be stable only at one value, several values or an infinite number of values in a certain range. The aim of the experiments was to determine, whether the stable intracellular K^+ is a continuous function of extracellular K^+ or rather a stepwise function, indicating that only certain stable K^+ concentrations can be kept by the cell.

Two experiments were suggested during the modeling process to clarify this question; see Figure 2.6. In the first experiment, the cytosolic K^+ is determined after growing the cells overnight at different concentrations of KCl. This measurement reveals a relationship between the external K^+ and the stable cytosolic K^+ reached after several hours of growth. This experiment led to the finding, that cells are able to maintain a stable intracellular potassium concentration around 300 mM
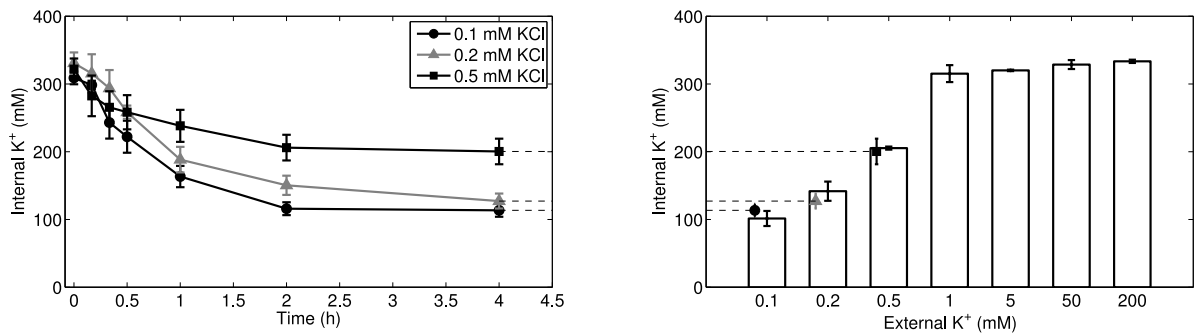
Figure 2.6: *Left panel: Course of the internal potassium concentration for cells grown in 20* mM *KCl and shifted to 100, 200 or 500* μM. *The dynamics looks similar to the potassium starvation experiments in Figure 2.5. The values that are reached after four hours are the same asfor cells grown overnight in the respective potassium concentration. Right panel: Two independent repetitions of the stable intracellular potassium experiment. Cells were grown overnight in a certain amount of KCl. The intracellular potassium concentration is stable for values above 1* mM *KCl. Below that value, the regulation of the maximum potassium concentration fails. The additional errorbars (1.96* $\cdot \sigma$*) for 0.1, 0.2 and 0.5* mM *give the final potassium concentrations reached after four hours in the potassium shortage experiment (left panel).*

for external potassium concentrations above 1 mM. Below that critical value the internal potassium concentration becomes continuously smaller in response to a decreasing external potassium.

The second experiment is similar to the starvation experiment of Navarrete et al. (2010) and is meant to support the findings of the above experiment. The yeast cells were prepared exactly like in Navarrete et al. (2010) and transfered to three different external KCl concentrations: 100, 200 and 500 μM (instead of 15 μM). Following the transfer to the medium with a reduced potassium concentration, the loss of potassium is monitored over several hours. After four hours of potassium starvation, the cells reach a new stable intracellular K$^+$.

The comparison of both experiments shows, that the stable $[K^+]_i$ for cells grown in a certain amount of potassium is comparable to the stable $[K^+]_i$ finally reached by the cells, which were shifted to a medium with that amount of potassium. Since either *growth in* or *shift to* a certain potassium concentration leads to the same stable internal potassium concentration, it is hypothesized, that the same mechanism, adapting $[K^+]_i$ in response to $[K^+]_o$ controls the course of potassium under starvation.

2.1.5 Expression level of the carbonic anhydrase

$\boxed{\circlearrowleft}$ As a result of decarboxylation reactions (e.g. during fermentation), the metabolism releases CO_2. In liquid solution CO_2 reacts with water to carbonic acid, which further dissociates into bicarbonate and protons (see Section 2.2.13).

Since CO_2 related reactions rarely happen spontaneously under physiological conditions, they are triggered by the carbonic anhydrase enzyme. To support a model hypothesis of an altered metabolic CO_2 production (see Section 3.2.3), Joaquin Ariño[5] measured the expression of the related gene *NCE103* under the conditions of the potassium starvation experiment of Navarrete et al. (2010). For the wildtype, the expression level increases to a maximum after 60 minutes of starvation. Afterwards, the expression level decreases again, whereas the velocity of the decrease

---

[5]Department de Bioquimica i Biologia Molecular, Facultat de Veterinaria, Universitat Autonoma de Barcelona, Bellaterra Spain
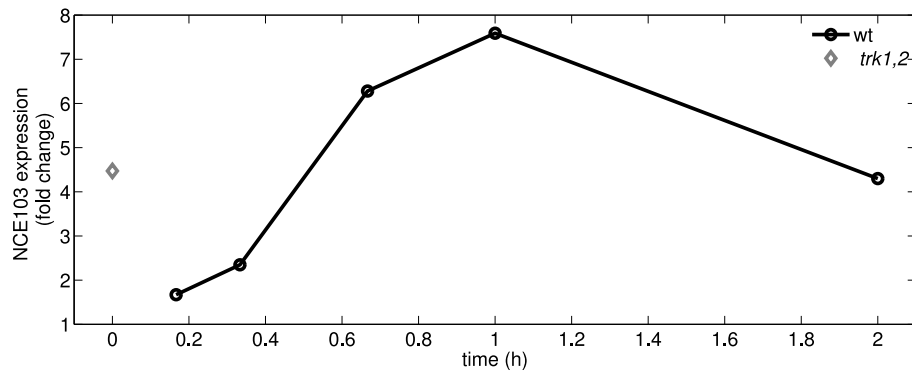
Figure 2.7: *Fold change of the RNA of the yeast carbonic anhydrase gene NCE103. For trk1,2Δ mutants only one value before starvation is available. The data-points for the wildtype start ten minutes after the shift to the potassium free medium.*

is more slowly than the observed increase. For *trk1,2*Δ mutants only one expression value for cells right before the starvation procedure is available (see Figure 2.7).

For the wildtype the expression level shows an increase reaches a maximum after 60 minutes of starvation. Afterwards, the expression level decreases again, whereas the velocity of the decrease is more slowly than the observed increase.

The expression level of the *trk1,2*Δ mutants was obtained under 50 mM potassium and is not directly comparable to the data for the wildtype. Assuming, that the expression level in the wildtype does not undergo significant changes in the first ten minutes of starvation, the expression level of *NCE103* is three times higher in *trk1,2*Δ mutants than the wildtype before starvation.

[↻] To support the findings of the microarray experiment Joaquin Ariño recently (Oct. 2011) measured the mRNA expression level of *NCE103* using the quantitative PCR technique. He found a more than four fold higher mRNA level in *trk1,2*Δ mutants compared to the wildtype at time point zero (ratio 4.1, stand. dev. 0.82, four samples). He also found a four fold increase of mRNA in the wildtype after 60 minutes of starvation (ratio 4.31 , stand. dev. 0.58, three samples). Both findings indicate, that the microarray experiment reflects the cytosolic amount of carbonic anhydrase.

2.1.6 Activity of the ATP hydrolysis of Pma1

[↻] To confirm a model model hypothesis about Pma1 regulation (see Section 3.2.3), the activity of Pma1's ATP hydrolysis was measured[6]. The cells were prepared according to the starvation protocol of Navarrete et al. (2010). At certain time points the cells were collected and the cell membrane was purified to prepare a sample with an enriched Pma1 enzyme concentration.

In an appropriate reaction buffer the inorganic phosphate concentration, P_i, was measured for 20 minutes. Since the reaction buffer contained specific inhibitors for other ATPases, it is assumed, that measured P_i stems mainly from Pma1. The subtraction of an additional control measurement including Pma1 inhibitors ensures, that the measurement reflects the of the hydrolytic activity of Pma1 itself.

It is further assumed the procedure preserved the phosphorylation state of Pma1 and that its activity is constant during the assay time (20 minutes). Thus, the relationship of the P_i concentra-

---

[6]Experimenters: Lynne Paula Yenush, Vicent Llopis Torregrosa, Instituto de Biologia Molecular y Celular de Plantas UPV-CSIC, Ciudad Politecnica de la Innocacion, Universidad Politecnica de Valencia
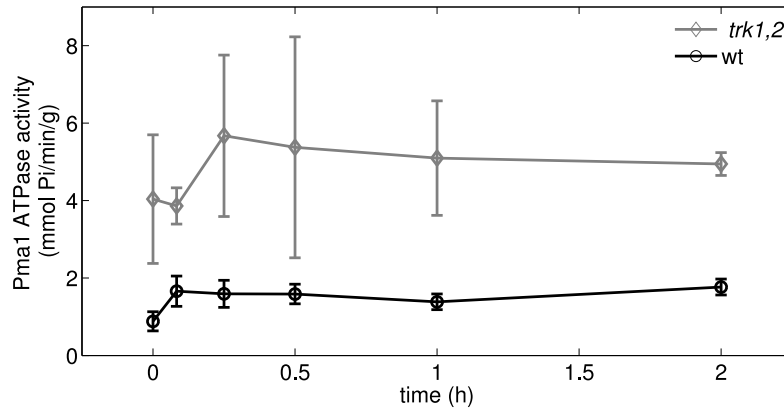
Figure 2.8: *Time course of the Pma1 ATPase activity under the potassium starvation experiment of Navarrete et al. (2010). The time point zero corresponds to the transfer to the potassium free medium.*

tion and the assay time serves as an estimate of the P_i production rate at the time point the cell sample was drawn.

Figure 2.8 shows the result for the wildtype and *trk1,2Δ* mutants. Despite large confidence intervals, the level of Pma1's ATP hydrolysis is clearly higher in the *trk1,2Δ* mutant. This result was also confirmed in three preceding experiments (not shown). The experimenters found no difference in the Pma1 content between the in the wildtype and the *trk1,2Δ* mutant. This indicates, that the higher activity is not due to a different expression level, but due to a structural state of Pma1.

The dynamic behavior is the same in wildtype and *trk1,2Δ*. At the moment of the external potassium drop the activity rapidly increases and reaches a maximum after 10-20 minutes. Afterwards, one can observe a slower relaxation. A similar behavior was already observed for the *NCE103* expression level.

Unit conversion

Knowing from Serrano (1988) that one H^+ is transported for 1 molecule of ATP allows to estimate the proton flux/current through Pma1 activity. Lets assume a proportionality between P_i production and H^+ flux. The original data is given in $\frac{mmol}{min\,g}$, where g refers to the total protein weight of Pma1. For conversion to an appropriate unit, one has to multiply with the protein weight to volume ratio. Knowing the number of Pma1 molecules from Ghaemmaghani (2003), $n = 1\,260\,000$, and the protein weight from the amino acid sequence, $99.6\,kDa$, (www.yeastgenome.org) the conversion yields

$$\frac{mmol}{60\,s\,g} \cdot \frac{n \cdot 99.6\,kDa}{50 \cdot 10^{-12}cm^3} = \frac{mmol}{60\,s\,g} \cdot \frac{n \cdot 99600\,Da}{50 \cdot 10^{-12}cm^3} \tag{2.27}$$

$$= \frac{mmol}{60\,s\,g} \cdot \frac{n \cdot 99600 \cdot 1.66 \cdot 10^{-24}g}{50 \cdot 10^{-12}cm^3} = 7 \cdot 10^{-5} \cdot \frac{mmol}{s\,cm^3} . \tag{2.28}$$

Thus one can derive the relationships

$$\frac{mmol}{s\,g} \,\hat{=}\, 10^{-5} \cdot \frac{mmol}{s\,cm^3} \tag{2.29}$$

$$\frac{mmol}{s\,g} \,\hat{=}\, 30.87 \frac{\mu A}{cm^2} . \tag{2.30}$$

It is worth to emphasize, that this measurement does not reflect the activity of Pma1 in the living organism. The proton flux via Pma1 also depends on the internal and external pH as well as the membrane potential; see Section 2.2.9. Those parameters are not available under the given procedure. The measurement reflects the biophysical property of the Pma1 enzyme to hydrolyze ATP and is thus rather comparable to the parameter I_{Pma1}^{max}, reflecting the maximum pump activity; see Section 2.2.9.

2.2 Model building

This chapter describes the development of the model from the basic ideas towards advanced versions. The biophysical system is modeled by the currents/fluxes mediated by the cellular transport systems as well as the membrane potential.

Model framework

The model describes intracellular concentrations changes, which are determined by mass fluxes mediated by the different transport systems. The simplest model approach treats the whole cell as a single compartment. Intracellular structures like the vacuole, endosomes or mitochondria are neglected. This simplification accounts for the missing experimental tractability of related transport activities, concentration changes and other related parameters. The resulting model is therefor an effective model which treats the effects of intracellular compartments only as the parameter values and does not account for dynamic effects related to intracellular transport events.

The basic model was designed for an acidic external pH[7] and covers the potassium, protons and the related membrane transporters Trk1,2, Tok1, Nha1 and Pma1. Additionally a leak current for each species is taken into account, which mimics further systems of low affinity or unspecific processes, e.g. Nsc1[8]. Especially in the case of protons the leak accounts for the proton gradient driven uptake of nutrients, sugars, amino acids etc. The proton and potassium fluxes are coupled by the membrane potential. The structure of the modeling is given by

$$\frac{d}{dt}[K^+]_i \;=\; -J_K = -\left(J_K^{Trk1,2} + J_K^{Tok1} + J_K^{Nha1} + J_K^{leak} \right) \tag{2.31}$$

$$\frac{d}{dt}pH_i \;=\; \frac{1}{\beta} \cdot J_H = \frac{1}{\beta} \cdot \left(J_H^{Pma1} + J_H^{Nha1} + J_H^{leak} \right) \tag{2.32}$$

$$\frac{d}{dt}V_m \;=\; -\frac{1}{c_m}\left(I_K + I_H \right). \tag{2.33}$$

where J denote the respective mass fluxes and I the respective current densities. The superscript indicates the transport system and the subscript the transported specie. For example, $J_K^{Trk1,2}$ describes the mass flux of potassium via Trk1,2. The parameter β is the proton buffer capacity, which is defined according to Grabe and Oster (2001) as $\frac{d[H^+]}{d\,pH}$ (more details will be given in Section 2.2.11). Details about the description of the membrane potential and the usage of the specific membrane capacitance c_m will be given in Section 2.2.3.

Besides regulation processes such as phosphorylations and post-transcriptional modifications, the

---

[7]An external pH above 7 means a stress condition for the cell and leads to a couple of specific mechanisms, e.g. the activation of Ena1 and the deactivation of Nha1.

[8]The divalent cations (Ca^{2+}, Mg^{2+}) in the external medium (see Table) will cause at least a very low Nsc1 activity.

fluxes mainly depend on internal and external concentrations as well as the membrane potential. Most of what is known about transporters and channels is deduced from electro-physiological measurements. The approaches used to model the different transport systems are common scientific standard, see Fall (2002); Hille (2001); Keener and Sneyd (2004); Weiss (1996a, b).

The movement of charged particles generates an electric current and the different cellular structures are treated as a part of an electric circuit. The transport systems can be thought of as resistors. The cell membrane insulates the cytosol from the surrounding species and charges. Since it separates areas of different electrochemical potentials, the membrane can be assumed as a capacitor storing energy and this energy can be used to energize the transport systems. However, the capacitor itself is continuously charged by the activity of the proton pump, which converts chemical into electrochemical energy by maintaining the difference in proton concentration. The plasma membrane ATPase is therefore considered as a battery in an electric circuit.

In the following the approaches to the modeling of the different transport systems are described. According to the treatment of a cellular transporter as a kind of resistor, the basic description follows Ohm's law, which relates the electric current, the voltage and the conductance. The conductance can either be constant or a function of the membrane voltage (voltage gating). With exception of the proton pump Pma1, all transporters are modeled according to Ohm's law or a gated channel approach.

2.2.1 Ohm's law

Electrical phenomena occur when charges of opposite sign become separated. A net flow of charges is called current (measured in amperes, A). The size of a current is determined by two factors: the potential difference[9] (measured in volts, V) and the work needed to move a unit charge across a 1 V potential. The measure of the ease of flow of a current between two points is called conductance (measured in Siemens, S). The reciprocal of the conductance is called the resistance (measured in ohm, Ω). In the case of a constant conductance g, the current I equals the product of the conductance g and voltage V

$$I = g\,V\,. \tag{2.34}$$

In a biological context Ohm's law can be used to describe a transporter current by

$$I = g \cdot (V_m - E)\,, \tag{2.35}$$

with the membrane potential V_m and the transporters equilibrium potential E. In case of a simple uniport E is the Nernst-potential. The difference $(V_m - E)$ can be thought as a kind of driving force for a transport systems. As long as the membrane potential does not equal the equilibrium potential, the transport system can mediate a transport in one or the other direction.

2.2.2 Voltage gating

According to Fall (2002) channels can be thought to have gates. These gates regulate the permeability of an ion. If these gates are regulated by the membrane voltage one talks about voltage gated

---
[9]Frequently the terms potential, voltage and voltage difference were used for the same thing
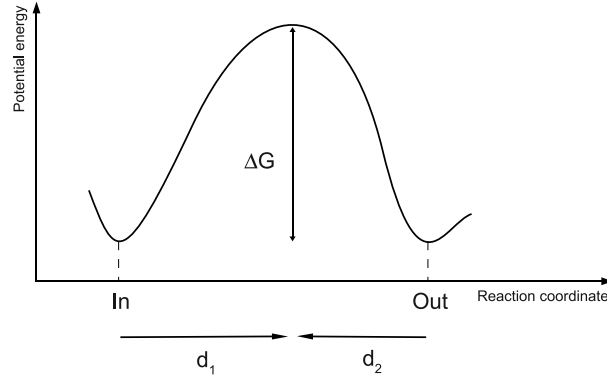
Figure 2.9: *Profile of the potential energy. A charged particle passing from state In to state Out must overcome a peak (ΔG) in the potential energy. The parameters d_1 and d_2 represent the fractional distance of the energy barrier from the membranes inner and outer surface. Figure based on Keener and Sneyd (2004).*

channels. In this case the constant conductance g is replaced by a voltage dependent expression.

The idea is, that an ion moving through a channel jumps over a number of free energy barriers (Eyring et al. (1949) cited in Keener and Sneyd (2004)). At the different ion binding sites, the potential energy of the ion reaches a local minimum. According to the theory of chemical reaction rates, the rate (k) of the transition between two states depends exponentially of the free energy difference (ΔG) between these states.

The electrical field of the membrane contributes to the energy peak and in dependence of the charge of the respective ion, the membrane potential either enlarges or diminishes the barrier. This concept can also be used for the voltage dependent opening and closing of a channel. According to Tombola et al. (2006), the voltage sensitivity of a transporter requires a charged region, which changes its conformation/location in response to changes in the membrane potential.

In the following the voltage dependent transition between an active and an inactive state is considered. If a constant number (N) of transporters is either in an open state (N_O) or in a closed state (N_C), the fraction of open or closed transporters can be defined as $f_O = \frac{N_O}{N}$ and $f_C = \frac{N_C}{N}$.

If the switch between both states follows the reaction scheme
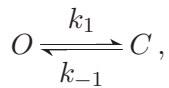
$$O \underset{k_{-1}}{\overset{k_1}{\rightleftharpoons}} C \,,$$

the change of the open state can than be written as

$$\frac{f_O}{dt} = k_1 \cdot f_O - k_{-1} \cdot f_C \,.$$

In equilibrium

$$0 = k_1[O] - k_{-1}[C] \tag{2.36}$$

$$0 = k_1[O] - k_{-1}(1 - [O]) \tag{2.37}$$

$$f_O = \frac{k_{-1}}{k_1 + k_{-1}} \,. \tag{2.38}$$

The voltage dependence can be introduced into the rate constants by assuming

$$k_1 = k_1^0 e^{\frac{1}{RT}\Delta G + zF \cdot d_1 \cdot V_m} \tag{2.39}$$

$$k_{-1} = k_{-1}^0 e^{\frac{1}{RT}\Delta G + zF \cdot d_2 \cdot V_m} , \tag{2.40}$$

where z is the valence, F Faradays constant, R ideal gas constant, T temperature and d_1 and d_2 satisfy $d_1 - 1 = d_2$. The parameters d_1 and d_2 describe the fractional distance of the energy barrier in the electrical field (see Figure 2.9). Defining a dimensionless membrane potential $u = V_m \frac{zF}{RT}$ equation (2.38) becomes

$$f_O = \frac{k_{-1}^0 e^{d_2 u}}{k_1^0 e^{d_1 u} + k_{-1}^0 e^{d_2 u}} \tag{2.41}$$

$$= \frac{1}{1 + \frac{k_1^0}{k_{-1}^0} e^{(d_1 - d_2) u}} . \tag{2.42}$$

Substituting

$$d = d_1 - d_2 \tag{2.43}$$

$$u_{1/2} = \frac{\ln \frac{k_1^0}{k_{-1}^0}}{d_2 - d_1} \tag{2.44}$$

into

$$f_O = \frac{1}{1 + \frac{k_1^0}{k_{-1}^0} e^{(d_1 - d_2) u}} \tag{2.45}$$

yields the voltage dependent expression for the transport system to be in an active/open state

$$f_O = \frac{1}{1 + e^{d(u - u_{1/2})}} \tag{2.46}$$

$$= \frac{1}{1 + e^{d\frac{zF}{RT}(V_m - V_{1/2})}} , \tag{2.47}$$

where $V_{1/2}$ defines the voltage for a half maximal activation. The parameter d controls the transition between the active and inactive state. The sign of d determines whether the gate inactivates or activates under hyperpolarization; see Figure 2.10. Equation (2.46) is often called Boltzmann factor or Boltzmann equation.

2.2.3 The membrane as a capacitor

The cell's lipid bilayer separates intra and extracellular solutions. Since the membrane itself is almost impermeable to charged particles, the membrane insulates the internal and external charges from each other. At any time, the cell maintains an electroneutral state. That means, that the intracellular positive and negative charges are always balanced. Under natural and experimental conditions the surrounding of the cell is large compared to the cell volume and involves vast amounts of various particles, which tend to counterbalance their different charges. Thus, the environment of the cell also can be considered as electroneutral.
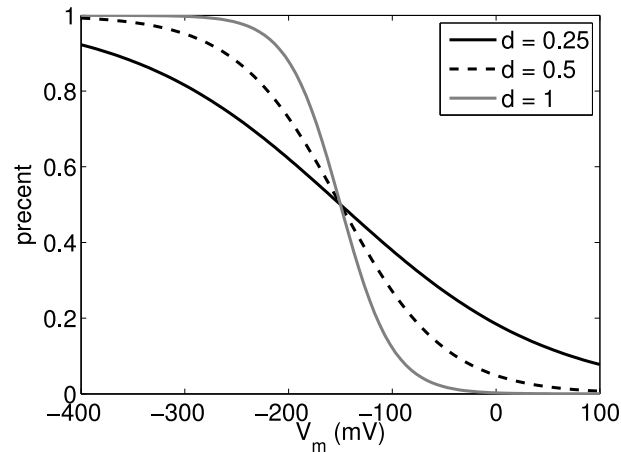
Figure 2.10: *Illustration of the Boltzmann factor. The parameter d controls the steepness of the curve, while* $V_{1/2} = -150\,\text{mV}$ *gives the half maximal activation.*
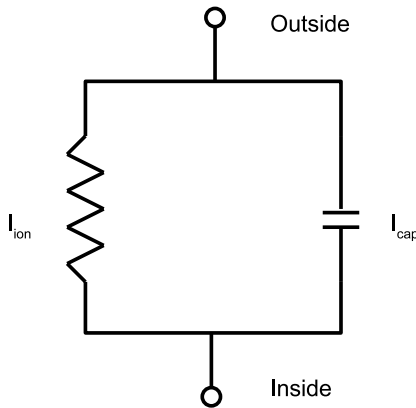
Figure 2.11: *Electrical circuit of the cell membrane; based on Hille (2001)*

The potential difference arises from an excess of positive charges on the extracellular side and the excess of negative charges on the intracellular side of the cell membrane. This potential drops exponentially with the distance from the membrane. The violation of the electroneutrality takes place only in the range of the so called Debye length, which is around 1 nm. Thus, the amount of charges needed to set up the membrane potential is rather low. For an estimation how many charges are required to set up the membrane potential the reader is referred to Appendix 4.9.

The capacitance (measured in Farad) is a measure of how much charge (Q, measured in coulomb) needs to be transferred from one conductor to another to set up a given potential difference.

The charge (Q) stored in a capacitor is proportional (factor C) to the potential difference (V)

$$C\,V = Q\,.\tag{2.48}$$

Taking the derivative with respect to the time yields

$$\frac{dV}{dt} = \frac{1}{C}\frac{dQ}{dt} = \frac{1}{C}I\,,\tag{2.49}$$

where the change of charges over the time is a current I measured in amperes.

Figure 2.11 visualizes the related electrical circuit of the cell membrane as a capacitor, working in parallel with a resistor. The resistor represents the cellular ion transport systems. Since there can be no net buildup of charges on either side of the membrane, the sum of the capacitive current I_{cap} and the ion current I_{ion} must equal zero. This is also known as *Kirchhoff's circuit law*, stating that at each point of a circuit the sum of all incoming and outgoing currents must equal zero at any time.

Excess of charges

In the context of cellular fluxes and currents, the membrane potential is often expressed by the excess of charges. The approach uses the idea, that a potential difference is set up by the excess of positive charges on one side of a membrane and excess of negative charges on the other side. Thus, the concentration difference of the involved ions defines the membrane potential.

$$V_m = \frac{-1}{c_m} F \mathcal{R} \left(z_K \left([K^+]_o - [K^+]_i \right) + z_H \left([H^+]_o - [H^+]_i \right) + \ldots - [X] \right) , \qquad (2.50)$$

where $c_m = 1 \frac{\mu F}{cm^2}$ is the specific membrane capacitance, F is Faraday's constant, $z_.$ is the respective valence and $\mathcal{R}$ is the volume to surface ratio. The species X mimics all other species, such as large impermeable macro molecules. When taking into account a proton buffer capacity β (unit $\frac{mmol}{pH\,cm^3}$, see Section 2.2.11) the above equation can be written as (Boron and de Weer 1976)

$$V_m = \frac{-1}{c_m} F \mathcal{R} \left(z_K \left([K^+]_o - [K^+]_i \right) + z_H \, \beta \, (pH_i - pH_o) + \ldots - [X] \right) . \qquad (2.51)$$

The magnitude of the prefactor (assuming a volume of $50\,fL$)

$$\mathcal{F} = -\frac{F \cdot \mathcal{R}}{c_m} = -7350 V \cdot \frac{cm^3}{mmol} \qquad (2.52)$$

ensures, that only a few charges are required to set up a considerable potential difference. Approximately, the excess of 6000 charges per μm^2 and are sufficient to shift the membrane potential by $100\,mV$, which is in agreement with (Alberts et al. 1998, 419), see Appendix 4.9 for detailed calculations.

Differential equation

The above derivation yields an expression for the membrane potential, which is similar to the capacitor equation. The external concentrations as well as X are assumed to be constant

$$
\begin{aligned}
\frac{d}{dt} V_m &= \frac{-1}{c_m} F \mathcal{R} \frac{d}{dt} \left(z_K \left([K^+]_o - [K^+]_i \right) + z_H \, \beta \, (pH_i - pH_o) - X \right) & (2.53) \\
&= \frac{-1}{c_m} F \mathcal{R} \frac{d}{dt} \left(-z_K [K^+]_i + z_H \, \beta \, pH_i \right) & (2.54) \\
&= \frac{-1}{c_m} F \mathcal{R} \left(z_K J_K + z_H J_H \right) & (2.55) \\
&= \frac{-1}{c_m} \cdot \left(I_K + I_H \right) , & (2.56)
\end{aligned}
$$

where $\frac{d}{dt}[K^+]_i = -J_K$, $\frac{d}{dt}[H^+]_i = -J_H$, $\frac{d[H^+]_i}{d\,pH_i} = \beta$ and the electric current densities I are related to the mass flux by $I = z \cdot F \cdot J \cdot \mathcal{R}$. The general description is

$$\frac{d}{dt} V_m = -\frac{1}{c_m} \sum_j I_j , \qquad (2.57)$$

where j indicates the various ion species. The external concentrations, as well as constant impermeable intra- and extracellular charges are not considered explicitly in the this approach. They
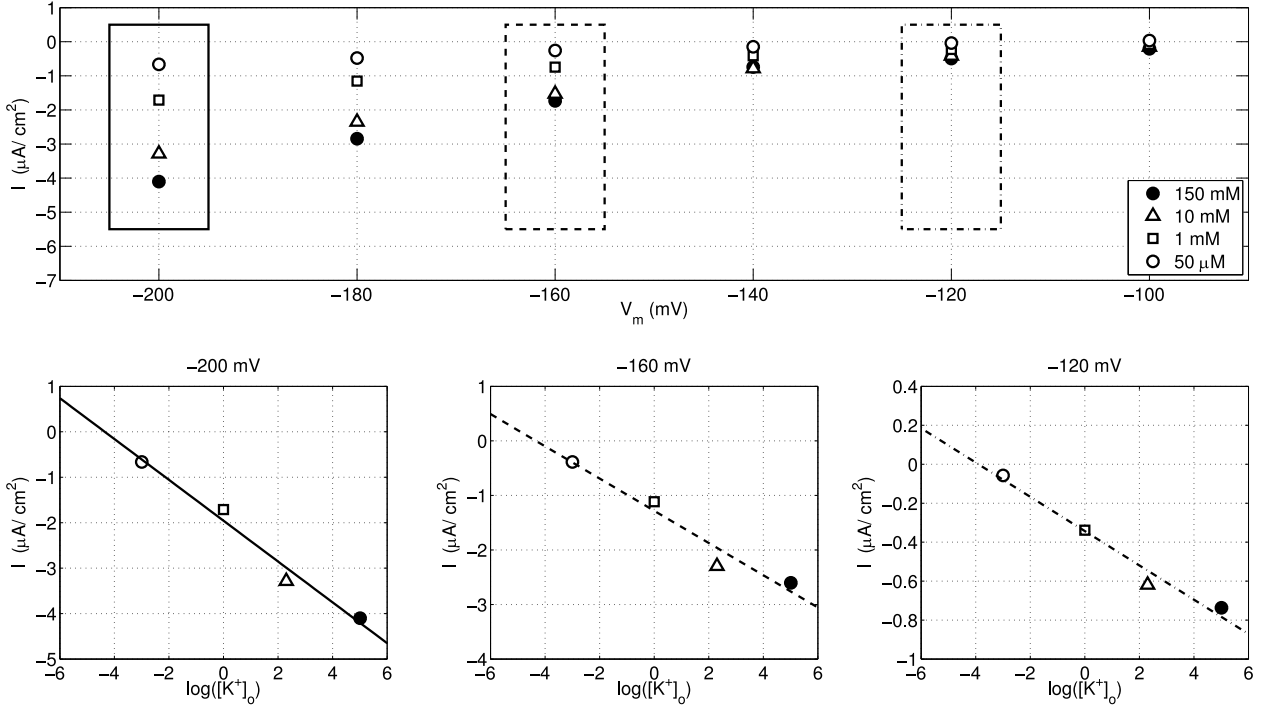
Figure 2.12: *The picture on the top gives the raw data of Kuroda et al. (2004), Fig. 9c. The boxes marks the concentration dependent current for a fixed membrane voltage. The figures below represent the linear dependence of the current on the logarithm of the extracellular potassium concentration.*

are set implicitly by the initial conditions for the various species. The constant arising from the indefinite integration of equation (2.53) and covers the sum of all fixed charges.

2.2.4 Trk1,2

A detailed kinetic model for the description of the concentration and voltage dependent transport current of the Trk1,2 system was not able to represent the data. There is simply not enough information about the detailed mechanisms of transport or its dependence on the electrochemical gradient. Therefore phenomenological models were used.

A detailed analyses of Kuroda et al. (2004)'s data revealed, that for a fixed membrane potential, the mediated current is approximately linearly dependent on the logarithm of the external potassium concentration. This relationship is a good description for voltages in the range of -200 to -120 mV. In the area above, the data points are to dense to be reliably included in such a consideration. Figure 2.12 shows the respective result for three different voltages. The reader is also reminded to the data of Haro and Rodriguez-Navarro (2002) presented in Figure 2.2, where the Trk1 mediated rubidium flux is depends linearly on the logarithm of the external Rb^+.

This is consistent with Ohm's law since

$$I_K = g \cdot (V_m - E_K) \quad = \quad g_{Trk1,2} \cdot \left(V_m - \frac{RT}{zF} \ln \frac{[K^+]_o}{[K^+]_i} \right) \tag{2.58}$$

$$= \quad -g \cdot \frac{RT}{zF} \ln[K^+]_o - g \cdot \frac{RT}{zF} \ln[K^+]_i + g \cdot V_m \,. \tag{2.59}$$

In the case of a constant conductivity g, intracellular potassium $[K^+]_i$ and membrane potential V_m the current depends only on the external concentration $[K^+]_o$. These conditions are fulfilled
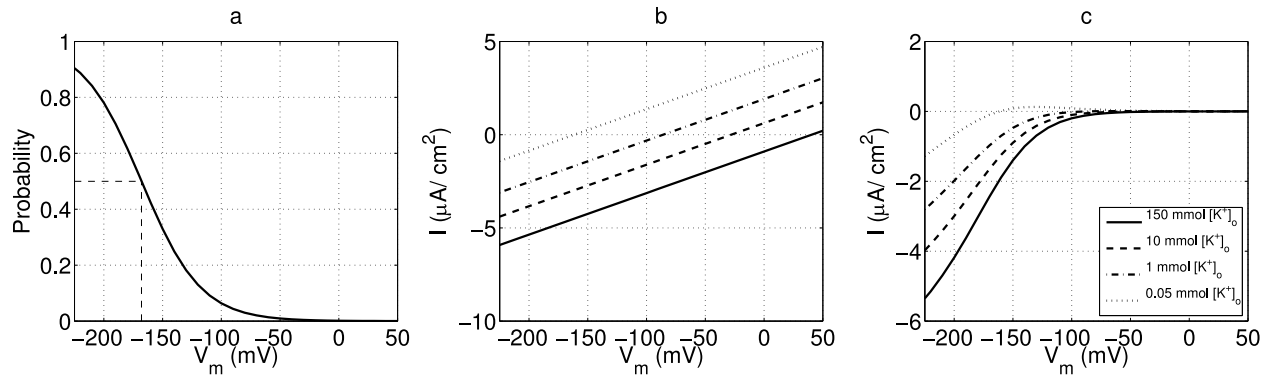
Figure 2.13: *The figure visualizes the data fit of the raw data of Kuroda et al. (2004), Fig. 9c and supports the interpretation of the used approach. (a) gives the voltage dependent probability for the transport system to be active, (b) gives the linear part $g_{Trk1,2}(V_m - E_{Trk1,2})$ and (c) gives the product of a and b, which is the fitted current voltage relationship.*

in the electrophysiological measurements. A related approach is the voltage gated channel approach, where the conductance parameter itself is dependent on the membrane voltage. A fit of equation (2.46) to the data provides the parameter estimates

$$g_{Trk1,2} \quad = \quad 22.28 \, \frac{\mu S}{cm^2} \tag{2.60}$$

$$d_{Trk1,2} \quad = \quad 0.99 \tag{2.61}$$

$$V_{1/2,Trk1,2} \quad = \quad -0.168 \, V \, . \tag{2.62}$$

The nonlinear fit was robust to different initial values or parameter boundaries of the fitting routine. Details of the fitting routine are given in Table 2.5. Figure 2.13 visualizes the details of the data fit with only three different parameters. Figure 2.14 gives the raw data of the four data sets as well as the respective model fit. Based on suggestions in the literature a data fit under the assumption of a K^+/K^+ and H^+/K^+ symporter was tried. However, the zero crossing of the data does not match with the equilibrium potential for such transporters and thus, no satisfactory data fit was possible.

Summary Trk1,2

The potassium currents mediated by Trk1,2 can be expressed by

$$I_K^{Trk1,2} \quad = \quad \frac{g_{Trk1,2}}{1 + e^{d_{Trk1,2} \cdot \frac{zF}{RT}\left(V_m - V_{1/2,\,Trk1,2}\right)}} \cdot \left(V_m - \frac{RT}{zF} \ln \frac{[K^+]_o}{[K^+]_i}\right) \, . \tag{2.63}$$

Matlab function	`lsqnonlin`
Norm Residual	0.8078
Exit criteria	Norm of residual changed less than tolerance 1e-12
Iterations	15
Initial values	$g_{Trk1,2} = 100$, $d_{Trk1,2} = 0.5$, $V_{1/2,Trk1,2} = -0.25$
Upper bound	$g_{Trk1,2} = 250$, $d_{Trk1,2} = 0$, $V_{1/2,Trk1,2} = 0$
Lower bound	$g_{Trk1,2} = 0$, $d_{Trk1,2} = 1$, $V_{1/2,Trk1,2} = -1$

Table 2.5: *Method and parameters used for the data fit of the Trk1,2 current.*
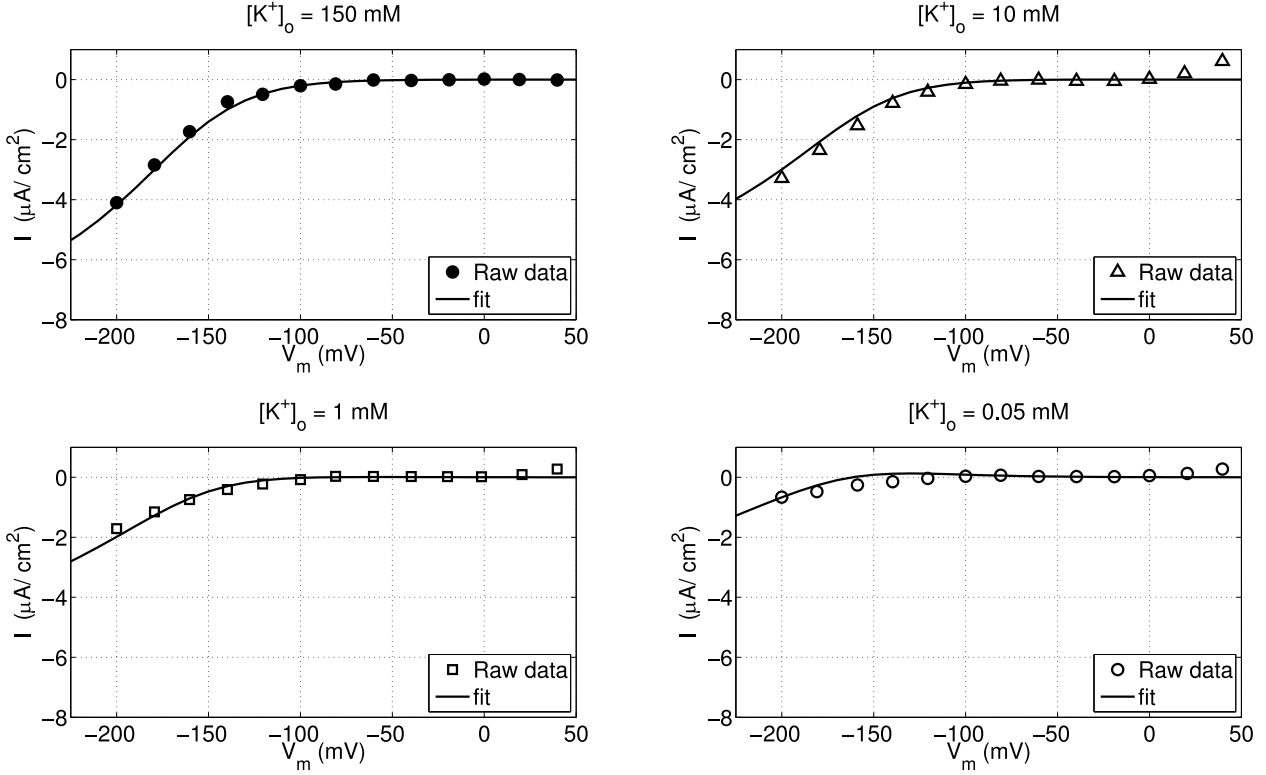
Figure 2.14: *Data fit and raw data in parallel. Three different parameters were needed to describe the four datasets at once.*

Parameters

$$g_{Trk1,2} \;=\; 23\,\frac{\mu S}{cm^2} \tag{2.64}$$

$$d_{Trk1,2} \;=\; 1 \tag{2.65}$$

$$V_{1/2,\,Trk1,2} \;=\; -0.168\,V\,. \tag{2.66}$$

2.2.5 Nha1

Besides the leak currents, the Nha1 transport system is the only system for which no data (flux and electrophysiological measurements) was available. Initially, we assume a simple ohmic current-voltage relationship. It turned out, however, that a voltage gating needs to be be applied when simulating the potassium starvation experiment. The model version using the ohmic model is referred as $\mathcal{M}_1$ and the model with voltage gating $\mathcal{M}_2$; see Table 3.1.

A central issue in using the ohmic approach is the determination of the equilibrium potential of the respective transporter, which can be easily given in the case of uniporters and symporters. The equilibrium potential for Nha1 or any other antiporter is more difficult to determine.To definitely answer the question, the approach of Endresen et al. (2007) considering the total work done by a transport system was used. Nha1 uses the inward directed electrochemical proton gradient to reduce the potassium content or detoxify sodium. Two protons take the elevator down and thus provide energy to lift one potassium/sodium from the cytosol to the external environment (Ohgaki et al. 2005). The net charge movement is the uptake of one positive charge per cycle. Since sodium plays a minor role in the simulated potassium starvation experiment (see Chapter 3), Na^+ is not included in the description of Nha1.

	1 h	3 h	6 h
overexpr. Nha1	$405 \pm 38\,\text{nmol/mg}$	$349 \pm 61\,\text{nmol/mg}$	$302 \pm 37\,\text{nmol/mg}$
Nha1	$426 \pm 38\,\text{nmol/mg}$	$367 \pm 36\,\text{nmol/mg}$	$298 \pm 24\,\text{nmol/mg}$
nha1Δ	$488 \pm 37\,\text{nmol/mg}$	$397 \pm 37\,\text{nmol/mg}$	$288 \pm 30\,\text{nmol/mg}$

Table 2.6: *Intracellular potassium content after certain hours of starvation in potassium free medium (Bañuelos et al. 2002). Values given plus/minus $1.96 \cdot \sigma$. After six hours of starvation the potassium content is similar in all three cases. That the presence, absence or even over-expression of Nha1 has no influence on the potassium content after six hours of starvation implies a deactivation of Nha1 under starvation.*

For Nha1, the total work (ΔG, measured in Joule) is composed of the work performed by the proton and potassium movements. The energy provided by the electrochemical proton gradient is consumed by potassium transport. Thus, the total work is reduced by the transport of potassium, which explains the negative sign in equation (2.68) (Gibb's free energy)

$$\Delta G_H = +2\mathbf{e}(V_m - E_H) \tag{2.67}$$
$$\Delta G_K = -1\mathbf{e}(V_m - E_K) \tag{2.68}$$

where $\mathbf{e}$ is the elementary charge, converting the unit Volt to Joule. E_K is the equilibrium potential for potassium.

$$E_K = \frac{RT}{zF} \ln \frac{[K^+]_o}{[K^+]_i} \, . \tag{2.69}$$

The total work is the sum of ΔG_H and ΔG_K

$$\Delta G_{tot} = \Delta G_H + \Delta G_K \tag{2.70}$$
$$= 2\mathbf{e}(V_m - E_H) - \mathbf{e}(V_m - E_K) \tag{2.71}$$
$$= 2\mathbf{e}V_m - 2\mathbf{e}E_H - \mathbf{e}V_m + \mathbf{e}E_K \tag{2.72}$$
$$= \mathbf{e}V_m - 2\mathbf{e}E_H + \mathbf{e}E_K \, . \tag{2.73}$$

Solving for the voltage, where $\Delta G_{tot} = 0$ yields,

$$0 = \Delta G_{tot} \tag{2.74}$$
$$0 = \mathbf{e}V_m - 2\mathbf{e}E_H + \mathbf{e}E_K \tag{2.75}$$
$$V_m = 2E_H - E_K \, . \tag{2.76}$$

Thus the equilibrium potential E_{Nha1} can be written as

$$E_{Nha1} = \frac{RT}{F} \ln \frac{[H^+]_o^2 \cdot ([K^+]_i)}{[H^+]_i^2 \cdot ([K^+]_o)} \, . \tag{2.77}$$

Since two protons are transported in exchange with one potassium, the proton current I_H^{Nha1} and the potassium current I_K^{Nha1} are related by

$$I_H^{Nha1} = -2 \cdot I_K^{Nha1} \tag{2.78}$$

Summary Nha1

In the initial model version, $\mathcal{M}_1$, (see Table reftab:models) a constant conductivity was used

$$I_K^{Nha1} \;=\; -g_{Nha1} \cdot (V_m - E_{Nha1}) \tag{2.79}$$

$$I_K^{Nha1} \;=\; -2 \cdot I_K^{Nha1} \,. \tag{2.80}$$

The improved model version $\mathcal{M}_2$ uses a voltage gating

$$I_K^{Nha1} \;=\; -\frac{g_{Nha1}}{1 + e^{d_{Nha1} \cdot \frac{F}{RT}\left(V_m - V_{1/2,\,Nha1}\right)}} \cdot (V_m - E_{Nha1}) \tag{2.81}$$

$$I_K^{Nha1} \;=\; -2 \cdot I_K^{Nha1} \,. \tag{2.82}$$

The parameters were tentatively chosen as

$$g_{Nha1} \;=\; 10\,\frac{\mu\mathsf{S}}{\mathsf{cm}^2} \tag{2.83}$$

$$d_{Nha1} \;=\; -1 \tag{2.84}$$

$$V_{1/2,\,Nha1} \;=\; -0.3\,\mathsf{V}\,. \tag{2.85}$$

$$\tag{2.86}$$

For Nha1, no data was available. The value of the conductance parameter was tentatively chosen. Assuming, that the values for all other systems are suitable, the conductance parameter of Nha1 depicts a free dimension in the parameter space. To get an idea of g_{Nha1}, several model simulations with different values for g_{Nha1} were made. Knowing the typical cellular concentration of potassium, the pH and the membrane potential, the values for g_{Nha1}, yielding physiological simulation results were considered to be appropriate between 8-12 $\mu\mathsf{S}/\mathsf{cm}^2$.

2.2.6 Potassium leak

Apart from the major potassium uptake system Trk1,2, the yeast cell can have various unspecific or even unknown potassium transporters. To mimic these systems in the model, an ohmic potassium leakage current is proposed. The idea of a linear relationship between the potassium leakage current and the voltage is supported by the measurements of the potassium leak in Kuroda et al. (2004) (see Figure 2.1). The data does not depict a pure cellular potassium leak, but covers also leakage currents from the experimental set up (e.g. electrode leak etc.).

Although, the leakage data of Kuroda et al. (2004) represents not only a cellular leak, the data was used to get an idea of the conductance parameter $g_{K,leak}$. Determining the slope of each of the four data sets by a linear regression, the value $5\frac{\mu\mathsf{S}}{\mathsf{cm}^2}$ was considered as suitable for the potassium leak.

The current is described as

$$I_K^{leak} = g_{K,leak} \cdot \left(V_m - \frac{RT}{zF} \ln \frac{[K^+]_o}{[K^+]_i} \right) \,. \tag{2.87}$$

Parameter

$$g_{K,leak} = 5\,\frac{\mu\mathsf{S}}{\mathsf{cm}^2} \,. \tag{2.88}$$

2.2.7 Proton leak

Many transport systems are driven by the electrochemical gradient of protons. Actually, the cell utilizes this gradient to take up sugars, amino acids and other nutrients. Additionally channels like Nsc1 or other transporters mediate an unspecific proton transport. In a personal communication Clifford L. Slayman[10] states, that at least in *Neurospora crassa* about 80% of the pumped out protons return attracted by the membrane voltage. Similar to the potassium leak, the proton leak deserves further investigations. There are electrophysiological observations in *N. crassa* confirming a large linear proton leak (Gradmann et al. 1978; Sanders et al. 1981). Thus, the proton leak was modeled by Ohm's law. The value for the conductance parameter is based on Sanders et al. (1981).

The current is described as

$$I_H^{leak} = g_{H,leak} \cdot \left(V_m - \frac{RT}{zF} \ln \frac{[H^+]_o}{[H^+]_i} \right) . \tag{2.89}$$

Parameter

$$g_{H,leak} = 25 \frac{\mu S}{cm^2} . \tag{2.90}$$

2.2.8 Tok1

The Tok1 channel is closed under physiological conditions. It is a system, which is well characterized by electrophysiological measurements. The article of Johansson and Blatt (2006) gives several current-voltage relationships for Tok1 and also presents an appropriate description of the Tok1 mediated currents by a gated channel approach. The approach is adopted in the model without further modifications. The description includes the known voltage gating for negative membrane potentials, meaning that Tok1 only opens for positive membrane voltages. In the later model simulations, positive membrane potentials are never observed. Thus, Tok1 is always inactive and does not contribute significantly to the model results. It is included in the model, since it may be relevant in future model versions or the simulation of very special conditions.

The potassium currents mediated by Tok1 can be expressed by

$$I_K^{Tok1} = \frac{g_{Tok1}}{1 + e^{d_{Tok1} \cdot \frac{zF}{RT}\left(V_m - V_{1/2, Tok1}\right)}} \cdot \left(V_m - \frac{RT}{zF} \ln \frac{[K^+]_o}{[K^+]_i} \right) . \tag{2.91}$$

$$\tag{2.92}$$

Parameters

$$g_{Tok1} = 9 \frac{\mu S}{cm^2} \tag{2.93}$$

$$d_{Tok1} = -1.04 \tag{2.94}$$

$$V_{1/2, Tok1} = -0.0034 \, V . \tag{2.95}$$

$$\tag{2.96}$$

---

[10]Yale University, Department of Cellular & Molecular Physiology

2.2.9 Pma1

A special case of transport system is the proton pump Pma1, since it is not driven by concentration gradients or the membrane voltage, but by the energy provided by the ATP hydrolysis. As the primary generator of driving force for all other processes, the role of the pump is equivalent to a battery in an electrical circuit. The equilibrium potential for the pump is shifted from the Nernst potential for protons by the energy of the ATP hydrolysis ΔG_{ATP}.

$$E_H^{Pma1} = E_H + \frac{\Delta G_{ATP}}{F} \,, \tag{2.97}$$

where Faraday's constant F converts the units of ΔG_{ATP} to voltage. Under standard conditions the value of ΔG_{ATP} is around $-30 \frac{kJ}{mol}$. Measurements in *Neurospora crassa* indicate a more negative value in the range of $-50 \frac{kJ}{mol}$ (Gradmann et al. 1978; Rodriguez-Navarro 2000). Since no experimental values for *S. cerevisiae* are available, additional assumptions had to be made.

The equilibrium potential for the proton pump determines the lower limit for the membrane potential. Values more negative than this critical limit would cause the pump to reverse its favored pump direction. The consideration of a lower limit for the membrane potential can be used to adapt the value of ΔG_{ATP} to the conditions in *S. cerevisiae*. For $\Delta G_{ATP} = -50 \frac{kJ}{mol}$, $pH_i = 7\,pH$ and $pH_o = 5.5\,pH$ the equilibrium potential for the pump is

$$E_H^{Pma1} = E_H + \frac{\Delta G_{ATP}}{F} \approx -400mV \,. \tag{2.98}$$

This value is generally believed to be too negative; Rodriguez-Navarro (2000) and references therein. Therefore, a value of $\Delta G_{ATP} = -40 \frac{kJ}{mol}$ was chosen, leading to an $E_H^{Pma1} = E_H + \frac{\Delta G_{ATP}}{F} \approx -300mV$. This is in agreement with the lower limit for the membrane potential suggested by Rodriguez-Navarro (2000). More negative values yielded too negative membrane voltages and more positive values caused a reversed Pma1 activity. Although, the value for the ATP hydrolysis is left for further investigations and must not necessarily treated as constant, the proposed value was suitable in the model simulations and could be used to adjust the membrane potential.

The description of the pump current is based on (Endresen et al. 2007, Section C). The pump is considered to change between two states, characterized by pointing a proton to the inside or to the outside. The net reaction is

$$H_i^+ \rightleftharpoons H_o^+ \,. \tag{2.99}$$

The total change in Gibbs free energy is

$$\Delta G_{Pma1} = \mathbf{e} \left(V_m - \left(E_H + \frac{\Delta G_{ATP}}{F} \right) \right) \,, \tag{2.100}$$

where $\mathbf{e}$ is the elementary charge, converting Volt to Joule and E_H is the Nernst potential for protons.

The ratio between the forward and backward reaction is exponentially dependent on the total

change of energy (Boltzmann distribution)

$$\frac{k_1}{k_{-1}} = e^{\frac{-\Delta G_{Pma1}}{RT}} \,. \tag{2.101}$$

At equilibrium, the sum of the rate constants describing the change of the two states is assumed to be constant, since in equilibrium, the forward reaction must balance the reverse reaction.

$$\lambda = k_1 + k_{-1} \tag{2.102}$$

Substituting k_{-1} one obtains

$$\frac{k_1}{\lambda - k_1} = e^{\frac{-\Delta G}{RT}} \tag{2.103}$$

$$k_1 = \frac{\lambda e^{\frac{-\Delta G}{RT}}}{e^{\frac{-\Delta G}{RT}} + 1} \,. \tag{2.104}$$

Substituting k_1 yields

$$\frac{\lambda - k_{-1}}{k_{-1}} = e^{\frac{-\Delta G}{RT}} \tag{2.105}$$

$$k_{-1} = \frac{\lambda}{e^{\frac{-\Delta G}{RT}} + 1} \,. \tag{2.106}$$

The net transport current can be given as

$$I_{Pma1} = N \cdot \mathbf{e} \cdot (k_1 - k_{-1}) \,, \tag{2.107}$$

where N is the transporter density ($1/\text{cm}^2$) and $\mathbf{e}$ the elementary charge. The difference of the rate constants is

$$
\begin{aligned}
k_1 - k_{-1} &= \lambda \frac{e^{\frac{-\Delta G}{RT}} - 1}{e^{\frac{-\Delta G}{RT}} + 1} \cdot \frac{e^{\frac{\Delta G}{2RT}}}{e^{\frac{\Delta G}{2RT}}} \tag{2.108} \\
&= \lambda \frac{e^{\frac{-\Delta G}{2RT}} - e^{\frac{\Delta G}{2RT}}}{e^{\frac{-\Delta G}{2RT}} + e^{\frac{\Delta G}{2RT}}} \tag{2.109} \\
&= \lambda \frac{-\left(e^{\frac{\Delta G}{2RT}} - e^{\frac{-\Delta G}{2RT}}\right)}{e^{\frac{-\Delta G}{2RT}} + e^{\frac{\Delta G}{2RT}}} \tag{2.110} \\
&= \lambda \frac{-\sinh\left(\frac{-\Delta G}{2RT}\right)}{\cosh\left(\frac{-\Delta G}{2RT}\right)} \tag{2.111} \\
&= \lambda \tanh\left(\frac{\Delta G}{2RT}\right) \,. \tag{2.112}
\end{aligned}
$$

Finally this yields

$$I_H^{Pma1} = I_{Pma1}^{max} \cdot \tanh\left(\frac{F}{2RT} \cdot (V_m - E_{Pma1})\right) \,. \tag{2.113}$$

with $E_{Pma1} = E_H + \frac{\Delta G_{ATP}}{F}$.

Thus, for the pump only one parameter, giving the maximum pump current is required. For *S. cerevisiae* no current-voltage relationships could be found in the literature. However, since Serrano

(1988) reports a homology of 74% between the nucleotide sequences of Pma1, the electrophysiological measurements for the related ascomycete *Neurospora crassa* can be used to identify a suitable value for I_{Pma1}^{max}. Based on Gradmann et al. (1978) $I_{Pma1}^{max} = 16 \frac{\mu A}{cm^2}$ was chosen as parameter value.

For comparison: the turnover rate of Pma1 is given as 20-100 H^+ per second by Serrano (1988). The respective mass flux is given by

$$J_H^{Pma1} \frac{n_H \cdot n_{Pma1}}{N_A \cdot V} , \qquad (2.114)$$

where n_H is the turnover rate, $n_{Pma1} = 1\,260\,000$ the number of Pma1 molecules, $N_A = 6 \cdot 10^{26}\,1/mmol$ Avogadros constant and $V = 50 \cdot 10^{-12} cm^3$ the cell volume. For the given turnover rates this yields a mass flux of $8 \cdot 10^{-4}$ to $4 \cdot 10^{-3} \frac{mmol}{cm^3\,s}$ and a current density of 6-30 $\frac{\mu A}{cm^2}$.

Summary Pma1

The pump current is described by

$$I_H^{Pma1} = I_{Pma1}^{max} \cdot \tanh \left(\frac{V_m - \left(\frac{RT}{zF} \ln \frac{[H^+]_o}{[H^+]_i} + \frac{\Delta G_{ATP}}{F} \right)}{2RT} \right) . \qquad (2.115)$$

Parameters

$$\Delta G_{ATP} = -40 \cdot 10^6 \frac{\mu J}{mmol} \qquad (2.116)$$

$$I_{Pma1}^{max} = 16 \frac{\mu A}{cm^2} . \qquad (2.117)$$

2.2.10 Simulated current voltage relationships

In the sections above mathematical expressions for each single transport systems were given. These descriptions allow the simulation of current voltage relationships for the transporters. The consideration of those relationships is a useful tool to understand, how the current is affected by concentration or membrane potential changes. Figure 2.15 shows the simulated current-voltage relationships. The parameters follow the values given in the respective sections. Additional parameters are $[K^+]_o = 10\,mM$, $[K^+]_i = 250\,mM$, $pH_o = 5.8\,pH$, $pH_o = 6.8\,pH$ and $V = 50\,fL$. It is recommended to consult Figure 2.15, while reading the results in Chapter 3.

In the stationary state, the net transport of all ions must equal zero (see Equation (2.31)). Assuming that the given concentrations are stationary, the sum of all transporter currents determines the stationary membrane potential by the zero crossing of the total current with the voltage axes. Figure 2.16 shows the respective considerations for the current-voltage relationships given in Figure 2.15.

The Tables 2.7 and 2.8 gives the Nernst potential for various internal and external concentrations. This allows the reader to follow the equilibrium potential caused by concentration changes.
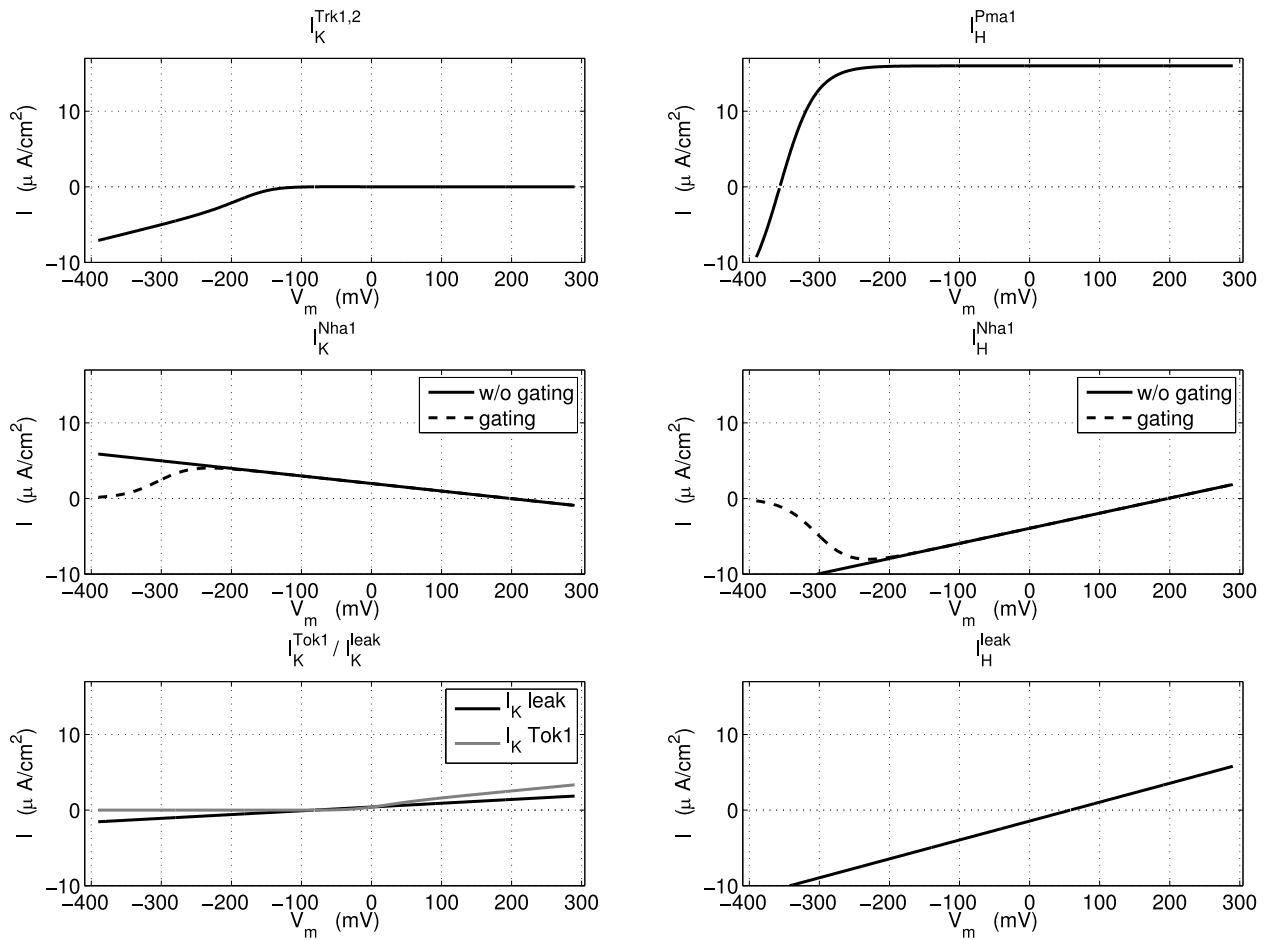
Figure 2.15: *Simulated current voltage relationships for Trk1,2, Nha1, Pma1, Tok1 as well as proton and potassium leak. In the case of Nha1 the potassium and the proton current is shown. The dashed line represents the current-voltage relationship with a voltage gating for Nha1. The panel on the bottom-left, shows the relationship for the potassium leak (black) and Tok1 (gray).*
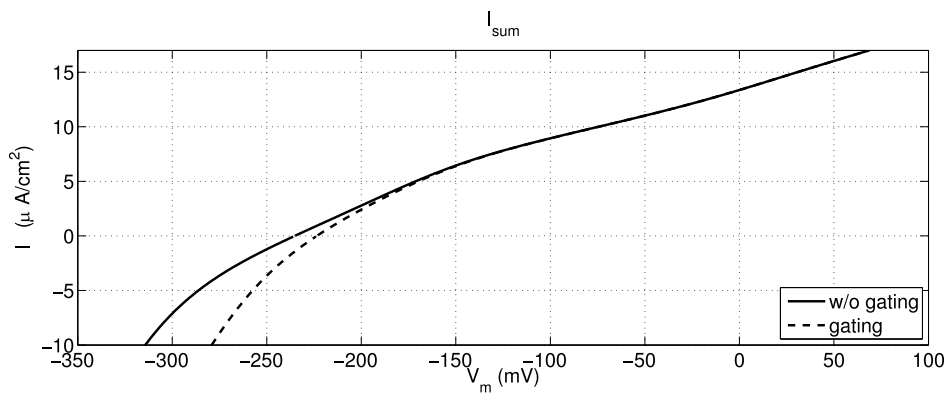
Figure 2.16: *Total sum of all currents presented in Figure 2.15 (solid line). The shattered line shows the respective result including the voltage gating of Nha1. The zero crossing of the total current corresponds to the stationary membrane potential, which is approx. $-230\,\text{mV}$.*

		$[K^+]_i$(mM)				
		1	10	100	200	300
	0.015	-106	-164	-222	-240	-250
$[K^+]_o$(mM)	1	0	-58	-116	-134	-144
	10	58	0	-58	-76	-86
	50	99	41	-18	-35	-45

Table 2.7: *Nernst potential (given in* mV*) for different external and internal potassium concentrations. The rows indicate* $[K^+]_o$ *and the columns* $[K^+]_i$.

		pH_i			
		5.5	6	6.5	7
	4.5	58	87	116	145
pH_o	5	29	58	87	116
	5.5	0	29	58	87
	6	-29	0	29	58

Table 2.8: *Nernst potential (given in* mV*) for different external and internal proton concentrations. The rows indicate* pH_o *and the columns* pH_i.

2.2.11 Constant proton buffer capacity

For many decades it is known that yeast cells tend to acidify their surrounding (Lopéz et al. (1999) and references therein). This is caused by the release of protons from various processes in metabolic active cells. Despite these large proton efflux the yeast cell keep a physiological pH around 7 pH. For this purpose the cell relies not only on the regulation of cellular transport processes, but also on a proton buffer capacity, β (unit mmol/pH/cm^3). It is defined as (Boron and de Weer 1976)

$$\beta = \frac{d\,[H^+]}{d\,pH}\,. \tag{2.118}$$

In this context, the reader is reminded to the mechanism of potassium uptake. The proton pump, Pma1, extrudes H^+ and the loss of positive charges energizes the charge compensatory uptake of K^+. This suggests a 1:1 relationship of potassium uptake and proton extrusion, which is, however, not really the case due to the parallel transport of other charged species. Nevertheless, the well proven mechanism of potassium uptake requires a cellular proton concentration far more than 10^{-7} mol/L (7 pH).

By means of the Avogadro constant, $k_A = 6 \cdot 10^{23} \frac{1}{mol}$ the absolute number of protons and potassium inside the cell can be estimated, assuming a cell volume of $V = 50\,\text{fL} = 50 \cdot 10^{-15}\,\text{L}$.

$$[H^+]_i \cdot V \cdot k_A \;=\; 10^{-7}\text{mol/L} \cdot 50 \cdot 10^{-15}\,\text{L} \cdot 6 \cdot 10^{23}\frac{1}{mol} = 3\,000 \tag{2.119}$$

$$[K^+]_i \cdot V \cdot k_A \;=\; 0.2\text{mol/L} \cdot 50 \cdot 10^{-15}\,\text{L} \cdot 6 \cdot 10^{23}\frac{1}{mol} = 10^9 \tag{2.120}$$

Thus, to exchange relevant amounts of protons and potassium, the cell needs to have a proton storage and release system. It arises from the property of large negative charged macromolecules, amino acids, metabolic intermediates etc. to catch and release protons. As a result, not every proton entering or leaving the cell contributes directly to the cellular pH (but to the charge balance!).

The model will deal with a constant proton buffering capacity using the parameter β as a constant

Description	β mM/pH	Reference
Golgi complex	10	Farinas & Verkman, 1999, cited in Grabe and Oster (2001)
Golgi complex	40	Wu et al., 2000, cited in Grabe and Oster (2001)
Endopl. ret.	6	Wu et al., 2000, cited in Grabe and Oster (2001)
Endosomes	50	Rybak et al., 1997, Grabe and Oster (2001)

damping factor. Although, the proton buffer capacity is crucial in living cells, the literature does not provide very much information about possible values for β. The value used in this work

$$\beta = 0.2 \, \frac{\text{mmol/cm}^3}{\text{pH}} \tag{2.121}$$

is based on literature, theoretical thoughts and experimental support.

Theoretical estimates   Yeast cells typically has an internal potassium concentration of around $200 - 300$mM and a pH of 7. Potassium starved cells are able to keep a residual potassium concentration around 100 mM. Due to the lack of energizing glucose the proton pump will reduce its activity during potassium starvation, what yields a pH of 5.7-5.9 pH (Lopéz et al. 1999). Supporting this finding, Rodriguez-Navarro (2000) states, that during starvation the loss of positive charges (potassium) is partly compensated by protons, which will lead to a reduced pH.

If a starved cell is put into a rich medium, it can be expected that the maximum potassium concentration is restored after a short time (see potassium uptake measurements Appendix 4.4). This corresponds, a potassium concentration change of up to 200mM and an equivalent H^+ extrusion. However the pH of starved and well supplied cells differs by 1 pH unit. Thus, a simple estimate for a constant buffer capacity, β, can be given by relating the required proton concentration change to the observed pH change.

$$\beta = \frac{200\text{mM}}{1\text{pH}} = 200 \, \frac{\text{mM}}{\text{pH}} \, . \tag{2.122}$$

Supporting literature   In (Grabe and Oster 2001) references to the proton buffer capacity of some organelle systems are given. The values for the three compounds given in Grabe and Oster (2001) sum up to $66 - 96$ mM/pH, whereas the cytosol and further cell structures are not taken into account. It is thus likely, that the overall buffer capacity of the cell is higher than 100 mM/pH.

The proton buffer capacity of the whole cell was measured by Blatt and Slayman (1987) in *Neurospora crassa*. Under various conditions (treatment with certain drugs), the buffer capacity was estimated to be $42 - 202$ mM/pH. Since *N. crassa* is a related ascomycete the values can, in principle, hold as an estimate for *S. cerevisiae*. However, the range of the values is rather broad. In addition the conditions in this work are far from being comparable to those in the literature above.

Experimental support   ⟳   In the early stages of the present work, potassium uptake measurements were used to calibrate the model parameters. Relating the overall proton extrusion during potassium uptake to the change of the intracellular pH allows an estimate of the cytosolic proton buffer capacity. For further details see Appendix 4.4 and especially Table 4.2.

2.2.12 Cell volume

Yeast grows in the range of micro-molar to molar concentrations of potassium. This gives not only rise to the question, how the cells are able to maintain a certain cytosolic concentration, but also rises the question, how the cells can resist the remarkable changes in the osmotic pressure. As mentioned above, potassium is known to be one player in the osmoregulation of the yeast cell. This means, that the cytosolic potassium concentration helps to maintain a certain cell volume. The net loss of potassium results in a reduction of cell volume (Navarrete et al. 2010). This effect arises from the concomitantly decrease of osmotic pressure.

The osmoregulation via the change of concentrations involves two counteracting processes: The higher the concentration inside the cell, the more water is attracted and hold. This results in an increase of cell volume. But since the concentration is dependent on the dilution of an amount of substance in a certain volume, the concentrations decrease with growing volume, reducing the effect of attracting water. However, these two processes can not treated in isolation, but in combination with the activity of the transport systems. The decrease of concentration due to the swelling of the cell could stimulate the uptake of a certain particle in order to restore the concentration (and *vice versa*). For further informations about the coupling of the volume, concentrations and the membrane potential, see Jakobsson (1980).

Because the tight coupling of volume and transport, the volume regulation is incorporated in all model versions. The mathematical description is based on the ideas of Gennemark et al. (2006) who gives a simple model of glycerol controlled osmoregulation under hyper-osmotic conditions in *S. cerevisiae*.

The change of the volume can be described by

$$\frac{d}{dt}V = L_p \cdot A \cdot (\Pi_i - \Pi_o - \Pi_t) \ , \tag{2.123}$$

where L_p is the hydraulic conductivity and A is the cell surface. Π_i, Π_o and Π_t are the internal, external osmotic pressure and the turgor pressure. The hydraulic conductivity is a parameter describing the resistance of the cell membrane to changes of pressure and defined as

$$L_p \quad = \quad 4 \cdot 10^{-11} \frac{\mathsf{cm}^4}{\mathsf{s} \cdot \mu \mathsf{J}} \ , \tag{2.124}$$

where $\mathsf{N} = \mathsf{Pa} \cdot \mathsf{m}^2$ and $\mathsf{J} = \mathsf{N} \cdot \mathsf{m}$ was used to convert the original units of Gennemark et al. (2006).

External osmotic pressure

The external osmotic pressure can be estimated from the composition of the medium. According to (Gennemark et al. 2006) the total osmotic pressure of a solvent with a couple of solutes can be approximated by

$$\Pi_o = RT \cdot \sum_l n_l \, [c]_l \, \phi_k \ , \tag{2.125}$$

with l indexing all contributing solutes $[c]$ and n the number of moieties the substance dissociates in. For example potassium chloride has a value of $n = 2$. The equation can be derived from the ideal gas equation, which relates pressure, volume and temperature via the ideal gas constant.

Since a solution depicts no ideal gas, and therefore interactions between solvent and solute can be expected, the coefficient ϕ covers the degree of deviation from idealism. It dependents on the concentration of the solute and has to be determined experimentally for a certain substance under certain conditions. Robinson and Stokes (1959) gives e.g. $\phi_{KCL}(0.1\,\text{mM}) = 0.93$. The coefficient can be interpreted as the fraction of the solute, which is not in close interaction with the solvent. The lower the concentration, the closer is the osmotic coefficient to one.

In a solvent with several solutes the interaction between the different substances can not neglected, when calculating the overall osmotic pressure Π_o. However, the effect of these interactions can not predicted and quantified in a common case. Thus the value of Π_o is only a reasonable approximation for the true osmotic pressure. Such a calculation has been already demonstrated in Section 2.1.3 for the data of Navarrete et al. (2010).

Internal osmotic pressure

Whereas under most experimental conditions the surrounding medium is known in detail, the intracellular concentrations and substances are not under control. This makes the internal osmotic pressure more complicated to estimate. Gennemark et al. (2006) estimates the total concentration of osmotic active substances to be around 600-700 mM. This value covers all macromolecules, cellular structures and concentrations present in the cell. It also covers potassium, which is not treated as a variable in the model of Gennemark et al. (2006). Regarding the typical potassium concentration of up to 300 mM shows, that potassium generates approximately one half to the total osmotic pressure.

In this work the internal osmotic pressure is estimated by

$$\Pi_i = RT \cdot V \cdot \frac{[Z]_i + \sum_l [c]_l}{V - f_V \cdot V(0)}, \tag{2.126}$$

where V is the volume, $V(0)$ a reference volume, f_V the fraction of non-osmotic volume, l indexing all contributing solutes $[c]$, such as potassium, free protons etc. and $[Z]_i$ covers all impermeable particles. Subtracting the maximal potassium content of around $300\,\text{mM}$ from the total concentration of osmotic substances, a value of $[Z]_i = 300\,\text{mM}$ is suggested. According to Gennemark et al. (2006) around one third of the cell volume is loaded with cellular structures such as organelles and macromolecules. Thus, the internal osmotic pressure needs to be corrected for the osmotic inactive volume, which is achieved by the dimensionless parameter $f_V = 0.37$.

For the internal osmotic pressure, the osmotic coefficients are neglected. For 300 mM KCl the respective value is $\phi = 0.9063$ (Robinson and Stokes 1959). Thus, the osmotic coefficient for the most abundant specie is already close to one. Implementing this factor does not lead to a visible change in the simulation results. The uncertainties in the estimation of Π_i are such large, that the inclusion of the osmotic coefficients pretend an accuracy where none can be achieved.

Turgor pressure

In most experimental and natural surroundings, the intracellular osmotic pressure exceeds the extracellular one. This would in principle lead to a steady influx of water, causing the cell to swell and burst. However, this is prevented by the cell wall, which creates an inward directed pressure, the so called turgor pressure (Gennemark et al. (2006) and references therein), which adds a certain

value to the external pressure to balance the intracellular osmotic effects. The equilibrium condition can be given as

$$\Pi_i = \Pi_o + \Pi_t \,. \tag{2.127}$$

Since the external salt concentrations can be in the micromolar range, while the cytosolic concentrations are always in the millimolar range, it becomes clear that the cell wall has to be a very tight structure, to create a sufficient pressure.

According to Levin (1979), the turgor pressure can be expressed as

$$\Pi_t(t) = p^I + \Pi_t(0) \tag{2.128}$$

where $\Pi_t(0)$ is the initial turgor pressure and p^I is the intracellular hydrostatic pressure. The hydrostatic pressure is related to the elasticity of the cell wall and the volume by

$$\epsilon \;=\; V \cdot \frac{d\,p^I}{d\,V} \tag{2.129}$$

$$\frac{\epsilon}{V} \cdot dV \;=\; d\,p^I \,, \tag{2.130}$$

where ϵ is the so called volumetric elastic modulus, covering the elasticity of the cell wall. If ϵ is not dependent on the volume, the equation can be integrated to finally yield the turgor pressure as

$$\Pi_t(t) = \epsilon \cdot \ln \frac{V}{V(0)} + \Pi_t(0) \,. \tag{2.131}$$

Using the approximation $\ln(1 + x) \approx x$, the expression is further simplified to

$$\Pi_t(t) = \epsilon \cdot \left(\frac{V}{V(0)} - 1 \right) + \Pi_t(0) \,. \tag{2.132}$$

The above expression is adopted and modified by Gennemark et al. (2006). Since the parameter ϵ is not easy to interpret, it is replaced by a parameter, $V^{\Pi_t=0}$, describing the volume, for which the turgor pressure is zero

$$\Pi_t(t) \;=\; \epsilon \cdot \ln \frac{V}{V(0)} + \Pi_t(0) = 0 \tag{2.133}$$

$$V^{\Pi_t=0} \;=\; V(t) = V(0) \cdot \left(1 - \frac{\Pi_t(0)}{\epsilon} \right) \tag{2.134}$$

$$\epsilon \;=\; \frac{\Pi_t(0) \cdot V(0)}{V(0) - V^{\Pi_t=0}} \,. \tag{2.135}$$

Substituting ϵ into Equation (2.132) yields

$$\Pi_t(t) \;=\; \frac{\Pi_t(0) \cdot V(0)}{V(0) - V^{\Pi_t=0}} \cdot \left(\frac{V}{V(0)} - 1 \right) + \Pi_t(0) \tag{2.136}$$

$$=\; \frac{\Pi_t(0) \cdot V(0) \cdot V(t) - \Pi_t(0) \cdot V(0)^2}{V(0)^2 - V^{\Pi_t=0} \cdot V(0)} + \Pi_t(0) \tag{2.137}$$

$$=\; \frac{\Pi_t(0) \cdot V(0) - \Pi_t(0) \cdot V(0) + \Pi_t(0) \cdot V(0) - \Pi_t(0) \cdot V^{\Pi_t=0}}{V(0) - V^{\Pi_t=0}} \tag{2.138}$$

$$=\; \Pi_t(0) \cdot \frac{V(t) - V^{\Pi_t=0}}{V(0) - V^{\Pi_t=0}} \,. \tag{2.139}$$

where $V^{\Pi_t=0}$ is expressed as a certain fraction, k_V, of the initial volume $V^{\Pi_t=0} = k_V \cdot V(0)$. Since the elasticity of the cell wall should not be able to yield a negative pressure, the values for $\Pi_t(t)$ are restricted to positive values.

Influence of the volume on the transporters conductivities

The conductivities of the transport systems are given in $\mu S/cm^2$. Since the conductivities are related to the cell surface, the change of the cell volume affects the conductivity parameters. For example: if a constant number of transporters is placed in a certain area of the cell surface and this area is increased, then the surface related conductivity is decreased. In the model simulations the conductivities are scaled by a dimensionless factor

$$S = \frac{A(0)}{A} \, , \tag{2.140}$$

where $A(0)$ is the initial surface and A the actual surface.

Summary

The volume change is modeled as

$$\frac{d}{dt}V(t) = L_p \cdot A \cdot (\Pi_i - \Pi_o - \Pi_t) \, , \tag{2.141}$$

where

$$\Pi_i = RT \cdot V \cdot \frac{[Z]_i + \sum_l [c]_l}{V - f_V \cdot V(0)} \tag{2.142}$$

$$\Pi_o = RT \cdot \sum_l n_l \, [c]_l \, \phi_k \tag{2.143}$$

$$\Pi_t = \Pi_t(0) \cdot \frac{V(t) - V^{\Pi_t=0}}{V(0) - V^{\Pi_t=0}} \tag{2.144}$$

$$\Pi_t(0) = \Pi_i(0) - \Pi_o(0) \tag{2.145}$$

$$L_p = 4 \cdot 10^{-11} \frac{cm^4}{s \cdot \mu J} \tag{2.146}$$

$$[Z]_i = 300 \, mM \tag{2.147}$$

$$V^{\Pi_t=0} = k_V \cdot V(0) \tag{2.148}$$

$$k_V = 0.99 \tag{2.149}$$

$$f_V = 0.37 \tag{2.150}$$

When the external medium does not change, Π_o is constant and the volume change only depends on Π_i and Π_t. The turgor pressure depends on the volume volume, which means, that the volume is governed mainly by the increase or decrease of the internal osmotic pressure Π_i. An increase in Π_i causes an increase of the cell volume. This results in an increase of the turgor pressure until Π_i is balanced. In this respect, the role of the parameter k_V can be clarified. The denominator of Π_t becomes very small for $k_V \to 1$. This means, the closer k_V to 1, the more sensitive the turgor pressure reacts to changes of the volume, and the internal osmotic pressure is balanced more quickly by Π_t.
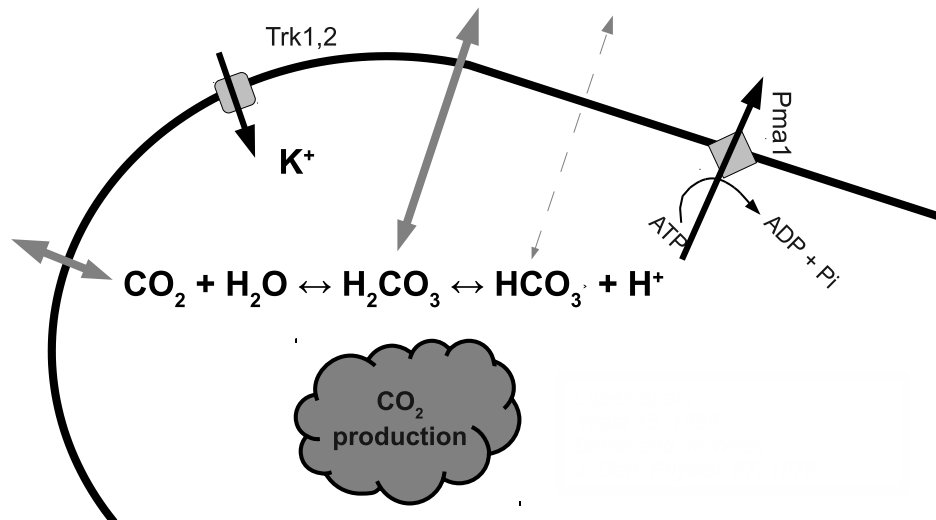
Figure 2.17: *Effect of CO_2 production according to Lopéz et al. (1999). CO_2 reacts with water to carbonic acid, which dissociates into bicarbonate and protons. While CO_2 and carbonic acid can freely permeate the cell membrane, bicarbonate is accumulated inside the cell. The protons are pumped out which energizes the uptake of potassium via Trk1,2.*

2.2.13 Bicarbonate extension

The property of buffering protons plays a crucial role in the regulation of intracellular pH. The proton buffer must be capable of storing, but also of providing protons, when the cytosolic pH reaches a very low level. In metabolic active cells, there is always a net extrusion of protons observable by an acidification of the medium. Thus, these protons are assumed to arise from various metabolic processes.

The observed discrepancy between H^+ extrusion and the amount of free protons in the cell during potassium uptake leads to the question of how protons are stored and released in side the cell. The fact that the presence of glucose in the medium enhance the H^+ extrusion suggests that glycolysis contributes to the release of protons. While glycolysis itself does not lead to a net production of protons, the aerobic (Krebs-cycle) and anaerobic (fermentation) reactions steps related to pyruvate, produce carbon dioxide (Alberts et al. 1998). In liquid solutions the essential reaction is

$$CO_2 + H_2O \rightleftarrows H_2CO_3 \rightleftarrows HCO_3^- + H^+ . \tag{2.151}$$

In a biological context the hydration of CO_2 to H_2CO_3 is catalyzed by the enzyme carbonic anhydrase. Actually, the reactions related to bicarbonate depict a well known proton buffer system used by many organisms.

Based on the work of Antonio Peña and coworkers (Peña et al. 1967, 1972, 1969; Peña 1975) the authors of Lopéz et al. (1999) suggest a functional connection between CO_2 and potassium uptake. Since HCO_3^- is rather impermeable to the cell membrane it is accumulated inside the cell, while H^+ is pumped out in order to restore the pH. This H^+ extrusion energizes the uptake of potassium; see Figure 2.17.

Boron and de Weer (1976) present a model to study the effects of the extracellular CO_2 concentration of the intracellular pH in the giant squid axon. Their ideas are used to formulate a model
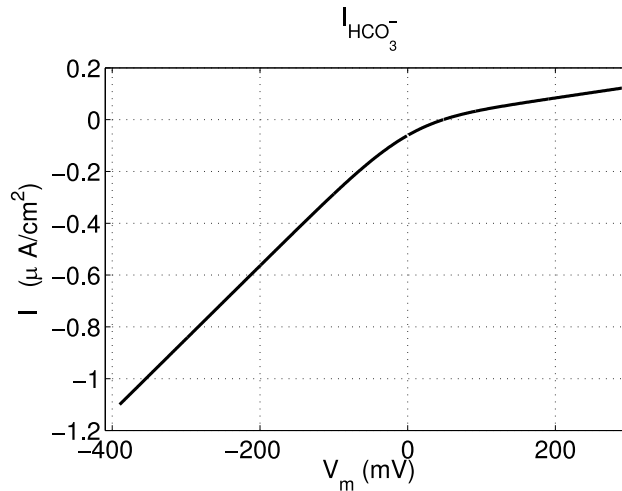
Figure 2.18: *Current-voltage relationship for the HCO_3^- leak. $P_{HCO_3^-} = 5e-7\,\frac{cm}{s}$, $[CO]_o = 1\,mM$, $[CO]_i = 2\,mM$, $pH_o = 5.8\,pH$, $pH_i = 6.8\,pH$. For physiological membrane potentials, the current density is negative, which means efflux for anions.*

of proton buffering and production. The model covers the concentrations of H_2CO_3, HCO_3^- and H^+ as variable and describes the change of the total weak acid $[H_2CO_3]_i + [HCO_3^-]_i$.

A rapid equilibrium is assumed for the first reaction step in Equation (2.151). Thus, the model covers the concentration of H_2CO_3, HCO_3^- and H^+ as variables, to describe the changes of the total weak acid ($[H_2CO_3]_i + [HCO_3^-]_i$) and the protons. Fick's law is used to describe the H_2CO_3 flux across the membrane

$$J_{H_2CO_3} = -P_{H_2CO_3} \frac{1}{\mathcal{R}} \left([H_2CO_3]_o - [H_2CO_3]_i \right),$$ (2.152)

with the constant permeability $P_{H_2CO_3}$ (unit $\frac{cm}{s}$) and $\mathcal{R} = \frac{volume}{surface}$. A positive flux occurs, when the intracellular concentration exceeds the extracellular one.

Concerning the anionic species HCO_3^- the Goldmann-Hodgkin-Katz (GHK) equation can be used to describe a passive leakage flux

$$J_{HCO_3^-} = -P_{HCO_3^-} \frac{1}{\mathcal{R}} \frac{V_m F}{RT} \frac{[HCO_3^-]_o - [HCO_3^-]_i \, e^{\frac{-V_m F}{RT}}}{1 - e^{\frac{-V_m F}{RT}}},$$ (2.153)

with the constant permeability $P_{HCO_3^-}$ (unit $\frac{cm}{s}$) and $\mathcal{R} = \frac{volume}{surface}$. Since $exp\left(\frac{-V_m F}{RT}\right) \in \left[3 \cdot 10^3; 2 \cdot 10^4\right]$ for membrane voltage $V_m \in [-0.25\,V; -0.2\,V]$, a positive flux $J_{HCO_3^-}$ can be expected, unless $[HCO_3^-]_o$ exceeds $[HCO_3^-]_i$ by four orders of magnitude. Taking into account that a negative membrane voltage energizes the efflux of negative particles this finding appears reasonable.

The usage of the GHK equation instead of the model typical Ohm's law approach is motivated by the fact, that Boron and de Weer (1976) gives an estimation for the permeability $P_{HCO_3^-}$. Since it is not possible to convert a permeability into a conductance and since no conductance parameter for yeast could be found in the literature the usage of that approach appears to be a sensible solution.

Carbon-dioxide is expected to turn quickly into carbonic acid (Lopéz et al. (1999) $10^{-pK_A} = 10^{-6.35}$), which dissociates into hydrogen carbonate and protons. In the model it is assumed that the total CO_2 concentration can be expressed by $[CO_2] = [HCO_3^-] + [H_2CO_3]$. The partitioning of
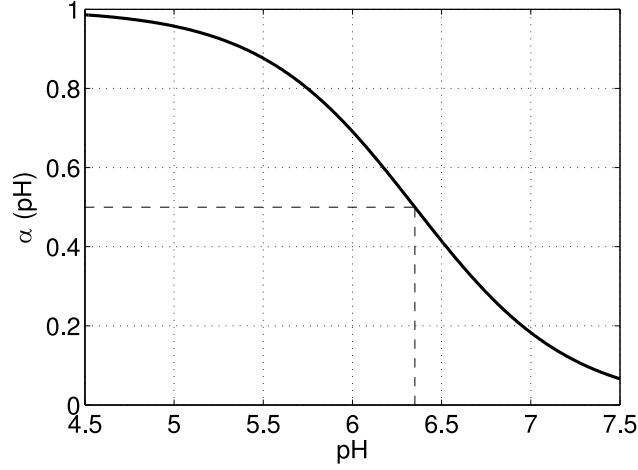
Figure 2.19: *Fraction of H_2CO_3 remaining undissociated in dependence of the pH.*

a $[HCO_3^-]$ and $[H_2CO_3]$ is dependent on the surrounding pH. This allows to calculate the internal $[HCO_3^-]$ and $[H_2CO_3]$ via

$$[CO_2]_i = [H_2CO_3]_i + [HCO_3^-]_i . \tag{2.154}$$

Accordingly, the change of $[CO_2]_i$ is given by

$$\frac{d[CO_2]_i}{dt} = -J_{CO_2} = -\left(J_{H_2CO_3} + J_{HCO_3^-} \right) . \tag{2.155}$$

In a final step the concentrations of $[H_2CO_3]_i$ and $[HCO_3^-]_i$ have to be expressed in terms of $[CO_2]_i$. The fraction α of the intracellular weak acid is

$$\alpha = \frac{[H_2CO_3]_i}{[H_2CO_3]_i + [HCO_3^-]_i} = \frac{[H^+]_i}{[H^+]_i + K_A} , \tag{2.156}$$

where the equation $[H_2CO_3]_i = \frac{[H^+]_i [HCO_3^-]_i}{K_A}$ was used. In the original approach the equilibrium constant is chosen to be $K_A = 10^{-6}$. In the present work the value from Lopéz et al. (1999) was used: $K_A = 10^{-pK_A} = 10^{-6.35}$. Now $[H_2CO_3]_i = \alpha[CO_2]_i$ and $[HCO_3^-]_i = (1-\alpha)[CO_2]_i$. [11]. The change of the intracellular pH (or proton concentration respectively) can be expressed as

$$\frac{d\,pH_i}{dt} = \frac{1}{\beta} \left((1-\alpha) J_{H_2CO_3} - \alpha J_{HCO_3^-} + J_H^{transp} \right) \tag{2.157}$$

$$\frac{d\,pH_i}{dt} = \frac{1}{\beta} \left(J_H^{react} + J_H^{transp} \right) , \tag{2.158}$$

where $(1-\alpha)$ describes the fraction of H_2CO_3 dissociating into HCO_3^- and H^+, α represents the fraction of HCO_3^- binding to H^+, β is a constant buffer capacity, J_H^{transp} sums all proton fluxes via cell membrane transporters and $J_H^{react} = (1-\alpha) J_{H_2CO_3} - \alpha J_{HCO_3^-}$ substitutes the proton fluxes arising from the CO_2 reaction. The buffer capacity still appears as a necessary damping factor,

---

[11]Because K_A is in the order of magnitude of the cytosolic proton concentration, α can change considerably (see Figure 2.19). The rate constants for the effective reaction $HCO_3^- + H^+ \underset{q_{-1}}{\overset{q_1}{\rightleftharpoons}} CO_2 + H_2O$ are given as $q_1 = 3.437 \cdot 10^{10}$ mol $\cdot$ s and $q_{-1} = 2.73 \cdot 10^4$ s^{-1} by Martin et al. (2011) (human cells)

because it can not be expected, that the CO_2 buffer system covers all buffering processes.

The changes of H_2CO_3 and HCO_3^- due to the association and dissociation processes must not taken into account in equation (2.155) because the release of one species goes along with the release of the other species. It is also worth to note, that $(1 - \alpha) J_{H_2CO_3}$ and $\alpha J_{HCO_3^-}$ describe electroneutral processes and induce no net electrical current.

Inclusion of carbon dioxide production

After introducing the basic concept of proton buffering, a source flux, $J_{CO_2}^{prod}$, arising from metabolic processes is taken into account. Due to the definition in Equation (2.154) the production of CO_2 also means a production of carbonic acid and hydrogen carbonate. Thus the production flux has to be split up into

$$
\begin{aligned}
J_{H_2CO_3}^{prod} &= \alpha \, J_{CO_2}^{prod} & (2.159) \\
J_{HCO_3}^{prod} &= (1 - \alpha) \, J_{CO_2}^{prod}, & (2.160)
\end{aligned}
$$

where $J_{CO_2}^{prod}$ represents any convenient function (production is equal to influx. Sign convention: production negative). Teusink et al. (2000) uses $J_{CO_2}^{prod} = 2.5 \cdot 10^{-3} \frac{\text{mmol}}{\text{cm}^3 \, \text{s}}$ (original unit 154 mM/s) in a kinetic model of glycolysis. However, it can be expected that this parameter strongly depends on the metabolic state, the strain and external conditions.

The fluxes of H_2CO_3 and HCO_3^- can now be written as

$$
\begin{aligned}
J_{H_2CO_3} &= -\frac{P_{H_2CO_3}}{\mathcal{R}} \left([H_2CO_3]_o - \alpha \, [H_2CO_3]_i \right) + J_{H_2CO_3}^{prod} & (2.161) \\
J_{HCO_3^-} &= -\frac{P_{HCO_3^-}}{\mathcal{R}} \frac{F \, V_m}{R \, T} \frac{[HCO_3^-]_o - [HCO_3^-]_i \, \exp(-\frac{V_m F}{R T})}{1 - \exp(-\frac{V_m F}{R T})} + J_{HCO_3^-}^{prod}. & (2.162)
\end{aligned}
$$

For an overview of all fluxes related to the bicarbonate model extension see Figure 2.20.
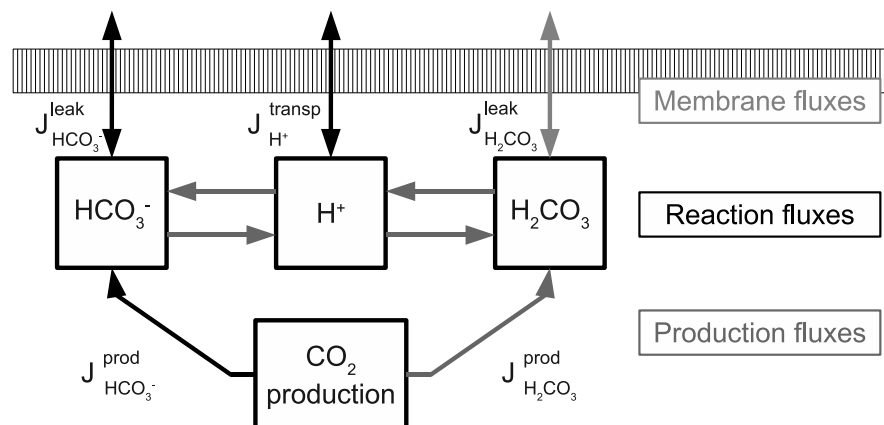
Figure 2.20: *Schematic of fluxes related to the CO_2 model extension. Grey arrows indicate electroneutral and black arrows indicate charge carrying fluxes.*

Model system including bicarbonate reaction

$$
\begin{aligned}
\frac{d}{dt}[K^+]_i &= -(J_K^{Trk1,2} + J_K^{Tok1} + J_K^{Nha1} + J_K^{leak}) \\
\frac{d}{dt}[CO_2]_i &= -(J_{H_2CO_3} + J_{HCO_3^-}) \\
\frac{d}{dt}pH_i &= \frac{1}{\beta}(J_H^{Pma1} + J_H^{leak} + J_H^{Nha1} + (1-\alpha)J_{H_2CO_3} - \alpha J_{HCO_3^-}) \\
&= \frac{1}{\beta}(J_H^{Pma1} + J_H^{leak} + J_H^{Nha1} + J_H^{react}) \\
\frac{d}{dt}V_m &= -\frac{1}{c_m}\left(I_K^{Trk1,2} + I_K^{Tok1} + I_K^{Nha1} + I_K^{leak} \right. \\
&\qquad\qquad \left. I_H^{Pma1} + I_H^{leak} + I_H^{Nha1} + I_{HCO_3^-} \right)
\end{aligned}
$$

From the change of CO_2, only the charge carrying flux $J_{HCO_3^-}$ is incorporated in the membrane potential (H_2CO_3 is uncharged). Electroneutral fluxes $(1-\alpha)J_{H_2CO_3}$ and $\alpha J_{HCO_3^-}$) are not taken into account. In the stationary state the following conditions must be fulfilled

(1) $J_K = 0$

(2) $-J_{H_2CO_3} = J_{HCO_3^-}$

(3) $J_H^{transp} = -(1-\alpha)J_{H_2CO_3} + \alpha J_{HCO_3^-}$

(4) $J_H^{transp} = J_{HCO_3^-}$.

In the following considerations J_K can be neglected. From (2) and (3) it follows that $-J_{H_2CO_3} = J_H^{transp}$. Inserting (4) into (3) yields expression (2): $-J_{H_2CO_3} = J_{HCO_3^-}$. Both conditions together result in $-J_{H_2CO_3} = J_{HCO_3^-} = J_H^{transp}$. In words: In the stationary state, the net influx/production of carbonic acid is compensated by an equivalent net efflux of hydrogen carbonate and protons (*vice versa*). This appears reasonable since the dissociation products of carbonic acid should be constantly removed from the cell. The model including the bicarbonate reaction scheme is referred as model version $\mathcal{M}_3$; see Table 3.1.

3 Results

A useful mathematical model can to make testable predictions which provide deeper insights and suggest new experiments. An important step of modeling is the calibration to experimental data. This step is essential for the systems biology cycle of prediction, experimental validation and model improvement (see Figure 1.1).

The goal of this thesis is a deeper mechanistic understanding of potassium homeostasis under starvation conditions. The data basis for that is provided by the experiments of Navarrete et al. (2010) that were described in Section 2.1.3. As a result it is predicted that the antiporter Nha1 decreases its activity in response to potassium shortage.

The bicarbonate reaction is another important process involved in potassium homeostasis. It is shown that the transient activation of this reaction is essential for homeostatic regulation. A new mathematical approach, called reverse tracking algorithm was developed for this purpose. The predictions were experimentally verified and change the prevailing view of potassium homeostasis.

3.1 Initial model
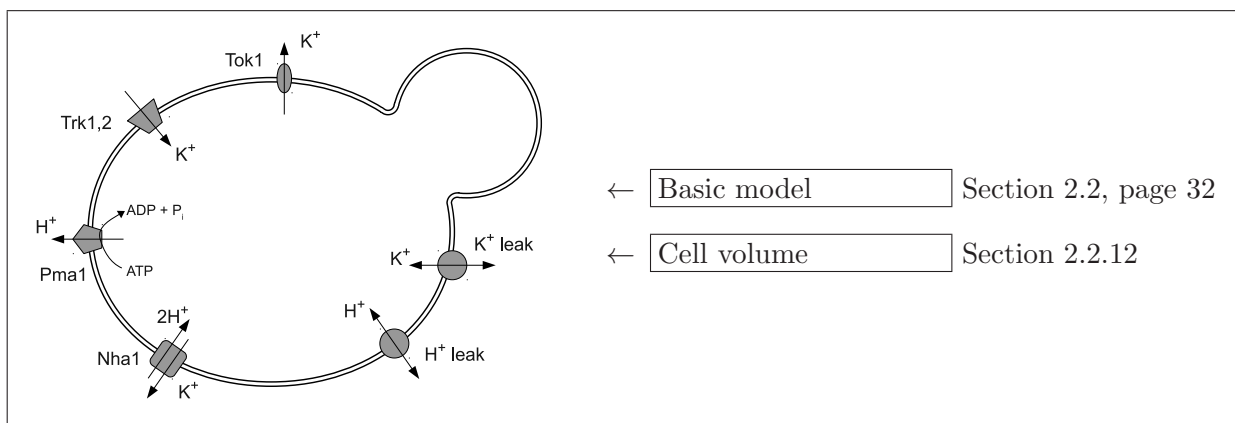
Figure 3.1: *Scheme of the first approach. The cell is considered as one compartment and the transport systems for potassium and protons are Trk1,2, Nha1, Tok1, Pma1 as well as the leakage currents.*

In this section the initial model versions $\mathcal{M}_1$ and $\mathcal{M}_2$ are introduced which are further improved in Section 3.2 (version $\mathcal{M}_3$); see Table 3.1. The first model describes the cell as a single compartment and incorporates only potassium and protons. The related transport systems are Trk1,2, Nha1, Tok1, Pma1 as well as the leakage currents for protons and potassium (see Figure 3.1). For both species influx and efflux systems are included in the model.

The primary source of energy is the ATP driven efflux of protons via Pma1. This establishes an inward directed proton gradient, which energizes Nha1 and the proton leak. Both systems mediate an uptake of protons. The extrusion of protons by Pma1 generates and maintains the membrane

Model $\mathcal{M}_1$	Nha1 w/o gating	/
Model $\mathcal{M}_2$	Nha1 gating	/
Model $\mathcal{M}_3$	Nha1 gating	bicarbonate react.

Table 3.1: *Overview of the three different model versions used in this section. $\mathcal{M}_1$ uses the ohmic model for Nha1, while $\mathcal{M}_2$ assumes a voltage gating. This model version is further extended by the bicarbonate reaction system ($\mathcal{M}_3$).*

voltage. This energizes the uptake of potassium via Trk1,2.

This uptake is balanced by the extrusion of potassium via Nha1. Tok1 is also known to mediate an potassium efflux. However, it was found to be inactive in the model simulations.

All transport processes are coupled by the membrane potential and the volume. The buffering of protons is covered by a constant buffer capacity. A special case is chloride, which is not considered as a transported ion due to its very low cytosolic concentration, but has to be taken into account for the external osmotic pressure.

Before the model approach is described in detail, the reader is reminded to the following conventions. Sign convention of the mass fluxes (J):

- Influx $J < 0$

- Efflux $J > 0$

Relationship between current density (I) and mass flux (J)

$$I = z \cdot F \cdot J \cdot \mathcal{R} \,. \tag{3.1}$$

Parameters and units can be found in Section 2.2. For a better understanding of the model behavior, the current-voltage relationships for the transport systems in Figure 2.15 might be helpful.

The complete model system is described below

$$\frac{d}{dt}[K^+]_i = -J_K \quad = \quad -\left(J_K^{Trk1,2} + J_K^{Nha1} + J_K^{Tok1} + J_K^{K,leak} \right) \tag{3.2}$$

$$\frac{d}{dt}pH_i = \frac{1}{\beta}J_H \quad = \quad \frac{1}{\beta}\left(J_H^{Pma1} + J_H^{Nha1} + J_H^{H,leak} \right) \tag{3.3}$$

$$\frac{d}{dt}V \quad = \quad L_p \cdot A \cdot (\Pi_i - \Pi_o - \Pi_t) \,. \tag{3.4}$$

The different transport systems are modeled as

$$I_K^{Trk1,2} \quad = \quad \frac{g_{Trk1,2} \cdot \mathcal{S}}{1 + e^{d_{Trk1,2} \cdot \frac{zF}{RT}(V_m - V_{Trk1,2}^{1/2})}} \cdot (V_m - E_{Trk1,2}) \tag{3.5}$$

$$I_K^{Nha1} \quad = \quad -\frac{g_{Nha1} \cdot \mathcal{S}}{1 + e^{d_{Nha1} \cdot \frac{zF}{RT}(V_m - V_{Nha1}^{1/2})}} \cdot (V_m - E_{Nha1}) \tag{3.6}$$

$$I_K^{Tok1} \quad = \quad \frac{g_{Tok1} \cdot \mathcal{S}}{1 + e^{d_{Tok1} \cdot \frac{zF}{RT}(V_m - V_{Tok1}^{1/2})}} \cdot (V_m - E_{Tok1}) \tag{3.7}$$

$$I_K^{K,leak} \quad = \quad g_{K,leak} \cdot \mathcal{S} \cdot (V_m - E_{K,leak}) \tag{3.8}$$

$$I_H^{Pma1} \;=\; I_{Pma1}^{max} \cdot \mathcal{S} \cdot \tanh\left(\frac{zF}{2RT}\left(V_m - \left(E_H + \frac{\Delta G_{ATP}}{F}\right)\right)\right) \tag{3.9}$$

$$I_H^{Nha1} \;=\; -2 \cdot I_K^{Nha1} \tag{3.10}$$

$$I_H^{H,leak} \;=\; g_{H,leak} \cdot \mathcal{S} \cdot (V_m - E_{H,leak}) \;. \tag{3.11}$$

Equation (3.6) incorporates already a voltage gating mechanism for Nha1 ($\mathcal{M}_2$). This is compared to a simpler description with a constant conductivity $\mathcal{M}_1$.

The membrane potential is calculated by the charge difference; see Section 2.2.3

$$V_m \;=\; -\frac{F \cdot \mathcal{R}}{c_m}\left(\beta pH_i - [K^+]_i - [X]\right) \tag{3.12}$$

$$V_m \;=\; \mathcal{F}\left(\beta pH_i - [K^+]_i - [X]\right) , \tag{3.13}$$

where $[X]$ sums up all fixed charges. In each model simulation $[X]$ was defined by the choice of $[K^+]_i(0)$, $pH_i(0)$, $V(0)$ and $V_m(0)$.

Equilibrium potentials

$$E_{Trk1,2} = E_{K,leak} = E_{Tok1} \;=\; \frac{RT}{zF}\ln\frac{[K^+]_o}{[K^+]_i} \tag{3.14}$$

$$E_{Nha1} \;=\; \frac{RT}{zF}\ln\left(\frac{[K^+]_i}{[K^+]_o} \cdot \frac{[H^+]_o^2}{[H^+]_i^2}\right) \tag{3.15}$$

$$E_{H,leak} = E_H \;=\; \frac{RT}{zF}\ln\frac{[H^+]_o}{[H^+]_i} \;. \tag{3.16}$$

Osmotic pressure

$$\Pi_o \;=\; \left([K^+]_o + [H^+]_o + [Cl^-]_o + [Z]_o\right) \cdot RT \tag{3.17}$$

$$\Pi_i \;=\; \frac{V}{V - f_V \cdot V(0)} \cdot \left([K^+]_i + [H^+]_i + [Z]_i\right) \cdot RT \tag{3.18}$$

$$\Pi_t \;=\; \Pi_t(0) \cdot \frac{V - V^{\Pi_t=0}}{V(0) - V^{\Pi_t=0}} \tag{3.19}$$

$$\Pi_t(0) \;=\; \Pi_i(0) - \Pi_o(0) \tag{3.20}$$

$$V^{\Pi_t=0} \;=\; k_V \cdot V(0) \;. \tag{3.21}$$

In the starvation experiment, external potassium is removed in a washing procedure. In the model this is described by the following process

$$[K^+]_o(t) = [Cl^-]_o(t) = \begin{cases} 0.05\,\frac{\mathsf{mmol}}{\mathsf{cm}^3}, & \text{for } t < 0\,\mathsf{s}, \\ 15 \cdot 10^{-6} + \left(0.05 - 15 \cdot 10^{-6}\right) \cdot \exp\left(-\left(\frac{t-\mu}{\sigma}\right)^2\right)\,\frac{\mathsf{mmol}}{\mathsf{cm}^3}, & \text{otherwise} \end{cases} \tag{3.22}$$

where $\mu = 0$ and $\sigma = 0.04 \cdot 60^2\,sec$. The definition is similar to the classic Gaussian curve. The choice of σ controls the duration of the potassium drop. Larger values mean a longer time to switch between the concentrations (and *vice versa*). Here, the value of σ means a potassium drop from 50 mM to 15 μM in less than ten minutes. According to a personal communication with the authors of Navarrete et al. (2010), this time corresponds roughly to the time it took to wash the cells twice in potassium free medium. The washing procedures is meant to reduce the potassium adhered at the cell sample. This can hardly be thought as a kind of binary concentration switch, since the

Variable	Value	Unit	Description	Reference
$[K^+]_i(0)$	0.2	mmol/cm^3	initial $[K^+]_i$	
$pH_i(0)$	6.9	pH	initial pH_i	
$V(0)$	48	fL	initial volume	
$V_m(0)$	-0.2	V	initial membr. pot.	
c_m	1	μF/cm^2	specific membrane capacitance	Hille (2001)
β	0.2	mmol/cm^3/pH	H$^+$ buffer capacity	Section 2.2.11
$g_{Trk1,2}$	23	μS/cm^2	conductance Trk1,2	Section 2.2.4
$d_{Trk1,2}$	1	dimensionless	voltage sensitivity	Section 2.2.4
$V_{1/2,Trk1,2}$	-0.168	V	half maximal voltage	Section 2.2.4
g_{Tok1}	8	μS/cm^2	conductance Tok1	Section 2.2.8
d_{Tok1}	-1	dimensionless	voltage sensitivity	Section 2.2.8
V_{Tok1}	-0.0034	V	half maximal voltage	Section 2.2.8
g_{Nha1}	12	μS/cm^2	conductance Nha1	Section 2.2.5
d_{Nha1}	-1	dimensionless	voltage sensitivity	Section 2.2.5
$V_{1/2,Nha1}$	-0.315	V	half maximal voltage	Section 2.2.5
I_{Pma1}^{max}	16	μA/cm^2	maximal pump current	Section 2.2.9
ΔG_{ATP}	$-40 \cdot 10^6$	μJ/mmol	energy ATP hydrolysis	Section 2.2.9
$g_{K,leak}$	5	μS/cm^2	conductance	Section 2.2.6
$g_{H,leak}$	25	μS/cm^2	conductance	Section 2.2.7
$[K^+]_o$	0.05 to $15 \cdot 10^{-6}$	mmol/cm^3	external potassium	Section 2.1.3
$[Cl^-]_o$	0.05 to $15 \cdot 10^{-6}$	mmol/cm^3	external potassium	Section 2.1.3
pH_o	5.8	pH	external pH	Section 2.1.3
A		cm^2	cell surface	
$\mathcal{R}$		cm	volume to surface ratio	
$\mathcal{S}$		dimensionless	surface scaling $A(0)/A$	Section 2.2.12
L_p	$4 \cdot 10^{-11}$	cm^4/μJ/s	hydraulic conductivity	Section 2.2.12
k_V	0.5	dimensionless	elasticity of the cell wall	Section 2.2.12
f_V	0.37	dimensionless	fraction of non-osmotic volume	Section 2.2.12
Π		μJ/cm^3 = Pa	osmotic pressure	
$[Z]_o$	0.23	mmol/cm^3	osmotic active conc. extern	Section 2.1.3
$[Z]_i$	0.2	mmol/cm^3	osmotic active conc. intern	Section 2.2.12

Table 3.2: *Parameters used in the basic model. Parameter values for the different transport systems were either taken from literature or adapted to the experimental data.*

subsequent centrifugation after the washing goes along with a denser packing of the cells, where the cells might sense a potassium loss of their neighbors. Thus, the assumption a smooth transition between both concentrations appears reasonable.

According to personal communication with José Ramos, the ratio of cell volume to medium volume is 1:10 000. In addition the sample is continuously stirred. This justifies the assumption of a constant external potassium concentration. The internal sodium concentration is around 10-15 mM in the whole period of the measurements (personal communication with the authors). The external potassium is at 1.7 mM. Since the internal concentration does not change and the external sodium is rather low, it is unlikely, that sodium is transported in relevant amounts under these conditions. Thus, sodium is excluded from the following considerations.

With the initial values from Table 3.2 the system relaxes to the stationary values $[K^+]_i = 0.2\,$mmol/cm^3, $pH_i = 6.9\,$pH, $V = 48\,$fL and $V_m = -0.214\,$V. At the stationary state a linear stability analysis was performed. The general solution of a linear homogeneous system of n differential
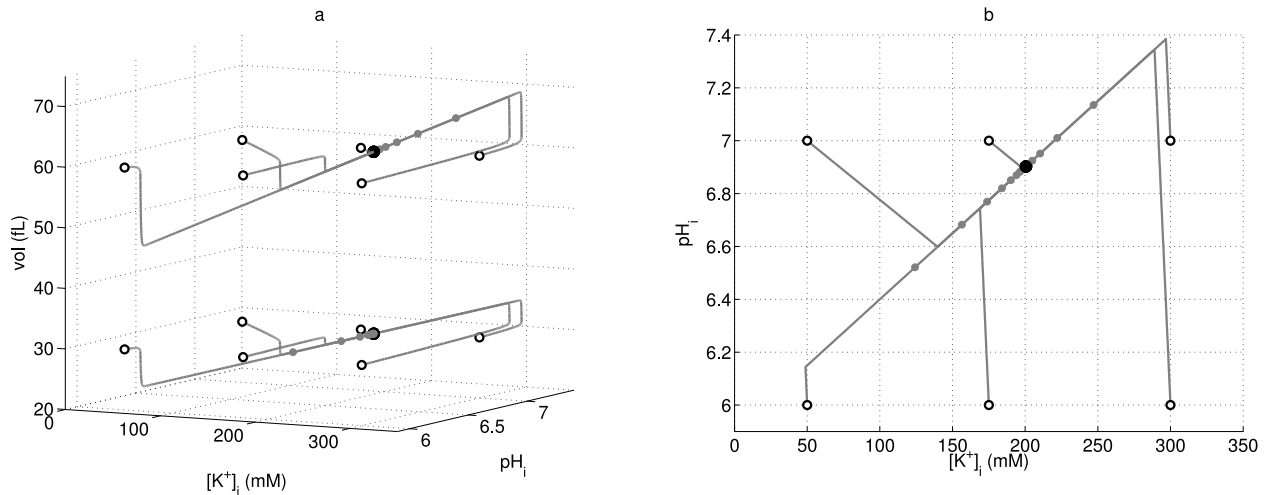
Figure 3.2: *Phaseportrait: relaxation from initial values (open circles) to the stationary state (black solid circle). Grey dots on the trajectories for the initial values $[K^+]_i(0) = 50\,\text{mM}$, $pH_i(0) = 6\,\text{pH}$, $V(0) = 30\text{fL}$ and $[K^+]_i(0) = 300\,\text{mM}$, $pH_i(0) = 7\,\text{pH}$, $V(0) = 70\text{fL}$ indicate 5 minutes steps. (a) three dimensional phase-portrait of the whole model system. (b) phaseportrait for model system with a constant volume of 48 fL.*

equations

$$\dot{\mathbf{y}} = \mathbf{A}\,\mathbf{y}\,, \tag{3.23}$$

has the form

$$\mathbf{y}(t) = \sum_{i=1}^{n} c_i \mathbf{v}_i e^{\lambda_i t}\,, \tag{3.24}$$

with $1 \times n$ vector $\mathbf{y}$, $n \times n$ matrix $\mathbf{A}$, eigenvalues λ_i, eigenvectors $\mathbf{v}_i$ and constants c_i defined by the initial conditions.

Here, all eigenvalues have a negative sign which indicates a stable stationary state; see Table 3.3. Positive or imaginary values were never observed in any model simulation. The eigenvalues define three different time scales, where the fast systems dynamics is mainly governed by λ_1. As a consequence, the system relaxes quickly to a manifold in the $\mathbf{v}_2$, $\mathbf{v}_3$ plane for time $t > \frac{1}{|\lambda_1|}$; see Figure 3.2. This corresponds to the fast loss of potassium after starvation; see Section 3.1.1.

eigenvalues	eigenvectors
$\lambda_1 = -83.5$	$\mathbf{v}_1 = (-0.15,\, 0.99,\, 0)^T$
$\lambda_2 = -0.0024$	$\mathbf{v}_2 = (-0.2,\, 0.98,\, 0)^T$
$\lambda_3 = -1.3$	$\mathbf{v}_3 = (0.15,\, -0.99,\, 0)^T$

Table 3.3: *Eigenvalues and eigenvectors at the stationary state.*

To quantify and compare the influence of the parameter changes on the stationary state, a sensitivity analyses was performed. The sensitivity, S, gives the percentage change of the stationary variable per percentage change of the respective parameter. Generally, the sensitivity of a variable
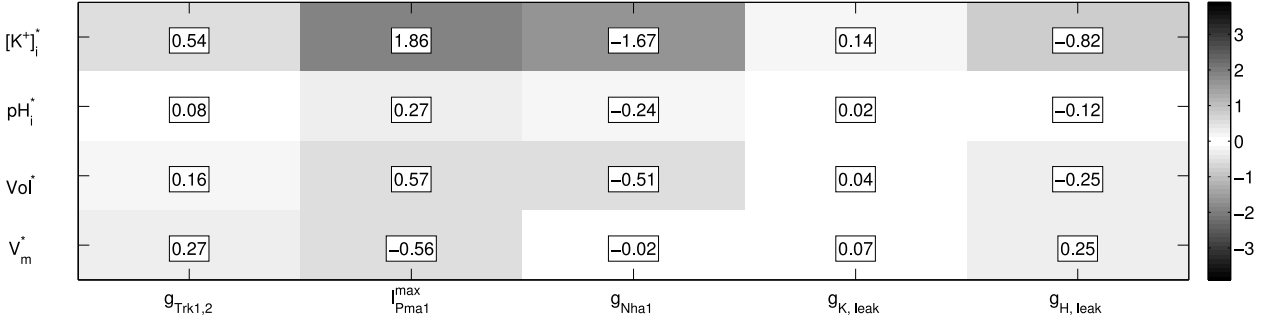
Figure 3.3: *Sensitivity of the stationary state. For each of the variables indicated on the x-axis the sensitivity of the stationary value indicated on the y-axes was calculated. The sign indicates, whether the component increases (positive) or decreases (negative) with a growth in the different parameters.*

y to a parameter x is defined as (Klipp et al. 2005)

$$\frac{x}{y}\frac{\partial y}{\partial x} \approx \frac{x}{y}\frac{\Delta y}{\Delta x}, \tag{3.25}$$

where Δ indicates finite differences. Approximating the derivatives, the sensitivity of the stationary potassium concentration, pH, membrane potential and volume to chnages in the conductivity $g_{Trk1,2}$ can be given as (other parameters follow analogously)

$$\mathbf{S}^*_{Trk1,2} = \begin{pmatrix} \frac{g_{Trk1,2}}{[K^+]^*_i} \cdot \frac{^{up}[K^+]^*_i - [K^+]^*_i}{(1+p-1)g_{Trk1,2}} \\[2mm] \frac{g_{Trk1,2}}{pH^*_i} \cdot \frac{^{up}pH^*_i - pH^*_i}{(1+p-1)g_{Trk1,2}} \\[2mm] \frac{g_{Trk1,2}}{V^*} \cdot \frac{^{up}V^* - V^*_m}{(1+p-1)g_{Trk1,2}} \\[2mm] \frac{g_{Trk1,2}}{|V^*_m|} \cdot \frac{^{up}V^*_m - V^*_m}{(1+p-1)g_{Trk1,2}} \end{pmatrix} = \begin{pmatrix} \frac{1}{[K^+]^*_i} \cdot \frac{^{up}[K^+]^*_i - [K^+]^*_i}{p} \\[2mm] \frac{1}{pH^*_i} \cdot \frac{^{up}pH^*_i - pH^*_i}{p} \\[2mm] \frac{1}{V^*} \cdot \frac{^{up}V^* - V^*_m}{p} \\[2mm] \frac{1}{|V^*_m|} \cdot \frac{^{up}V^*_m - V^*_m}{p} \end{pmatrix}, \tag{3.26}$$

where $p = 0.1$ gives an increase in $g_{Trk1,2}$, superscript * denotes the stationary values and superscript ^{up} denotes the stationary value obtained with the increased parameter value. The respective results for $g_{Trk1,2}$, g_{Nha1}, I^{max}_{Pma1}, $g_{K^+,leak}$ and $g_{H^+,leak}$ can be found in Figure 3.3. This consideration allows also to prove, whether the role of a transporter in the model system matches the expected physiological properties.

In all cases, the stationary potassium concentration shows the highest sensitivity to parameter changes, especially to g_{Nha1} and I^{max}_{Pma1}. The influence of Trk1,2 is apparently lower compared to Nha1 and Pma1. These findings will be discussed further in Section 3.2.

Trk1,2 and K^+ leak   The influence of Trk1,2 and the potassium leak is very similar, whereas the effect of Trk1,2 is more pronounced: An increase in the respective conductivity leads to an increase in the stationary potassium value. Due to the uptake of positive charges, this goes in parallel with a depolarization of the membrane and an increase in the volume. The stationary pH is also increased, because the uptake of potassium is driven and balanced by the extrusion of protons.

Pma1 and H$^+$ leak An increased I_{Pma1}^{max} leads to a hyperpolarization and an increase of the potassium concentration. Concomitantly, the pH is growing due to the extrusion of protons. This reflects the accepted mechanism of proton extrusion driven potassium uptake.

Being a proton influx system, changes in the proton leak yield opposite results compared to Pma1.

Nha1 The increase of g_{Nha1} decreases each stationary value. The reduction of the intracellular potassium mirrors the potassium extrusion via Nha1. The concomitant uptake of protons leads to a decrease of the pH. These results could be expected from Nha1's physiological function. A counterintuitive result is the decrease of the membrane potential, since the net uptake of Nha1 is 1 positive charge per turn. Thus, a depolarization could have been expected. However, the present observation can be explained by the coupling of the systems variables and the involvement of two counteracting processes. The one is the uptake of positive charges, which leads in principle to a depolarization. The other effect stems from the resulting pH decrease. The lower the pH, the lower is the equilibrium potential for Pma1; see Section 2.2.10. This leads to a higher Pma1 current, which goes along with a hyperpolarization. Together, both concurrent processes result in a weak hyperpolarization.

This observation is in agreement with the hyperpolarization in Nha1 overexpressing cells reported by Kinclova-Zimmermannova et al. (2006).

3.1.1 Simulated potassium starvation experiment

The internal concentration change of potassium, the course of the pH as well as the relative membrane potential are known from the measurements. The data points give the constraints for the results of the model simulation. For the membrane potential, only the qualitative behavior can be assessed, since absolute values are not available.

After analyzing basic properties of the model system the potassium starvation experiment of Navarrete et al. (2010) is simulated; see Section 2.1.3. The mathematical expressions for the transporters as well as the respective parameter values follow the description given at the beginning of this section. The initial values were taken from Table 3.3. Model versions $\mathcal{M}_1$ and $\mathcal{M}_2$ are analyzed in parallel.

Potassium For the internal potassium, there are two results:

- When the external potassium drops, the internal potassium rapidly decreases within minutes, whereas the data shows a decrease over several hours

- Without the Nha1 voltage gating, the internal potassium is almost completely lost. The voltage dependent Nha1 deactivation allows a stationary potassium concentration around 30 mM.

Both findings point to the central topics of this work. The experience, that after the external potassium drop a non-zero $[K^+]_i$ could only achieved by a deactivation of Nha1 led to the indispensable implementation of the Nha1 voltage gating (model $\mathcal{M}_2$). As a vital part of the model, all following simulations deal with the Nha1 gating.
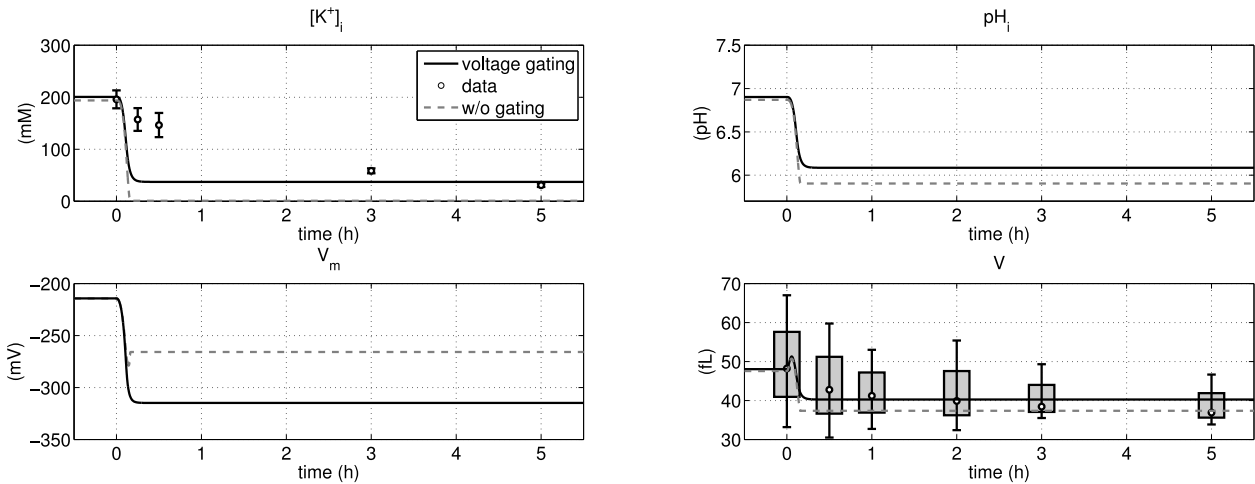
Figure 3.4: *Simulated potassium starvation experiment. The result is shown for the case of a Nha1 voltage gating (black line) and without gating (gray line). The data points represent the data of Navarrete et al. (2010); see also Section 2.1.3. The errorbars gives the 95% confidence interval. The drop of external potassium occurs at time point 0. In case of $[K^+]_i$, the Nha1 voltage gating prevents the total loss of potassium. The simulated potassium concentration reaches a stationary value at 30 mM. Contrary to the experimental data, $[K^+]_i$ is reduced rapidly. For pH_i the data shows a rather constant value, where the simulation shows a decrease of the pH. This decrease is higher in the case without Nha1 gating. The membrane potential, V_m, shows a hyperpolarization as a result of the potassium drop. The volume, V, shows a transient increase at time point zero. Overall, all variables follow the dynamic behavior of the external potassium.*

The other point is the dynamics of the system. The central aim of this work is to understand the mechanisms governing the internal potassium dynamics under low external potassium. The main efforts were focused on the development of regulatory systems, which allow a slower reduction of the internal potassium.

pH   The other variables follow the course of potassium. The internal pH rapidly drops by approximately one pH unit. Due to the constraint of electroneutrality, the loss of the positively charged potassium must be compensated by the uptake of protons. This leads to the reduced pH, which was reported for potassium starved cells in the literature; (Rodriguez-Navarro 2000) and references therein. This finding is in contradiction with the rather constant pH observed in Navarrete et al. (2010). [↻]   However, several repetitions of the experiment[1] confirmed a slow pH decrease during starvation. These preliminary data sets indicate, that the simulated pH drop is qualitatively correct.

Membrane potential   Following the general behavior of the internal potassium, the membrane potential hyperpolarizes as a direct effect of the loss of positive charges. The potassium loss is up to the activity of Nha1. Since the there is a net uptake of one positive charge per turn, the larger potassium reduction in the ohmic approach, goes is parallel with the uptake of more positive charges compared to the case of the Nha1 voltage gating. This explains, why the membrane voltage stays more positive in the case of the ohmic approach. A value for $V_m < -300$ mV may appear as too low for *S. cerevisiae*.

---

[1]Experimenters: Daniel Ganser, Jost Ludwig, Universität Bonn, Institut für Zelluläre und Molekulare Botanik (IZMB); Silvia Petrezsélyová, Olga Kinclova, Institute of Physiology, Academy of Sciences of the Czech Republic, Prague

Volume   Despite a low and transient increase, the volume follows closely the dynamics of the internal potassium. With constant external conditions, the volume changes only with the internal osmotic pressure, Π_i, which mainly depends on $[K^+]_i$. In this case, the external potassium drops more rapidly than the internal potassium. This causes a transient increase in the difference of the internal and external osmotic pressure, $\Pi_i - \Pi_o$. Since *in vivo* there will be a time delay between the external potassium drop and the sensing of the external osmotic pressure change, this increase can be considered rather as an artifact. In addition the parameter, $k_V = 0.5$, means a very flexible cell wall, which supports a sensitive reaction on osmotic changes. The original work of Gennemark et al. (2006), deals with a very rigid cell wall ($k_V = 0.99$). Using this value in the current simulation would lead to an almost constant cell volume.

Transport systems

The modeling of each single transport system allows to observe the simulated activity of a certain system, which can hardly be experimentally observed. Figure 3.6 shows the simulated potassium currents for Trk1,2, Nha1, Pma1 and the leak.

The transporter currents are weakly affected by the proposed voltage gating and the general behavior is very similar for both Nha1 approaches. When the external potassium is removed, the systems react with a transient change and reach a new stationary level after ten minutes of starvation. However, these changes are so small that they can be hardly detected by experiments. This finding rules out the possibility to prove the proposed voltage gating indirectly by a special behavior of a certain system.

Figure 3.6 gives the total potassium and proton currents $I_K = I_K^{Trk1,2} + I_K^{Nha1} + I_K^{Tok1} + I_K^{K,leak}$ and $I_H = I_H^{Pma1} + I_H^{Nha1} + I_H^{H,leak}$. The constraint of electroneutrality requires the compensation of the potassium efflux by an equivalent proton uptake.
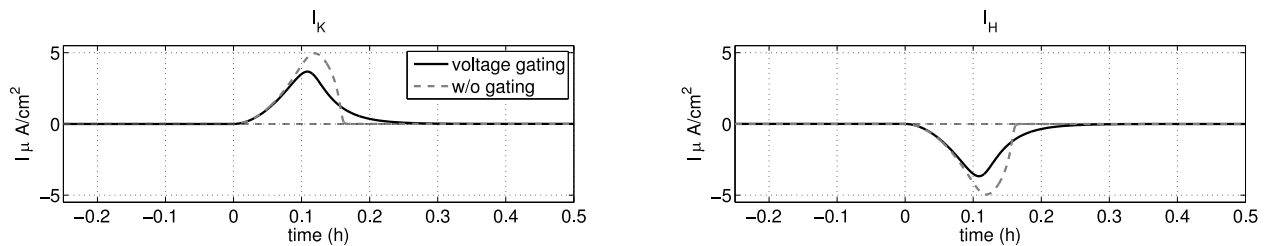
Figure 3.5: *Total sum of transporter currents for potassium and protons. The black line indicates the result for $\mathcal{M}_2$ and the gray line for $\mathcal{M}_1$. Before and several minutes after the external potassium drop (t = 0), the net currents of potassium and protons are zero, which indicates, that the influx of a species is balanced by an equivalent efflux. The external potassium reduction disturbs this equilibrium. The positive potassium current shows an efflux of potassium (left panel). Due to the constraints of the electro-neutrality, this efflux is compensated by a parallel uptake of protons (right panel). Without the voltage gating, the potassium current reaches higher values. Respectively, this causes a higher efflux of potassium. This rapid extrusion depletes all most all potassium and the system returns to a net potassium current of zero. In the case of the voltage gating, the return to the stationary current is apparently smoother.*
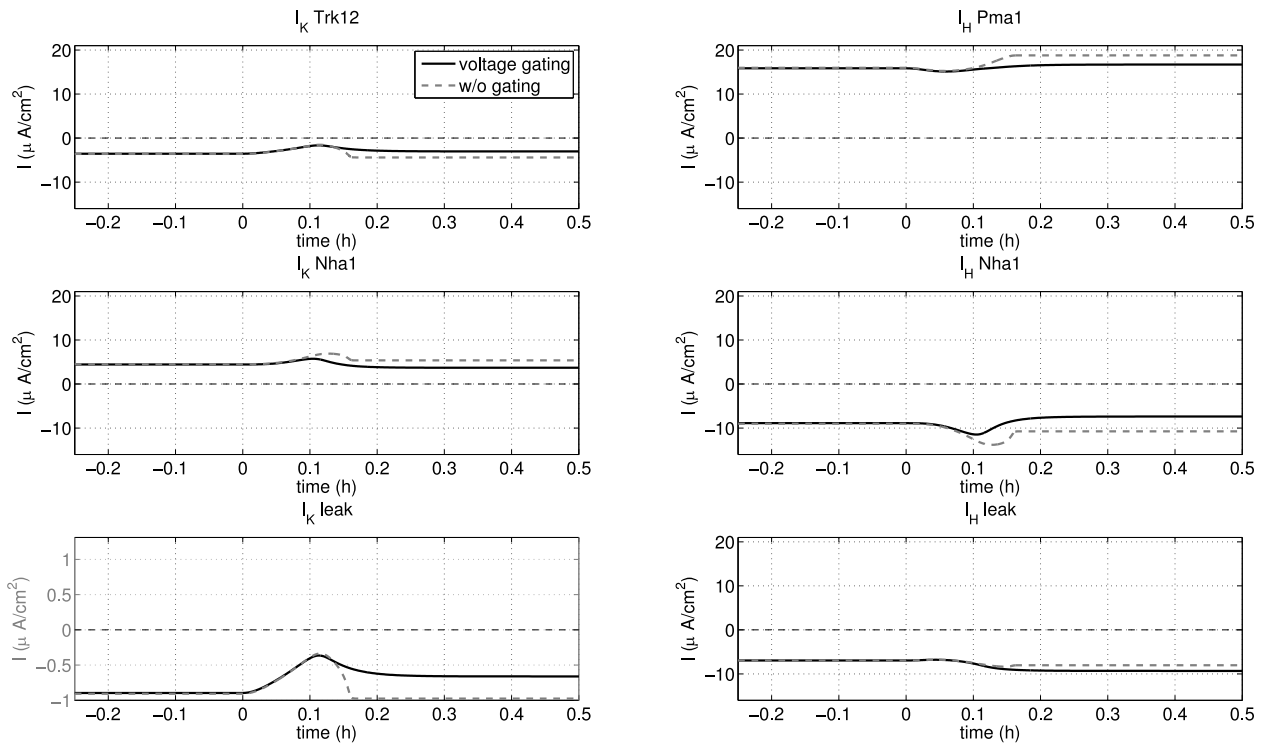
Figure 3.6: *Simulated current mediated by the transport systems. The potassium drop occurs at time point zero. Before and some minutes after the potassium drop, the currents are on a stationary level. The gray line represent the simulation of $\mathcal{M}_1$ and the black $\mathcal{M}_2$. The time axis is limited to the region, where the potassium drop occurs. Before and after that region the activity of the transporters stays constant. When the external potassium is reduced, the influx of potassium via Trk1,2 is reduced.*

3.1.2 Fast dynamics problem

Despite systematic studies of the transporters parameters, a change in the dynamic behavior of the system was not observed. The eigenvalues are not influenced in sign or magnitude. Two possible solutions were proposed.

Additional species

In the basic model versions $\mathcal{M}_1$ and $\mathcal{M}_2$ the charges of potassium are completely balanced by protons. Additional species might break the tight coupling of protons and potassium and introduce new degrees of freedom to the model. Bicarbonate and ammonium appeared as the most promising candidates.

Under the given conditions ammonium is the most abundant cation in the medium (around 90 mM, see 2.1.3). Due to Hess et al. (2006) ammonium can enter the cell via potassium transporters under potassium limiting conditions and it is reported, that ammonium can even reach toxic concentrations under such conditions. A respective model extension was developed, however, it turned out, that it can not describe the key aspects of homeostasis. Moreover, experimental findings by Joaquin Ariño and José Ramos showed a low influence of ammonium under starvation.

The role of bicarbonate in attracting potassium was investigated and discussed since the late 1960's in the work of Antonio Peña and coworkers (Peña et al. 1967, 1972, 1969; Peña 1975). A detailed mechanism of the connection between potassium and the bicarbonate fluxes was suggested

by Lopéz et al. (1999). Since the bicarbonate reaction is also a known proton buffer system, the metabolic release of CO_2 seems worth to study. The respective model extension turned out as promising; see Section 3.2.

Dynamic parameters

No single parameter was identified, which remarkably influences the systems dynamics. This led to the idea, that some parameters should be rather treated as dynamic variables to achieve the required flexibility. Parameters with a relatively high sensitivity coefficient appeared as most promising parameters; see Figure 3.3.

Key facts Section 3.1

- Key results
    - The dynamics of the system follows the dynamics of the external potassium drop. Certain parameters, parameter relationships or the combination of simple regulation mechanisms are not sufficient to slow down the systems dynamics
    - Additional species are suggested to break the tight coupling of potassium and proton fluxes. Ammonium and bicarbonate are considered as likely candidates

- Qualitative predictions in agreement with current knowledge
    - Pma1 driven potassium uptake
    - Hyperpolarization under potassium starvation
    - pH decrease under potassium starvation
    - volume reduction for decreased cytosolic K^+

- Testable model predictions
    - Nha1 must be deactivated in order to prevent the total loss of potassium under starvation. A voltage gating is suggested.
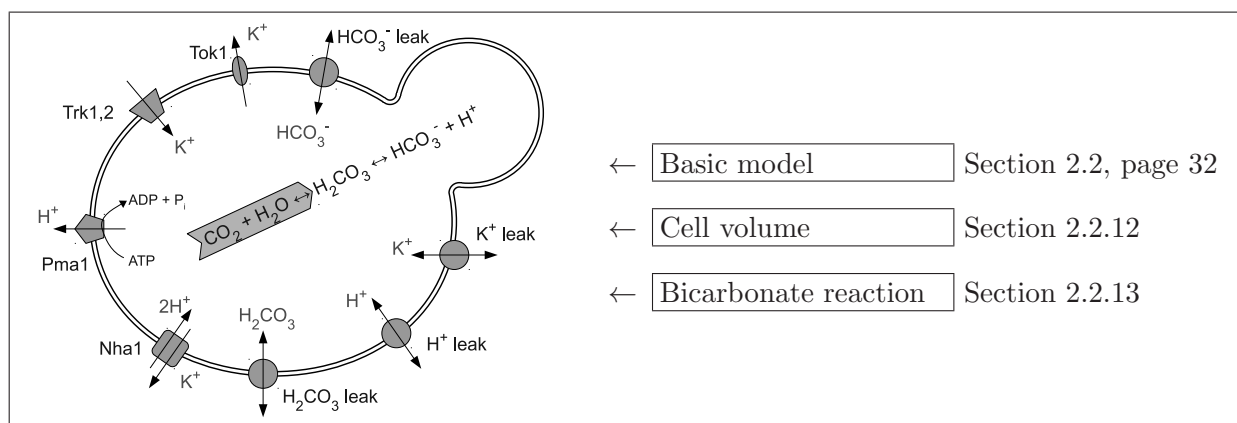
3.2 Bicarbonate model

Figure 3.7: *Schematic of a yeast cell. The respective model is composed from the initial model, osmotic effects and the bicarbonate reaction sequence.*

The inclusion of the bicarbonate reactions system turned out to be a crucial improvement of the model (version $\mathcal{M}_3$). However, the implementation of the CO_2 production *per se* did not slow down the dynamics of the potassium loss. It will be discussed later, that the reverse tracking approach for identifying unmodeled regulatory processes is a key advancement of this thesis. The related hypothesis were finally validated by experiments.

The bicarbonate reaction generates negative charges by producing impermeable HCO_3^- ions. This causes a lower membrane potential which counteracts the loss of potassium. However, the accumulation of HCO_3^- is restricted, since HCO_3^- and H^+ can form carbonic acid, which passively diffuses through the cell membrane; see Section 2.2.13.

The complete model equations for model version $\mathcal{M}_3$ are

$$\frac{d}{dt}[K^+]_i = -\left(J_K^{Trk1,2} + J_K^{Nha1} + J_K^{Tok1} + J_K^{leak} \right) \tag{3.27}$$

$$\frac{d}{dt}[CO_2]_i = -\left(J_{H_2CO_3} + J_{HCO_3^-} \right) \tag{3.28}$$

$$\frac{d}{dt}pH_i = \frac{1}{\beta}\left(J_H^{Pma1} + J_H^{Nha1} + J_H^{leak} + \right. \tag{3.29}$$

$$\left. +(1-\alpha)J_{H_2CO_3} - \alpha J_{HCO_3^-} \right) \tag{3.30}$$

$$\frac{d}{dt}V = L_p \cdot A \cdot (\Pi_i - \Pi_o - \Pi_t) . \tag{3.31}$$

The equilibrium conditions are equivalent to the findings in Section 2.2.13

$$J_{H_2CO_3} = -J_{HCO_3^-} = -J_H^{transp} . \tag{3.32}$$

The transport systems are modeled as

$$I_K^{Trk1,2} = \frac{g_{Trk1,2} \cdot \mathcal{S}}{1 + e^{d_{Trk1,2} \cdot \frac{zF}{RT}(V_m - V_{Trk1,2}^{1/2})}} \cdot (V_m - E_{Trk1,2}) \tag{3.33}$$

$$I_K^{Nha1} = -g_{Nha1} \cdot \mathcal{S} \cdot (V_m - E_{Nha1}) \tag{3.34}$$

$$I_K^{Tok1} = \frac{g_{Tok1} \cdot \mathcal{S}}{1 + e^{d_{Tok1} \cdot \frac{zF}{RT}(V_m - V_{Tok1}^{1/2})}} \cdot (V_m - E_{Tok1}) \tag{3.35}$$

$$I_K^{K,leak} = g_{K,leak} \cdot \mathcal{S} \cdot (V_m - E_{K,leak}) \tag{3.36}$$

$$I_H^{Pma1} = I_{Pma1}^{max} \cdot \mathcal{S} \cdot \tanh\left(\frac{zF}{2RT}\left(V_m - \left(E_H + \frac{\Delta G_{ATP}}{F} \right) \right) \right) \tag{3.37}$$

$$I_H^{Nha1} = -2 \cdot I_K^{Nha1} \tag{3.38}$$

$$I_H^{H,leak} = g_{H,leak} \cdot \mathcal{S} \cdot (V_m - E_{H,leak}) \tag{3.39}$$

$$J_{H_2CO_3} = \frac{P_{H_2CO_3}}{-\mathcal{R}}([H_2CO_3]_o - [H_2CO_3]_i) + J_{H_2CO_3}^{prod.} \tag{3.40}$$

$$J_{HCO_3^-} = \frac{P_{HCO_3^-}}{-\mathcal{R}}\frac{V_m F}{RT} \cdot \frac{[HCO_3^-]_o - [HCO_3^-]_i\, e^{\frac{-V_m F}{RT}}}{1 - e^{\frac{-V_m F}{RT}}} + J_{HCO_3^-}^{prod.} . \tag{3.41}$$

The membrane potential is modeled by the charge balance equation (see Section 2.2.3)

$$V_m = \mathcal{F}\left(\beta pH_i - [K^+]_i + [HCO_3^-]_i - [X]\right) \tag{3.42}$$

$$= \mathcal{F}\left(\beta pH_i - [K^+]_i + \frac{10^{-pH_i}}{10^{-pH_i} + 10^{-pK_A}}[CO_2]_i - [X]\right), \tag{3.43}$$

where $[X]$ sums up all fixed charges and is defined by the choice of $[K^+]_i(0)$, $pH_i(0)$, $V(0)$, $[CO_2]_i(0)$ and $V_m(0)$.

The fluxes related to the bicarbonate reaction are described as

$$J_H^{transp.} = J_H^{Pma1} + J_H^{Nha1} + J_H^{leak} \tag{3.44}$$

$$J_H^{CO_2 react.} = (1-\alpha)J_{H_2CO_3} - \alpha J_{HCO_3^-} \tag{3.45}$$

$$J_{H_2CO_3}^{prod.} = \alpha \cdot J_{CO_2}^{prod.} \tag{3.46}$$

$$J_{HCO_3^-}^{prod.} = (1-\alpha) \cdot J_{CO_2}^{prod.} \tag{3.47}$$

$$\alpha = \frac{[H^+]_i}{[H^+]_i + 10^{-pK_A}}, \tag{3.48}$$

with any convenient function $J_{CO_2}^{prod.}$. Note: The production rate is related to the volume the production rate has to be scaled according to

$$J_{CO_2}^{prod.} = \tilde{J}_{CO_2}^{prod.} \cdot \frac{V(0)}{V(t)}, \tag{3.49}$$

where $V(0)$ gives the initial volume. This covers the fact, that the produced amount of CO_2 should not change with the volume.

The equilibrium potentials are defined as

$$E_{Trk1,2} = E_{K,leak} = E_{Tok1} = \frac{RT}{zF}\ln\frac{[K^+]_o}{[K^+]_i} \tag{3.50}$$

$$E_{Nha1} = \frac{RT}{zF}\ln\left(\frac{[K^+]_i}{[K^+]_o} \cdot \frac{[H^+]_o^2}{[H^+]_i^2}\right) \tag{3.51}$$

$$E_{H,leak} = E_H = \frac{RT}{zF}\ln\frac{[H^+]_o}{[H^+]_i}. \tag{3.52}$$

The osmotic pressure and turgor pressure is calculated by

$$\Pi_o = \left([K^+]_o + [H^+]_o + [Cl^-]_o + [CO_2]_o + [Z]_o\right) \cdot RT \tag{3.53}$$

$$\Pi_i = \frac{V}{V - k_V \cdot V(0)} \cdot \left([K^+]_i + [H^+]_i + [CO_2]_i + [Z]_i\right) \cdot RT \tag{3.54}$$

$$\Pi_t = \Pi_t(0) \cdot \frac{V - f_V \cdot V(0)}{V(0) - f_V \cdot V(0)} \tag{3.55}$$

$$\Pi_t(0) = \Pi_i(0) - \Pi_o(0). \tag{3.56}$$

Variable	Value	Unit	Description	Reference
β	0.2	mmol/cm^3/pH	H$^+$ buffer capacity	Section 2.2.11
$g_{Trk1,2}$	23	μS/cm^2	conductance Trk1,2	Section 2.2.4
$d_{Trk1,2}$	1	dimensionless	voltage sensitivity	Section 2.2.4
$V_{1/2,Trk1,2}$	-0.168	V	half maximal voltage	Section 2.2.4
$\tilde{J}^{prod.}_{CO_2}$	8e-5	$\frac{mmol}{cm^3 s}$	CO$_2$ production rate	tentative
g_{Tok1}	9	μS/cm^2	conductance Tok1	Section 2.2.8
d_{Tok1}	-1	dimensionless	voltage sensitivity	Section 2.2.8
V_{Tok1}	-0.0034	V	half maximal voltage	Section 2.2.8
g_{Nha1}	13	μS/cm^2	conductance Nha1	tentative
d_{Nha1}	-1	dimensionless	voltage sensitivity	tentative
$V_{1/2,Nha1}$	-0.310	V	half maximal voltage	tentative
I^{max}_{Pma1}	13	μA/cm^2	maximal pump current	Section 2.2.9
ΔG_{ATP}	$-40 \cdot 10^6$	μJ/mmol	energy ATP hydrolysis	Section 2.2.9
$g_{K,leak}$	5	μS/cm^2	conductance	Section 2.2.6
$g_{H,leak}$	25	μS/cm^2	conductance	Section 2.2.7
$P_{H_2CO_3}$	$6 \cdot 10^{-3}$	cm/s	permeability	Boron and de Weer (1976)
$P_{HCO_3^-}$	$5 \cdot 10^{-7}$	cm/s	permeability	Boron and de Weer (1976)
pK_A	6.35	dimensionless	acidity constant H$_2$CO$_3$	Lopéz et al. (1999)
A		cm^2	cell surface	
$\mathcal{R}$		cm	volume to surface ratio	
$\mathcal{S}$		dimensionless	surface scaling $A(0)/A$	Section 2.2.12
L_p	$4 \cdot 10^{-11}$	cm^4/μJ/s	hydraulic conductivity	Section 2.2.12
k_V	0.5	dimensionless	elasticity of the cell wall	Section 2.2.12
f_V	0.37	dimensionless	fraction of non-osm. vol.	Section 2.2.12
Π		μJ/cm^3 = Pa	osmotic pressure	
$[Z]_o$	0.23	mmol/cm^3	osmotic active conc. extern	Section 2.1.3
$[Z]_i$	0.2	mmol/cm^3	osmotic active conc. intern	Section 2.2.12

Table 3.4: *Chosen Parameters for the bicarbonate model extension.*

	Initial value	stat. value		eigenvalues	eigenvector
$[K^+]_i$	180 mM	197 mM		$\lambda_1 = -86.3$	$v_1 = (0.18, -0.03, -0.98, 0)^T$
$[CO_2]_i$	5 mM	4.1 mM		$\lambda_2 = -16.1$	$v_2 = (-0.15, 0.45, -0.88, 0)^T$
pH_i	6.9 pH	7.01 pH		$\lambda_3 = -0.003$	$v_3 = (0.2, 0.01, 0.98, 0)^T$
V	48 fL	49 fL		$\lambda_4 = -1.1$	$v_4 = (0.24, 0, 0.97, 0)^T$
V_m	-200 mV	-197 mV			

Table 3.5: *Initial values as well as the respective stationary values for the bicarbonate model extension. The eigenvalues at the stationary state are similar to those in the model versions $\mathcal{M}_1$ and $\mathcal{M}_2$. A qualitative change in the systems behavior can not be expected. Parameter changes or the application of simple regulation schemes did not change the eigenvalues drastically.*

3.2.1 Sensitivity of the stationary state

In the first model approach, the sensitivity of the stationary state to parameter changes was analyzed. The same consideration was made for the bicarbonate model to investigate the effect of the inclusion of CO$_2$. The sensitivities in Figure 3.8 were estimated by forward differences, by increasing the parameters $g_{Trk1,2}$, I^{max}_{Pma1}, g_{Nha1}, $g_{K,leak}$, $g_{H,leak}$ and $J^{prod}_{CO_2}$ by ten percent relative to their respective value given in Table 3.4.

Compared with the simple model (see Figure 3.3), the sensitivity of the stationary K$^+$, pH and
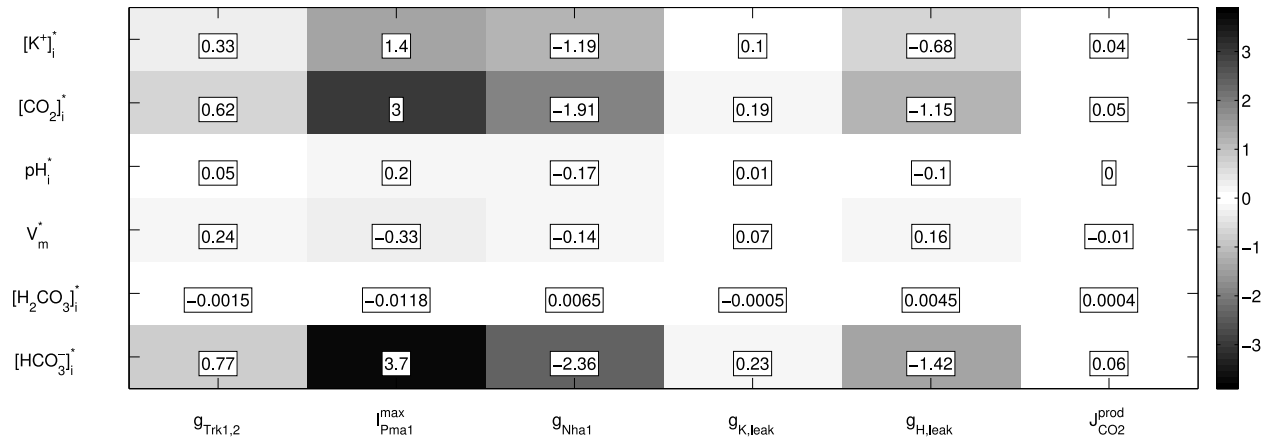
Figure 3.8: *Sensitivity of the stationary state. For each of the systems indicated on the x-axis the sensitivity of the stationary value indicated on the y-axes was calculated. The sign indicates, whether the variable increases (positive) or decreases (negative) with a increase in the different parameters. For all systems the effect in $[HCO_3^-]_i^*$ is most prominent. The scaling of the colorbar is the same as in Figure 3.3 to allow a convenient comparison.*

membrane potential is very similar, both in the magnitude and sign; see Section 3.1 and Figure 3.3. The parameter's influence on $[CO_2]_i$, $[H_2CO_3]_i$ and $[HCO_3^-]_i$ can be directly linked to their effect on the pH.

To understand the relationship between $[CO_2]_i$ and the pH, the reader is reminded to Figure 2.19, where the pH dependent partitioning of $[H_2CO_3]_i$ and $[HCO_3^-]_i$ was shown: the lower the pH, the more H_2CO_3 will remain undissociated. Thus, a pH dependent growth in H_2CO_3 will always result in an opposite behavior of HCO_3^- (the only exception occurs for the CO_2 production rate, where the source flux yields an increase both in H_2CO_3 and HCO_3^-). That the latter is the variable with the highest sensitivity can be explained by two effects: The pH dependent fraction of CO_2 forming HCO_3^- is a rather steep function around $pH_i = 7\,\mathsf{pH}$; see Figure 2.19. Thus, a small change in the pH leads to a considerable change in the HCO_3^- fraction. The same holds for H_2CO_3. However, the high permeability of carbonic acid lowers the effect on its concentration. Excess H_2CO_3 is extruded from the cell.

In Figure 3.8 it can be seen that a higher CO_2 production rate causes an increase in pH. At the first sight this is counterintuitive, since the dissociation of H_2CO_3 generates protons what should lower the pH. However, the production of protons stimulates the pump Pma1 to extrude protons, what has the opposite effect on the pH. This is another example for the coupling of the different processes involved in potassium transport.

3.2.2 Reverse Tracking Approach

Preliminary model simulations revealed, that a constant CO_2 production rate does not influence the systems dynamics (not shown).

In addition, a variety of hypothetical regulation systems was studied which potentially could slow down the loss of potassium. For example, an increase of the activity of Trk1,2 in response to external or internal concentration changes was assumed in the model by using simple kinetic relationships. Similarly, a K^+ concentration dependent decrease of the Nha1 conductivity was also

investigated computationally. All these approaches did not lead to a significant decrease in the velocity of the potassium loss and thereby to a better agreement with the experiments. These results show that at least one central process of potassium homeostasis is not covered by the model versions $\mathcal{M}_1 - \mathcal{M}_3$.

There are many possible reasons for the failure of the current model, including the lack of additional ions, metabolic effects or compartments storing potassium or protons. It is impossible to explicitly model theses effects, since the current qualitative understanding is limited and the required data will not available in near future.

Given that the model accounts for the major transport systems that are known to be relevant for homeostasis but still can not explain the data for potassium starvation, the question arises, which other dynamic processes alter the transport systems and at which point in the transport network they act on. To handle such unmodeled dynamic processes it is assumed that parameters in the model could be in fact not parameters, but time dependent functions. This time dependent functions represent the unknown regulatory processes required for active homeostatic control.

Instead of explicitly modeling these alterations, the model is kept as parsimonious as possible and a reverse engineering approach (called reverse tracking method) was followed to infer these time dependent input functions. This approach provides information about the most important dynamic regulation events which are triggered by other processes not explicitly described in the model.

The central idea of the reverse tracking method is to replace a parameter in the model by an unknown input function which will then be inferred from the experimental time course data. The respecting parameter is thus a potential point of application for the regulatory process not explicitly covered by the model. In control theory terms this is called an actuator. The inferred input function represents the effect of the regulatory processes on the actuator.

As candidate points of application, the conductance parameters of Trk1,2, Nha1, Pma1 and the leak currents, as well as the maximal pump current for Pma1 and the CO_2 production rate were chosen. For each of the respective variables it is tried to estimate the time course, which reproduces the experimental data.

This corresponds to the solution of the optimal control problem

$$||[K^+]_i^{sim}(p(t), \theta) - [K^+]_i^{ref}|| = \min! \, , \tag{3.57}$$

with the data based time course $[K^+]_i^{ref}$ (see Figure 2.3 for the respective spline fit of the raw data) and the simulated potassium concentration $[K^+]_i^{sim}(p(t), \theta)$, depending on a time dependent parameter $p(t)$ and further constant parameters θ.

One possible numerical method to solve this problem is given by the solution of the following ODE, which integrates the tracking error $e(t) = [K^+]_i^{sim}(p(t), \theta) - [K^+]_i^{ref}$

$$\frac{d}{dt}p(t) = -\eta \cdot \left([K^+]_i^{sim}(p(t), \theta) - [K^+]_i^{ref}\right) \, , \tag{3.58}$$

with an appropriate amplification factor $\eta > 0$. In control theory, this method is called integral controller (I-controller). The approach uses the the capability of an I-controller to adapt a dynamic variable to a certain reference value (Åström and Murray 2009). Since the reference value is itself
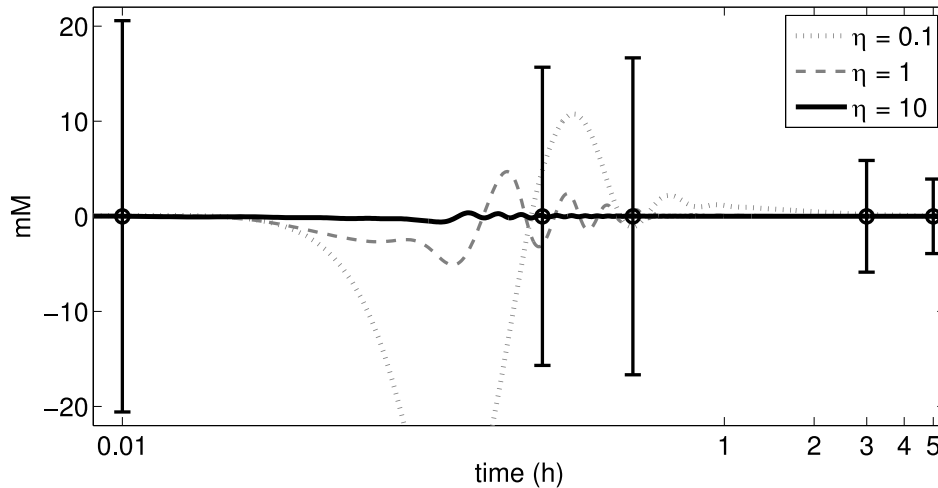
Figure 3.9: *The tracking error $e(t) = [K^+]_i^{sim}(p(t), \theta) - [K^+]_i^{ref}$ for the tracking of the wildtype starvation data by an adapted Pma1 activity. A low amplification factor η yields large error.*

time dependent, the I-controller follows its respective time course.

Identification of an appropriate η The amplification factor η was tentatively chosen in each individual case to reduce the oscillations produced by the I-controller. The manual approach was to start with low values and monitor the deviation from $[K^+]_i^{ref}$. This was repeated several times with a gradually increased η until the residual is almost zero. As an example, Figure 3.10 demonstrates this procedure for the tracking of the wildtype starvation data by Pma1. With a weak amplification factor, the I-controller reacts slowly, which results in a large tracking error. An increase of η (faster reaction of the I-controller) diminishes the amplitude of the deviation, however, the frequency of the oscillations is also increased.

Transport systems

In case of the transport systems $p(t)$ was used as a kind of regulation function for a constant conductivity parameter g and pump current I_{Pma1}^{max} (see equations (3.33)-(3.39))

$$\frac{d}{dt}p(t) = -\eta \cdot \left([K^+]_i^{sim}(p(t), \theta) - [K^+]_i^{ref} \right) \tag{3.59}$$

$$\bar{g}(t) = p(t) \cdot g, \tag{3.60}$$

where $\bar{g}(t)$ gives a time dependent conductance parameter ($\bar{I}_{Pma1}^{max}(t)$ respectively). For the following approaches, only the parameters related to the reverse tracking are shown. A comprehensive list of all parameters used for the results can be found in the Appendix Tables 4.5-4.7.

Trk1,2 and potassium leak ($g_{Trk1,2} = 23 \frac{\mu S}{cm^2}$, $\eta = 1$, $p(0) = 1$) For the reverse tracking approach, three different cases were analyzed.

- Trk1,2 as a K^+ uniport (model standard)

- Trk1,2 as a $2K^+$ symport

- Trk1,2 as a $1H^+/1K^+$ symport

Figure 3.10: *Estimated control signal for Trk1,2. The left panel shows the estimated conductivity of Trk1,2 and the right panel shows the respective data fit. In none of the three tested cases, a suitable control signal for Trk1,2 was found.*
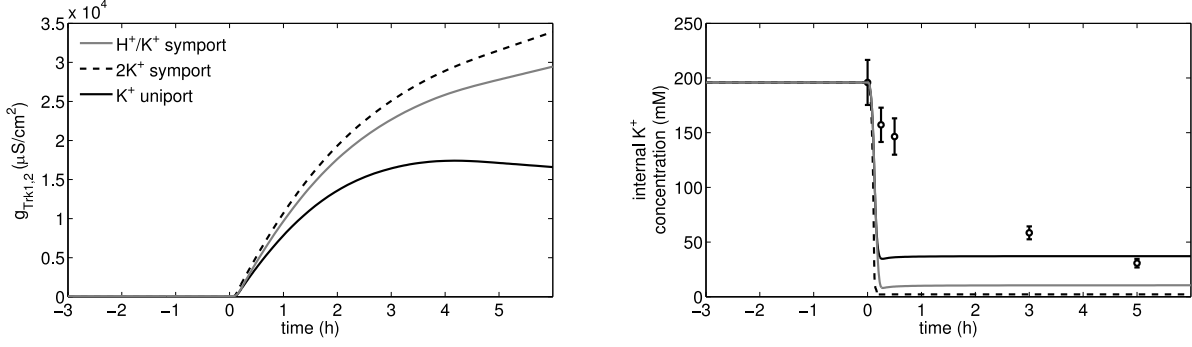
Each case yielded similar results (see Figure 3.10). When the external potassium is dropped at time point zero, the conductance is tremendously increased (magnitude 10^4). Nevertheless, this increase does not prevent the rapid loss of internal potassium (Figure 3.10).

As the high affinity uptake system, the literature reports Trk1,2 as a most relevant transporter under potassium limiting conditions. Surprisingly, the system does not react very sensible on changes in $g_{Trk1,2}$. However, the low influence of Trk1,2 was already observed in Figures 3.8 and 3.3.

The incapability of tracking the potassium data must lead to the exclusion of Trk1,2 as a potential actuator of potassium homeostasis. An early indication for a minor role of Trk1,2 could have been derived from a comparison of the potassium time courses in Figure 2.5, where the dynamics of the system is insensitive to the deletion of Trk1,2. As an explanation of this finding, it is suggested, that the micromolar concentration of potassium in the medium is not enough to ensure the potassium supply. Literally spoken: opening the doors is of no use, if nothing is outside.

A similar result was obtained for the potassium leak and no suitable control signal could be estimated for the conductivity parameter $g_{K,leak}$. This is in the line with the very low influence of $g_{K,leak}$ observed in previous considerations.

Pma1 and proton leak (wildtype: $I_{Pma1}^{max} = 15 \frac{\mu A}{cm^2}$, $\eta = 10$, $p(0) = 1$; *trk1,2*Δ; $I_{Pma1}^{max} = 15 \frac{\mu A}{cm^2}$, $\eta = 120$, $p(0) = 1$). The control problem for Pma1 was successfully solved. When the external potassium drops, the maximum pump current is rapidly increased followed by a slower reduction to a new stationary state; see Figure 3.11. In both cases, the predefined time course was accurately tracked and the residual is almost zero, since $[K^+]_i$ is weakly affected by the oscillations produced by the I-controller.

The high influence of Pma1 on the systems variables was already found in the former sensitivity studies. for the *trk1,2*Δ a higher activity of Pma1 compared to the wildtype is predicted. This reflects the higher energy required to maintain a higher potassium concentration in the mutant.

For the proton leak the required control signal could also be estimated (not shown). In order to almost perfectly track the internal potassium, $g_{H,leak}$ shows the opposite behavior compared to I_{Pma1}^{max}. When the external potassium drops, $g_{H,leak}$ is rapidly reduced to almost zero within 10-15 minutes. After this first response, the parameter grows again to reach a new stationary value.
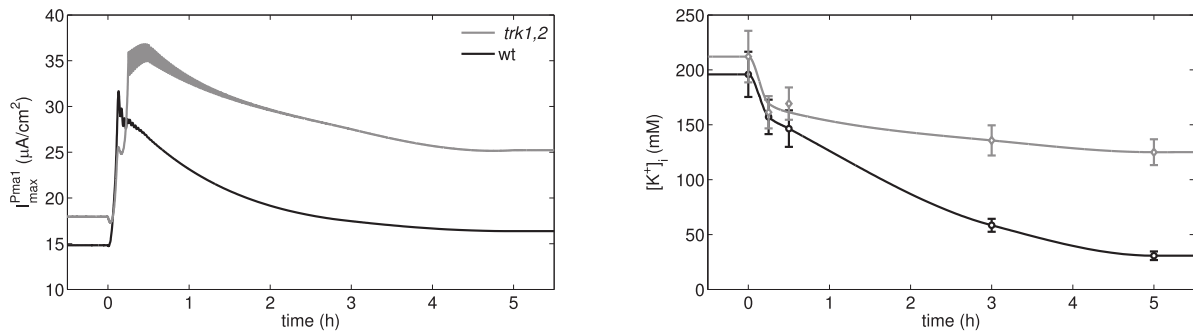
Figure 3.11: *Predicted response of Pma1 to potassium starvation for wt and trk1,2Δ. Left panel: time course of I_{Pma1}^{max}. The parameter is rapidly increased, followed by a slow relaxation. For trk1,2Δ the current is higher compared to wt. The oscillation are artifacts from the numerical method (I-controller). Right panel: Data fit using the estimated control signal.*

Nha1 (wildtype: $g_{Nha1} = 10 \, \frac{\mu S}{cm^2}$, $\eta = 2$) For Nha1 four different possibilities were tested with the reverse tracking approach

- Nha1 as a $2H^+$:$1K^+$ antiporter modeled by Ohm's law with a voltage gating for the conductivity

- Nha1 as a $2H^+$:$1K^+$ antiporter modeled by Ohm's law with a constant conductivity

- Nha1 as a $2H^+$:$1K^+$ antiporter modeled by Ohm's law with a potassium inhibition

- Nha1 as a $1H^+$:$1K^+$ antiporter

The potassium inhibition was modeled by multiplying the constant conductivity parameter q_{Nha1} with a potassium dependent expression $f([K^+]_i) = \frac{1}{1 + \frac{q_{Nha1}}{[K^+]_i}}$, where q_{Nha1} controls the half maximal activation.

The sensitivity analysis has identified Nha1 as a transporter with a high influence on the systems variables. Consequentially, the estimation of a control signal was successful. Each of the four tested approaches was capable to track the experimental data (see Figure 3.12). However, the estimated control signal shows a behavior which appears not plausible at first. At the moment of the external potassium drop, Nha1 is rapidly deactivated to prevent the potassium loss. This is followed by a phase, where Nha1 is activated again, which causes the loss of potassium (see Figure 3.12). The possibility, that the cell has developed a regulation pathway, which extrudes potassium under potassium limiting conditions appears rather counter-intuitive. The time course of internal potassium under starvation shows two phases for the wild-type, the *trk1,2Δ* and *nha1Δ* mutant. In the first hour the potassium loss is rapid, followed by a slower reduction of potassium (see Figure 2.5). Because this dynamic behavior is insensible to the deletion of Nha1, it is concluded, that Nha1 is not involved in the underlying regulation process.

In addition, the increased activity of Nha1 under starvation is contradictory to the findings of Bañuelos et al. (2002). The authors report, that the differences in the potassium content of the wildtype, *nha1Δ* mutants and a strain overexpressing Nha1 are no longer present after 6 hours of starvation. This implies a deactivation of Nha1 under potassium starvation (see Table 2.6).
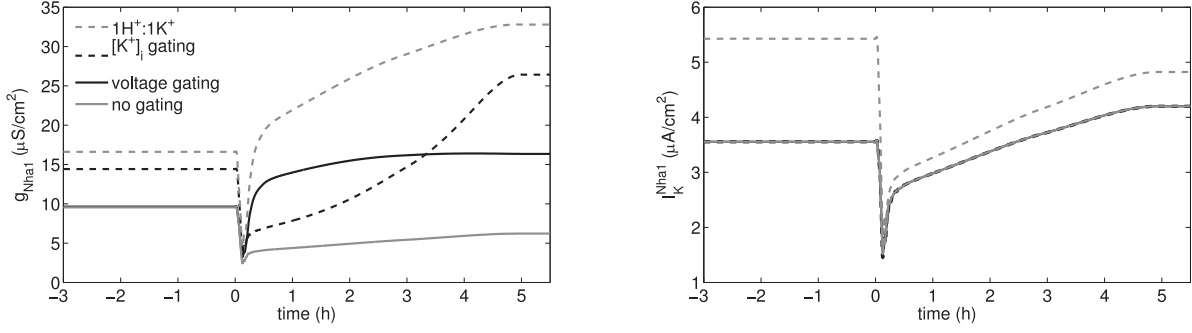
Figure 3.12: *Estimated control signal for Nha1. The left panel shows the estimated conductivity and the right panel shows the simulated Nha1 current. In each case, Nha1 is quickly deactivated followed by an increase in the activity. This is contradictory to the findings of Bañuelos et al. (2002).*

Carbon dioxide production

(wildtype: $\bar{J}_{CO_2}^{prod.}(0) = 5e - 4$, $\eta = 1e - 3$; *trk1,2*Δ; $\bar{J}_{CO_2}^{prod.}(0) = 5e - 4$, $\eta = 1e - 2$) The tracking equation for the carbon dioxide production rate reads (compare with Equation (3.49))

$$\frac{d}{dt}\bar{J}_{CO_2}^{prod.}(t) = -\eta \cdot \left([K^+]_i^{sim}(\bar{J}_{CO_2}^{prod.}(t), \theta) - [K^+]_i^{ref}\right) \cdot \frac{V(0)}{V(t)}. \tag{3.61}$$

As it was the case for the proton pump Pma1, it was possible to estimate a control signal for the carbon dioxide production rate (residual almost zero). Figure 3.13 shows, that a sudden increase followed by a slow relaxation recovers the experimental data. A similar shape was already observed for Pma1. The effect of the raised CO_2 production is a source flux of protons, which finally drives the potassium uptake.

Except from the initial phase of few minutes, the CO_2 production in *trk1,2*Δ mutants is higher compared to the wildtype. As an effect of the slower potassium loss in *trk1,2*Δ mutants, the increase of the control signal is less steep and shows a smoother transition to the phase of relaxation.
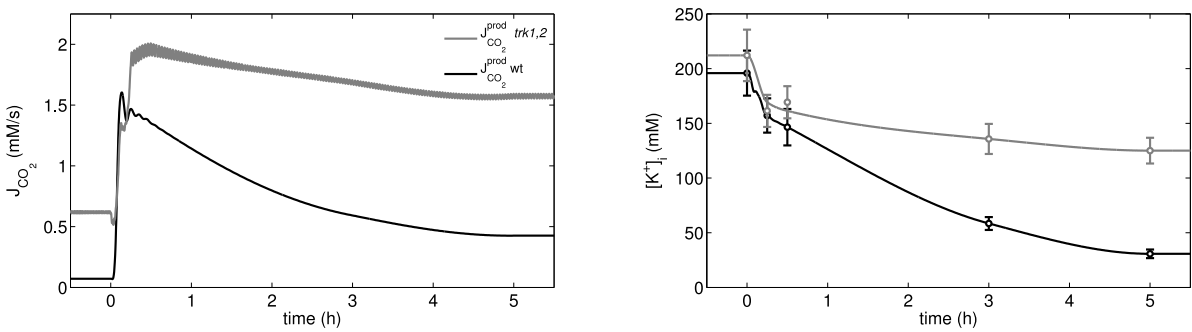
Figure 3.13: *Left panel: Estimated control signal for the CO_2 production rate (wildtype and trk1,2Δ mutant). The steep increase followed by a slow relaxation was already observed for Pma1. Right panel: Data fit of $[K^+]_i$ using the estimated control signal.*

3.2.3 Potential actuators of potassium homeostasis

Parameters, for which a respective time course could be found, are considered as potential actuators of potassium homeostasis. The potassium leak and Trk1,2 are both not capable to track the potassium concentration. Remarkably, all potential systems (Nha1, H^+ leak, Pma1, CO_2 production)

are related to proton fluxes.

However, the proton leak as an unspecific transport process is hardly subject of the organisms response to a potassium depletion. Nha1 can be also excluded from the list of actuators since the predicted control signal is in contradiction with experimental findings (Bañuelos et al. 2002).

The remaining candidates are the proton pump Pma1 and the CO_2 production rate. The effect of both systems is the extrusion of protons, either directly by the proton pump or indirectly by the intracellular release of protons, which triggers their extrusion. Thus, the function of both processes is to energize the potassium uptake via Trk1,2 and the leak. Although a net loss of potassium occurs, the K^+ uptake counterbalances the potassium efflux and achieves a slow internal potassium reduction.

Experimental validation

The proposed mechanism was subsequently validated by experiments. The measurements related to the Pma1 activity and bicarbonate reaction system were already presented in Section 2.1.5 and 2.1.6 and are shown again for a direct comparison with model predictions in Figure 3.14.
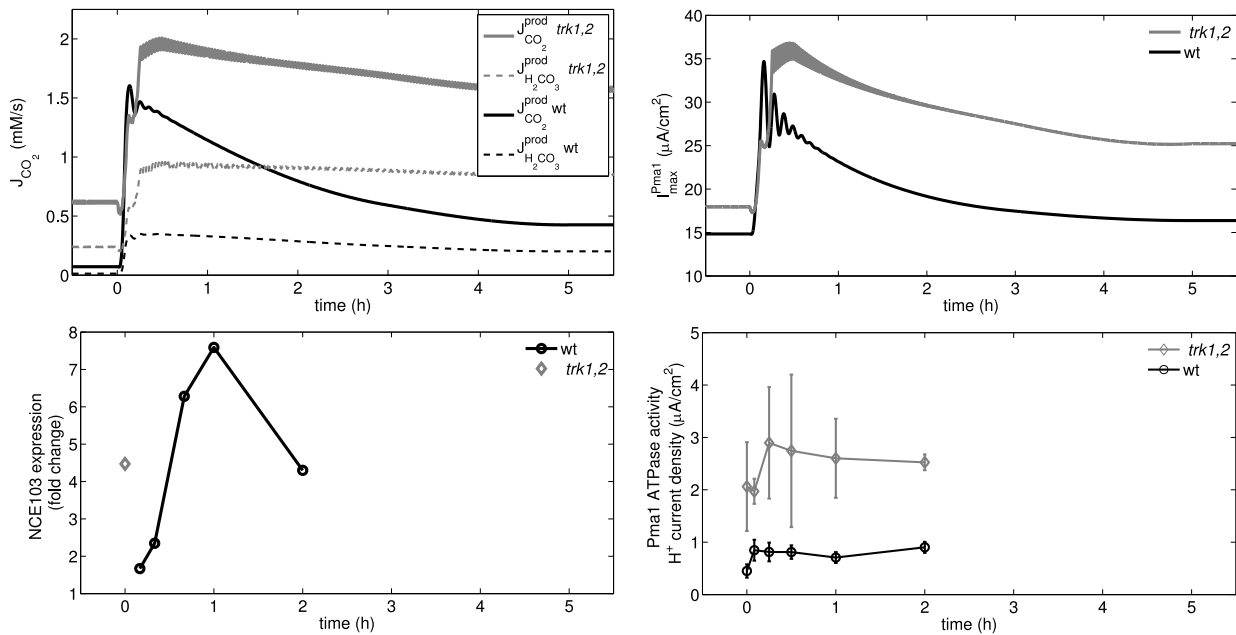
Figure 3.14: *Comparison of the predicted control signals (upper panels) for Pma1 and CO_2 production and the respective experimental validation (lower panels). A qualitative agreement is obvious. The predicted control CO_2 production fluxes are shown in parallel with the pH dependent production fluxes of carbonic acid. All fluxes show a rapid increase at the moment of the external potassium drop. The following relaxation to new stationary values is more prominent in the CO_2 fluxes compare to the H_2CO_3 fluxes. The expression level of the NCE103 gene encoding the carbonic anhydrase reaches a maximum after one hour of potassium starvation. For the trk1,2Δ the single expression value implicates a higher expression compared to the wildtype. The measured Pma1 activity was converted to $\mu A/cm^2$ according to the calculations in Section 2.1.6.*

Pma1 activity The shape of the estimated control signal for Pma1 is in qualitative agreement with the measurements: The data shows a rapid increase followed by a slower relaxation. These changes happen on the same timescale as the estimated signal. In addition, the experiment confirms the predicted higher Pma1 activity in *trk1,2Δ* mutants. However, converted to $\mu A/cm^2$, the measurements are 10-20 fold lower than the prediction. This could be up to uncertainties in the

unit conversion. Moreover, the experiment uses crude membrane preparation procedures and it is likely that the experiment can not reflect the *in vivo* ATPase activity. Thus, the measurement P_i gives only an indirect information about the proton flux.

As it was described in Section 2.1.6 the experiment monitors the inorganic phosphate production by Pma1, as a measure of Pma1's activity. A significant difference between the amount of Pma1 in the wildtype and *trk1,2Δ* could not be detected by the experimenters. This gives rise to the notion, that Pma1 is the target of a capable regulation mechanism, which sets Pma1 to a state where an increased level of ATP hydrolysis -and thus H^+ transport- is possible. In support of this idea, Eraso et al. (2006) reports a phosphorylation of Pma1 by the Ptk2 kinase, which increases the transport capacity and Estrada et al. (1996) found the kinases Yck1,2 to decrease Pma1's activity.

Carbon dioxide production   It was not possible to measure the metabolic release of CO_2 directly. As an alternative, the expression of NCE103 encoding the carbonic anhydrase was measured, since it was shown earlier that protein and mRNA levels of carbonic anhydrase are highly correlated (Amoroso et al. 2005). The assumption was, that an altered CO_2 production should be visible in the activity of the carbonic anhydrase.

Figure 3.14 shows the qualitative agreement between the expression level of NCE103 and the estimated CO_2 production rate in the wildtype. However, NCE103 increases more slowly and reaches its maximum after one hour of potassium starvation. The delay can be explained as follows: The experiment measures the RNA expression of the carbonic anhydrase gene, which can according to Amoroso et al. (2005) be assumed to be proportional to the amount of protein. However, the reverse tracking predicts the time course of bicarbonate reaction fluxes. Nevertheless, changes in the CO_2 production flux might trigger changes in the amount of enzyme.

For the *trk1,2Δ* mutant only one expression value is available. However, the level is higher than initially measured for the wildtype, which matches the prediction of a higher CO_2 production rate in *trk1,2Δ* mutants. These expression data were also confirmed by quantitative PCR techniques; see Section 2.1.5.

Mechanism of potassium homeostasis

The predicted and experimentally validated activation patterns for Pma1 and the bicarbonate reaction system show both a fast response. This implies that the signal triggering these responses must be also fast. The only fast variables in the model simulations are external potassium and the membrane potential, where the latter results probably from an insufficient mathematical description (see Section 3.2.4).

This suggests that the cell must trigger changes in proton fluxes in response to changes of external, but not internal potassium. The idea of an external potassium sensor is supported by the experimental findings of the stable potassium experiment given in Figure 2.6, where it was demonstrated, that the internal potassium is adjusted in dependence of $[K^+]_o$.

Figure 3.15 shows the proposed mechanism of potassium homeostasis: Aputative potassium sensor reacts to a fast signal (external potassium or even the hyperpolarization). The sensor signal triggers a control signal for Pma1 and the bicarbonate reaction system. Both systems contribute to an enlarged proton efflux, which finally energizes the uptake of potassium.
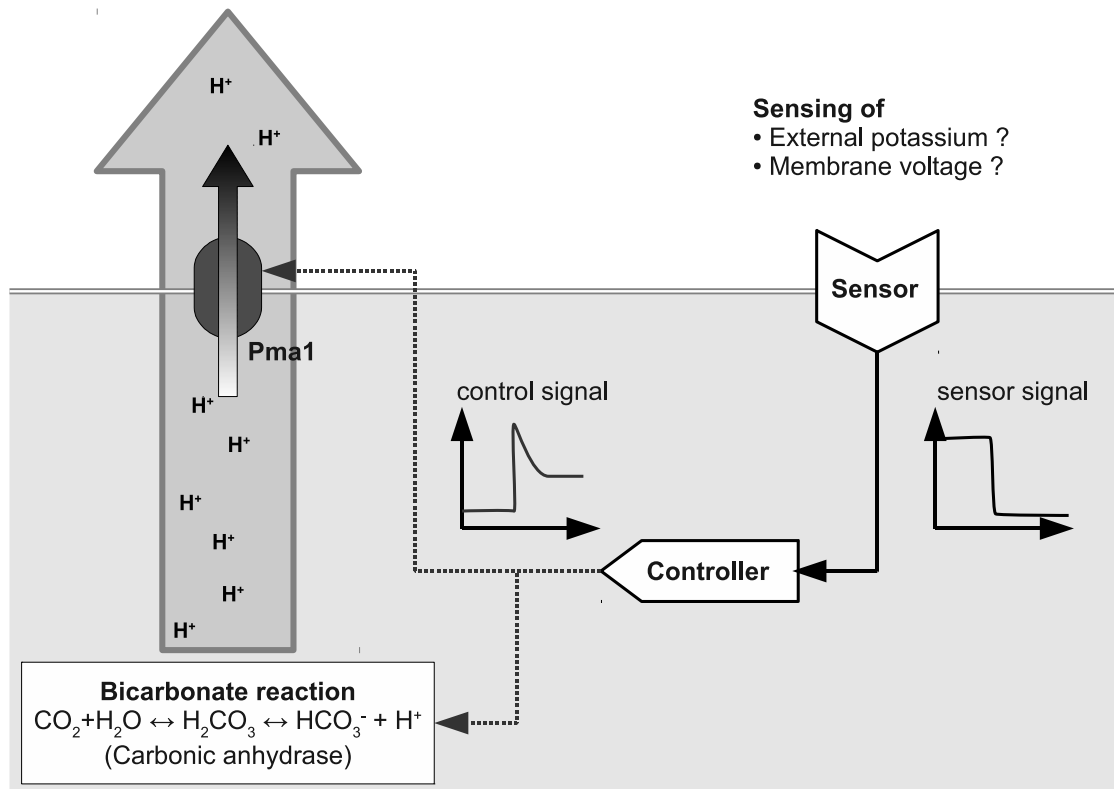
Figure 3.15: *Proposed mechanism of potassium homeostasis. In response to changes in the external potassium or the membrane potential, a control signal is generated to trigger Pma1 and the bicarbonate reaction system. Both systems are involved in proton extrusion, which energizes the potassium uptake.*

It is suggested, that the core of potassium homeostasis is rather the regulation of proton efflux, than the regulation of the potassium transporters. Their minor role is evident from the fact, that potassium homeostasis is still possible in *trk1,2Δ* and *nha1Δ*. However, this does not mean, that these systems do not contribute to the maintenance of potassium. It simply means, that there is an mechanism, which can compensate the lack of those systems.

While Pma1 is commonly accepted as the *driver* of potassium uptake, it was never reported that Pma1 is also the *regulator* for the internal potassium concentration. The similar shape of the estimated CO_2 production and Pma1 activity implies a connection between processes, possibly via ATP: The increased ATP demand by Pma1 could be compensated by an increased ATP production rate, which goes in parallel with the metabolic release of CO_2.

Such a connection implies a parallel work, where the bicarbonate reaction system is the donor of the protons, which are pumped out by Pma1. However, the interplay of both systems and a detailed characterization of the sensing and signal processing steps is still a subject of research.

3.2.4 Artificial feedback controller

Knowing the actuators and their respective control signal raises the ambition to generate the signal directly from a systems variable. Since the signal changes on a very short timescale, variables with a rapid dynamics were considered as promising. The respective variables are $[K^+]_o$, as an external variable and the membrane potential V_m (see Figure 3.16), as an internal variable. However, the experimental data shows a slower dynamics of the membrane potential than the model simulation;

compare Figure 2.4 and 3.16. In addition, the membrane potential can be affected by very few charges and it is assumed, that the vital regulation of potassium homeostasis should not depend on a signal which can be easily disturbed. Thus, the membrane potential is not considered as a regulation signal for the actuators.

The missing characterization of potential sensor systems requires a black box model, which effectively covers the unknown sensing and regulation processes. Such a description allows model simulations independent from an estimated signal. The required control signal could finally generated by a combination of a proportional and integral control of the error $e(t) = [K^+]_o - [K^+]_o^{ref}$ (PI-controller)

$$\frac{d}{dt}u(t) = a_P \cdot \frac{d}{dt}[K^+]_o + a_I(t) \cdot \left([K^+]_o - [K^+]_o^{ref}\right) , \tag{3.62}$$

with the control signal $u(t)$, the constant parameter a_P and the reference value $[K^+]_o^{ref} = 50\,\text{mM}$. The amplification factor, $a_I(t)$, is chosen to be time dependent

$$a_I(t) = \tilde{a}_I \cdot e^{-\frac{\ln 2}{t_I}t} , \tag{3.63}$$

with a constant parameter $\tilde{a}_I$ and t_I controlling the fade out of the I-controller.

For the CO_2 production rate the implementation reads; compare Equations (3.49) and (3.61)

$$\frac{d}{dt}\bar{J}_{CO_2}^{prod.} = u(t) \cdot \frac{V(0)}{V} \tag{3.64}$$

and for Pma1 respectively; compare Equations (3.37) and (3.59)

$$\frac{d}{dt}\bar{I}_{Pma1}^{max} = u(t) \cdot I_{Pma}^{max} . \tag{3.65}$$

The proportional part of the controller serves to increase the signal at the moment of the external potassium drop. The I-controller reduces the signal in the second phase. With a constant factor a_I, the I-controller would produce a linear decrease in the signal, which would finally lead to a negative control signal. The function $a_I(t)$ serves to exponentially fade out the influence of the I-controller.

With appropriate parameter values, the artificial feedback controller allows a quantitative data fit of the presented starvation experiments. The parameter values were set by a manual search. Two examples for the application of the artificial feedback controller are given below. A comprehensive list of all respective parameter values can be found in the following tables

1. Starvation in almost zero potassium (Navarrete et al. 2010)

   • wild-type and *trk1,2*: Table 4.8

2. Starvation in 100, 200 or 500 μM potassium (see Figure 2.6)

   • wild-type: Table 4.9

Example 1

This example demonstrates the quantitative data fit of the potassium starvation data (Navarrete et al. 2010) for the wildtype and *trk1,2*Δ controlling the CO_2 production rate. The parameters for the controller can be found in Table 3.6. For all other parameters see Appendix Table 4.8 The

	wildtype	$trk1,2\Delta$
$\bar{J}^{prod}_{CO_2}(0)$	$8e-5\frac{\text{mmol}}{\text{cm}^3\cdot\text{s}}$	$7e-4\frac{\text{mmol}}{\text{cm}^3\cdot\text{s}}$
a_P	$-3.2e-2$	$-3e-2$
$\tilde{a}_I$	$7e-6$	$6e-6$
t_I	$0.7\cdot 60^2\text{s}$	$0.7\cdot 60^2\text{s}$

Table 3.6: *Parameters for the artificial feedback controller in Section 3.2.4, Example 1.*

controller is specified by

$$\frac{d}{dt}\bar{J}^{prod}_{CO_2} = \left[a_P\cdot\frac{d}{dt}[K^+]_o + a_I(t)\cdot\left([K^+]_o - [K^+]_o^{ref}\right)\right]\cdot\frac{V(0)}{V(t)} \tag{3.66}$$

$$a_I(t) = \tilde{a}_I\cdot e^{-\frac{\ln 2}{t_I}t} \tag{3.67}$$

$$\left[K^+\right]_o^{ref} = 0.05\text{mmol/cm}^3\,. \tag{3.68}$$

Figure 3.16 gives the resulting CO_2 production rate as well as the respective data fit. The CO_2 production rate generated by the external potassium dependent controller shows the familiar shape of rapid increase and slow relaxation (Figure 3.16 a). This yields a suitable data fit for the potassium starvation data (Figure 3.16 b).

The simulated time course for the internal pH shows a decrease during starvation, whereas $trk1,2\Delta$ mutants show a lower pH. The pH dynamics are similar to the internal potassium. These findings are in qualitative agreement with unpublished material by Daniel Ganser and Jost Ludwig[2].

Compared to $trk1,2\Delta$ the internal CO_2 concentration is higher in the wildtype (Figure 3.16 d). This might appear contradictory to the higher CO_2 production rate in $trk1,2\Delta$. However, the reader is reminded on the definition $[CO_2]_i = [H_2CO_3]_i + [HCO_3^-]_i$ and the pH dependent partitioning of $[H_2CO_3]_i$ and $[HCO_3^-]_i$, see Section 2.2.13. Since the low pH in $trk1,2\Delta$ yields a high fraction of $[H_2CO_3]_i$, which easily diffuses through the cell membrane, the overall $[CO_2]_i$ stays lower despite a high CO_2 production rate. Nevertheless, this model prediction is strongly dependent on the internal pH.

In agreement with several publications, the model predicts a hyperpolarization in $trk1,2\Delta$ (Figure 3.16 e). The dynamics of the membrane potential follows the external potassium drop, which reflects the influence of $[K^+]_o$ on the potassium equilibrium potential. However, the measurements of Navarrete et al. (2010) indicate a slower dynamics, see Figure 2.4. Since the membrane potential is considerably affected by the movement of few charges, the involvement of additional processes is likely. It might be also the case that the dynamics of the measured data is slower because of the insufficient time resolution of the fluorescence dye used in the measurements.

Example 2

The artificial feedback controller is also capable to yield quantitative data fits of the experiments where the cells transfered from 50 mM KCl to a medium with 100, 200 or 500 μM potassium; see Figure 2.6. In this example the external potassium is used as the sensing signal and the maximum

---

[2]Universität Bonn, Institut für Zelluläre und Molekulare Botanik (IZMB)
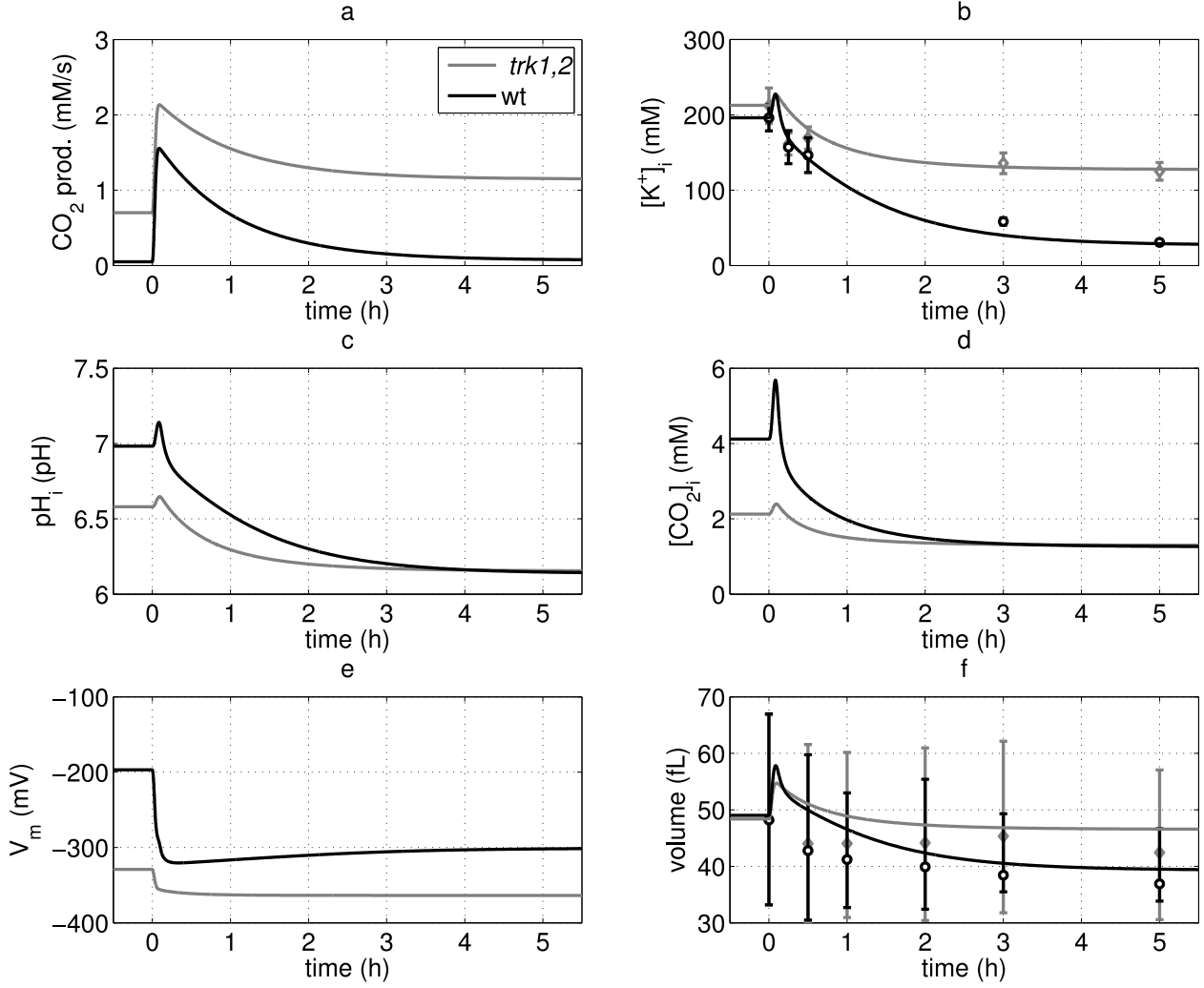
Figure 3.16: *Quantitative data fit for the wildtype and trk1,2Δ starvation data from (Navarrete et al. 2010); see Section 2.1.3. (a) CO₂ production rate generated by the feedback controller. (b) internal potassium time course, (c) internal pH time course, (d) CO₂ concentration, (e) membrane potential, (f) cell volume.*

Pma1 pump current, $\bar{I}^{max}_{Pma1}$, as the control signal

$$\frac{d}{dt}\bar{I}^{max}_{Pma1} = \left[a^K_P \cdot \frac{d}{dt}[K^+]_o + a^K_I(t) \cdot \left([K^+]_o - [K^+]^{ref}_o\right)\right] \cdot I^{max}_{Pma1} \qquad (3.69)$$

$$I^{max}_{Pma1} = 16\frac{\mu A}{cm^2} \qquad (3.70)$$

$$a^K_I(t) = \tilde{a}^K_I \cdot e^{-\frac{\ln 2}{t^K_I} t} \qquad (3.71)$$

$$\left[K^+\right]^{ref}_o = 0.05 \text{mmol/cm}^3 \,. \qquad (3.72)$$

where the superscript K indicates one of the three different external potassium concentrations. It was not possible to find *one* set of parameters, $\{a^K_P, \tilde{a}^K_I, t^K_I\}$, which holds in all cases. However, it
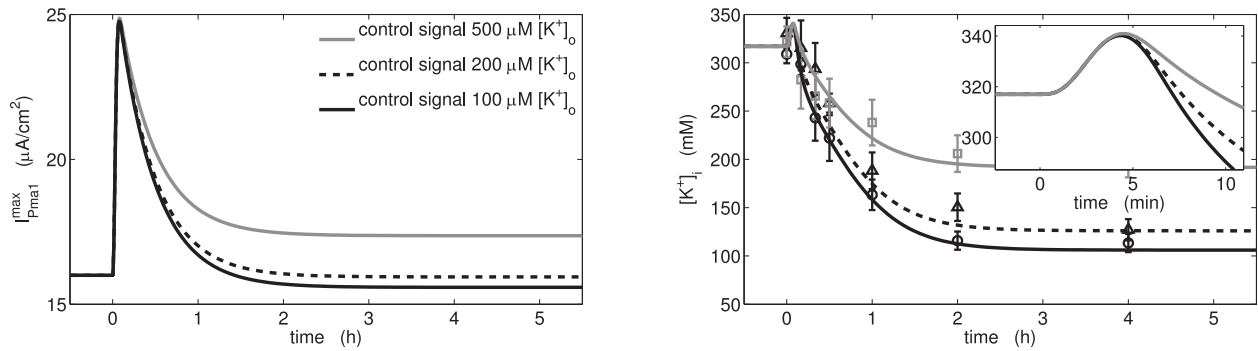
Figure 3.17: *Application of the artificial feedback controller to the starvation experiment, where the cells were transfered from 50 mM KCl to a medium with 100, 200 or 500 μM KCl (Figure 2.6). The left panel shows the three different control signals generated by the controller in response to the external potassium drop. The right panel shows the resulting data fit. The rapid activation of the controller at t = 0 causes a low, transient uptake of potassium (see inset for details).*

was possible to reduce the number of necessary parameters by setting

$$t_I^{100} = t_I^{200} = t_I^{500} = 0.3 \cdot 60^2 \text{s} \tag{3.73}$$

$$a_P^{100} = a_P^{200} = a_P^{500} = -200 \,, \tag{3.74}$$

which means, that only $\tilde{a}_I^K$ needs to be changed for each external potassium concentration

$$\tilde{a}_I^{100} = 1.45e - 1 \tag{3.75}$$

$$\tilde{a}_I^{200} = 1.4e - 1 \tag{3.76}$$

$$\tilde{a}_I^{500} = 1.2e - 1 \,. \tag{3.77}$$

For all other parameter values see Appendix Table 4.9.

Figure 3.17 shows the three different control signals generated by the artificial feedback controller and the respective data fit. The control signals show the familiar shape. When the external potassium drops, the signal is rapidly increased followed by a slow reduction to a new stationary state. The final potassium concentrations reflect the different levels of Pma1 activity. The $[K^+]_o$ dependent controller causes a transient uptake of potassium after the external potassium drop. Such an artifact was not observed when the actuators are controlled by V_m. The reason lies in the slightly different timescales of the external variable $[K^+]_o$ and internal variable $[K^+]_i$. Since the internal variables of the system changes in response to the external disturbance, there is a delay between the dynamics of $[K^+]_o$ and $[K^+]_i$, what allows a potassium uptake, before the the internal potassium concentration is affected by the potassium drop.

3.2.5 Structure of the system

The linearized system has a very large negative eigenvalue and this property is not changed by any parameter. This gives rise to the notion, that the high stability is a property of the system itself. Figure 3.18 shows the simplified structure of the system and indicates the coupling of the different transporters and systems variables. The activity of the transporters affect the concentration of protons and potassium. As a result, the membrane potential (V_m) changes. Both processes,
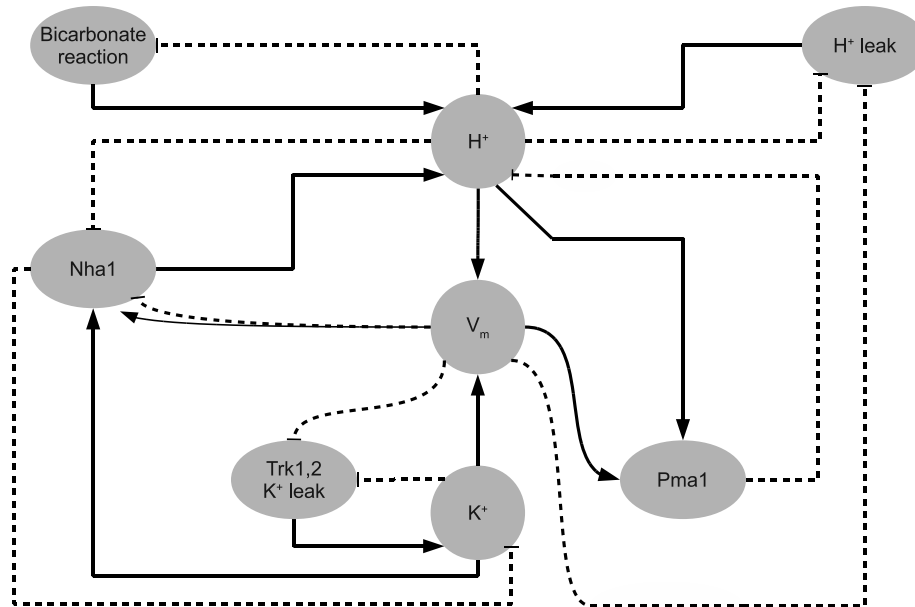
Figure 3.18: *Coupling of the transporters and variables. Each transporter receives a feedback from the altered concentrations and membrane potential. Dashed line: decrease of activity/concentration, solid line: increase of activity/concentration.*

concentrations and V_m give a feedback to the transporters activity. To follow the considerations below, it is recommended to have a repeated look at the simulated current-voltage relationships in Figure 2.15.

- The bicarbonate reaction system releases protons, which increases the intracellular H^+. The resulting pH change alters the fraction of H_2CO_3 remaining undissociated (see Figure 2.19). Therefore, the lower the intracellular pH, the more H_2CO_3 stays undissociated and less protons are released. This means, that the proton release gives itself a negative feedback, which protects the cell from acidification.

- The proton leak also provides protons to the cytosol. The increased $[H^+]_i$ leads to a more negative equilibrium potential for the proton leak. For a constant V_m, the shift of $E_{H,leak}$ leads to a reduced influx of protons. Another explanation is, that the uptake of protons reduces the inward directed proton gradient, which drives the proton uptake. Thus, an increasing intracellular H^+ means a negative feedback for the proton leak. In addition, the uptake of H^+ increases the membrane potential (depolarization!). Therefore, less energy is available for the uptake of positive charges. Again, the proton leak causes effects, which counteracts its own activity.

- Similar considerations can be made for Trk1,2 and the potassium leak. The uptake of K^+ shifts the equilibrium potential and causes also a depolarization. Both effects reduce the influx of potassium.

- The proton pump Pma1 reduces the internal H^+ concentration. This yields a more positive equilibrium potential, which results in a reduced activity of Pma1 (assume $V_m = const.$). A similar explanation: the efflux of protons enlarges the inward directed proton gradient, which

aggravates the extrusion of protons. This effect is further supported by the decrease of the membrane potential (hyperpolarization).

- The antiporter Nha1 couples the proton and potassium fluxes. It increases the protons and decreases potassium. The increase of $[H^+]_i$ shifts the equilibrium potential for Nha1 in the negative direction, which reduces its activity. The opposite holds for potassium, which causes a more positive E_{Nha1} and increases the efflux of potassium. Nha1's net uptake is one positive charge per cycle, which causes an increase of the membrane potential. In tendency, a depolarization results in a reduced activity of Nha1. However, the voltage gating causes a narrow area in which the depolarization can lead to an increase of the activity. Therefore, the feedback from the membrane potential depends on the actual value of the membrane potential.

In any case the transport systems give themselves a negative feedback. The only exception can occur for Nha1, when the membrane potential increases in the area, where the voltage gating is active. However, this is only a transient effect, which occurs in a certain range of the membrane potential.

A high stability of the system is a desirable property for homeostasis. It is hypothesized, that this is a result of the systems configuration, where each process is damped by its own effects. The coupling of all variables via the membrane potential allows the different transporters to balance each other and to hinder the build-up of disturbances.

Key facts Section 3.2

- The biophysical properties of the transport systems, as well as simple regulation schemes can not explain the systems dynamics, this implies the existence of an unmodeled dynamics.

- Instead of trying further regulation mechanism, the reverse tracking approach was used to identify the potential actuators of potassium homeostasis: Pma1 activity and CO_2 production

- Both systems trigger the proton efflux, which energizes the potassium uptake

- The estimated control signals for Pma1 and CO_2 are in qualitative agreement with experimental findings. These findings indicate, that both systems work in parallel

- The Pma1 activity might be connected to the CO_2 production via the increased generation of ATP

- It is suggested, that cellular transport is tightly coupled to metabolic processes

- Model simulations show the known hyperpolarization in Trk1,2 mutants

- Hypothesis: K_i^+ is regulated in response to K_o^+

- An artificial controller is suggested as an effective black box model for the actuator regulation

- It is hypothesized, that the dynamic system gains a *structural stability* by a negative feedback of each transport system

4 Summary and Discussion

This work was aimed to develop a predictive model for potassium homeostasis as a useful tool to increase the biological knowledge about *S. cerevisiae*. The model calibration to the data of Navarrete et al. (2010) led to deeper insight of the potassium dynamics under starvation.

4.1 Summary

The basic model concept describes the flux via each transport system in dependence on internal and external concentrations as well as the membrane potential. Current-voltage relations, where all these variables are under control served for parameters estimations and led to the idea of treating transport systems as resistors in an electric circuit. Since a comprehensive electrophysiological characterization of each transport system was not available for *S. cerevisiae*, measurements of these systems for the related ascomycete *Neurospora crassa* were also taken into account (Pma1, H^+ leak). The only system for which no experimental data was available at all was Nha1. Thus, a parsimony approach was chosen. The biophysical model was extended for the cell volume and the bicarbonate reaction system.

This model approach was able to qualitatively simulate known findings like the hyperpolarization in *trk1,2Δ* mutants and potassium starved cells and the pH decrease under potassium limiting conditions. Furthermore, the model covered the mechanism of proton extrusion driven potassium uptake and allowed insights in the interaction of the different transport systems. Thus, it is concluded, that the model is a valid basis for future developments of more refined models.

The first testable model hypothesis derived from simulations with model version $\mathcal{M}_1$ was the proposition of a Nha1 voltage gating (model version $\mathcal{M}_2$). This assumption was found to be a crucial postulate to limit the potassium efflux. Such a deactivation under potassium shortage is not only intuitive, but was already observed by Bañuelos et al. (2002), although the detailed mechanism is not known. This model prediction is currently (Oct. 2011) investigated by electrophysiological measurements by Vadim Volkov and Christopher Palmer, Institute for Health Research and Policy, London Metropolitan University. These experiments will also clarify the transport stoichiometry of protons and potassium, which is still under discussion.

Although the model has many free parameters, it was not possible to simulate a slow potassium loss. Thus, it was concluded, that at least one of the initially constant parameters should be treated as time dependent. The model version $\mathcal{M}_3$ introduced the bicarbonate reaction system. Using $\mathcal{M}_3$, the idea of the reverse tracking approach was to identify all parameters, which are able to reproduce the observed potassium time course. The respective numerical task could be solved by the usage of an integral-controller.

This analysis led to the proposition of Pma1 and the bicarbonate reaction system as potential actuators of yeast potassium homeostasis. Surprisingly, no appropriate control signal for Trk1,2 could

be found, although the relevance of Trk1,2 is well proven in publications. The experimental observation of the potassium starvation experiments that *trk1,2*Δ and *nha1*Δ mutants are viable and do not show an altered dynamics under starvation led to the conclusion, that potassium homeostasis is mainly governed by proton fluxes.

As an indirect support of the estimated regulation time courses for Pma1 and CO_2 production, the expression level of the NCE103 gene encoding the carbonic anhydrase and Pma1's inorganic phosphate release were monitored. In both experimental approaches a striking similarity between the estimation and the experimental data was found. In addition, not only the shape, but also the predicted higher Pma1 activity and CO_2 production in *trk1,2*Δ mutants was supported. This suggests an explanation for the known hyperpolarization and higher potassium content in *trk1,2*Δ mutants.

Based on the stable potassium experiments (see Section 2.1.4), it was hypothesized, that the necessary control signal for Pma1 and CO_2 is generated in response to external potassium. Since a putative potassium sensor is not known for yeast, additional sensor and signaling properties of potassium transport systems were assumed. Systematic studies of modified potassium starvation experiments using various mutants are currently under development and should reveal the proposed functionality in near future. Experimenter: José Ramos, Departemento Microbiología, Edificio Severo Ochoa, Campus de Rabanales, Universidad de Córdoba, Spain.

Although, there was experimental support for the suggested sensor and the control signal of the actuators, the signal transduction and modification remains a black-box. The gap was closed by an effective description using a modified proportional-integral controller.

In all model versions the system has negative eigenvalues; positive or imaginary values were never observed. Parameter changes did not influence the sign or the magnitude of the eigenvalues. Thus it was hypothesized, that the high stability is a property of the system itself. The negative feedback between the activity of the transporters and the systems variables was suggested as a possible explanation.

Key achievements
  ▶ Model building, improvement and calibration. Chapters 2 and 3
      − Osmotic effects. Section 2.2.12
      − Bicarbonate. Section 2.2.13
      − Ammonium. Appendix 4.8

  ▶ Testable predictions. Chapter 3
      − Nha1 gating. Section 3.1.1
      − Pma1 regulation. Section 3.2.2
      − CO_2 production. Section 3.2.2

  ▶ Understanding of potassium homeostasis
      − Regulation by H^+ fluxes in response to external potassium sensor. Section 3.2.3
      − Actuators: Pma1, Bicarbonate system. Section 3.2.3

  ▶ New method: reverse tracking. Section 3.2.2

  ▶ Initiation of several experiments. Appendix 4.5

4.2 Discussion

Despite the model's capability to make testable predictions, there are limitations, which deserve further investigation. A general constraint is the description of certain mutants. Since the cell can adapt the number and biophysical properties of all other systems, the simulation of e.g. *trk1,2Δ* is far more than setting the conductivity $g_{Trk1,2} = 0$. It is not a trivial, yet a worthwhile problem to understand what happens, when a certain system is missing.

4.2.1 Proton buffer

The proton buffer is a composition of the constant capacity parameter β and the bicarbonate reaction system. The model simulations can only qualitatively describe the pH changes. In order to achieve a quantitative prediction, which also follows the dynamic behavior of the internal pH a more sophisticated approach seems to be necessary. This could be aimed on a variable buffer capacity β or the complex interplay between all considered substances (including amino acids). An improved description of the pH will possibly require the characterization of influencing processes like sequestration and metabolism. Besides unclear physiological processes, the modeling of the pH suffers from the fact, that intracellular pH measurements are very delicate and reproducible data is hard to achieve.

4.2.2 Volume

The volume model predicts mainly the volume changes according to the uptake or loss of osmotic active substances, where potassium is the most relevant. However, additional effects like cell division processes, cell growth and volume regulation are presumably present in the data of Navarrete et al. (2010) and the quantification of theses processes suffers from many uncertainties. A refinement of the volume description requires experiments, which are designed especially for that purpose. For example the osmotic pressure of the starvation medium can be corrected for the missing 50 mM KCl by the addition of an equivalent concentration of osmotic active, yet impermeable substances to allow for a distinction between growth and osmotic effects.

That the simulated cell volume follows the uptake and loss of potassium demonstrates the ability of the model to qualitatively predict a well known effect. However, a model is expected to make new, testable predictions and this can not be achieved for volume effects by the current model version.

4.2.3 Membrane potential

The membrane potential was modeled as a capacitor equation. This description is apparently not suitable since the measurements and the simulation show a different dynamics. A possible solution could be the usage of the Goldman-Hodgkin-Katz equation, where the permeabilities of each ion provide additional points of adjustment. However, this requires the estimation of the permeabilities of each ion. Furthermore, the permeabilities itself could depend on the membrane voltage as well as concentrations. Thus, the Goldman-Hodgkin-Katz equation provides some degrees of freedom, but also introduces some new disadvantages.

Since the membrane potential is maintained by the actuator Pma1, a different description has implications for the course of Pma1's control signal under starvation. Therefore, an improved equation is required for a detailed understanding of Pma1's control mechanism.

4.2.4 Tok1

The role of Tok1 requires further investigation. The current-voltage relations in the literature indicate a deactivation for negative membrane voltages. Under most experimental and natural conditions, the membrane potential does not reach positive values. Thus, in the model simulation Tok1 is always inactive and an exclusion from the model would have no effect. However, the literature as well as unpublished material indicate Tok1's significant influence on the potassium content and membrane potential. Thus, Tok1 may be also involved in additional sensor or signaling mechanisms. Another explanation could be, that Tok1 opens under certain conditions to release relevant amounts of potassium. But to allow Tok1 to extrude potassium, the membrane voltage must be more positive than Tok1's equilibrium potential (Nernst-potential of potassium), which is not the case for membrane voltages near -250 mV. Possibly, the stoichiometry of the potassium transport changes under certain conditions or the membrane potential is much more positive than assumed.

4.2.5 Nha1

Nha1 was the only system with no available electro-physiological data and is modeled according to a parsimony description. Nevertheless, Nha1 plays a central role in the model simulation. The proposed voltage gating is a vital part of the model and the systems variables are very sensitive to changes in g_{Nha1}. Although the existence of numerous organelle proton-potassium exchangers implies the relevance of a direct coupling of proton and potassium fluxes, Nha1 is the only K^+/H^+ antiporter in the model. However, Jennings and Cui (2008) suggest, that the vacuole potassium/proton antiporter Nhx1 is more powerful in regulating the internal pH than Nha1. Furthermore, Nha1 is the only model system which extrudes relevant amounts of potassium. In the living organism, a part of this extrusion could be done by unspecific leak processes or even Tok1, which has no influence in the model so far. Thus it is hypothesized, that the role of Nha1 is overestimated in the current model version.

At the very end of this work, the assumed $2H^+:1K^+$ stoichiometry of Nha1 was doubted by the experimenters, since the only support comes from Ohgaki et al. (2005). Respective model simulations showed, that a $1\tilde{H}^+:1\tilde{K}^+$ stoichiometry also leads to the prediction of Pma1 and the CO_2 production as potential actuators. However, under this condition, Trk1,2 can be additionally identified as an actuator; see Appendix 4.7. This finding implies, that the role of Trk1,2 might be underestimated in the current model.

The uncertainty about Nha1 hinders further model improvements. Changes in the Nha1 transporter have implications for the influence of Trk1,2 and also other systems. The development of a detailed controller for potassium homeostasis can be hardly achieved on such a weak basis.

On the long run it might be necessary to discriminate between the effects of the organelle and the membrane proton/potassium antiporters. However, this requires more knowledge about Nha1 and the characterization of the intracellular transport. The latter is up to recent experimental work by

José Ramos, University of Cordoba/Spain.

4.2.6 Reverse Tracking

The reverse tracking is a key achievement which is of general applicability in other situations, where the dynamic behavior of a system needs to be understood. For example in a signaling network the identification of the driver nodes may lead to hypothesis about the network structure, like additional input signals or feedback loops or the crosstalk between different processes. These questions are subject to current investigations.

Although this method is intuitive and quickly to implement in a model system it suffers from several disadvantages

- the amplification factor needs to be defined manually

- a constant amplification factor may not appropriate, when the dynamics of the tracking signal changes

- the oscillations

- a mathematical proof of the method is not obvious

- only one parameter can be estimated

The latter point is most relevant in this work, where Pma1 and the bicarbonate reaction are regulated in parallel. Thus, the estimated signal represents the combined effect of both processes and necessarily deviates from even a precise experimental measurement. In the present case the estimated signals are in qualitative agreement with the data. However, this must not hold in other situations.

The artificial feedback controller, which generates the control signal from external potassium was developed at a time, when it was hypothesized that either Pma1 *or* the bicarbonate reaction sequence is the actuator. However, this hypothesis was rejected by the experimental validation. Since Pma1, CO_2 production and maybe also Trk1,2 (see Appendix 4.7) are regulated in parallel, the proposed description of the controller becomes of minor use. The definition of an appropriate controller of potassium homeostasis is currently quite speculative. The shape of the respective control signals is not known in detail. It is even not possible to quantify the influence of Pma1 and the bicarbonate reaction system. These questions, arising from model limitations can only be addressed by further experiments.

4.2.7 Mechanism of potassium homeostasis

Currently it is not clear how the cell senses external potassium. The model hypothesis of an external potassium sensor is based on the stable potassium experiment (see Section 2.1.4) as well as the rapid control signal for the actuators (see Section 3.2.3). An early indication of a putative potassium sensor is given by Rothstein and Demis (1953) who reports an induction of fermentation by external, but *not* internal potassium. The same authors highlight the coupling of proton efflux and potassium uptake: "During fermentation of glucose, there is a temporary accumulation of potassium, which is associated with an exchange of metabolically produced hydrogen ion from the

cell" (Rothstein and Demis 1953, p. 19). However, the identification of a respective sensor requires further experiments.

While an additional sensor and signaling function can be hypothesized for the potassium transporters, the signal transduction and generation of the control signals for the actuators remains obscure. The experimental validation proved a mutual regulation of both potential actuators. The connection between both processes might be via the ATP demand, where an increased ATP consumption by Pma1 might be compensated by an enlarged ATP production what goes along with CO_2 release. Although the physiological link between Pma1 activity and CO_2 production is plausible the detailed interaction mechanism is not obvious. Two general possibilities are a (1) parallel stimulation of both processes or (2) a sequential activation, where e.g. the Pma1 activity itself or a decreasing ATP level triggers the production of ATP (and thus CO_2). Furthermore it is not clear whether *NCE103* expression is triggered directly by a $[K^+]_o$ dependent signal or by e.g. the CO_2 concentration or other indirectly influenced parameters.

At least for Pma1 the kinases Ptk2 and Yck1,2 are known to increase or decrease Pma1's activity (Eraso et al. 2006; Estrada et al. 1996). Thus, they might be a starting point for further investigations. A first step could be to prove their involvement in the given problem. A systematic search for interaction partners may then allow the construction of a putative signal transduction network. At this time, there is a tremendous number of possible signaling pathways. Thus, modeling can not produce reasonable model hypothesis and only specific experiments can bring further insights.

Maintaining potassium against a steep concentration gradient is an energy consuming task. Moreover, since the stationary concentration is controlled by a steady influx and efflux and large part of the pumped out protons return via Nha1 and in symport with nutrients. While Pma1 is known as the primary (and vital) driver of all transport processes, this work showed Pma1's role as a regulator of the intracellular potassium dynamics. This reflects, that potassium homeostasis is closely related to the provision of energy, what has implications for glucose transport, glycolysis, CO_2 production and the whole metabolic state of a cell.

The configuration of the transport systems is characterized by (1) the tight coupling of proton and potassium fluxes and (2) a negative feedback of the transporters activity (see Section 3.2.5). It is hypothesized that this enables the stability of the system.

A high stability is desirable for homeostasis. In the living organism the tight coupling of proton and potassium fluxes, ensured by many potassium/proton antiporters may allow a quick adaption to external and internal disturbances. The maintenance of a steady state is energy demanding, but cell's benefit is a very stable intracellular state. The configuration of the transporters might be a key to understand yeast's high salt tolerance under various conditions.

4.3 Conclusion and outlook

The bicarbonate reaction sequence serves as a proton buffer mechanism in many organisms. The findings of this work have implications especially for cells which energize their transport systems by the extrusion of protons. Although, mammalian cells usually use a sodium-potassium pump mechanism Huber et al. (2010) investigated the effect of proton extrusion in human cancer cells. Corresponding to a higher level of glucose consumption, these cells tend to acidify their surrounding by the extrusion of protons arising from the bicarbonate reaction. While the cancer cells can cope

with a slight acidic external pH, normal cells are inhibited in growth or get even killed by a pH differing from neutral. This led to the theory of acidic pH driven tumor invasion (Martin et al. 2011), what demonstrates that the study of the bicarbonate reaction sequence is also relevant in other organisms than yeast.

An electro-physiological model for yeast was developed for the first time. After some improving steps, the model was able to make predictions, which were successfully validated. These model predictions raised a lot of questions and implications for further investigations and future model versions.

Nevertheless, the model is highly advanced. Further model improvements may aim on several topics like the inclusion of organelle transporters, further species, kinetic regulation models of transport systems, sensing and signaling mechanisms or metabolic effects on proton buffering and production. However, for all these topics there is a weak experimental basis for valid model hypothesis. Moreover, the experimental observability of variables like (time-resolved) enzyme concentrations, membrane potential, signal transduction, gene regulation etc. is only partly given. To avoid any speculative model extensions, new insights, data and experimental techniques have to be developed.

The major benefit of this work is not a certain mathematical model but the revelation of the central role of proton fluxes. This allows experimenters to focus on the most relevant issues. And even this means a lot of work and time.

In several years, a model of potassium homeostasis in yeast may look completely different than today. However, what will remain is the finding, that instead of the potassium transporters, the regulation of the proton efflux is the central key to understand the maintenance of potassium. Anything what affects the proton fluxes affects the potassium concentration. Thus, it is predicted, that potassium homeostasis will not be understood without the detailed knowledge about metabolic proton production and the regulation of proton fluxes.

Appendix

The appendix includes further material, results and additional comments. It supports the present work and should allow a deeper understanding. It also ensures a fluent reading of the main part: helpful, but not necessary informations, which are too long to fit in a footnote can be found in the appendix. It is also a pool of things that were developed, but finally not used in this thesis. Since the additional material would fill fills dozens of pages, the description is shortened to a minimum.

The appendix does not only give an impression of what has been tried without success, it also gives hints for further investigations. It is highly coupled with the main part of this work. Respective cross-references should allow the reader to easily navigate through the document.

4.4 Potassium uptake

> Related to
> ► Section 3, page 59
>
> ► Section 2.2.11, page 48

The following data was kindly provided by Sergey and Lana Shabala, University of Tasmania, Hobart, School of Agricultural Science. The experiment follows a protocol originally developed by Jost Ludwig, University of Bonn, Institute for cellular and molecular botany. To investigate the uptake of potassium yeast, cells were grown and harvested in the stationary phase. Afterwards, they were starved for more than four hours in distilled water, to reduce the potassium content and bring the cells in a need of potassium. The following observation of the potassium uptake consists of two steps. First a certain amount of potassium is added to the medium. This results in a very low potassium uptake. This indicates that the presence of potassium in the medium is not sufficient for an appropriate potassium supply. In the next step, glucose is added to the medium. The uptake of glucose by a cell leads on the one hand to the production of ATP, as well as a direct stimulation of the proton pump by glucose itself (Serrano 1983). As a result, the activity of the proton pump is increased[1]. This finally energizes the uptake of potassium via Trk1,2 and other systems. That not only Trk1,2 is energized by an increased Pma1 activity, but also other unspecific transporters can be observed in the potassium uptake measurements in *trk1,2Δ* mutants. An overview of the potassium uptake data for the wildtype and *trk1,2Δ* mutant can be found on page VIII. In any case, the data implies, that potassium is taken up mainly in exchange with protons.

The resulting potassium and proton fluxes were measured by using the MIFE® technique (microelectrode ion flux estimation)[2]. A cell sample is fixed as a mono layer on a microplate. Above the surface of the sample (in the micrometer range), an ion selective micro-electrode is placed. The basic idea is that the concentration of a substance released from a sample is higher near the surface than farther away (and *vice versa* for a substance taken up). MIFE® utilizes ion-selective microlelectrodes which tips are moved in a short time between two vertical positions above the surface of the sample. The change of the electrochemical potential between the two positions is used together with the Nernst-Planck equation to indicate the net flux of an ion over the membranes of a cell sample (Shabala et al. 2006). For a detailed physical explanation and a deeper insight in the technique the reader is referred to Newman (2001).

The specific experimental procedure as it was kindly provided by Sergey Shabala:

- Cells (strain PLY232) were grown in appropriate growth media

- Cell suspensions were transferred to appropriate centrifugation tubes and spinned down (5 min, 4000 g)

- The supernatant was discarded and cells resuspended in the same volume of bi-distillate water

- The above two steps were repeated one more time

- The supernatant was discarded again, and resuspended cells were transferred in double distilled water to Erlenmeyer flask and left stirred at 4 C overnight

---

[1] At the beginning there were some discussions, whether Pma1 is stimulated only pulse-wise (around 10 minutes) or for a long period of time (hours). A well investigated fact is the tendency of metabolic active cells to acidify their medium. It is also known, that glucose stimulates the metabolism. It can be concluded, that as long as glucose is available, the cells are metabolic active and therefore extrude protons. Due to the inward directed proton gradient, the only way of proton extrusion is via Pma1. A pulse-wise Pma1 stimulation in the model, would lead only to a transient increase of potassium.

[2] Visit `www.mife.com` for detailed information

- On the next day, cell suspensions were transferred to centrifugation tubes and spinned down (5 min, 4000 g)

- The supernatant was discarded and cells resuspended in 1 mM MES buffer

- Cells were immobilized on a cover slip and placed in the measuring chamber with 1 mM MES buffer

- Measurements were started (e.g. nearly zero at [K+] and no sugar) and net K^+ fluxes measured for 4-5 min

- KCl was added from stock solution to give required final KCl concentrations - one of 10 μM, 100 μM, 1 mM and 10 mM, and measurements taken for another 5 min

- Glucose solution (made in 1 mM MES) was added to give a final glucose concentration of 5%, and fluxes measured for 15 more minutes

The external pH is adjusted to 5.5 pH at the beginning of the recording. The cell volume is assumed to be 110 fL.

The MIFE$^{®}$ data was originally used to calibrate the biophysical model. During the TRANSLUCENT project the MIFE$^{®}$ technique was unavailable for extensive studies. Thus, the experimental verification of related hypothesis was not possible. Due to many uncertainties and experimental problems the work on this data was finally discontinued, since it appeared less promising. Anyway, the related thoughts and efforts may serve for future investigations. An additional modeling approach can be found in Gerber (2011).

4.4.1 Unit conversion

The original data is given in the unit $nmol/(m^2\,s)$. Again, the size of the used cells is not known; here 6 μm (sphere shape) is assumed. The conversion is done by multiplying with the surface to volume ratio[3]

$$\frac{\text{nmol}}{\text{m}^2\,\text{s}} \cdot \frac{surf}{vol} = 10^{-6} \frac{\text{mmol}}{10^4 \text{cm}^2\,\text{s}} \cdot \frac{surf}{vol} \tag{4.1}$$

$$= 10^{-10} \frac{\text{mmol}}{\text{cm}^2\,\text{s}} \cdot \frac{1.131 \cdot 10^{-6}\,\text{cm}^2}{1.131 \cdot 10^{-10}\,\text{cm}^3}\,. \tag{4.2}$$

This yields the relationship for the flux as

$$\frac{\text{nmol}}{\text{m}^2\,\text{s}} \;\hat{=}\; 10^{-6} \frac{\text{mmol}}{\text{cm}^3\,\text{s}}\,. \tag{4.3}$$

Multiplying with Faraday's constant and the volume to surface ratio results in the relationship

$$\frac{\text{nmol}}{\text{m}^2\,\text{s}} \;\hat{=}\; 0.0096 \frac{\mu\text{A}}{\text{cm}^2}\,. \tag{4.4}$$

4.4.2 Data analysis

Figure 4.1 shows the potassium and proton fluxes obtained with the MIFE$^{®}$ technique for the experiment described above (wildtype). The integration of the fluxes allows to estimate the theoretical concentration change inside the cell (Table 4.1). The concentration changes for potassium yield plausible results. Regarding the normal intracellular pH of 10^{-4} mM the values for the integrated proton flux might appear questionable, since far more protons are extruded than free protons are available in the cell. This implies the existence of a powerful proton buffer system; see Table 4.2.

	10 μM	100 μM	1 mM	10 mM
H^+ (mM)	60	89	92	119
K^+ (mH)	17	54	85	236
Difference	43	35	7	-117

Table 4.1: *Estimated concentration changes after glucose addition. Although potassium is apparently taken up in exchange with protons, a one to one relationship could not be detected. This implies, the involvement of other species and/or processes.*

---

[3]There might be some doubt, whether the surface in the MIFE$^{®}$ experiments is really related to the surface of the cell samples or the surface of the micro-plate. The suggested procedure of unit conversion was therefore discussed with Sergey Shabala. He stated, that he uses the same approach and considers the results as reasonable.
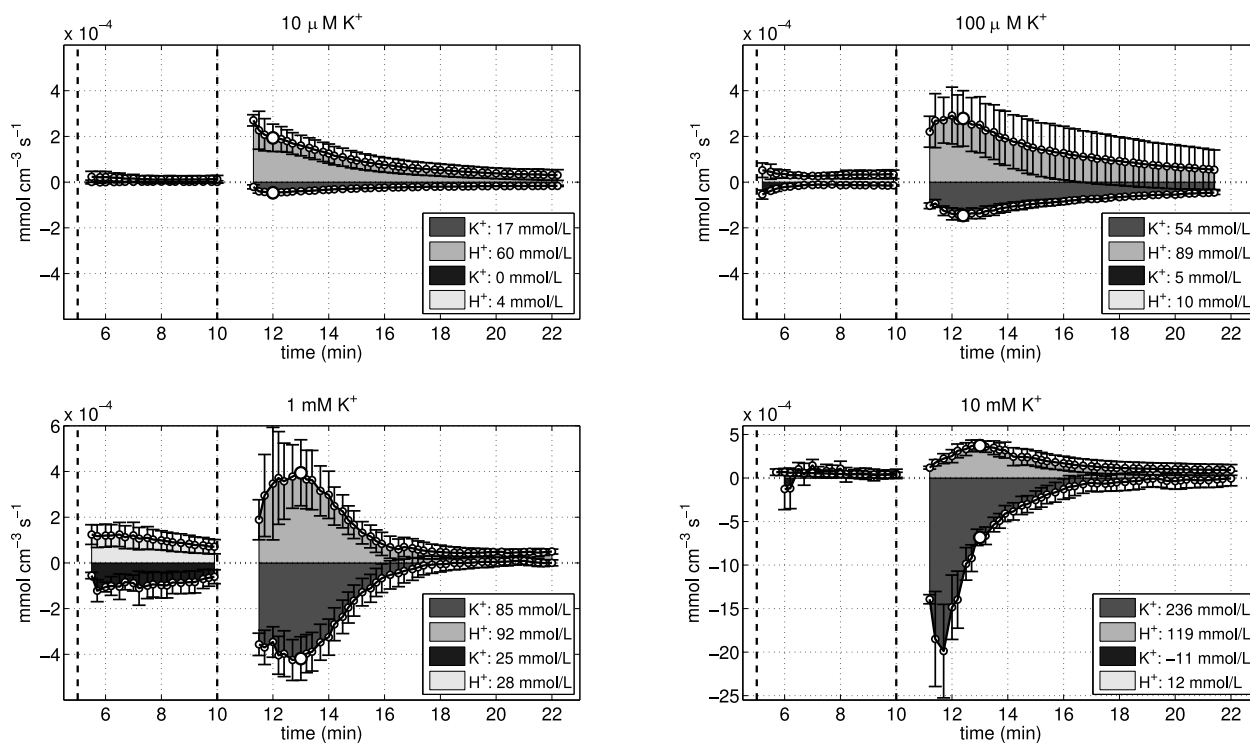
Figure 4.1: *Potassium and proton fluxes for four different KCl concentrations added to the medium. The x-axes indicates the time (minutes) and the y-axes the flux. The sign convention follows influx: negative. The vertical lines indicate the addition of KCl (at five minutes) and glucose (at ten minutes). Disturbances caused by this step are cut from the data. The errorbars represent the 95% confidence interval (five readings). The area under the curves represent the integrated fluxes. The respective values are given in the legend. The big open circle indicate the time point after which a linear relationship between the proton and potassium fluxes can be detected; see Figure 4.2.*

Only in the case of 1 mM KCl, there is almost an one to one relationship between protons and potassium. That for the most cases, the efflux of protons does not correspond exactly to the uptake of potassium indicates the involvement of other particles and/or processes. For the lower external potassium concentrations, the required electro neutrality implies a net extrusion of around 40 mM negative charges. In principal, this is equivalent to the uptake of positive charges, but the surrounding recording buffer does not include anything, which could expected to be taken up. For 10 mM KCl the required extrusion of anions turned into a need of anions (or extrusion of cations). The phase portrait of the proton and potassium fluxes (see Figure 4.2) shows a linear relationship after twelve minutes of the recording. The respective data points after which the relationship could be detected are marked as big open circles in Figure 4.1. A linear relationship might imply a certain stoichiometry between proton release and potassium uptake. This would highlight the tight coupling of proton and potassium fluxes.

Buffer capacity

Using the yeast strain BY4741, Jost Ludwig, University of Bonn, Institute for Cellular and Molecular Botany, repeated the above experiment.

	10 μM	100 μM	1 mM	10 mM
ΔH (mM)	60	89	92	119
ΔpH (pH)	0.29	0.29	0.42	0.6
$\Delta H/\Delta pH$ (mM/pH)	207	307	219	198

Table 4.2: *Estimation of the proton buffer capacity by relating the theoretical proton concentration change from the experiments of S. Shabala to the pH changes measured by J. Ludwig.*

He measured the intracellular pH changes by the help of a pH sensitive fluorescent protein (unpublished results). After glucose addition the pH increases rapidly and reaches a new stationary level after five to ten minutes. Relating the integrated proton flux after glucose addition to the pH change, allows to estimate a buffer capacity of the cytosol, see Table 4.2.
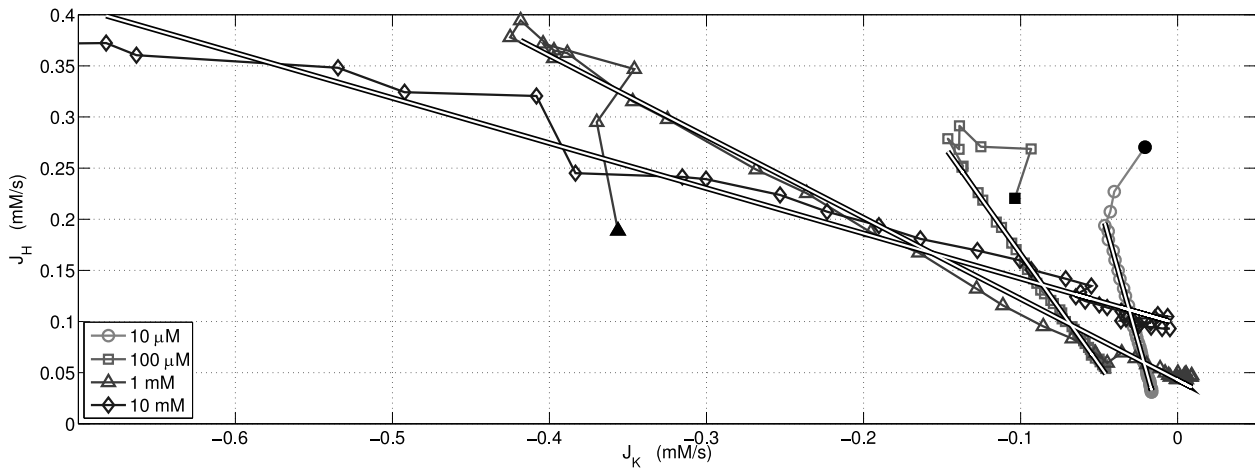
Figure 4.2: *Proton fluxes versus potassium fluxes from Figure 4.1. The figure shows the data after glucose injection. The filled data points corresponds to time point eleven minutes. The following data points represent time steps of six seconds. The solid lines are regression lines in the area, where the linear relationship between both fluxes is obvious.*

A direct comparison might be problematic since two different strains were used. Anyway, apart from the case of 100 μM KCl, the values indicate a constant buffer capacity of 200 mM/pH. Remembering the values reported for *S. cerevisiae* and *N. crassa* (see Section 2.2.11), the obtained buffer capacity appears valid.

4.4.3 Model simulation

The data of S. Shabala does not show a one to one correspondence of the proton and potassium fluxes. Only in the case of 1 mM KCl such a relationship can be observed. The missing ions or processes are still not identified. Related model approaches including a chloride leak and a chloride proton symport were tested without success. The required amounts of chloride could not be maintained in the simulations. A discussion of possible species involved is given at the end of this section. The unidentified fluxes hinders the simulation of each of the four experiments.

Variable	Value	Unit
β	0.2	mmol/cm^3/pH
$g_{Trk1,2}$	23	μS/cm^2
$d_{Trk1,2}$	1	dimensionless
$V_{1/2,Trk1,2}$	-0.168	V
g_{Tok1}	8	μS/cm^2
d_{Tok1}	-1	dimensionless
V_{Tok1}	-0.0034	V
g_{Nha1}	10	μS/cm^2
d_{Nha1}	1	dimensionless
V_{Nha1}	-0.310	V
I_{Pma1}^{max}	18	μA/cm^2
g_K^{leak}	5	μS/cm^2
g_H^{leak}	25	μS/cm^2
$[K^+]_i(0)$	0.15	mmol/cm^3
$pH_i(0)$	6.8	pH
$V_m(0)$	-0.2	V
V	110	fL

Table 4.3: *Parameters used for the data fit of the potassium uptake measurement for 1 KCl addition.*

However, the case of 1 mM KCl can be described by the model, demonstrating the ability of the model to simulate the potassium uptake experiments. The presented model approach covers only potassium and proton fluxes and includes the systems Trk1,2, Tok1, Nha1, Pma1 as well as leakage currents for protons

and potassium. The description of the transport currents follow the mathematical expressions given in Section 2.2.

The volume is not regarded because respective measurements of Clara Navarrete, University of Cordoba, Spain, (not published) indicate a constant volume during the experiments. This is most probably due to a very rigid cell wall, which is further strengthened under starvation conditions. Thus osmotic effects or volume regulation processes are not likely to be present or rather too small to be detected during the few minutes of the recording. This is an expedient fact, since the MIFE$^{\circledR}$ technique assumes the absence of water convection and uptake (Newman 2001).

The parameters and initial conditions used in the model simulation were shown in Table 4.3. The addition of KCl is modeled as an time dependent increase in the external potassium concentration. The stimulation of the proton pump after glucose injection is modeled by a time dependent increase of the parameter I_{Pma1}^{max}. Respective definitions are given below.

The potassium increase from $K_0 = 10\mu$M to $K_1 = 1$mM is modeled according to

$$[K^+]_o(t) = K_0 \frac{(K_1 - K_0)}{1 + e^{-s_1 \cdot (t - t_1)}} \,, \tag{4.5}$$

where $s_1 = 0.25$ controls the steepness and $t_1 = 0.25 \cdot 60^2$ s the time point of the potassium switch. The Pma1 stimulation is modeled as

$$\tilde{I}_{Pma1}^{max} = \left(1 + \frac{P_1}{1 + e^{s_2 \cdot (-t - t_2)}}\right) \cdot I_{Pma1}^{max} \,, \tag{4.6}$$

where $P_1 = 5$, $s_2 = 0.25$ and $t_2 = 0.365 \cdot 60^2$ s.

$$\frac{d}{dt}[K^+]_i \quad = \quad -J_K = -\left(J_K^{Trk1,2} + J_K^{Tok1} + J_K^{Nha1} + J_K^{leak}\right) \tag{4.7}$$

$$\frac{d}{dt}pH_i \quad = \quad \frac{1}{\beta} \cdot J_H = \frac{1}{\beta}\left(J_H^{Pma1} + J_H^{Nha1} + J_H^{leak}\right) \tag{4.8}$$

$$\frac{d}{dt}V_m \quad = \quad -\frac{1}{c_m}\left(I_H + I_K\right) \tag{4.9}$$

$$\tag{4.10}$$

The aim of the approach is to fit the simulated fluxes J_K and J_H to the raw data presented in Figure 4.1. The resulting data fit is shown in Figure 4.3. The simulated fluxes are in good qualitative agreement with the data. After the increase of the external potassium concentration and also after the increased Pma1 activity, the system reacts as expected with a potassium uptake and proton extrusion. After several minutes, the system returns to a stationary state, where the uptake and efflux processes are balanced and the net transport of protons and potassium is zero. The dynamics of the return to the stationary state could not described well by the model approach.

Figure 4.4, page VI shows the time courses of the internal potassium, pH and membrane potential. Potassium behaves as expected. Starting with a stable concentration of 100 mM, the external potassium increase leads to an increase in the internal potassium to 150 mM. The following activation of the proton pump yields an additional uptake of potassium to a final concentration of around 300 mM. This uptake of potassium requires an extrusion of protons in the order of 200 mM. Regarding the assumed proton buffer capacity of 200 mM/pH, it can be expected, that the internal pH change is nearly 1 pH unit. The simulated pH changes from 6.5 pH to above 7.4 pH. Although, these values may be slightly higher than the physiological values, the pH behaves like expected. The simulated membrane potential is a bit more complicated to explain. The increase of external potassium leads to a shift of the potassium equilibrium potential in the positive direction, which supports the uptake of potassium. Concomitantly, the membrane depolarizes due to the uptake of positive charges. This depolarization of the membrane is turned to a hyperpolarization at the moment Pma1 is stimulated and extrudes positive charges. Since the energy provided by this process is consumed by the potassium uptake systems, the hyperpolarization is only transient and a more positive membrane potential is achieved again.

Figure 4.5, page VII shows the activity of the different transport systems. The currents through Trk1,2 increase each with external potassium change and Pma1 stimulation. When regarding the currents of Pma1 it may confuse, that the current increase after the simulated stimulation is rather small. It may appear questionable, why such a small increase could drive the uptake of potassium. This question can be clarified, when looking at the Nha1 currents. The membrane potential reacts very sensitive on changes in the Pma1 activity. The model simulation predicts a transient hyperpolarization of the membrane in response to the stimulation of Pma1. This hyperpolarization enables the voltage gating of Nha1, which causes a reduction of the proton influx. Together with the small Pma1 activity increase, the net proton efflux is increased efficiently.
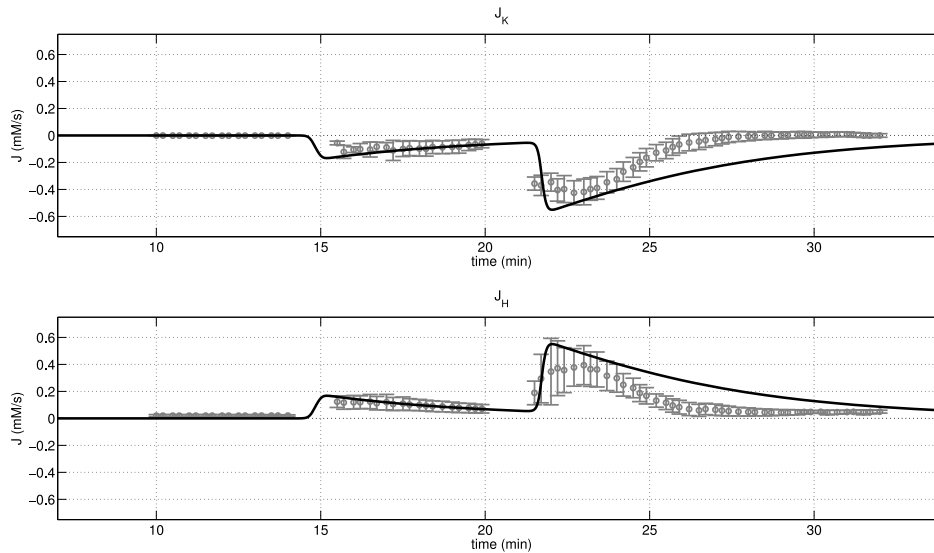
Figure 4.3: *Data fit of the model simulation for 1* mM *KCl. The grey data points with the 95% confidence interval is the proton and potassium flux data from the potassium uptake measurement shown in Figure 4.1. The black lines represent the simulated potassium and proton fluxes. A data fit covering the dynamics of the fluxes could not achieved. However, the simulation is in a good agreement with the data.*
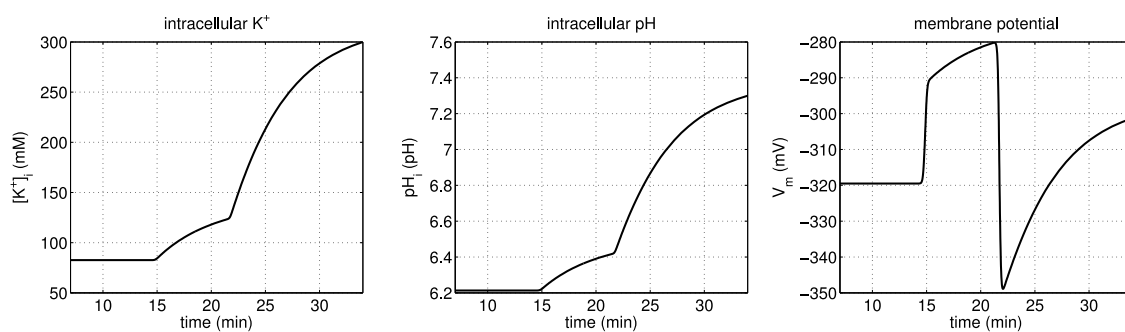
Figure 4.4: *Simulated internal potassium concentration, pH and membrane potential.*
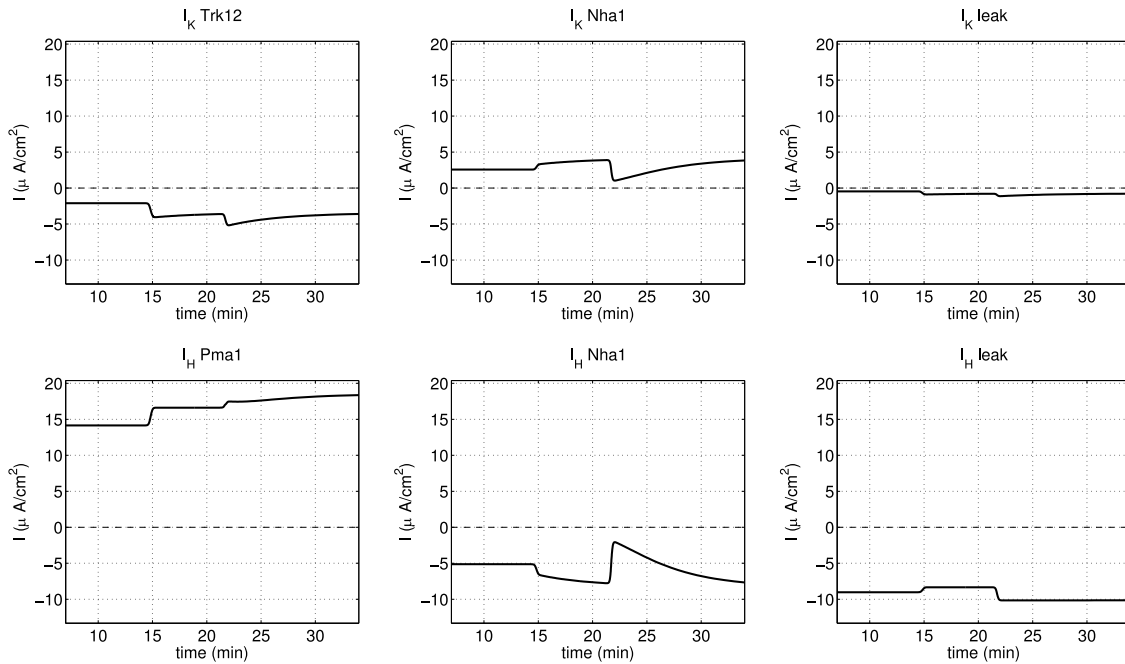
Figure 4.5: *Simulated activity of the transport systems. Tok1 is not shown since it is not active for the present conditions. The inset for Pma1 is a magnification showing the moment, when Pma1 is stimulated. The decrease of the Nha1 currents is a result of the Nha1 voltage gating in response the the transient hyperpolarization of the membrane, when Pma1 is stimulated.*

4.4.4 Discussion

Apart from the case of $[K^+]_o = 1\,\text{mM}$, the data does not show a 1:1 correspondence between proton and potassium fluxes. This gives rise to the notion, that there might exist additional (but not recorded) fluxes. From the data a clear tendency can be detected: for KCl < 1 mM, the proton extrusion exceeds the potassium uptake. At KCl $= 1$ mM almost a 1:1 correspondence is visible and for 10 mM KCl the potassium influx exceeds the proton release.

Assuming that one sort of ion is responsible for the observed effect, either a cation or an anion has to be taken into account. In order to maintain the required charge balance additional cations need to be taken up for low KCl and extruded for higher KCl. The recording buffer solution contains 10 mM CaCl$_2$, KCl and glucose. Calcium is rather a signaling molecule and the intracellular concentrations hardly exceed the micromolar range. Thus, the influx of further cations can be ruled out, since no cations are available.

In case of anions, the extrusion of anions for lower KCl and the uptake for higher KCl is needed. Since chloride is the only anion which is present in the external medium, the missing anion might be chloride. This means for lower KCl the extrusion around 40 mM and the uptake of around 100 mM for higher KCl.

The physiological cytosolic chloride concentration is given in the literature as around 1 mM. However it is reported that depolarized cells can keep higher amounts of chloride because of the efflux is energized by a negative membrane potential. In the present case, where the cells are starved in pure water for several hours, it is likely that the lack of energy providing glucose, leads to a reduced activity of the plasma membrane ATPase and thus a more positive membrane voltage. This would in principle support higher chloride concentrations. However, before a possible de-energization of the cell takes place, the membrane will hyperpolarize at the beginning of the starvation period due to the loss of potassium. This would support the efflux of chloride. Before starvation the cells kept in standard growth medium, and an accumulation of chloride far in the millimolar range is not reported in the literature for such a condition. For example, Kuroda et al. (2004) reports a large chloride efflux via Trk1,2, when the intracellular chloride is artificially raised beyond 1.2 mM. Concomitantly Trk1,2 becomes insensitive against external potassium. Both findings do not support the idea of a chloride accumulation.

The CO$_2$ production can also not hold as an explanation. The production yields H$^+$, uncharged H$_2$CO$_3$ and negative HCO$_3^-$. The latter one is rather impermeable to the membrane. Thus a CO$_2$ production would lead to an intracellular *accumulation* of HCO$_3^-$ and the data indicates, that 40 mM of negative charges needs to be *extruded* for lower KCl. When it is assumed, that only one specie can explain the missing fluxes, it needs to be justified, why the direction of that fluxes change with different concentrations of KCl. An ion, which could behave like this is not obvious. It is thus more likely, that more than one process is responsible for the observations.

It is predicted, that the elucidation of all the related problems and questions will turn out to be time consuming.
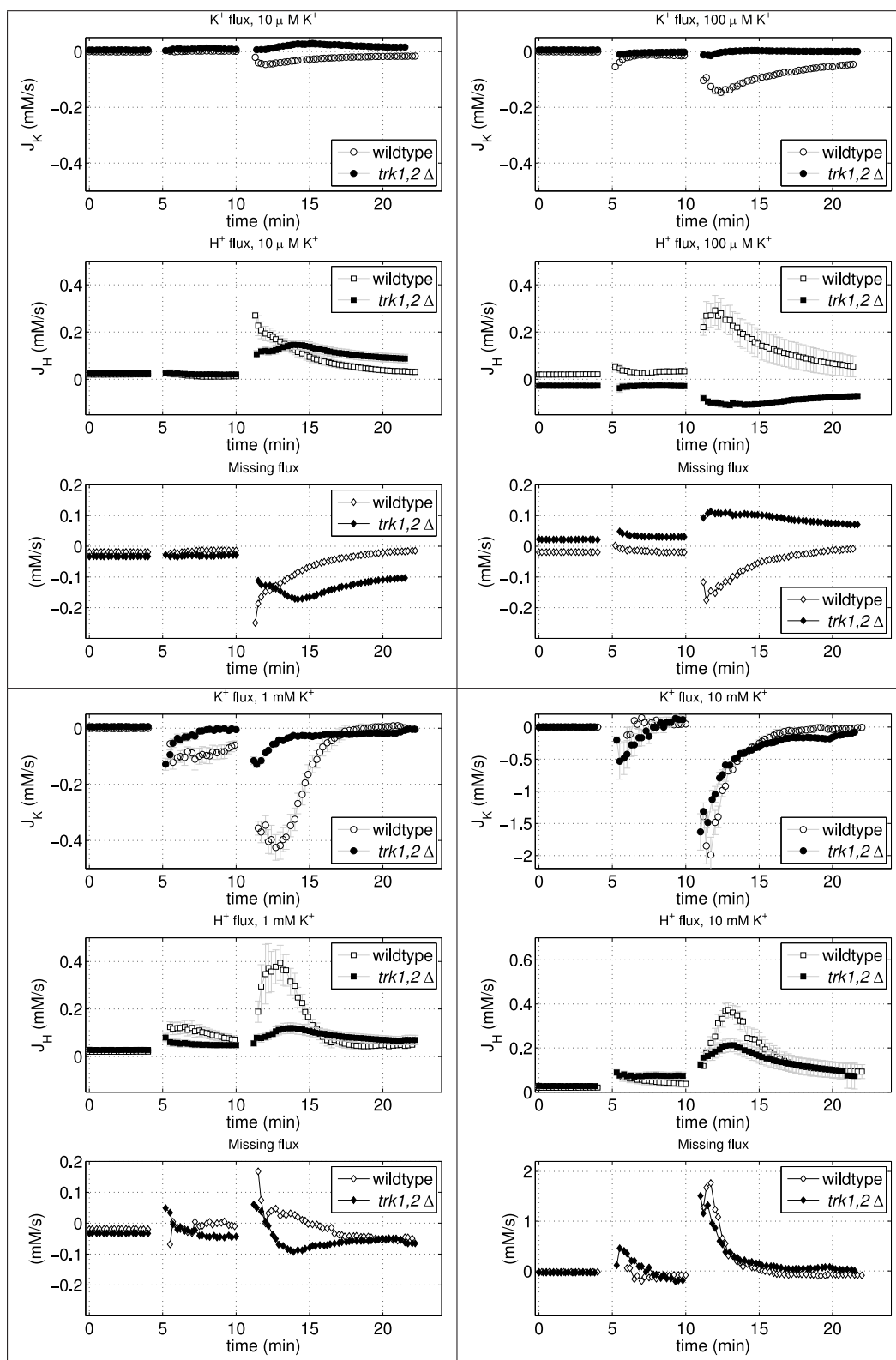
Figure 4.6: *Potassium uptake experiments from Sergey Shabala for the wildtype and trk1,2Δ. KCl addition at five minutes, glucose injection at ten minutes. The four panels represent the four different KCl concentrations added: 10 μM, 100 μM, 1 mM, 10 mM. Each panel shows the potassium and proton fluxes as well as their difference. For the trk1,2Δ mutant the addition of glucose apparently energizes the unspecific potassium uptake in case of 1 mM and 10 mM.*

4.5 Experimental wishlist

The aim of the model building process is to generate knowledge about the model organism. This requires a steady evaluation of model predictions. To support the modeling, the several experiments were planned by the author in cooperation with the wet lab scientists. The data is owned by the respective experimenters and is (in the most) cases not published yet.

The experimental wishlist was originally meant to complete the knowledge about the potassium starvation experiment by Navarrete et al. (2010) and the potassium uptake measurements by Sergey Shabala[6] (see Appendix 4.4). Additional experiments were designed to support several model hypothesis.

1. Potassium starvation experiments according to Navarrete et al. (2010)

   - Relative membrane potential; additional time points after four and five hours of potassium starvation. Status: the hyperpolarization is rather constant after one hour of potassium starvation; not published. Experimenter: Sylvia Petrezselyova[1]

   - Extracellular concentration changes. Status: changes are not expected due to the large volume of the medium. Experimenter: José Ramos[2]

   - Intracellular concentration changes of potassium. The experiment was repeated several times for the wildtype and different mutants; partially published; see Section 2.1.3. Status: wildtype, $nha1\Delta$, $trk1\Delta$, $trk2\Delta$, $trk1,2\Delta$, $sap155\Delta$, $sap185\Delta$ show similar dynamic behavior under potassium starvation. Experimenters: Sylvia Petrezselyova[1], José Ramos[2].

   - Intracellular ammonium concentration under potassium starvation for the wildtype. Status: the ammonium concentration increases from 4 mM before starvation to 10 mM after one hour of starvation, the concentration in; not published. Experimenter: Lina Patricia Barreto[3], Joaquin Ariño[3],

   - Volume changes. Several repetitions were performed for wildtype and $trk1,2\Delta$. Differing to Navarrete et al. (2010) the wildtype cells increase their volume after one hour of starvation. This supports the notion of possible growth effects in Navarrete et al. (2010); not published. Experimenter: Sylvia Petrezselyova[1]

   - Concentration of non permeable substances. Status: an estimate could be derived from Gennemark et al. (2006); see Section 2.2.12.

   - Fraction of non-osmotic volume. Status: an estimate can be given based on Gennemark et al. (2006); see Section 2.2.12.

   - Fraction of free and bound/buffered cytosolic species like potassium. Status: a related experiment was not possible

   - Time course of the intracellular pH. Status: in progress, preliminary results indicate a pH drop of 0.5 units; not published. Experimenter: Sylvia Petrezselyova[1], Olga Kinclova[1]

   - Glucose uptake fluxes. Status: this experiment can potentially be done by Joaquin Ariño[3].

   - Cell population size during starvation. Status: available from Navarrete et al. (2010).

   - Time resolved expression level of the carboanhydrase. Status: published, see Section 2.1.5. Experimenter: Joaquin Ariño[3]

   - Time resolved Pma1 activity. Status, published, see Section 2.1.6. Experimenter: Lynne Yenush, Vicent[7] Llopis Torregrosa[7]

2. Potassium uptake experiments according to Sergey Shabala[6]

   - Relative membrane potential before and five minutes after KCl addition. Status: the membrane hyperpolarizes due to the uptake of positive charges; not published. Experimenter: Sylvia Petrezselyova[1].

   - Extracellular concentration changes of various species like K^+, Cl^-, H^+ and Na^+ (MIFE technique). Status: not published. Experimenter: Hella Lichtenberg[4].

   - Intracellular concentration changes of various species. Given an initial concentration, the intracellular concentrations can be estimated from measured fluxes. Initial concentrations were determined for several mutants. Status: not published. Experimenter: José Ramos[2].

   - Transport fluxes of various species (MIFE technique). Status: not published. Experimenter: Hella Lichtenberg[4].

   - Volume changes after the addition of glucose and KCl. Status: the volume does not change; not published. Experimenter: Clara Navarrete[2].

   - Fraction of free and bound/buffered cytosolic species like potassium. Status: a related experiment was not possible.

   - Time course of the cytosolic pH during glucose induced potassium uptake. Status: the pH increases roughly 0.5 units; not published. Experimenter: Sylvia Petrezselyova[1], Jost Ludwig[4].

   - Rough estimate of the proton buffer capacity. Status: work in progress. Experimenter: Jost Ludwig[4].

- Cell population size during overnight starvation in pure water. Status: the cells survive to almost 100%; not published. Experimenter: Guido Hasenbrink[4].

3. Stable potassium experiments

   - Stable potassium experiment. Finished for wildtype; see Section 2.1.4. Repetitions for various mutants in progress. Experimenter: José Ramos[2].

   - Preliminary intracellular pH measurements were performed by Daniel Ganser[4], not published. Status: the intracellular pH shows similar behavior than potassium. For lower external KCl the pH is rather 6 pH and becomes stable for higher KCl.

   - Measurements for the relative membrane potential were performed by Sylvia Petrezselyova[1], not published. Status: The membrane potential shows stable values for external KCl above 1 mM. Below, a hyperpolarization in dependence of the external KCl can be observed.

4. Electro-physiological measurements

   - Current-voltage relationships for Nha1 expressed in oocytes. Status: in progress. Experimenter: Chris Palmer[5], Vadim Volkov[5]

   - Current-voltage relationships for Trk1,2, Pma1 and Tok1. Status: planned. Experimenter: Chris Palmer[5], Vadim Volkov[5]

[1] Institute of Physiology, Academy of Sciences of the Czech Republic, Prague

[2] Departamento Microbiologia, Campus Rabanales, University of Cordoba, Spain

[3] Department de Bioquimica i Biologia Molecular, Facultat de Veterinaria, Universitat Autonoma de Barcelona, Bellaterra, Spain

[4] Universität Bonn, Institut für Zelluläre und Molekulare Botanik (IZMB)

[5] Institute for Health Research and Policy, Metropolitan University, London

[6] University of Tasmania, School of Agricultural Science

[7] Universidad Politécnica de Valencia, Valencia, Spain

4.6 Cell weight and volume

Related to
▶ Section 2.1.3, page 27

In Section 2 the cell weight and the physical density of a yeast cell was used for the purpose of unit conversion. For a historic view, the article of Seliber and Katznelson (1929) could be interesting. The authors give an estimate for the wet weight of a yeast cell under different conditions. The Tables I-XV gives the minimal and maximal cell weight estimation for each condition. Pooling all mentioned values, one find a mean of

$$\bar{w}_{Zelle} = 1.94\,10^{-7}\,\mathsf{mg}$$

and a median of

$$\hat{w}_{Zelle} = 1.45\,10^{-7}\,\mathsf{mg}\,.$$

According to this results, a yeast cell of $1.94\,10^{-7}$ mg and an assumed density of $1.1\,\mathsf{g/cm^2}$ would have diameter of around $7\,\mu$m (sphere shape). It can be presumed, that the material does not consist of *one* strain. Nevertheless, the plausible result implies, that the modern theoretic thoughts about the cell weight are in good agreement with the ancient measurements.

4.7 Trk1,2 as a possible actuator

Related to
▶ Section 3.2, page 69

▶ Section 4, page 88

The model prediction of Pma1 and CO_2 as actuators of potassium homeostasis could be verified by experiments. A surprising result is the exclusion of Trk1,2 as a potential actuator. On the one hand, this could be understood as a hint on a minor role of Trk1,2 in regulating homeostasis. It can be hypothesized, that regulating the proton efflux is more relevant than the regulation of the potassium uptake systems. However, the importance of Trk1,2 is out of question. Several articles (Ariño et al. (2010) and references therein) show Trk1,2's influence on the potassium content and its regulation in response to external potassium changes.
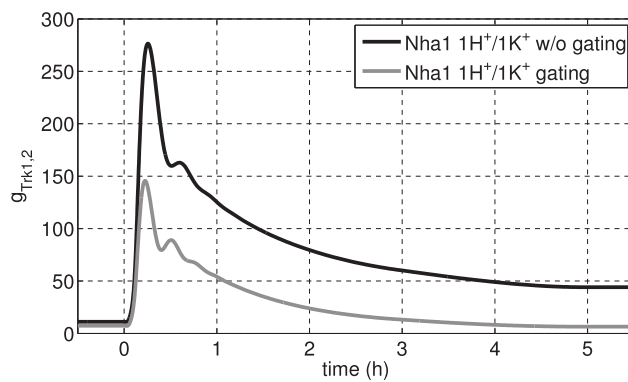

Figure 4.7: *Reverse tracking for Trk1,2. Nha1 was assumed to be an electroneutral antiporter with a $1H^+:1K^+$ stochiometry. Trk1,2 can serve as an actuator regardless whether a voltage gating is assumed or not. The shape of the estimated control signals is similar to those of Pma1 and CO_2 production (left panel). The right panel shows the respective data fit.*

It is not obvious why the cell spends energy for the regulation of a less relevant system. It is also questionable, if one should trust the prediction of a very first modeling approach more than the conviction of designated experts. A reasonable explanation arose from the investigation of Nha1.

At the very beginning of this work, the proposition of Ohgaki et al. (2005) as electrogenic was "cutting-edge-science". However, the lack of further experimental support led finally to the conviction of an electroneutral transporter. At the very end of this work, electrophysiological data for Nha1 was not available. Anyway, the assumption of a $2H^+:1K^+$ stoichiometry of Nha1 was more and more in doubt, since the only support comes from Ohgaki et al. (2005) and no other electrogenic potassium/proton antiport is known in *S. cerevisiae* or a related organism.

Although the model prediction of CO_2 and Pma1 as potential actuators was already verified, it was investigated what happens if Nha1 is not treated as electrogenic. Again, for each system it was tried to estimate a control signal; see Table 4.4.

The original model hypothesis about the role of CO_2 and Pma1 could be derived also with Nha1 as an electroneutral $1H^+:1K^+$ antiporter. In addition, Trk1,2 can also serve as an actuator. If no voltage gating is applied to Nha1, Trk1,2 is even

the only actuator of the system; see Figure 4.7.

These findings suggest, that the role of Trk1,2 is probably underestimated in the current model version. They also demonstrate Nha1's capability to change the model prediction. Thus, a detailed knowledge about Nha1 is crucial for further model versions.

	Nha1			
	$2H^+/K^+$ gate	$2H^+/K^+$ w/o gate	H^+/K^+ gate	H^+/K^+ w/o gate
Trk1,2 K^+ uniport	x	x	$\checkmark$	$\checkmark$
Trk1,2 $2K^+$ symport	x	x	x	x
Trk1,2 $H^+:K^+$ symport	x	x	x	x
Nha1	x	x	x	x
CO_2 production	$\checkmark$	x	$\checkmark$	x
Pma1 activation	$\checkmark$	x	$\checkmark$	x

Table 4.4: *Overview of possible actuators. The rows indicate the actuators and the columns the transporter type of Nha1. The symbol $\checkmark$ marks the actuators for which a control signal could successfully be estimated. Apparently the voltage gating of Nha1 is a crucial point for explaining the systems dynamics. The respective parameter values used can be found in the tables in the Appendix 4.10.*
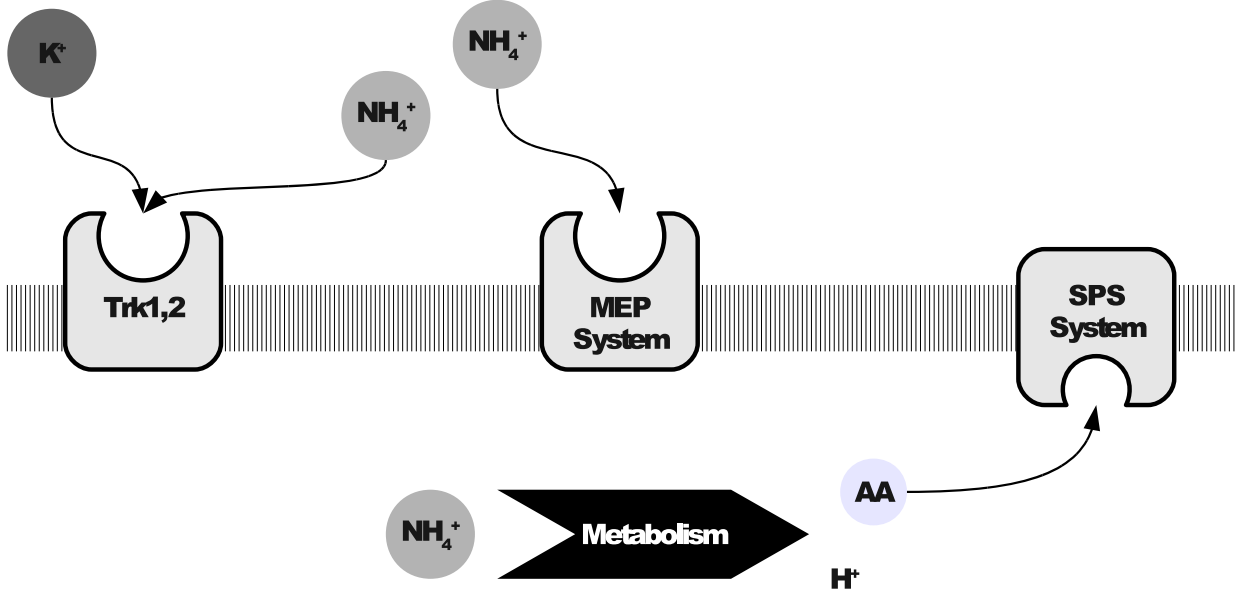
Figure 4.8: *Scheme of the ammonium model extension. Ammonium competes with potassium to be transported via Trk1,2. Additionally ammonium is taken up via the MEP system. One ammonium is degraded into one electroneutral amino acid and one proton. Amino acids were extruded by the SPS system.*

4.8 Ammonium model extension

In the experiments of Navarrete et al. (2010) the NH_4^+ concentration is around 90 mM; see Section 2.1.3, page 26. When calibrating the model to the potassium starvation data, the involvement of ammonium was in suspect to explain the dynamics of the potassium loss. Therefore the ammonium model extension was developed.

Assumptions:

- ammonium enters the cell via the MEP system

- ammonium competes with potassium to be transported via Trk1,2

- one NH_4^+ is degraded into one amino acid, which is considered as electroneutral

- to keep the positive charge of ammonium, it is assumed that the metabolic degradation yields one proton per amino acid

- amino acids are removed from the cell via the SPS system

4.8.1 Transport systems

The ammonium transport via the MEP system is modeled according to Ohm's law

$$I_{NH_4^+}^{MEP} = g_{MEP} \cdot \left(V_m - \frac{RT}{zF} \ln \frac{[NH_4^+]_o}{[NH_4^+]_i} \right) \text{, with } g_{MEP} = 1 \frac{\mu S}{cm^2} \tag{4.11}$$

The degradation of ammonium to amino acids is described by an ammonium concentration dependent flux

$$J_{AA}^{prod} = -p_{AA}^{prod} \cdot [NH_4^+]_i \,, \tag{4.12}$$

where $p_{AA}^{prod} = 0.01 \frac{1}{s}$ is a rate constant. Concerning the minus sign, the reader is reminded to the sign convention: influx negative. The amino acid membrane transport is modeled according to a simple diffusion approach

$$J_{AA}^{SPS} = -p_{AA}^{SPS} \cdot ([AA]_o - [AA]_i) \cdot \frac{1}{\mathcal{R}} \,, \tag{4.13}$$
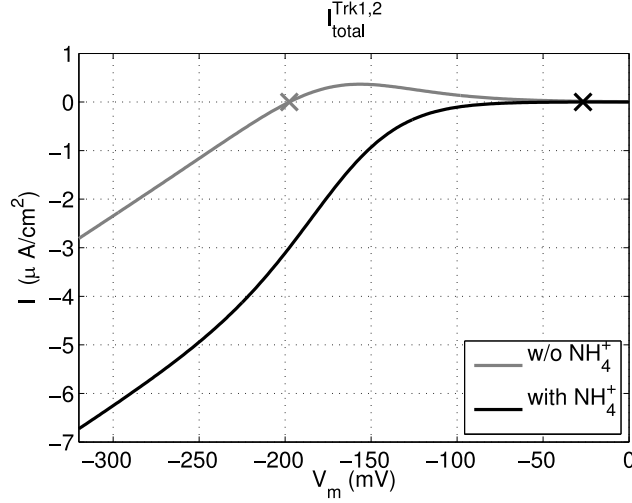
Figure 4.9: *Current-voltage relationship for Trk1,2 without (gray) and with NH_4^+ included (black) in the equilibrium potential. The cross indicates the equilibrium potential for both cases. Ammonium causes a shift of the current-voltage relationship in the positive direction. For a rather constant V_m this means an increase in the total Trk1,2 current. $[K^+]_o = 0.1\,\mathrm{mM}$, $[K^+]_i = 250\,\mathrm{mM}$ $[NH_4^+]_o = 90\,\mathrm{mM}$, $[NH_4^+]_i = 10\,\mathrm{mM}$.*

where $p_{AA}^{SPS} = 0.01\,\frac{\mathrm{cm}}{\mathrm{s}}$. For Trk1,2 it is assumed, that the transporter can not distinct between potassium and ammonium. Thus, the equilibrium potential for Trk1,2 can be expressed as

$$E_{K^+/NH_4^+} = \frac{RT}{zF} \ln \frac{[K^+]_o + [NH_4^+]_o}{[K^+]_i + [NH_4^+]_i} . \tag{4.14}$$

The involvement of ammonium causes the equilibrium potential to shift in the positive direction. Remembering the current voltage relationship of Trk1,2 (see Figure 2.15), and assuming a constant V_m, the shift results in an increase of the total Trk1,2 current. Thus, although a certain fraction of the total current is up to ammonium, the shift of the equilibrium potential could contribute to a higher potassium uptake. From this finding it can be hypothesized, that the physiological reason for transporting ammonium via Trk1,2 under potassium shortage may lie in the support of the potassium uptake.

The complete description of Trk1,2 including ammonium is given as

$$I_{total}^{Trk1,2} = -\frac{g_{Trk1,2}}{1 + e^{d_{Trk1,2} \cdot \frac{zF}{RT} \left(V_m - V_{1/2,\,Trk1,2}\right)}} \cdot \left(V_m - \frac{RT}{zF} \ln \frac{[K^+]_o + [NH_4^+]_o}{[K^+]_i + [NH_4^+]_i}\right) \tag{4.15}$$

$$I_K^{Trk1,2} = \gamma \cdot I_{total}^{Trk1,2} \tag{4.16}$$

$$I_{NH_4}^{Trk1,2} = (1 - \gamma) \cdot I_{total}^{Trk1,2}, \tag{4.17}$$

where γ describes the fraction of the potassium flux of the total current.

4.8.2 Complete model system

$$\frac{d}{dt}[K^+]_i = -(J_K^{Trk1,2} + J_K^{Tok1} + J_K^{Nha1} + J_K^{leak})$$

$$\frac{d}{dt}pH_i = \frac{1}{\beta}(J_H^{Pma1} + J_H^{leak} + J_H^{Nha1} + J_{AA}^{prod})$$

$$\frac{d}{dt}[NH_4^+]_i = -(J_{NH_4}^{Trk1,2} + J_{NH_4}^{MEP} - J_{AA}^{prod})$$

$$\frac{d}{dt}[AA]_i = -(J_{AA}^{prod} + J_{AA}^{SPS})$$

$$\frac{d}{dt}V_m = -\frac{1}{c_m}\left(I_K^{Trk1,2} + I_K^{Tok1} + I_K^{Nha1} + I_K^{leak}\right.$$

$$I_{NH_4}^{Trk1,2} + I_{NH_4}^{MEP}$$

$$\left. I_H^{Pma1} + I_H^{leak} + I_H^{Nha1}\right)$$

$$NH_4^+ \rightarrow \boxed{AA} + H^+$$

$$\boxed{CA}$$

$$CO_2 + H_2O \leftrightarrow H_2CO_3 \leftrightarrow \boxed{HCO_3^-} + H^+$$
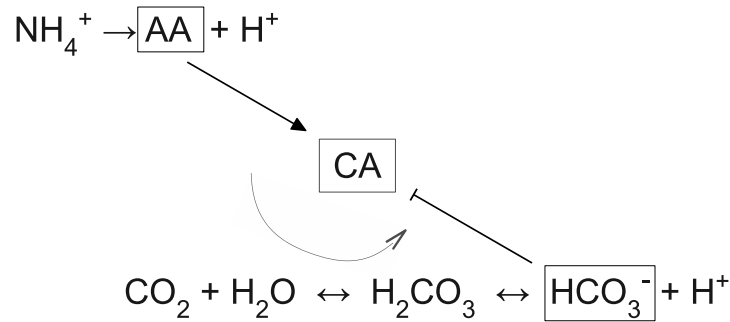
Figure 4.10: *Connection between the ammonium and bicarbonate model extension. The upper reaction shows the metabolic degradation of ammonium to amino acids (AA) and protons, as it was supposed by the ammonium model. Certain amino acids could serve to activate the carbonic anhydrase (CA), which supports the reaction of CO_2 and water. One reaction product is bicarbonate, which is a deactivator of the carbonic anhydrase. In future model versions this connection may be a worthwhile system to study.*

Note: the degradation of ammonium does not change the charge balance and is therefore not involved in the membrane potential.

In the stationary state the following conditions must be fulfilled

(1) $J_K^{transp} = 0$

(2) $J_H^{transp} = -J_{AA}^{prod}$

(3) $-J_{NH_4}^{transp} = -J_{AA}^{prod}$

(4) $J_{AA}^{SPS} = -J_{AA}^{prod}$

(5) $J_K^{transp} = -\left(J_{NH_4}^{transp} + J_H^{transp}\right)$.

From (1) and (5) it follows

$$-J_K^{transp} = J_{NH_4}^{transp} + J_H^{transp} = 0\,. \tag{4.18}$$

This means, that the net potassium transport must be compensated by the sum of the transport fluxes of ammonium or protons. It also means, that the uptake of potassium and ammonium must completely balanced by the extrusion of protons, which is a reasonable finding. Another result can be obtained from (2), (3) and (4):

$$J_{NH_4}^{transp} = -J_{AA}^{SPS} = -J_H^{transp}\,. \tag{4.19}$$

It means, that the influx of ammonium corresponds to the efflux of protons as well as the efflux of amino acids.

4.8.3 Future perspectives

The promising bicarbonate model includes the reaction of carbon dioxide and water to carbonic acid; see Section 3.2. In yeast cells, this reaction is accelerated by the carbonic anhydrase enzyme Lopéz et al. (1999). Isik et al. (2009) and Isika et al. (2010), report an activation mechanism of this enzyme by certain amino acids. This means, that the uptake and metabolic degradation of ammonium could bolster the CO_2 related reactions. In turn, Isik et al. (2008) and Isika et al. (2010) mention the suppressing function of bicarbonate on the carbonic anhydrase. Thus, the counteracting influence of bicarbonate and certain amino acids is a subsystem, which is worth to study in future model versions (see Figure 4.10).

The SPS system, amino acids and the ammonium metabolism are also involved as regulators in the mitochondrial retrograde signaling pathway, which configures the cell metabolism to defects in mitochondria Liu and Butow (2006). Since the suppression of mitochondrial genes is known for high glucose concentrations (Klemme 2004) an activation of this pathway appears likely.

4.9 Charges needed to set up the membrane potential

> Related to
> ► Section 2.2.3, page 35
>
> ► Section 1.1, page 4

The equation allows to calculate the number of charges which are required to set up a certain membrane potential. Assuming a membrane potential of $-0.25\,\mathsf{V}$ and a cell volume of $50\,\mathsf{fL} = 50 \cdot 10^{-12}\,\mathsf{cm}^3$. The respective surface of the cell is $6.5634 \cdot 10^{-7}\mathsf{cm}^2 = 65,634\,\mu\mathsf{m}^2$ the following equation gives the concentration of charges needed.

$$0.25\,\mathsf{V} \quad = \quad \frac{96485 \cdot 10^3\mu\mathsf{C}/\mathsf{mmol} \cdot 50 \cdot 10^{-12}\,\mathsf{cm}^3}{6.5634 \cdot 10^{-7}\mathsf{cm}^2 \cdot 1\mu\mathsf{F}/\mathsf{cm}^2} \cdot [X] \tag{4.20}$$

$$0.25\,\mathsf{V} \quad = \quad 7.3502\mathsf{V}/\mathsf{mmol}/\mathsf{cm}^3 \cdot [X] \tag{4.21}$$

$$3.4013 \cdot 10^{-5}\mathsf{mmol}/\mathsf{cm}^3 \quad = \quad [X] \tag{4.22}$$

The total amount of substance can be given by

$$s_{tot} = 3.4013 \cdot 10^{-5}\mathsf{mmol}/\mathsf{cm}^3 \cdot 50 \cdot 10^{-12}\mathsf{cm}^3 = 1.7 \cdot 10^{-18}\mathsf{mol} \tag{4.23}$$

Multiplying the result with Avogadros constant, k_A, yields the number of particles

$$n \quad = \quad s_{tot} \cdot k_A \tag{4.24}$$

$$n \quad = \quad 1.7 \cdot 10^{-18}\mathsf{mol} \cdot 6 \cdot 10^{23}1/\mathsf{mol} = 1.0204 \cdot 10^6 \tag{4.25}$$

Relating this number to the cell surface gives a kind of charge density, q_d, at the cell wall

$$q_d = \frac{1.0204 \cdot 10^6}{65,634\,\mu\mathsf{m}^2} = 15\,5461/\mu\mathsf{m}^2 \tag{4.26}$$

Lumping all calculation steps together, reveals that q_d is independent of the volume or surface

$$\frac{|V_m| \cdot c_m}{\frac{Vol}{Surf} \cdot F} \quad = \quad [X] \tag{4.27}$$

$$[X] \cdot Vol \cdot k_A = \frac{|V_m| \cdot c_m \cdot Surf}{F} \cdot k_A \quad = \quad n \tag{4.28}$$

$$\frac{|V_m| \cdot c_m \cdot k_A}{F} \quad = \quad \frac{n}{Surf} \tag{4.29}$$

Beware of the right units! Thus the number of charges needed depends linearly on the potential difference. In (Alberts et al. 1998, 419) it is stated, that $6\,000$ charges per $1/\mu\mathsf{m}^2$ are enough to shift the membrane potential by $100\,\mathsf{mV}$. According to the this information one needs $2.5 \cdot 6\,000 = 15\,000$ charges to shift the membrane potential by $250\,\mathsf{mV}$, which matches perfectly the results obtained above.

4.9.1 Surface potential

While the membrane potential (V_m) is a direct effect of changes in the lumenal and extracellular concentrations Endresen et al. (2007), the inner (φ_i) and outer (φ_o) surface potential of a cell membrane arises from anionic phospholipid on both sides of the membrane. Cerbon and Calderon (1994) found for *Saccharomyces carlsbergensis* that the charged lipids on the internal surface exceeds that of the outer surface up to three fold. This asymmetric distribution is maintained by the in-out translocation of phospholipids.

The surface potential leads to a local change of the concentration of charged particles, which can be approximated by weighting the concentrations (X) with a Boltzmann factor $[\tilde{X}] = [X] \cdot e^{-\frac{zF}{RT}\varphi}$ Läuger et al. (2009). Thus a negative potential φ leads to a local increase of positive charges, whereas anionic species are repelled. The authors of Grabe and Oster (2001) propose to regard this effect in electrophysiological models.

For the Nernst-potential (E_0) of a specie X the inclusion of the surface potential means a shift of $\Delta\varphi =$

$\varphi_i - \varphi_o$

$$
\begin{aligned}
E_0 &= \frac{R\,T}{z\,F}\,\ln\frac{[X]_o\,e^{-\frac{z\,F}{R\,T}\varphi_o}}{[X]_i\,e^{-\frac{z\,F}{R\,T}\varphi_i}} && (4.30)\\[2mm]
&= \frac{R\,T}{z\,F}\,\ln\frac{[X]_o}{[X]_i} + \ln e^{-\varphi_o+\varphi_i} && (4.31)\\[2mm]
&= \frac{R\,T}{z\,F}\,\ln\frac{[X]_o}{[X]_i} + \varphi_i - \varphi_o && (4.32)\\[2mm]
&= \frac{R\,T}{z\,F}\,\ln\frac{[X]_o}{[X]_i} + \Delta\varphi\,. && (4.33)
\end{aligned}
$$

The transmembrane potential was estimated by Cerbon and Calderon (1994) $\Delta\varphi \approx -20\,mV$. Presuming that this result can hold for *S. cerevisae*, the expected effect of the surface potential is rather negligible. Such a small shift can hardly distinguished from shifts which occur by random change of the stoichiometry or variable affinities of a transport system. In addition, it is questionable to define φ_o directly at the outer cell surface or in the area of cell wall, which contains a bunch of negative charged molecules. However, Borst-Pauwels (1981) reports that the kinetic parameters for Rb^+ uptake does not differ from that of yeast cells with a artificially removed cell wall. Therefore Rodriguez-Navarro (2000) concludes that the influence of the negative groups of the cell wall on the electrical field near the transport sites is rather low. The uncertainties related to the surface potential and -even more important- the missing experimental tractability make it not promising to include the surface potential in a model. Predictions that were made on such a basis can not be tested in near future and are therefore of minor benefit.

4.10 Parameters for reverse tracking and feedback controller

Variable	wt, Trk1,2, K^+	wt, Trk1,2, $2K^+$	wt, Trk1,2, H^+/K^+	unit
$[K^+]_i(0)$	0.2	0.2	0.2	$\frac{\text{mmol}}{\text{cm}^3}$
$[CO_2]_i(0)$	0.01	0.01	0.01	$\frac{\text{mmol}}{\text{cm}^3}$
$pH_i(0)$	7	7	7	pH
$V_m(0)$	-0.2	-0.2	-0.2	V
$V(0)$	48e-12	48e-12	48e-12	cm^3
$g_{Trk1,2}$	23	23	23	$\frac{\mu\text{S}}{\text{cm}^2}$
$p(0)$	1	1	1	/
pH_o	5.8	5.8	5.8	pH
$[CO_2]_o$	1e-3	1e-3	1e-3	$\frac{\text{mmol}}{\text{cm}^3}$
η	1	1	1	/
c_m	1	1	1	$\frac{\mu\text{F}}{\text{cm}^2}$
β	0.2	0.2	0.2	$\frac{\text{mmol}}{\text{pH}\times\text{cm}^3}$
$g_{Trk1,2}$	n.a.	n.a.	n.a.	$\frac{\mu\text{S}}{\text{cm}^2}$
$d_{Trk1,2}$	1	1	1	/
$V_{1/2,Trk1,2}$	-0.168	-0.168	-0.168	V
g_{Tok1}	9	9	9	$\frac{\mu\text{S}}{\text{cm}^2}$
d_{Tok1}	-1	-1	-1	/
V_{Tok1}	-0.0034	-0.0034	-0.0034	V
g_{Nha1}	10	10	10	$\frac{\mu\text{S}}{\text{cm}^2}$
d_{Nha1}	-1	-1	-1	/
V_{Nha1}	-0.31	-0.31	-0.31	V
I_{Pma1}^{max}	15	15	15	$\frac{\mu\text{A}}{\text{cm}^2}$
ΔG_{ATP}	-40e+6	-40e+6	-40e+6	$\frac{\text{kJ}}{\text{mmol}}$
g_K^{leak}	5	5	5	$\frac{\mu\text{S}}{\text{cm}^2}$
g_H^{leak}	25	25	25	$\frac{\mu\text{S}}{\text{cm}^2}$
$P_{H_2CO_3}$	6e-3	6e-3	6e-3	$\frac{\text{cm}}{\text{s}}$
$P_{HCO_3^-}$	5e-7	5e-7	5e-7	$\frac{\text{cm}}{\text{s}}$
$J_{CO_2}^{prod}$	1e-4	1e-4	1e-4	$\frac{\text{mmol}}{\text{cm}^3\times\text{s}}$
pK_A	-6.35	-6.35	-6.35	/
L_p	4e-11	4e-11	4e-11	$\frac{\text{cm}^4}{\text{s}\times\mu\text{J}}$
f_V	0.5	0.5	0.5	/
k_V	0.37	0.37	0.37	/
$[Z]_o$	0.23	0.23	0.23	$\frac{\text{mmol}}{\text{cm}^3}$
$[Z]_i$	0.2	0.2	0.2	$\frac{\text{mmol}}{\text{cm}^3}$

Table 4.5: *Reverse tracking approach: Parameters used to estimate the time courses of CO_2 production for the potassium starvation in the wild-type. These parameters were used to generate Figure 3.10. The values hold also for the approach using Nha1 as an electroneutral transporter, see Appendix Section 4.7.*

Variable	Nha1	Nha1 K^+ gating	Nha1 no gating	Nha1 $1H^+:1K^+$	unit
$[K^+]_i(0)$	0.2	0.2	0.2	0.2	$\frac{mmol}{cm^3}$
$[CO_2]_i(0)$	0.01	0.01	0.01	0.01	$\frac{mmol}{cm^3}$
$pH_i(0)$	7	7	7	7	pH
$V_m(0)$	-0.2	-0.2	-0.2	-0.2	V
$V(0)$	48e-12	48e-12	48e-12	48e-12	cm^3
g_{Nha1}	10	10	10	10	$\frac{\mu S}{cm^2}$
$p(0)$	1	1	1	1	/
pH_o	5.8	5.8	5.8	5.8	pH
$[CO_2]_o$	1e-3	1e-3	1e-3	1e-3	$\frac{mmol}{cm^3}$
η	2	2	2	2	/
c_m	1	1	1	1	$\frac{\mu F}{cm^2}$
β	0.2	0.2	0.2	0.2	$\frac{mmol}{pH \times cm^3}$
$g_{Trk1,2}$	23	23	23	23	$\frac{\mu S}{cm^2}$
$d_{Trk1,2}$	1	1	1	1	/
$V_{1/2,Trk1,2}$	-0.168	-0.168	-0.168	-0.168	V
g_{Tok1}	9	9	9	9	$\frac{\mu S}{cm^2}$
d_{Tok1}	-1	-1	-1	-1	/
V_{Tok1}	-0.0034	-0.0034	-0.0034	-0.0034	V
g_{Nha1}	n.a	n.a.	n.a.	n.a.	$\frac{\mu S}{cm^2}$
d_{Nha1}	-1	n.a.	n.a.	-1	/
V_{Nha1}	-0.31	n.a.	n.a.	-0.31	V
q_{Nha1}	n.a.	n.a.	0.1	n.a.	$\frac{mmol}{cm^3}$
I_{Pma1}^{max}	15	15	15	15	$\frac{\mu A}{cm^2}$
ΔG_{ATP}	-40e+6	-40e+6	-40e+6	-40e+6	$\frac{kJ}{mmol}$
g_K^{leak}	5	5	5	5	$\frac{\mu S}{cm^2}$
g_H^{leak}	25	25	25	25	$\frac{\mu S}{cm^2}$
$P_{H_2CO_3}$	6e-3	6e-3	6e-3	6e-3	$\frac{cm}{s}$
$P_{HCO_3^-}$	5e-7	5e-7	5e-7	5e-7	$\frac{cm}{s}$
$J_{CO_2}^{prod}$	1e-4	1e-4	1e-4	1e-4	$\frac{mmol}{cm^3 \times s}$
pK_A	-6.35	-6.35	-6.35	-6.35	/
L_p	4e-11	4e-11	4e-11	4e-11	$\frac{cm^4}{s \times \mu J}$
f_V	0.5	0.5	0.5	0.5	/
k_V	0.37	0.37	0.37	0.37	/
$[Z]_o$	0.23	0.23	0.23	0.23	$\frac{mmol}{cm^3}$
$[Z]_i$	0.2	0.2	0.2	0.2	$\frac{mmol}{cm^3}$

Table 4.6: *Reverse tracking approach: Parameters used to estimate the time courses of CO_2 production for the potassium starvation in the wild-type. These parameters were used to generate Figure 3.12. The values hold also for the approach using Nha1 as an electroneutral transporter, see Appendix Section 4.7.*

Variable	wt, CO_2	wt, Pma1	$trk1,2$, CO_2,	$trk1,2$, Pma1	unit
$[K^+]_i(0)$	0.2	0.2	0.2	0.2	$\frac{mmol}{cm^3}$
$[CO_2]_i(0)$	0.01	0.01	0.01	0.01	$\frac{mmol}{cm^3}$
$pH_i(0)$	7	7	6.5	6.5	pH
$V_m(0)$	-0.2	-0.2	-0.2	-0.2	V
$V(0)$	48e-12	48e-12	48e-12	48e-12	cm^3
$\bar{J}_{CO_2}^{prod}(0)$	5e-4	n.a.	5e-4	n.a.	$\frac{mmol}{cm^3 \times s}$
$\bar{I}_{Pma1}^{max}(0)$	n.a.	15	n.a.	15	$\frac{\mu A}{cm^2}$
$p(0)$	n.a.	1	n.a.	1	/
pH_o	5.8	5.8	5.8	5.8	pH
$[CO_2]_o$	1e-3	1e-3	1e-3	1e-3	$\frac{mmol}{cm^3}$
η	1e-3	10	1e-2 (5e-2)	120 (200)	/
c_m	1	1	1	1	$\frac{\mu F}{cm^2}$
β	0.2	0.2	0.2	0.2	$\frac{mmol}{pH \times cm^3}$
$g_{Trk1,2}$	23	23	23.	23	$\frac{\mu S}{cm^2}$
$d_{Trk1,2}$	1	1	1	1	/
$V_{1/2,Trk1,2}$	-0.168	-0.168	-0.168	-0.168	V
g_{Tok1}	9	9	9	9	$\frac{\mu S}{cm^2}$
d_{Tok1}	-1	-1	-1	-1	/
V_{Tok1}	-0.0034	-0.0034	-0.0034	-0.0034	V
g_{Nha1}	10	10	10	10	$\frac{\mu S}{cm^2}$
d_{Nha1}	-1	-1	-1	-1	/
V_{Nha1}	-0.31	-0.31	-0.31	-0.31	V
I_{Pma1}^{max}	15 (10)	n.a.	15	n.a.	$\frac{\mu A}{cm^2}$
ΔG_{ATP}	-40e+6	-40e+6	-40e+6	-40e+6	$\frac{kJ}{mmol}$
g_K^{leak}	5	5	5	5	$\frac{\mu S}{cm^2}$
g_H^{leak}	25	25	25	25	$\frac{\mu S}{cm^2}$
$P_{H_2CO_3}$	6e-3	6e-3	6e-3	6e-3	$\frac{cm}{s}$
$P_{HCO_3^-}$	5e-7	5e-7	5e-7	5e-7	$\frac{cm}{s}$
$J_{CO_2}^{prod}$	n.a.	1e-4	n.a.	1e-4	$\frac{mmol}{cm^3 \times s}$
pK_A	-6.35	-6.35	-6.35	-6.35	/
L_p	4e-11	4e-11	4e-11	4e-11	$\frac{cm^4}{s \times \mu J}$
f_V	0.5	0.5	0.5	0.5	/
k_V	0.37	0.37	0.37	0.37	/
$[Z]_o$	0.23	0.23	0.23	0.23	$\frac{mmol}{cm^3}$
$[Z]_i$	0.2	0.2	0.2	0.2	$\frac{mmol}{cm^3}$

Table 4.7: *Reverse tracking approach: Parameters used to estimate the time courses of CO_2 production and Pma1 regulation for the potassium starvation in wild-type and trk1,2. The values hold also for the approach using Nha1 as an electroneutral transporte, see Appendix Section 4.7. Exceptions are given in round brackets.*

| | wiltype | | $trk1,2\Delta$ | | |
| | Signal: CO_2 | Signal: Pma1 | Signal: CO_2 | Signal: Pma1 | |
Variable	Sensor: $[K^+]_o$	Sensor: $[K^+]_o$	Sensor: $[K^+]_o$	Sensor: $[K^+]_o$	unit
$[K^+]_i(0)$	0.2	0.2	0.2	0.2	$\frac{mmol}{cm^3}$
$[CO_2]_i(0)$	0.01	0.01	0.01	0.01	$\frac{mmol}{cm^3}$
$pH_i(0)$	7	7	6.5	6.5	pH
$V_m(0)$	-0.2	-0.2	-0.2	-0.2	V
$V(0)$	48e-12	48e-12	48e-12	48e-12	cm^3
$\bar{J}^{prod}_{CO_2}(0)$	8e-5	n.a.	7e-4	n.a.	$\frac{mmol}{cm^3\times s}$
$\bar{I}^{max}_{Pma1}(0)$	n.a.	15	n.a.	15	$\frac{\mu A}{cm^2}$
$g_{Trk1,2}(0)$	…	…	n.a.	n.a.	$\frac{\mu S}{cm^2}$
pH_o	5.8	5.8	5.8	5.8	pH
$[CO_2]_o$	1e-3	1e-3	1e-3	1e-3	$\frac{mmol}{cm^3}$
$[K^+]^{Ref}_o$	0.05	0.05	n.a.	n.a.	$\frac{mmol}{cm^3}$
$\tilde{a}_I$	7e-6	1.5e-1	6e-6	1.2e-2	/
t_I	0.7×60^2	0.5×60^2	0.7×60^2	0.7×60^2	s
a_P	-0.032	-400	-3.5e-2	-225	/
c_m	1	1	1	1	$\frac{\mu F}{cm^2}$
β	0.2	0.2	0.2	0.2	$\frac{mmol}{pH\times cm^3}$
$g_{Trk1,2}$	23	23	n.a.	n.a.	$\frac{\mu S}{cm^2}$
$d_{Trk1,2}$	1	1	n.a.	n.a.	/
$V_{1/2,Trk1,2}$	-0.168	-0.168	n.a.	n.a.	V
g_{Tok1}	9	9	9	9	$\frac{\mu S}{cm^2}$
d_{Tok1}	-1	-1	-1	-1	/
V_{Tok1}	-0.0034	-0.0034	-0.0034	-0.0034	V
g_{Nha1}	10	10	10	10	$\frac{\mu S}{cm^2}$
d_{Nha1}	-1	-1	-1	-1	/
V_{Nha1}	-0.31	-0.31	-0.31	-0.31	V
I^{max}_{Pma1}	15	n.a.	15	n.a.	$\frac{\mu A}{cm^2}$
ΔG_{ATP}	-40e+6	-40e+6	-40e+6	-40e+6	$\frac{kJ}{mmol}$
g^{leak}_K	5	5	5	5	$\frac{\mu S}{cm^2}$
g^{leak}_H	25	25	25	25	$\frac{\mu S}{cm^2}$
$P_{H_2CO_3}$	6e-3	6e-3	6e-3	6e-3	$\frac{cm}{s}$
$P_{HCO_3^-}$	5e-7	5e-7	5e-7	5e-7	$\frac{cm}{s}$
$J^{prod}_{CO_2}$	n.a.	1e-4	n.a.	1e-4	$\frac{mmol}{cm^3\times s}$
pK_A	-6.35	-6.35	-6.35	-6.35	/
L_p	4e-11	4e-11	4e-11	4e-11	$\frac{cm^4}{s\times\mu J}$
f_V	0.5	0.5	0.5	0.5	/
k_V	0.37	0.37	0.37	0.37	/
$[Z]_o$	0.23	0.23	0.23	0.23	$\frac{mmol}{cm^3}$
$[Z]_i$	0.2	0.2	0.2	0.2	$\frac{mmol}{cm^3}$

Table 4.8: *Artificial feedback controller: Parameter values, for a data-fit of the wild-type an trk1,2 starvation data. The headline of the columns indicates which variable is used as control signal (I^{max}_{Pma1} or CO_2 production rate). Examples for the implementation can be found on in Section 3.2.4.*

Variable	Signal: CO_2 Sensor: $[K^+]_o$	Signal: Pma1 Sensor: $[K^+]_o$	unit
$[K^+]_i(0)$	0.35	0.31	$\frac{\text{mmol}}{\text{cm}^3}$
$[CO_2]_i(0)$	0.01	0.01	$\frac{\text{mmol}}{\text{cm}^3}$
$pH_i(0)$	7	7	pH
$V_m(0)$	-0.2	-0.2	V
$V(0)$	48e-12	48e-12	cm^3
$\bar{J}_{CO_2}^{prod}(0)$	1e-4	n.a.	$\frac{\text{mmol}}{\text{cm}^3 \times \text{s}}$
$\bar{I}_{Pma1}^{max}(0)$	n.a.	16	$\frac{\mu\text{A}}{\text{cm}^2}$
$g_{Trk1,2}(0)$	n.a.	n.a.	$\frac{\mu\text{S}}{\text{cm}^2}$
pH_o	5.8	5.8	pH
$[CO_2]_o$	1e-3	1e-3	$\frac{\text{mmol}}{\text{cm}^3}$
$[K^+]_o^{Ref}$	0.05	0.05	$\frac{\text{mmol}}{\text{cm}^3}$
V_m^{Ref}	n.a.	n.a.	V
$\tilde{a}_I^{100}$	8.6e-6	1.45e-1	/
t_I^{100}	0.5×60^2	0.3×60^2	s
a_P^{100}	-0.02	-200	/
$\tilde{a}_I^{200}$	8e-6	1.4e-1	/
t_I^{200}	0.5×60^2	0.3×60^2	s
a_P^{200}	-0.02	-200	/
$\tilde{a}_I^{500}$	5.5e-6	1.2e-1	/
t_I^{500}	0.5×60^2	0.3×60^2	s
a_P^{500}	-0.02	-200	/
c_m	1	1	$\frac{\mu\text{F}}{\text{cm}^2}$
β	0.2	0.2	$\frac{\text{mmol}}{\text{pH}\times\text{cm}^3}$
$g_{Trk1,2}$	23	23	$\frac{\mu\text{S}}{\text{cm}^2}$
$d_{Trk1,2}$	1	1	/
$V_{1/2,Trk1,2}$	-0.168	-0.168	V
g_{Tok1}	9	9	$\frac{\mu\text{S}}{\text{cm}^2}$
d_{Tok1}	-1	-1	/
V_{Tok1}	-0.0034	-0.0034	V
g_{Nha1}	10	10	$\frac{\mu\text{S}}{\text{cm}^2}$
d_{Nha1}	-1	-1	/
V_{Nha1}	-0.31	-0.31	V
I_{Pma1}^{max}	15	n.a.	$\frac{\mu\text{A}}{\text{cm}^2}$
ΔG_{ATP}	-40e+6	-40e+6	$\frac{\text{kJ}}{\text{mmol}}$
g_K^{leak}	5	5	$\frac{\mu\text{S}}{\text{cm}^2}$
g_H^{leak}	25	25	$\frac{\mu\text{S}}{\text{cm}^2}$
$P_{H_2CO_3}$	6e-3	6e-3	$\frac{\text{cm}}{\text{s}}$
$P_{HCO_3^-}$	5e-7	5e-7	$\frac{\text{cm}}{\text{s}}$
$J_{CO_2}^{prod}$	n.a.	1e-4	$\frac{\text{mmol}}{\text{cm}^3 \times \text{s}}$
pK_A	-6.35	-6.35	/
L_p	4e-11	4e-11	$\frac{\text{cm}^4}{\text{s}\times\mu\text{J}}$
f_V	0.5	0.5	/
k_V	0.37	0.37	/
$[Z]_o$	0.23	0.23	$\frac{\text{mmol}}{\text{cm}^3}$
$[Z]_i$	0.2	0.2	$\frac{\text{mmol}}{\text{cm}^3}$

Table 4.9: *Artificial feedback controller: Parameter values, for a data-fit of the starvation data where the cells were shifted in 100, 200 and 500 µM KCl. The headline of the columns indicates which variable is used as a sensing signal ($[K^+]_o$ or V_m) and control signal (I_{Pma1}^{max} or CO_2 production rate). The values of the second column were used to generate Figure 3.17. An example for the implementation can be found on page 83.*

Bibliography

Alberts et al. 1998
ALBERTS, Bruce ; BRAY, Dennis ; JOHNSON, Alexander ; LEWIS, Julian: *Essential Cell Biology*. New York & London : Garland Publishing, 1998

Alberts et al. 2002
ALBERTS, Bruce ; JOHNSON, Alexander ; LEWIS, Julian ; RAFF, Martin ; ROBERTS, Keith ; WALTER, P.: *Molecular Biology of the cell*. 4. New York & London : Garland Science, 2002

Amoroso et al. 2005
AMOROSO, Gabriele ; MORELL-AVRAHOV, Lola ; MÜLLER, Dominik ; KLUG, Katharina ; SÜLTEMEYER, Dieter: The gene NCE103 (YNL036w) from Saccharomyces cerevisiae encodes a functional carbonic anhydrase and its transcription is regulated by the concentration of inorganic carbon in the medium. In: *Mol Microbiol* 56 (2005), Apr, Nr. 2, 549-558. http://dx.doi.org/10.1111/j.1365-2958.2005.04560.x

Ariño et al. 2010
ARIÑO, Joaquín ; RAMOS, José ; SYCHROVA, Hana: Alkali-metal-cation transport and homeostasis in yeasts. In: *Microbiol Mol Biol Rev.* 74 (2010), Nr. 1, P. 95–120

Åström and Murray 2009
ÅSTRÖM, Karl J. ; MURRAY, Richard M.: *Feedback Systems*. Princeton University Press, 2009

Bañuelos et al. 2002
BAÑUELOS, Maria ; RUIZ, Maris ; JIMÉ, Adriana ; SOUCIET, Jean-Luc ; POTIER, Serge ; RAMOS, José: Role of the Nha1 antiporter in regulating K$^+$ influx in Saccharomyces cerevisiae. In: *Yeast* 19 (2002), P. 9–15

Banuelos et al. 1998
BANUELOS, Maria ; SYCHROVA, Hana ; BLEYKASTEN-GROSSHANS, Claudine ; SOUCIET, Jean-Luc ; POTIER, Serge: The Nha1 antiporter of Saccharomyces cerevisiae mediates sodium and potassium efflux. In: *Microbiology* 144 (1998), P. 2749–2785

Bertl et al. 1998
BERTL, Adam ; BIHLER, Hermann ; REID, J. D. ; KETTNER, C. ; SLAYMAN, Clifford L.: Physiological characterization of the yeast plasma membrane outward rectifying K$^+$ channel, Duk1 (Tok1). In: *J. Membr. Biol.* 162 (1998), P. 67–80

Bertl et al. 2003
BERTL, Adam ; RAMOS, José ; LUDWIG, Jost ; LICHTENBERG-FRATÉ, Hella ; REID, John ; BIHLER, Hermann ; CALERO, Fernando ; MARTINEZ, Paula ; LJUNGDAHL, Per: Characterization of potassium transport in wild-type and isogenic yeast strains carrying all combinations of trk1, trk2 and tok null mutations. In: *Molecular Microbiology* 47 (2003), Nr. 3, P. 767–780

Bertl and Slayman 1990
BERTL, Adam ; SLAYMAN, Clifford L.: Cation selective channels in the vacuolar membrane of *Saccharomyces cerevisiae*: Dependence of calcium redox state and voltage. In: *Proc. Natl. Acad. Sci.* 87 (1990), P. 7824–7828

Bertl et al. 1993
BERTL, Adam ; SLAYMAN, Clifford L. ; GRADMANN, Dietrich: Gating and conductance in an outward-rectifying K$^+$ channel from the plasma membrane of Saccharomyces cerevisiae. In: *Journal of Membrane Biology* 132 (1993), P. 183–199

Bezanilla 2002
BEZANILLA, F.: *The nerve Impulse*. 2002 http://pb010.anes.ucla.edu

Bihler et al. 1998
BIHLER, Hermann ; SLAYMAN, Clifford L. ; BERTL, Adam: NSC1: A novel high-current inward rectifier for cations in the plasma membrane of *Saccharomyces cerevsiae*. In: *FEBS Letters* 432 (1998), P. 59–64

Bihler et al. 2002
BIHLER, Hermann ; SLAYMAN, Clifford L. ; BERTL, Adam: Low-affinity potassium uptake by Saccharomyces cerevisiae is mediated by NSC1, a calcium-blocked non-specific cation channel. In: *Biochimica et Biophysica Acta* 1558 (2002), P. 109–118

Blatt and Slayman 1987
BLATT, M.R. ; SLAYMAN, C.L.: Role of active potassium tranport in the regulation of cytoplasmic pH by nonanimal cells. In: *Proc. Natl. Acad. Sci USA* 84 (1987), P. 2737:2741

Bonner 1982
BONNER, Oscar D.: Osmotic and Activity Coefficients of Some Amino Acids and Their Hydrochloride Salts at 298.15 K. In: *J. Chem. Eng. Data* 27 (1982), P. 422–423

Boron and de Weer 1976
BORON, W. F. ; DE WEER, P.: Intracellular pH transients in squid giant axons caused by CO_2, NH_3 and metabolic inhibitors. In: *The Journal of General Physiology* 67 (1976), P. 91:112

Borst-Pauwels 1981
BORST-PAUWELS, G. W. F. H.: Ion transport in yeast. In: *Biochimica et Biophysica Acta* 650 (1981), P. 88–127

Borst-Pauwels 1993
BORST-PAUWELS, G. W. F. H.: Kinetical parameters of monovalent cation uptake in yeast calculated on accounting for the mutual interaction of cation uptake and membrane potential. In: *Biochimica et Biophysica Acta* 650 (1993), P. 201–206

Botstein and Fink 1988
BOTSTEIN, D. ; FINK, G. R.: Yeast: an experimental organism for modern biology. In: *Science* 240 (1988), P. 1439:1443

Bowman and Slayman 1979
BOWMAN, B. J. ; SLAYMAN, C. W.: The effects of vanadate on the plasma membrane ATPase of *Neurospora crassa*. In: *J. Biol. Chem.* 254 (1979), P. 2929–2934

Brett et al. 2006
BRETT, Christopher L. ; DONOWITZ, Mark ; RAO, Rajini: Does the proteome encode organellar pH? In: *FEBS Letters* 580 (2006), Nr. 3, 717 - 719. `http://dx.doi.org/DOI:10.1016/j.febslet.2005.12.103`. – DOI DOI: 10.1016/j.febslet.2005.12.103. – ISSN 0014–5793

Brett et al. 2005
BRETT, Christopher L. ; TUKAYE, Deepali N. ; MUKHERJEE, Sanchita ; RAO, Rajini: The yeast endosomal Na^+ (K^+/H^+) exchanger Nhx1 regulates cellular pH to control vesicle trafficking. In: *Molecular Biology of the Cell* 16 (2005), P. 1396:1405

Buch-Pedersen et al. 2006
BUCH-PEDERSEN, Morten J. ; RUDASHEVSKAYA, Elena L. ; BERNER, Torben S. ; VENEMA, Kees ; PALMGREN, Michael G.: Potassium as an Intrinsic Uncoupler of the Plasma Membrane H+-ATPase. In: *THE JOURNAL OF BIOLOGICAL CHEMISTRY* 281 (2006), Nr. 50, P. 38285–38292

Calero et al. 2000
CALERO, Fernando ; GOMEZ, Nestor ; ; NO, Joaquin A. ; RAMOS, José: Trk1 and Trk2 define the major K^+ transport system in fission yeast. In: *Journal of Bacteriology* 182 (2000), Nr. 2, P. 394–399

Cerbon and Calderon 1994
CERBON, Jorge ; CALDERON, Victor: Surface potential regulation of phospholipid compositions and in-out translocation in yeast. In: *European Journal of Biochemistry* 219 (1994), P. 195–200

Coury and Brodsky 1999
COURY, Larry A. ; BRODSKY, Julie McGeoch Guido Guidotti J.: The yeast Saccharomyces cerevisiae does not sequester chloride but can express a functional mammalian chloride channel. In: *FEMS Microbiological Letters* 179 (1999), P. 327–332

Cui and Kaandorp 2006
CUI, Jiangjun ; KAANDORP, Jaap: Mathematical modeling of calcium homeostasis in yeast cells. In: *Cell Calcium* 39 (2006), P. 337–348

Endresen et al. 2007
ENDRESEN, LP. ; HALL, K. ; HOYE, JS. ; MYRHEIM, J.: A theory for the membrane potential of living cells. In: *Biological Physics* 1 (2007), P. 1–22

Eraso et al. 2006
ERASO, Pilar ; MAZON, Maria J. ; PORTILLO, Francisco: Yeast protein kinase Ptk2 localizes at the plasma membrane and phosphorylates in vitro the C-terminal peptide of the H+-ATPase. In: *Biochimica et Biophysica Acta (BBA) - Biomembranes* 1758 (2006), Nr. 2, 164 - 170. `http://dx.doi.org/DOI:10.1016/j.bbamem.2006.01.010`. – DOI DOI: 10.1016/j.bbamem.2006.01.010. – ISSN 0005–2736

Estrada et al. 1996

ESTRADA, Enrique ; AGOSTINIS, Patrizia ; VANDENHEEDE, Jackie R. ; GORIS, Jozef ; MERLEVEDE, Wilfried ; FRANCOIS, Jean ; GOFFEAU, Andre ; GHISLAIN, Michel: Phosphorylation of Yeast Plasma Membrane H+-ATPase by Casein Kinase I. In: *The Journal of Biological Chemistry* 271 (1996), P. 32064–32072

Eyring et al. 1949

EYRING, H. ; LUMRY, R. ; WOODBURY, J. W.: Some applications of modern rate theory to physiological systems. In: *Record Chem. Prog.* 10 (1949), P. 100–114

Fairman et al. 1999

FAIRMAN, C. ; ZHOU, X.-L. ; KUNG, C.: Potassium uptake through the Tok1 K^+ channel in the budding yeast. In: *Membrane Biology* 168 (1999), P. 149–157

Fall 2002

FALL, Christopher ; MARLAND, Eric (Hrsg.) ; WAGNER, John (Hrsg.) ; TYSON, John (Hrsg.): *Computational Cell Biology.* Springer, Berlin, 2002

Follmann 2001

FOLLMANN, Hartmut: *Biochemie.* Teusink, 2001

Forment et al. 2002

FORMENT, Javier ; MULET, Jose M. ; VICENTE, Oscar ; SERRANO, Ramon: The yeast SR protein kinase Sky1p modulates salt tolerance, membrane potential and the Trk1,2 potassium transporter. In: *Biochimica et Biophysica Acta* 1565 (2002), Nr. 1, P. 36–40

Gaber et al. 1988

GABER, R. F. ; STYLES, C. A. ; FINK, G. R.: Trk1 encodes a plasma membrane protein required for high-affinity transport in Saccharomyces cerevisiae. In: *Mol. Cell. Biol.* 8 (1988), P. 2848–2859

Gennemark et al. 2006

GENNEMARK, Peter ; NORDLANDER, Bodil ; HOHMANN, Stefan ; WEDLIN, Dag: A simple mathematical model of adaption to high osmolarity in yeast. In: *In silico Biology* 6 (2006), Nr. 0018, P. 34

Gerber 2011

GERBER, Susanne: *In Silico Modeling of Cation Homeostasis in Saccharomyces cerevisiae*, Humboldt-Universität zu Berlin- Mathematisch-Naturwissenschaftliche Fakultät I, Diss., 2011

Ghaemmaghani 2003

GHAEMMAGHANI: Global analysis of protein expression in yeast. In: *Nature* 425 (2003), P. 737–741

Goffeau et al. 1996

GOFFEAU, A. ; BARRELL, B. G. ; BUSSEY, H. ; DAVIS, R. W. ; DUJON, B. ; FELDMANN, H. ; GALIBERT, F. ; HOHEISEL, J. D. ; JACQ, C. ; JOHNSTON, M. ; LOUIS, E. J. ; MEWES, H. W. ; MURAKAMI, Y. ; PHILIPPSEN, P. ; TETTELIN, H. ; OLIVER, S. G.: Studies on mechanisms of K^+ transport in yeast. In: *Science* 274 (1996), Nr. 5287, P. 546–567

Goosens et al. 2000

GOOSENS, Alain ; FUENTE, Natalia De L. ; FORMENT, Javier ; SERRANO, Ramon ; PORTILLO, Francisco: Regulation of Yeast H1-ATPase by Protein Kinases Belonging to a Family Dedicated to Activation of Plasma Membrane Transporters. In: *MOLECULAR AND CELLULAR BIOLOGY* 20 (2000), Nr. 20, P. 7654–7661

Gourlay et al. 2006

GOURLAY, C. W. ; DU, W. ; AYSCOUGH, K. R.: Apoptosis in yeast – mechanisms and benefits to a unicellular organism. In: *Mol. Microbiol.* 62 (2006), P. 1515–1521

Grabe and Oster 2001

GRABE, Michael ; OSTER, George: Regulation of Organell Acidity. In: *J. Gen. Physiol.* 117 (2001), P. 329–343

Gradmann et al. 1978

GRADMANN, D. ; HANSEN, U.P. ; LONG, W. S. ; SLAYMAN, C.L. ; WARNCKE, J.: Current voltage relationships for the plasma membrane and its principal electrogenic pump in *Neurospora crassa*: I. Steady-state conditions. In: *Journal of Membrane Biology* 39 (1978), P. 333–367

Haro and Rodriguez-Navarro 2002

HARO, R. ; RODRIGUEZ-NAVARRO, A.: Molecular analysis of the mechanism of the potassium uptake through the TRK1 transporter of *Saccharomyces cerevisiae*. In: *Biochimica et Biophysica Acta* 1564 (2002), P. 114:122

Hess et al. 2006
Hess, David C. ; Lu, Wenyun ; Rabinowitz, Joshua D. ; Botstein, David: Ammonium Toxicity and Potassium Limitation in Yeast. In: *PLoS Biology* 4 (2006), Nr. 11, P. 2012–2023

Hille 2001
Hille, Bertil: *Ion channels of excitable membranes.* Sinauer, 2001

Huber et al. 2010
Huber, Veronica ; Milito, Angelo De ; Harguindey, Salvador ; Reshkin, Stephan J ; Wahl, Miriam L ; Rauch, Cyril ; Chiesi, Antonio ; Pouyssegur, Jacques ; Gatenby, Robert A ; Rivoltini, Licia ; Fais, Stefano: Proton dynamics in cancer. In: *Journal of Translational Medicine* 8 (2010), P. 1–4

Isik et al. 2008
Isik, Semra ; Kockar, Feray ; Arslan, Oktay ; Guler, Ozen O. ; Innocenti, Alessio ; Supuran, Claudiu T.: Carbonic anhydrase inhibitors. Inhibition of the β-class enzyme from the yeast Saccharomyces cerevisiae with anions. In: *Bioorganic & Medicinal Chemistry Letters* 18 (2008), Nr. 24, P. 6327 – 6331

Isik et al. 2009
Isik, Semra ; Kockar, Feray ; Aydin, Meltem ; Arslan, Oktay ; Guler, Ozen O. ; Innocenti, Alessio ; Scozzafava, Andrea ; Supuran, Claudiu T.: Carbonic anhydrase activators: Activation of the β-carbonic anhydrase Nce103 from the yeast Saccharomyces cerevisiae with amines and amino acids. In: *Bioorganic & Medicinal Chemistry Letters* 19 (2009), Nr. 6, P. 1662 – 1665

Isika et al. 2010
Isika, Semra ; Ozensoy, Guler O. ; Kockar, Feray ; Aydin, Meltem ; Oktay, Arslan ; Supuran, Claudiu T.: Saccharomyces cerevisiae -Carbonic Anhydrase: Inhibition and Activation Studies. In: *Current Pharmaceutical Design* 16 (2010), P. 3327–3336(10)

Jakobsson 1980
Jakobsson, Eric: Interactions of cell volume, membrane potential and membrane transport parameters. In: *American Physiological Society* 238(5) (1980), 196-206. http://www.ncbi.nlm.nih.gov/pubmed/7377338?ordinalpos=2&itool=EntrezSystem2.PEntrez.Pubmed.Pubmed

Jennings and Cui 2008
Jennings, Michael L. ; Cui, Jian: Chloride homeostasis in Saccharomyces cerevisiae: high affinity influx, V-ATPase-dependent sequestration, and identification of a candidate Cl^- sensor. In: *J. Gen. Physiol.* 131 (2008), Nr. 4, P. 379:391

Johansson and Blatt 2006
Johansson, Ingela ; Blatt, Michael R.: Interactive domains between pore loops of the yeast K^+ channel Tok1 associate with extracellular K^+ sensitivity. In: *Bioche. J.* 393 (2006), P. 645:655

Keener and Sneyd 2004
Keener, James ; Sneyd, James: *Mathematical Physiology.* Springer, 2004

Ketchum et al. 1995
Ketchum, K. A. ; Joiner, W. J. ; Sellers, A. J. ; Kaczmarek, L. K. ; Goldstein, S. A.: A new family of outward rectifying potassium channel proteins with two pore domains in tandem. In: *Nature* 376 (1995), P. 690–695

Kinclova-Zimmermannova and Sychrova 2004
Kinclova-Zimmermannova, O. ; Sychrova, H.: Functional study of the Nha1p C-terminus: involvement in cell response to changes in external osmolarity. In: *Curr. Genet.* 49 (2004), P. 229–236

Kinclova-Zimmermannova et al. 2006
Kinclova-Zimmermannova, Olga ; Gaskova, Dana ; Sychrova, Hana: The $Na^+,K^+/H^+$-antiporter Nha1 influences the plasma membrane potential of *Saccharomyces cerevisiae.* In: *FEMS Yeast Research* 6 (2006), P. 792–800

Klemme 2004
Klemme, Jobst H.: *Angewandte Mikrobiologie.* Aachen : Shaker Verlag, 2004

Klipp et al. 2005
Klipp, E. ; Herwig, R. ; Kowald, A. ; Wierling, C. ; Lehrach, H.: *Systems Biology in Practice - Concepts Implementation and Application.* Wiley Verlag, 2005

Ko et al. 1990
Ko, Christopher H. ; Buckley, Ann M. ; Gaber, Richard F.: TRK2 Is Required for Low Affinity K+ Transport in Saccharomyces cerevisiae. In: *Genetics* 125 (1990), P. 305–312

Kolacna et al. 2005
KOLACNA, Lucie ; ZIMMERMANNOVA, Olga ; HASENBRINK, Guido ; SCHWARZER, Sarah ; LUDWIG, Jost ; LICHTENBERG-FRATÉ, Hella ; SYCHROVA, Hana: New phenotypes of functional expression of the mKir2.1 channel in potassium efflux-deficient Saccharomyces cerevisiae strains. In: *Yeast* 22 (2005), P. 1315–1323

Kuroda et al. 2004
KURODA, Teruo ; BIHLER, Hermann ; BASHI, E. ; SLAYMAN, Clifford ; RIVETTA, Alberto: Chloride channel function in the yeast TRK-potassium transporters. In: *Journal of Membrane Biology* 198 (2004), P. 177–192

Läuger et al. 2009
LÄUGER, Peter ; GEROLD, Adam ; STARK, Günther: *Physikalische Chemie und Biophysik.* 5. Berlin Heidelberg New York : Springer, 2009

Levin 1979
LEVIN, Ronald L.: Water Permeability of Yeast Cells at Sub-Zero Temperatures. In: *Journal of Membrane Biology* 46 (1979), P. 91–124

Liu and Butow 2006
LIU, Zhengchang ; BUTOW, Ronald A.: Mitochondrial Retrograde Signaling. In: *Annu. Rev. Genet.* 40 (2006), P. 159–185

Lopéz et al. 1999
LOPÉZ, R. ; ENRÍQUEZ, E. ; PEÑA, A.: Effects of weak acids on cation accumulation, ΔpH and $\Delta\Psi$ in yeast. In: *YEAST* 15 (1999), P. 1515–1521

Loukin and Saimi 1999
LOUKIN, S. H. ; SAIMI, Y.: K^+-dependent composite gating of the yeast K^+ channel, Tok1. In: *Biophys J* 77 (1999), Dec, Nr. 6, P. 3060–3070

Madrid et al. 1998
MADRID, R. ; GÓMEZ, M. J. ; RAMOS, J. ; RODRIGUEZ-NAVARRO, A.: Ectopic potassium uptake in trk1 trk2 Mutants of Saccharomyces cerevisiae correlates with a highly hyperpolarized membrane potential. In: *J. Biol. Chem.* 273 (1998), P. 14838–14844

Manlandro et al. 2005
MANLANDRO, Cara Marie A. ; HAYDON, Devon H. ; ROSENWALD, Anne G.: Ability of the Sit4p to promote K^+ efflux via Nha1 is modulated by Sap155p and Sap185p. In: *Eucaryotic Cell* 4 (2005), Nr. 6, P. 1041–1049

Maresova and Sychrova 2005
MARESOVA, Lydie ; SYCHROVA, Hana: Physiological characterization of *Saccharomyces cerevisiae* kha1 deletion mutants. In: *Mol. Microbiol.* 55 (2005), P. 588–600

Maresova et al. 2006
MARESOVA, Lydie ; URBANKOVA, Eva ; GASKOVA, Dana ; SYCHROVA, Hana: Measurements of plasma membrane potential changes in *Saccharomyces cerevisiae* cells reveal the importance of the Tok1 channel in the membrane potential maintenance. In: *FEMS Yeast Res.* 6 (2006), Nr. 2, P. 1039–1046

Marini et al. 1997
MARINI, Anna-Marie ; SOUSSI-BOUDEKOU, Said ; VISSERS, Stephan ; ANDRE, Bruno: A family of ammonium transporters in *Saccharomyces cerevisiae*. In: *Molecular and Cellular Biology* 17 (1997), Nr. 8, P. 4282–4293

Marini et al. 1994
MARINI, Anna-Marie ; VISSERS, Stephan ; ; URRESTARAZU, Antonio ; ANDRE, Bruno: Cloning and expression of the MEP1 gene encoding an ammonium transporter in *Saccharomyces cerevsiae*. In: *The EMBO Journal* 13 (1994), Nr. 15, P. 3456–3463

Martin et al. 2011
MARTIN, N. K. ; GAFFREY, E. A. ; GATENBY, R. A. ; GILLIES, R. J. ; ROBEY, I. F. ; MAINI, P. K.: A mathematical model of tumour and blood pHe regulation: The HCO_3^-/CO_2 buffering system. In: *Mathematical Biosciences* 230 (2011), P. 1–11

Martinez and Persson 1998
MARTINEZ, P. ; PERSSON, B. L.: Identification, cloning and characterization of a derepressible Na^+ coupled phosphate transporter in Saccharomyces cerevisiae. In: *Mol. Gen. Genet.* 258 (1998), P. 628–638

Martinez-Muñoz and Peña 2005
MARTINEZ-MUÑOZ, Gloria ; PEÑA, Antonio: In situ study of K^+ transport into the vacuole of *Saccharomyces cerevisiae*. In: *Yeast* 22 (2005), P. 689–704

Mendoza et al. 1994
Mendoza, Imelda ; Rubio, Francisco ; Rodriguez-Navarro, Alonso ; Pardo, Jose M.: The Protein phosphatase calcineurin is essential for NaCl tolerance of *Saccharomyces cerevisiae*. In: *Journal of Biological Chemnistry* 269 (1994), Nr. 12, P. 8792–8796

Merchan et al. 2004
Merchan, Stephanie ; Bernal, Dolores ; Serrano, Ramon ; Yenush, Lynne: Responses of the Saccharomyces cerevisiae Mpk1 mitogen-activated protein kinase pathway to increase in turgor pressure caused by loss of Ppz protein phosphatases. In: *EUKARYOTIC CELL* 3 (2004), Nr. 1, P. 100–107

Michel et al. 2006
Michel, Bertha ; Lozano, Carlos ; Rodriguez, Miriam ; Coria, Roberta ; Ramirez, Jorge ; Na, Antonio P.: The yeast potassium transporter TRK2 is able to substitute for TRK1 in its biological function under low K and low pH conditions. In: *Yeast* 23 (2006), P. 581–589

Morsomme et al. 2000
Morsomme, P. ; Slayman, C. ; Goffeau, A.: Mutagenic study of the structure, function and biogenesis of the yeast plasma membrane H^+-ATPase. In: *Biochim. Biophys. Acta* 1469 (2000), P. 133–157

Mulet et al. 1999
Mulet, Jose M. ; Leube, Martin P. ; Kron, Stephen J. ; Rios, Gabino ; Fink, Gerald R. ; Serrano, Ramon: A Novel Mechanism of Ion Homeostasis and Salt Tolerance in Yeast: the Hal4 and Hal5 Protein Kinases Modulate the Trk1-Trk2 Potassium Transporter. In: *MOLECULAR AND CELLULAR BIOLOGY* 9 (1999), Nr. 5, P. 3328–3337

Navarre and Goffeau 2000
Navarre, Catherine ; Goffeau, Andre: Membrane hyperpolarization and salt sensitivity induced by deletion of PMP3, a highly conserved small protein of yeast plasma membrane. In: *The EMBO Journal* 19 (2000), Nr. 11, P. 2515–2524

Navarrete et al. 2010
Navarrete, Clara ; Petrezsélyová, Sylvia ; Barreto, Lina ; Martínez, José L. ; Zahrádka, Jaromir ; No, Joaquín A. ; Ramos, José: Lack of main K^+ uptake systems in S. cerevisiae cells affects yeast cell physiological parameters both in potassium sufficient and limiting conditions. In: *FEMS Yeast Research* 10 (2010), Nr. 5, P. 508–517

Nelissen et al. 1997
Nelissen, Bart ; De Wachter, Rupert ; Goffeau, André: Classification of all putative permeases and other membrane plurispanners of the major facilitator superfamily encoded by the complete genome of *Saccharomyces cerevisiae*. In: *FEBS Microbiol Rev* 21 (1997), P. 113–134

Newman 2001
Newman, I. A.: Ion Transport in roots: measurement of fluxes using io-selective microelectrodes to characterize transporter function. In: *Plant, Cell and Environment* 24 (2001), P. 1–14

Nowikovsky et al. 2004
Nowikovsky, Karin ; Froschauer, Elisabeth ; Zsurka, Gabor ; Samaj, Jozef ; Reipert, Siegfried ; Kolisek, Martin ; Wiesenberger, Gerlinde ; Schweyen, Rudolf: The LETM1/YOL027 gene family encodes a factor of the mitochondrial K+ homeostasis with a potential role in the Wolf-Hirschhorn syndrome. In: *J Biol Chem* 279 (2004), Jul, Nr. 29, 30307-30315. http://dx.doi.org/10.1074/jbc.M403607200

Ohgaki et al. 2005
Ohgaki, Ryuichi ; Nakamura, Norihiro ; Mitsui, Keiji ; Kanazawa, Hiroshi: Characterization of the ion transport activity of the budding yeast Na+/H+ antiporter, Nha1p, using istolated secretory vesicles. In: *Biochimica et Biophysica Acta* 1712 (2005), P. 185–196

Peña et al. 1967
Peña, A. ; Cinco, G. ; Garcia, A. ; Puyou, A. G. ; Tuena, M.: Effects of externally added sodium and potassium ions on the glycolytic sequence of Saccharomyces cerevisiae. In: *Biochimica et Biophysica Acta (BBA) - General Subjects* 148 (1967), Nr. 3, 673 - 682. http://dx.doi.org/DOI:10.1016/0304-4165(67)90040-2. – DOI DOI: 10.1016/0304–4165(67)90040–2. – ISSN 0304–4165

Peña et al. 1972
Peña, A. ; Cinco, G. ; Gómez-Puyou, A. ; Tuena, M.: Effect of the pH of the incubation medium on glycolysis and respiration in Saccharomyces cerevisiae. In: *Archives of Biochemistry and Biophysics* 153 (1972), Nr. 2, 413 - 425. http://dx.doi.org/DOI:10.1016/0003-9861(72)90359-1. – DOI DOI: 10.1016/0003–9861(72)90359–1. – ISSN 0003–9861

Peña et al. 1969
PEÑA, A. ; CINCO, G. ; PUYOU, A.Gomez ; TUENA, M.: Studies on the mechanism of the stimulation of glycolysis and respiration by K+ in Saccharomyces cerevisiae. In: *Biochimica et Biophysica Acta (BBA) - Bioenergetics* 180 (1969), Nr. 1, 1 - 8. http://dx.doi.org/DOI:10.1016/0005-2728(69)90187-X. – DOI DOI: 10.1016/0005–2728(69)90187–X. – ISSN 0005–2728

Peña 1975
PEÑA, Antonio: Studies on mechanisms of K$^+$ transport in yeast. In: *Arch Biochem Biophys* 167 (1975), P. 397–409

Petrezsélyová et al. 2011
PETREZSÉLYOVÁ, Sylvia ; RAMOS, José ; SYCHROVA, Hana: Trk2 transporter is a relevant player in K$^+$ supply and plasma-membrane potential control in Saccharomyces cerevisiae. In: *Folia Microbiol (Praha)* 56 (2011), Nr. 1, P. 23–28

Platara et al. 2006
PLATARA, M. ; RUIZ, A. ; SERRANO, R.: The transcriptional response of yeast Na$^+$-ATPase ENA1 gene to alkaline stress involves three main signaling pathways. In: *The Journal of Biological Chemnistry* 281 (2006), Nr. 48, P. 36632:36642

Prior et al. 1996
PRIOR, C. ; PORTIER, S. ; SOUCIET, JL ; SYCHROVA, H.: Characterization of the NHA1 gene encoding a Na$^+$/H$^+$ antiporter of the yeast Saccharomyces cerevisiae. In: *FEBS Letters* 387 (1996), P. 89–93

Ramos et al. 1994
RAMOS, Jose ; ALIJO, Rafael ; HARO, Rosario ; RODRIGUEZ-NAVARRO, Alonso: TRK2 Is Not a Low-Affinity Potassium Transporter in Saccharomyces cerevisiae. In: *Journal of Bacteriology* 176 (1994), Nr. 1, P. 249–252

Ramos and Rodriguez-Navarro 1986
RAMOS, José ; RODRIGUEZ-NAVARRO, Alsonso: Regulation and interconversion of the potassium transport systems of Saccharomyces cerevisiae as revealed by rubidium transport. In: *European Journal of Biochemistry* 154 (1986), P. 307:311

Rao et al. 1993
RAO, R. ; DRUMMOND-BARBOSA, D. ; SLAYMAN, C. W.: Transcriptional regulation by glucose of the yeast PMA1 gene encoding the plasma membrane H$^+$-ATPase. In: *Yeast* 9 (1993), P. 1075–1084

Reed et al. 1987
REED, Robert ; CHUDEK, John ; FOSTER, Roy ; GADD, Geoffrey: Osmotic Significance of Glycerol Accumulation in Exponetially Growing Yeast. In: *Applied and Environmental Microbiology* 53 (1987), Nr. 9, P. 2119–2123

Rivetta et al. 2005
RIVETTA, Alberto ; SLAYMAN, Clifford ; KURODA, Teruo: Quantitative Modeling of Chloride Conductance in Yeast TRK Potassium Transporters. In: *Biophysical Journal* 89 (2005), P. 2412–2426

Roberts et al. 2001
ROBERTS, Stephen K. ; DIXON, Graha, K. ; FISCHER, Marc ; SANDERS, Dale: A novel low-affinity $H^+ - Cl^-$ co-transporter in yeast: characterization by patch clamp. In: *Mycologia* 93 (2001), Nr. 4, P. 626:633

Robinson and Stokes 1959
ROBINSON, R. A. ; STOKES, R. H.: *Electrolyte Solutions.* Second Revised Edition. Mineola, New York : Dover Publications, 1959

Rodriguez-Navarro et al. 1986
RODRIGUEZ-NAVARRO, Alonso ; R. BLATT, Michael ; L. SLAYMAN, Clifford: A potassium-proton symport in *Neurospora crassa*. In: *Journal of Genetics Physiology* 87 (1986), P. 649:674

Rodriguez-Navarro and Ramos 1984
RODRIGUEZ-NAVARRO, Alonso ; RAMOS, José: Dual System for Potassium Transportin *Saccharomyces cerevsiae*. In: *Journal of Bacteriology* 159 (1984), Nr. 3, P. 940–945

Rodriguez-Navarro 2000
RODRIGUEZ-NAVARRO, Alsonso: Potassium transport in fungi and plants. In: *Biochimica et Biophysica Acta* 1469 (2000), P. 1:30

Rosas et al. 1994
ROSAS, Gisele ; GOMEZ, Froylan ; NA, Antonio P.: Effect of potassium on amino acid transport in yeast. In: *Biochimia et Biophysica Acta* 1195 (1994), P. 223–228

Rothstein and Bruce 1958
    ROTHSTEIN, A. ; BRUCE, M.: The potassium efflux and influx in yeast at different potassium concentrations. In: *Journal of Cellular and Comparative Physiology* 51 (1958), P. 439–455

Rothstein and Demis 1953
    ROTHSTEIN, Aser ; DEMIS, Cenza: The relationship of the cell surface to metabolism. The stimulation of fermentation by extracellular potassium. In: *Archives of Biochemistry and Biophysics* 44 (1953), Nr. 1, 18-29. http://dx.doi.org/10.1016/0003-9861(53)90005-8. – DOI 10.1016/0003–9861(53)90005–8. – ISSN 0003–9861

Rubio et al. 1995
    RUBIO, F. ; GASSMANN, W. ; SCHROEDER, J.I.: Sodium-driven potassium uptake by the plant potassium transporter HKT1 and mutations conferring salt tolerance. In: *Science* 270 (1995), P. 1660–1663

Ruiz and Arino 2007
    RUIZ, Amparo ; ARINO, Joaquin: *The ENA yeast sodium ATPase system: Function and regulation.* 2007. – 2007

Sanders et al. 1981
    SANDERS, D. ; HANSEN, U.P. ; SLAYMAN, C.L.: Role of the plasma membrane proton pump in pH regulation in non-animal cells. In: *Proc. Natl. Acad. Sci USA* 78 (1981), P. 5903:5907

Sanders et al. 1983
    SANDERS, Dale ; SLAYMAN, Clifford ; PALL, Martin L.: Stochiometry of H^+/amino acid cotransport in *Neurospora crassa* revealed by current-voltage analysis. In: *Biochimica et Biohysica Acta* 735 (1983), P. 67–76

Seliber and Katznelson 1929
    SELIBER, G. ; KATZNELSON, R.: Der Einfluss der Zusammensetzung Nährbodens auf das Gewicht und den osmotischen Wert der Hefezelle. In: *Protoplasma* 7 (1929), Nr. 1, P. 204:231

Serrano 1980
    SERRANO, Ramon: Effect of ATPase inhibitors on the proton pump of respiratory-deficient yeast. In: *European Journal of Biochemistry* 105 (1980), P. 419–424

Serrano 1983
    SERRANO, Ramon: In vivo activation of the yeast plasma membrane ATPase. In: *Federation of European Biochemical Societies* 156 (1983), Nr. 1, P. 11–14

Serrano 1988
    SERRANO, Ramon: Structure and function of proton translocating ATPase in plasma membranes of plants and fungi. In: *Biochimica et Biophysica Acta* 947 (1988), P. 1–28

Shabala et al. 2006
    SHABALA, Lana ; ROSS, Tom ; MCMEEKIN, Tom ; SHABALA, Sergey: Non-invasive microelectrode ion flux measurements to study adaptive responses of microorganisms to the environment. In: *FEMS Microbiol Rev* 30 (2006), P. 472–486

Sychrova 2004
    SYCHROVA, H.: Yeast as a model organism to study transport and homeostasis of alkali metal cations. In: *Physiol Res.* 53 (2004), P. 91–98

Teusink et al. 2000
    TEUSINK, Bas ; PASSARGE, Jutta ; REIJENGA, Corinne A. ; ESHALGADO, Eugenia ; VAN DER WEIJDEN, Coen C. ; SCHEPPER, Mike ; WALSH, Michael ; BAKKER, Barbara ; VAN DAM, Karel ; WESTERHOFF, Hans ; SNOEP, Jacky: Can yeast glycolysis be understood in terms of in vitro kinetics of the constituent enzyme? Testing biochemnistry. In: *European Journal of Biochemnistry* 267 (2000), P. 5313–5329

Tombola et al. 2006
    TOMBOLA, F. ; PATHAK, M. M. ; ISACOFF, E. Y.: How does voltage open an ion channel. In: *Annu. Rev. Cell Dev. Biol.* 22 (2006), P. 23–52

Vargas et al. 2007
    VARGAS, Rita ; GARCIA-SALCEDO, Raul ; TENEIRO, Sandra ; TEIXEIRA, Miguel ; FERNANDES, Alexandra ; RAMOS, Jose ; SA-CORREIRA, Isabel: Saccharomyces cerevisiae Multidrug resistance transporter Qdr2 is implicated in potassium uptake, providing a physiological advantage to quinidine-stressed cells. In: *Eucaryotic Cell* 6 (2007), Nr. 2, P. 134–142

Vergani et al. 1998
    VERGANI, Paola ; HAMILTON, David ; JARVIS, Simon ; BLATT, M. R.: Mutations in the pore regions of the yeast K^+ channel YKC1 affect gating by extracellular K^+. In: *The EMBO Journal* 17 (1998), Nr. 24, P. 7190–7198

Vidal et al. 1995
    VIDAL, M. ; BUCKLEY, A.M. ; YOHN, C. ; HOEPPNER, D.J. ; GABER, R.F.: Identification of essential nucleotides in an upstream repressing sequence of Saccharomyces cerevisiae by selection of increased expression of Trk2. In: *PNAS* 92 (1995), P. 2370–2374

Warncke and Slayman 1980
    WARNCKE, Jens ; SLAYMAN, Clifford: Metabolic modulation of stoichiometry in a proton pump. In: *Biochimica et Biophysica Acta* 591 (1980), P. 224–233

Weiss 1996a
    WEISS, Thomas F.: *Cellular Biophysics - Electrical properties.* Bradford, 1996

Weiss 1996b
    WEISS, Thomas F.: *Cellular Biophysics - Transport.* Bradford, 1996

Yenush et al. 2005
    YENUSH, Lynne ; MERCHAN, Stephanie ; HOLMES, James ; SERRANO, Ramon: pH-Responsive, Post-translational Regulation of the Trk1 Potassium Transporter by the Type 1-Related Ppz1 Phosphatase. In: *Molecular and Cellular Biology* 25 (2005), Nr. 19, P. 8683–8692

Yenush et al. 2002
    YENUSH, Lynne ; MULET, J.M. ; NO, Joaquin A. ; SERRANO, Ramon: The Ppz protein phosphatases are key regulators of K^+ and pH homeostasis: implications for salt tolerance, cell wall integrity and cell cycle progression. In: *The EMBO Journal* 21 (2002), Nr. 5, P. 920–929

Zotova et al. 2010
    ZOTOVA, Ludmila ; ALESCHKO, Markus ; SPONDER, Gerhard ; BAUMGARTNER, Roland ; REIPERT, Siegfried ; PRINZ, Monika ; NOWIKOVSKY, Karin: Novel components of an active mitochondrial K^+/H^+ exchange. In: *The Journal of Biological Chemnistry* 285 (2010), Nr. 19, P. 14399–14414

Erklärung

Hiermit versichere ich, dass diese Dissertation von mir selbst und ohne unerlaubte Hilfsmittel angefertigt worden ist. Es wurden keine anderen als die angegebenen Hilfsmittel benutzt. Ferner erkläre ich, dass die vorliegende Arbeit an keiner anderen Hochschule als Dissertation eingereicht worden ist.

Paderborn, 21.06.2012, Matthias Kahm